

Letter from the Editors

This new issue of the journal begins, as is the tradition, with reviews. The first paper comes from a famous Novosibirsk school of bioorganic chemists (the Institute of Chemical Biology and Fundamental Medicine, Siberian Branch, Russian Academy of Sciences) and is devoted to escort aptamers. The review lays emphasis on innovative methods for the target delivery of drugs using oligoribonucleotides and deoxyribonucleotides that can recognize a variety of target cells. The next comprehensive review also pertains to modern “hotbeds of growth” (mesenchymal stem cells). It is by a world-renowned team working at the Department of Fundamental Medicine, Lomonosov Moscow State University. The work delves into both the fundamental aspects of the problem and the potential of stem cells in the repair and regeneration of tissues. Finally, a team from Lomonosov MSU and the Bach Institute of Biochemistry, Russian Academy of Sciences presents a classical review in the field of biotechnology and bioengineering.

The series of experimental papers opens with a presentation by a team from MSU, RAS Engelhardt Institute of Molecular Biology, and University Medical Center Hamburg-Eppendorf. The work centers on the development of prospective cell models intended for the screening of anti-HIV drugs. Scientists from the Institute for General Pathology and Pathophysiology, Russian Academy of Medical Sciences, and MSU report on the problems associated with the use of stem cells in regenerating the retina. The problem of protein expression in plants, which is topical today, is examined in a paper by researchers from the Belozersky Institute of Physico-Chemical Biology and

the Biological Department of MSU. In the paper, practical aspects of the expression of the epitopes of vaccine proteins are clearly laid out. Very topical studies in the field of innate immunity are presented by researchers from the Gamaleya Research Institute of Epidemiology and Microbiology. It should be stressed that the Nobel Prize in physiology and medicine was awarded in 2011 for the development of the concept of innate immunity. A practical paper dealing with the development of inhibitors-antibiotics targeted at the suppression of the activity of DNA-gyrases is by RAS institutes: the Engelhardt Institute of Molecular Biology and the Postovsky Institute of Organic Synthesis. A cell biology study on the change of the nucleolus during mitosis was penned by researchers at the Shemyakin and Ovchinnikov Institute of Bioorganic Chemistry, RAS. The anti-bacterial activity of photosensibilizing agents is the subject matter generalized in the paper by scientists of the Pirogov Russian National Research Medical University and Gamaleya Research Institute of Epidemiology and Microbiology. The series of experimental papers closes with a topical publication by researchers of the Shemyakin and Ovchinnikov Institute of Bioorganic Chemistry, who have discovered a new pathway of acid-base balance regulation in animals.

As usual, we at the journal could not abstain from vital issues of development related to Russian science. In the Forum section, we present an analytical review of the progress achieved in the “Life Sciences” program initiated by the Ministry of Education and Science.

The editorial board and the editorial council of *Acta Naturae* wish their readers success in research and invite them to cooperate. ●

Save 10% on Subscription for 2012

Details at www.actanaturae.ru

DISCUSSION

Modeling approaches are further improved by implementing new algorithms of the conformational search and new scoring functions (methods to estimate the free energy of ligand binding). Scoring functions may include either components of molecular mechanics force fields [2] or empirical terms, e.g. hydrogen bonds described by their geometrical parameters [4]. In this work we studied stacking interactions, which usually are not properly taken into account in widely used scoring functions.

THE PARAMETERS OF STACKING INTERACTIONS

Of all the various types of interactions in biomolecular complexes (such as hydrogen bonds, salt bridges, etc.), the stacking of aromatic substances deserves special attention. Most drugs include aromatic fragments in their chemical structure, and stacking often plays a notable role in their recognition by protein targets. We have recently shown that an explicit account of stacking in scoring functions increases the efficiency of ATP docking [5]. The aromatic interactions were identified by the mutual orientation of two cycles described by geometrical parameters: the height h and displacement d of one cycle relative to the other, and the angle between their planes (Fig. 1).

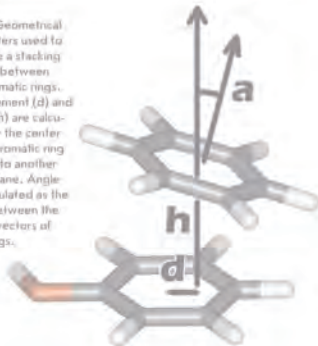
However, the range of these parameters, which corresponds to the presence or absence of a stacking contact, is still not very well defined and usually taken as arbitrary [6, 7]. Defining it more accurately would assist in developing more efficient scoring functions and should improve the prediction quality of the spatial structures of protein-ligand complexes by molecular modeling methods. With this aim in view, we performed an analysis of the spatial structures of protein-ligand complexes determined experimentally with atomic resolution where ligands contained aromatic moieties as a substructure.

The well-known example of stacking interactions is the parallel packing of purine and pyrimidine nucleosides in DNA [8, 9]. Some aromatic compounds tend to orient perpendicular to each other (T-shaped stacking), as has been shown for amino acids in proteins [7, 10] and for model systems of carbon aromatic cycles (benzene and naphthalene) [11–14]. Besides, such compounds participate in cation- π interactions, where a positively charged group interacts with the negatively charged cloud of aromatic π -electrons [15–17].

Taking all that into account, we analyzed the distribution of geometrical parameters h , d , and α for contacts of aromatic and guanine moieties of ligands with the aromatic side chains of receptor amino acids Phe, Tyr, Trp, and His, as well as with the positively charged guanidino group of Arg and amino group of Lys. The results obtained for guanine are presented in Fig. 2.

It can be seen that two distinct orientations are typical for Phe: parallel and perpendicular to the guanine plane (Fig. 3, shown in red and green, respectively). The displacement d lies in the same range (1–3 Å) for both types of contacts. Meanwhile, they differ in the value of height h , which is ≈ 3 Å for parallel and ≈ 1 Å for perpendicular orientation. Similar distributions were obtained for Tyr, Trp, and His, though the data are sparser in those cases. However, the T-shaped contact is not as typical for Tyr, Trp, and His as it is for Phe.

Fig. 1. Geometrical parameters used to describe a stacking contact between two aromatic rings. Displacement (d) and height (h) are calculated for the center of one aromatic ring relative to another ring's plane. Angle α is calculated as the angle between the normal vectors of both rings.



APRIL/JUNE 2009, No. 1

Acta Naturae



SYNTHETIC ANTIBODIES
FOR CLINICAL USE

REGULATING TELOMERASE IN ONCOGENESIS
P. 51

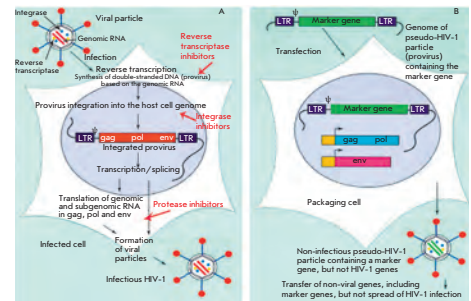
THE STRUCTURE OF THE MITOCHONDRIAL GENOME AS AN ACTIVATOR OF OPISTHORCHIASIS
P. 59

STACKING INTERACTIONS IN COMPLEXES OF FIBERS WITH ADENINE- AND GUANINE-CONTAINING LIGANDS

Screening of Potential HIV-1 Inhibitors/Replication Blockers Using Secure Lentiviral *in Vitro* System

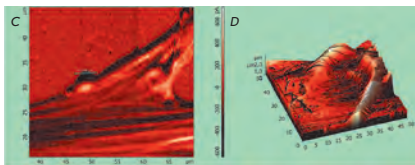
M.M. Prokofjeva, P.V. Spirin, D.V. Yanvarev, A.V. Ivanov, M.S. Novikov, O.A. Stepanov, M.B. Gottikh, S.N. Kochetkov, B. Fehse, C. Stocking, V.S. Prassolov

The development and usage of safe cell systems for testing agents which possess anti-HIV activity is a very important factor in the design of new drugs. We have described in detail a system we designed that is based on lentiviral vectors for swift and completely safe screening of potential HIV-1 replication inhibitors. The system enables one to test the efficiency of the inhibitory activity of compounds whose action is directed towards either wild-type HIV-1 reverse transcriptase or integrase, or mutant enzymes corresponding to the drug-resistant virus form. Application of this system substantially broadens the possibilities of preclinical anti-HIV drugs testing.



The life cycle of infectious HIV-1 (A) and production of recombinant pseudo-HIV-1 particles in packaging cells (B).

Behavior of Transplanted Multipotent Cells after *in Vitro* Transplantation into the Damaged Retina



The formation of synaptic connections between the transplanted MMSCs and retinal cells.

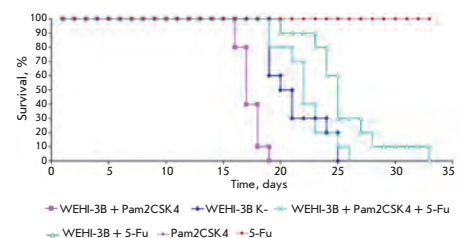
S.A. Sergeev, Y.V. Khranova, M.L. Semenova, I.N. Saburina, N.V. Kosheleva

The use of stem cell technologies in retinal defect reparation therapy has produced beneficial results. However, questions concerning the functional replacement of the missing retinal neurons by transplanted cells thus far remain unanswered. The organotypic culture protocol was used in this study in order to prove the possibility of transdifferentiation of bone marrow stromal cells (MMSCs) and neural stem/progenitor cells (NSPCs) from EGFP-positive mice and the functional integration of these cells. This technique enables a detailed characterization of cell behavior post-transplantation.

Triggering of Toll-like Receptor-2 in Mouse Myelomonocytic Leukaemia Cells WEHI-3B Leads to the Suppression of Apoptosis and Promotes Tumor Progression *in Vivo*

D.V. Shcheblyakov, D.Y. Logunov, I.V. Rakovskaya, M.M. Shmarov, B.S. Naroditsky, A.L. Ginzburg

Toll-like receptors are the essential components of innate immunity. It is shown that TLRs play an essential role in the immune resistance of an organism to bacterial and viral infections. The ability of TLR agonists to bolster the immune reaction makes them promising for use in the therapy of infectious diseases and in the chemotherapy of malignant neoplasms. However, different TLR ligands may have either antitumor activity (lipopolysaccharide, imiquimod, CpG) or, conversely, could beef up the resistance of tumor cells to apoptosis; stimulating their proliferation under certain conditions (lipopolysaccharide, lipopeptide). It has been shown that the TLR2-dependent signalling pathway in the myelomonocytic mouse leukaemia cell line WEHI-3B leads to the constitutive activation of the transcriptional factor NF- κ B, suppression of apoptosis in tumor cells, and progression of myelomonocytic mouse leukaemia *in vivo*, upon the addition of TLR2 agonist (synthetic lipopeptide Pam2CSK4) or following the infection of tumor cells with *Mycoplasma arginini*.



Influence of diacylated lipopeptide Pam2CSK4 on the proliferation rate and chemotherapy resistance of WEHI-3B tumor cells. Survival curves of BALB / c mice.

Founders

Ministry of Education and
Science of the Russian Federation,
Lomonosov Moscow State University,
Park Media Ltd

Editorial Council

Chairman: A.I. Grigoriev
Editors-in-Chief: A.G. Gabibov, S.N. Kochetkov

V.V. Vlassov, P.G. Georgiev, M.P. Kirpichnikov,
A.A. Makarov, A.I. Miroshnikov, V.A. Tkachuk,
M.V. Ugryumov

Editorial Board

Managing Editor: V.D. Knorre
Publisher: A.I. Gordeyev

K.V. Anokhin (Moscow, Russia)
I. Bezprozvanny (Dallas, Texas, USA)
I.P. Bilenkina (Moscow, Russia)
M. Blackburn (Sheffield, England)
S.M. Deyev (Moscow, Russia)
V.M. Govorun (Moscow, Russia)
O.A. Dontsova (Moscow, Russia)
K. Drauz (Hanau-Wolfgang, Germany)
A. Friboulet (Paris, France)
M. Issagouliants (Stockholm, Sweden)
A.L. Konov (Moscow, Russia)
M. Lukic (Abu Dhabi, United Arab Emirates)
P. Masson (La Tronche, France)
K. Nierhaus (Berlin, Germany)
V.O. Popov (Moscow, Russia)
I.A. Tikhonovich (Moscow, Russia)
A. Tramontano (Davis, California, USA)
V.K. Švedas (Moscow, Russia)
J.-R. Wu (Shanghai, China)
N.K. Yankovsky (Moscow, Russia)
M. Zouali (Paris, France)

Project Head: E.A. Novoselova

Editor: N.Yu. Deeva

Strategic Development Director: E.L. Pustovalova

Designer: K.K. Oparin

Photo Editor: I.A. Solovey

Art and Layout: K. Shnaider

Copy Chief: Daniel M. Medjo

Address: 119991 Moscow, Russia, Leninskiye Gory, Nauchny
Park MGU, vlad. 1, stroeniye 75G.

Phone/Fax: +7 (495) 930 80 06

E-mail: vera.knorre@gmail.com, enovoselova@strf.ru,
biomem@mail.ru

Reprinting is by permission only.

© ACTA NATURAE, 2011

Номер подписан в печать 28 ноября 2011 г.

Тираж 200 экз. Цена свободная.

Отпечатано в типографии «МЕДИА-ГРАНД»

Letter from the Editors 1

FORUM

E. V. Poverennaya, A. V. Lisitsa, A. N. Petrov,
A. A. Makarov, N. G. Luzgina

**A Statistical Analysis of Competitive Research
Contracting in the Field of Life Sciences 6**

REVIEWS

A. S. Davydova, M. A. Vorobjeva,
A. G. Venyaminova

**Escort Aptamers: New Tools for the Targeted
Delivery of Therapeutics into Cells 12**

N. I. Kalinina, V. Yu. Sysoeva, K. A. Rubina,
Ye. V. Parfenova, V. A. Tkachuk

**Mesenchymal Stem Cells in Tissue Growth
and Repair 30**

A.A. Alekseeva, S.S. Savin, V.I. Tishkov

**NAD⁺-dependent Formate
Dehydrogenase from Plants 38**

RESEARCH ARTICLES

M.M. Prokofjeva, P.V. Spirin, D.V. Yanvarev,
A.V. Ivanov, M.S. Novikov, O.A. Stepanov,
M.B. Gottikh, S.N. Kochetkov, B. Fehse,
C. Stocking, V.S. Prassolov

**Screening of Potential HIV-1 Inhibitors/
Replication Blockers Using Secure
Lentiviral *in Vitro* System. 55**

S.A. Sergeev, Y.V. Khranova, M.L. Semenova,
I.N. Saburina, N.V. Kosheleva

**Behavior of Transplanted Multipotent
Cells after *in Vitro* Transplantation
into the Damaged Retina66**

L. G. Tyulkina, E. V. Skurat, O. Yu. Frolova,
T. V. Komarova, E. M. Karger, I. G. Atabekov

**New Viral Vector for Superproduction
of Epitopes of Vaccine Proteins in Plants73**

D.V. Shcheblyakov, D.Y. Logunov,
I.V. Rakovskaya, M.M. Shmarov,
B.S. Naroditsky, A.L. Ginzburg

**Triggering of Toll-like Receptor-2
in Mouse Myelomonocytic Leukaemia
Cells WEHI-3B Leads to the Suppression
of Apoptosis and Promotes Tumor
Progression *in Vivo*83**

V.L. Tunitskaya, A.R. Khomutov,
S.N. Kochetkov, S.K. Kotovskaya,
V.N. Charushin

**Inhibition of DNA Gyrase by Levofloxacin
and Related Fluorine-Containing
Heterocyclic Compounds94**

K.V. Shishova, O.O. Zharskaya, O.V. Zatsepina

**The Fate of the Nucleolus during Mitosis:
Comparative Analysis of Localization
of Some Forms of Pre-rRNA
by Fluorescent *in Situ* Hybridization
in NIH/3T3 Mouse Fibroblasts100**

T.A. Shmigol, V.A. Bekhalo, E.V. Sysolyatina,
E.V. Nagurskaya, S.A. Ermolaeva,
A.Ya. Potapenko

**Effect of Sodium Chloride on Aggregation
of Merocyanine 540 and Photosensitized
Inactivation of *Staphylococcus aureus* and
Pseudomonas aeruginosa107**

I.E. Deyev, D.I. Rzhnevsky, A.A. Berchatova,
O.V. Serova, N.V. Popova, A.N. Murashev,
A.G. Petrenko

**Deficient Response to Experimentally
Induced Alkalosis in Mice with the
Inactivated *insrr* Gene114**

Guidelines for Authors118

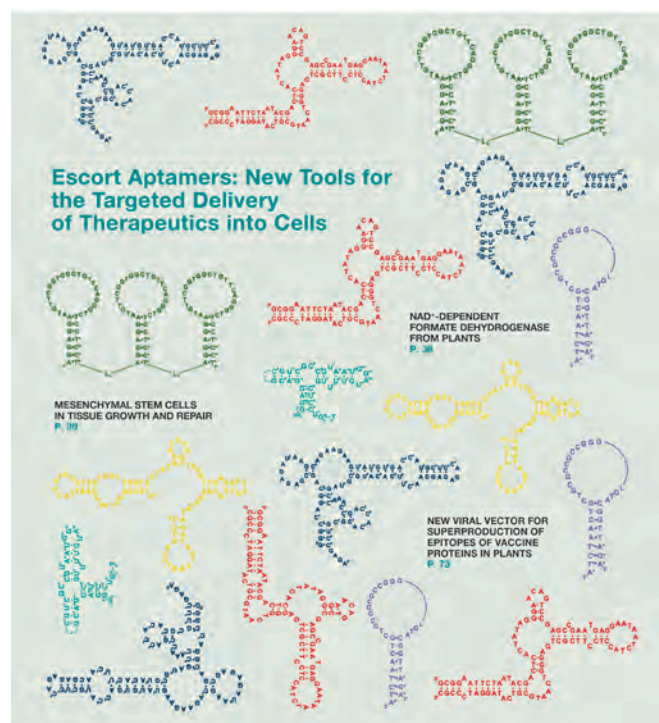


IMAGE ON THE COVER PAGE
The proposed secondary structure of aptamers.
(A. S. Davydova *et al.*)

A Statistical Analysis of Competitive Research Contracting in the Field of Life Sciences

E. V. Poverennaya^{1*}, A. V. Lisitsa¹, A. N. Petrov², A. A. Makarov³, N. G. Luzgina⁴

¹Orekhovich Institute of Biomedical Chemistry, Russian Academy of Medical Sciences

²Directorate of the CNTP at the Russian Ministry of Education and Science

³Engelhardt Institute of Molecular Biology, Russian Academy of Sciences

⁴Research Center of Clinical and Experimental Medicine, Siberian Branch, Russian Academy of Medical Sciences

*E-mail: k.poverennaya@gmail.com

Copyright © 2011 Park-media, Ltd. This is an open access article distributed under the Creative Commons Attribution License, which permits unrestricted use, distribution, and reproduction in any medium, provided the original work is properly cited.

Assessment of applications in open state calls for a competitive contracting is regulated by the Federal Law 94-FZ. Ratios of different criteria in assessing applications (price, terms, and quality of proposal) are set in the legislation and make it possible, as a result of calculations using a universal formula, to assign a score for each application. Using these rating scores, winners are selected. In this paper, we have attempted to characterize the correlation between the price and quality of the research proposed by the applicants and estimate how efficient it is to use the legally set weighted values of different criteria in assessing applications.

Russian Federal R&D Program the Federal Law 94-FZ [1] prescribes that for the state as a customer, the top priority is given to the lower costs of project implementation. In the framework of this principle was used for assessment and comparison of research applications. Normally, low price and quick performance are more important than the quality; however, such approach is poorly effective for research contracting.

From December 2010 to January 2011 in the framework of the Federal R&D Program two types of research lots were opened for applications. Lots for investigative research were opened with the maximum price tag of 6 mln rubles per 2-years, whereas applied research

calls were at the price 12 mln rubles for the same period of time. Each lot enabled to conclude research contracts with several top-scoring applicants. As scorings were dependent on the price diminishing, afterwards it has been concluded that price dumping in scientific competitions has reached 60% [3].

In terms of the development of the scientific-and-technological potential of the country, the calls were first opened under condition in which, to comply with the requirements of Resolution of the Russian Government No. 722 dated September 10, 2009 [4], the specific weight of the price in the gross assessment of the application comprised 55%. It should be noted that all the research contract calls were announced in a relatively short pe-

riod of time, i.e. the applicants had limited opportunity to alter their tactics in the competition.

We have analyzed the following data taken from the protocols of assessment and comparison of research proposals [5]:

- Maximum lot price;
- Name of the applicant;
- Expert assessment of application by criterion “scientific and technical level of research” (maximum 35 scores);
- Expert assessment by “professional reputation of the applicant” (maximum 40 scores);
- Expert assessment by “prior R&D experience” (maximum 25 scores);
- and
- Project implementation cost, demanded by the applicant.

A total of 41 lots were analyzed. In the contest for these lots, 183 scientific organizations took part, and each organization filed at least one application. A total of 421 applications were filed and included in this analysis. The results of the calls were taken from official protocols published by the Ministry of Education and Science of the Russian Federation. The price demanded by the participant was normalized to the maximum price of the lot, and the obtained value of the *price-drop* was expressed in percentage

points. Given the fact that expert assessments based on the criteria “scientific and technical level of research,” “professional reputation of the,” and “prior R&D experience” correlated with each other (the correlation coefficient exceeded than 0.73), the sum of the above-said criteria was considered the integral measure of assessment, which was further designated as *application quality*.

To calculate the statistical correction, we analyzed the dependence between the assessment of the application quality V and the price-drop C . To reveal this dependence, applications were selected, which came out of the 49 (from 183 organizations-participants) most active participants, i.e. those that filed at least three applications for different lots, and at least one application from those filed was a winner.

In the case if three or more applications were filed by one participant, we averaged the assessment of the application quality and price-drop, and, in accordance with the obtained means V and C , a point was plotted on the graph. If several data points (from different participants) corresponded to one value of price-drop, we excluded, before the averaging, outliers using the t-test ($p \geq 0.95$). The obtained scatter plot data was approximated using the linear equation $V = aC + b$, where the values of constants a and b were obtained with the help of the least square method (built-in tool of Microsoft Excel).

The value of constant a , defining the slope angle of the approximation linear equation curve, was used as a statistical correction, given the expression (1):

$$a = \frac{dV}{dC} = \frac{V - V'}{C' - C}, \quad (1)$$

where values V and C were obtained from averaged data presented in official protocols, and V' and C' were values corrected under

the assumption that the research quality must not be affected by the price. Assuming that the minimum value of the reduction of the price, not leading to a decrease in quality, comprises $C' = 0$, in order to calculate the *adjusted assessment of the application quality* V' , expression (1) was transformed into:

$$V' = V - |a|C. \quad (2)$$

(The module is used as the coefficient a is negative due to the reciprocal dependency between the application quality and price-drop.)

Using formula (2), we carried out a retrospective calculation of the adjusted values of assessments of the scientific quality for 421 applications. For each contest lot, the final score of applications was calculated using the formula listed in the official call documentation:

$$R = 0.45V' + 0.55C. \quad (3)$$

The lots were sorted (ranked) by descending degree of the final score R .

In order to compare the ratings of applications, the applications were sorted according to the final score, which accounts for the estimations of application quality. A series of model ratings were generated by changing the weight of the application quality from 0.45 to 1.00 with a step of 0.05. Modeled ratings were compared with the expert rating, obtained by formula (3). In agreement with different weights of the quality criterion, we changed the specific weight of the cost so that the sum of both criteria equaled one.

In order to compare the artificially generated model and expert ratings, we used the Spearman coefficient of rank correlation (CRC):

$$r_s = 1 - \frac{6 \sum d^2}{n(n^2 - 1)}, \quad (4)$$

where d is the difference between

the ranks for each application in the lot and n is the number of applications in the lot. CRC was computed for each lot separately; thereat, five lots were excluded from the analysis as they contained less than five applications. For the remaining 36 lots, we assessed the reliability of CRC using the critical value r_s at a given number of applications per lot. We selected the values of rank correlation which were reliable at a significance level $p \geq 0.95$, and the selected CRC values were averaged for all lots. The mean CRC values were put on the graph in accordance with the specific weights of the criterion “application quality,” for which ratings were computed. On the graph, using the least square method, we found two approximating equations, corresponding to linear sections of the CRC dependency. Equations were solved to define the optimal weight of the “application quality” criterion, exceeding which CRC did not significantly increase at the increase of the specific weight.

The data, presented in the protocols of assessment and comparison of applications, are summarized in *Fig. 1* in the form of a histogram indicating the number of filed applications depending on the price-drop intervals. Less than 5% of the applications (21 out of 421 applications) entered the contest with zero price-drop, i.e. the cost of the project equaled the initial (maximum) cost of the call. The mean price-drop was 30% for all applications surveyed.

As is seen from the histogram (*Fig. 1*), the distribution of applications has three clear peaks corresponding to price-drops of 15, 30, and 50%. The presence of these peaks allows for a discussion of the general considerations underlying a participant’s decision on the cost of their work. It can be presumed that a fall in the cost of up to 15%, which was the case in 155 applications, is

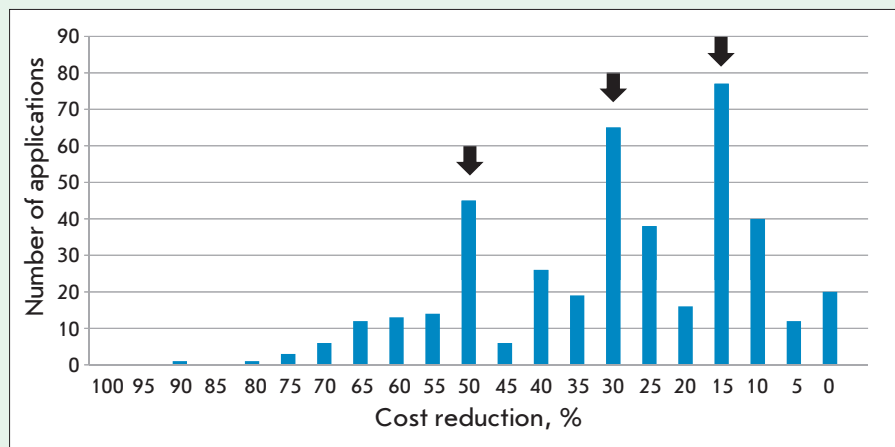


Fig. 1. Distribution of research applications depending on the degree of price-drop. Peaks are marked by arrows.

not critical for the research quality and can be achieved by a reduction in overhead expenses (coverage of overhead expenses from the applicant's internal resources). A 30% price reduction may point at sufficient applicant groundwork, e.g., a stock of consumables or reagents, readily available for the project implementation. A total of 119 applications (i.e. 28% of the total number) fell in the range of costs reductions of 15 to 30%. The next category includes 96 applications in which the cost reduction ranged from 30–50%. In this case, it could be suggested that the fall in costs will adversely affect the quality of the project implementation. Finally, in the histogram, a group is seen, with costs falling by more than 50%. This group includes 51 applications, which number is twice less than for the previously described categories of pricing. Lower number indicates that “raider” tactics drops out of the general concept pursued by the applicants when estimating the cost of their research work.

An analysis of the data published in the protocols of the research calls allows one to estimate the activity and efficiency of the participants. Most applications were filed by low-activity participants who put in most cases one, and sometimes,

two applications. As is seen from the histogram in *Fig. 2*, there were 132 such entities, i.e. substantially over half of the applications. The data obtained for one or two applications are not sufficient to draw statistical generalizations. Besides, as can be seen from *Fig. 2*, low-activity participants rarely win. Probably, sole applications are filed by institutions whose profile of activity is not fully compliant with general trends in

life science. Adaptation to a limited number of specific tasks generally lowers the competitiveness, which is reflected in the low efficiency of the participants who filed only one application – 23,5%.

High efficiency is typical for the participants who put in three or more applications (*Fig. 2*). For the participants who filed three to four applications, the efficiency exceeded 40%, i.e. nearly half of the applications awarded a contract. Hence, one can conclude that the work of the institution in several directions increases competitiveness and, most likely, such participants exert the greatest influence on the development of life sciences in Russia. Given the above considerations, we further analyzed the data on the quality of the applications of the participants who filed three and more applications. The number of such participants was 49.

Before we proceed to the analysis of the applications quality, we should note the tight interconnection between the categories of expert quality scorings. For instance,

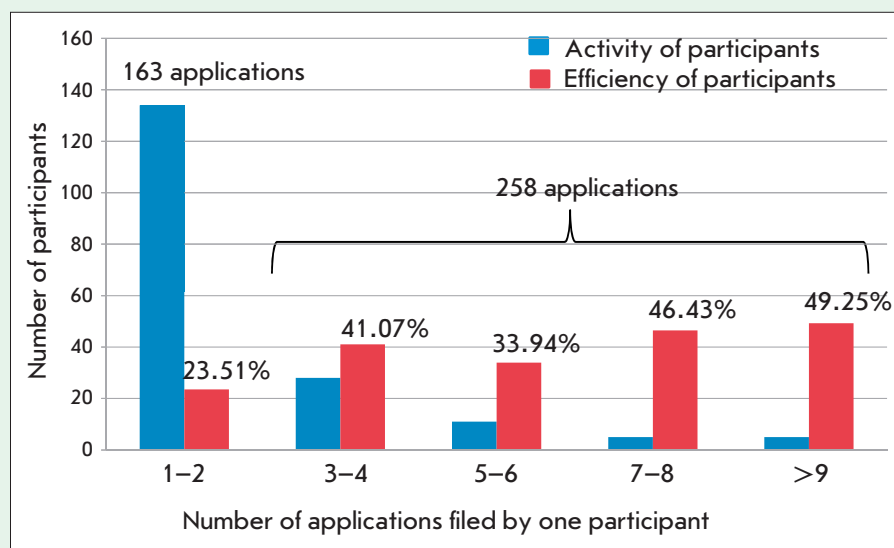


Fig. 2. Distribution of values of activity and efficiency of participants. Activity is calculated as the number of applications filed by the participant; efficiency, the ratio of the number of “winning” applications to the total number of applications filed by the participant.

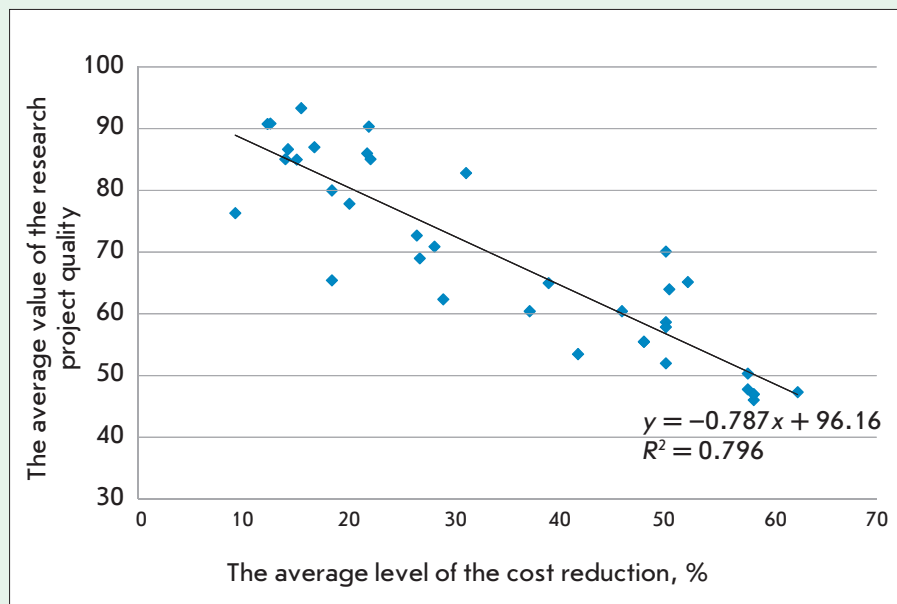


Fig. 3. The linear approximation of the dependence of the experts' quality assessment (V) and the price-drop in the application (C). Each point corresponds to one participant, and respective values of the price-drop and application quality are averaged by the winning applications.

the level of the research correlates well with the professional reputation of the applicant ($R^2 = 0.74$; $n = 421$), while the reputation, in turn, depends on experience ($R^2 = 0.73$; $n = 421$). Such a correlation is quite regular, which further permitted to use the sum of the scores in all three expert categories as the score of the quality of the research project submitted for the call.

Figure 3 shows data demonstrating the correlation between the application quality of the projects and reduction in the demanded price. The dependence has been obtained for 105 winning applications, which came up from the selected 49 active participants. If quality assessments coincided in several applications, the relevant values of cost reduction for these applications were averaged. Therefore, for example, the lowest reduction in cost according to the data in Fig. 3 amounts to 9% (not 0%, as follows from the histogram in Fig. 1).

Approximation of the data by the

linear dependence, in agreement with formula (2), allowed us to reveal the value of the absolute term $V = 96$ and adjustment multiplier $a = -0.787$, and include these terms for the calculation of the adjusted assessment of the application quality V' :

$$V' = 96 - 0.787 \times C. \quad (5)$$

The absolute term in the formula defines the limit for the score assessment of the research quality. The value obtained on the basis of the approximation results almost coincides with the maximum of the scores 100, set in the call official documentation. Substituting the values shown in Fig. 3 in formula (5), one can find the point $V = 47$; $C = 60\%$, at which the adjusted assessment of the research quality equals zero. This means that for the applications whose price is reduced by 60% and more, the risk of poor quality of results is so high that, in the expert opinion, it is impos-

sible in principle to implement the project.

The adjusted assessment of the research quality, obtained as a result of approximation, was substituted in formula (3) and a new total score was calculated for each lot, which was the weighted sum total of the indicators "application quality" and "price-drop." Applications filed in each lot were rearranged in accordance with the values of the total score. The obtained ranking of the applications was considered an expert rating, i.e. the rating in which the order of applications encapsulates the collective opinion of the experts about the link between the application's cost and its quality.

The expert rating was then compared with the model ratings obtained at different values of the weights of the cost and quality criteria, e.g., the values 0.4 and 0.6 were taken for the weights, respectively. The weights were used to compute the new value of the final score assessment for all applications, after which the applications were positioned within each lot in descending order. Such a model rating was compared with the expert rating previously obtained with the use of the adjusted assessment. The comparison was carried out with the use of the Spearman rank correlation coefficient (CRC), which is sensitive to the order of elements in sorted lists. In the described example case, when the weight of the quality criterion was set at 0.6, the value of CRC was 0.865. This value indicates that the order of applications in the expert rating matches well the model rating with the preset quality-to-cost ration 0.6/0.4/

On opposite case, when, for instance quality-to-cost was 0.4/0.6, the CRC value equaled only 0.75.

In Fig. 4, values of CRC are shown for 11 model ratings obtained at different quality-to-cost ratios. Along the ordinate axis the

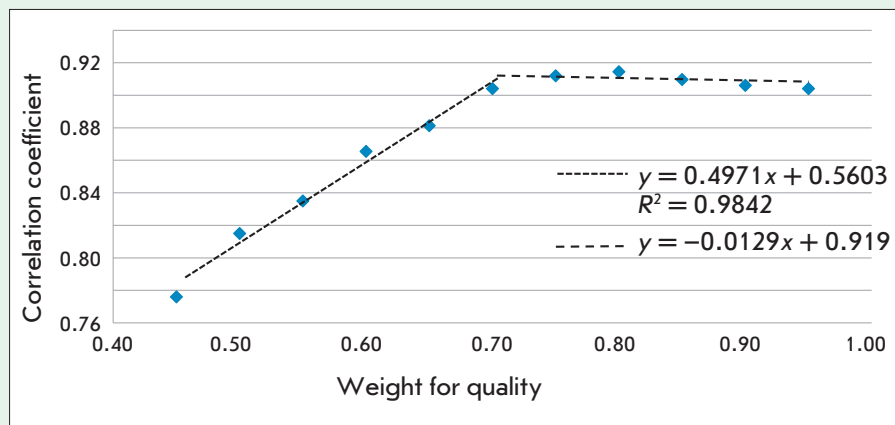


Fig. 4. Dependence of rank correlation of the expert rating and model ratings, obtained at different weights of the criterion “application quality.”

weights of the application quality used to generate the model ratings are plotted, and along the abscissa axis, values of CRC obtained as a result of comparing model ratings with the expert rating. It is seen from Fig. 4 that there is a clear dependence between the CRC and the weight of the quality criteria. The increase in the value of the correlation coefficient continues up to the level of values of the quality criterion of 0.7, at which CRC goes beyond 0.9. Further increase in the weight

of the quality criterion did not affect in any significant manner the CRC value.

For purposes of illustration, Fig. 4 shows approximation lines crossing at a point with the abscissa coordinate 0.703 (3). The slope of the straight line, approximating the plateau on the graph, may vary depending on the number of points used to draw the equation. The dynamics of the CRC increase changes up to the level of 0.7; therefore, it is purposeful to take this value for

the minimum weight at which optimal coincidence of the model and expert ratings is achieved.

CONCLUSIONS

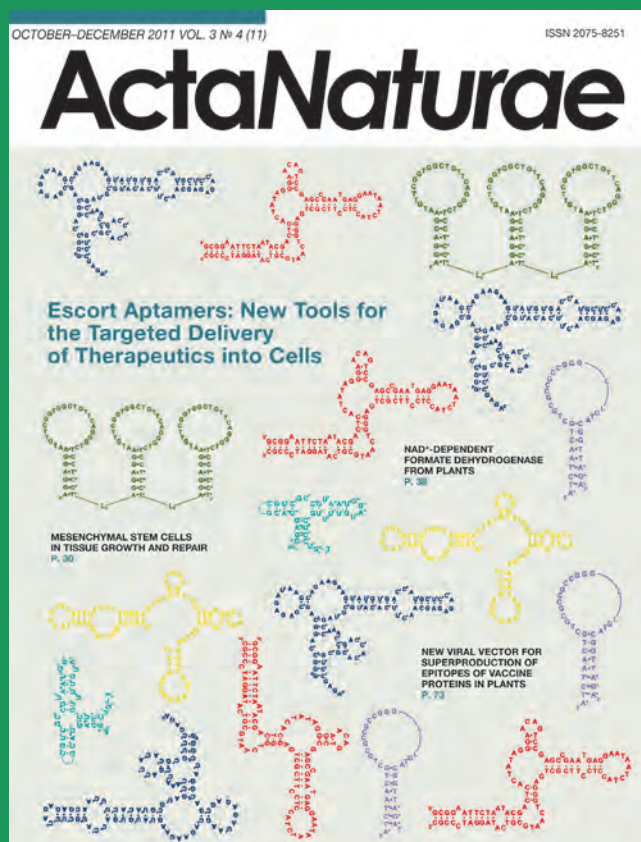
There exists a reciprocal dependency between the quality of the research project and reduction in its cost. If the price of the project drops by more than 60% against the initial estimation of the call budget the proper implementation of research becomes impossible. The legally established weights for the price and quality are currently inappropriate for the competitive research contracting, as these weights almost neglect the expert opinion while comparing the applications merely by the price. Using heuristic modeling, we have shown that optimal ranking of research applications can be achieved by using the quality to-cost ratio 0.7/0.3. ●

The authors are grateful to the members of the Live Systems Workgroup and K. Timirbaev (the MetaSyntez Corporation) for participation in the discussion of the paper.

REFERENCES

1. On the placement of orders for the supplies of goods, execution of works, and rendering of services for state and municipal needs: Federal Law dated July 21, 2005 No. 94 – FZ. The Code of Laws of the Russian Federation. 2005. No. 30. Clause 3105.
2. The Federal Target Program “Research and development in the priority directions of the development of the Russian scientific-and-technological complex for 2007–2012”: Resolution of the Government of the Russian Federation dated July 6, 2006 No. 977-r. The Code of Laws of the Russian Federation. 2006. No. 29. Clause 3258.
3. “The system of state purchases in the sphere of science and education requires radical changes”. Polit.ru. URL: <http://www.polit.ru/news/2011/08/05/sg/>
4. On the approval of the Rules of assessing applications for participation in the competition for the right to sign the state or municipal contract for the supplies of goods, execution of works, and rendering of services for state or municipal needs: Resolution of the Government of the Russian Federation dated September 10, 2009 No. 722. The Code of Laws of the Russian Federation. 2009. No. 38. Clause 4477.
5. Arrangement 1.2. “Carrying out problem-oriented investigative studies and creating the scientific-and-technical groundwork in technologies in the field of live systems”. Federal Target Program “Research and development in the priority directions of the development of the Russian scientific-and-technological complex for 2007–2013.” URL: <http://www.fcpir.ru/catalog.aspx?CatalogId=1044>

Acta Naturae is a new international journal on life sciences based in Moscow, Russia. Our goal is to present scientific work and discovery in molecular biology, biochemistry, biomedical disciplines and biotechnology. *Acta Naturae* is also a periodical for those who are curious in various aspects of biotechnological business, intellectual property protection and social consequences of scientific progress.



For more information and subscription please contact us at info@biorf.ru

Escort Aptamers: New Tools for the Targeted Delivery of Therapeutics into Cells

A. S. Davydova, M. A. Vorobjeva*, A. G. Venyaminova

Institute of Chemical Biology and Fundamental Medicine, Siberian Branch, Russian Academy of Sciences

*E-mail: maria.vorobjeva@gmail.com

Received 08.07.2011

Copyright © 2011 Park-media, Ltd. This is an open access article distributed under the Creative Commons Attribution License, which permits unrestricted use, distribution, and reproduction in any medium, provided the original work is properly cited.

ABSTRACT Escort aptamers are DNA or RNA sequences with high affinity to certain cell-surface proteins, which can be used for targeted delivery of various agents into cells of a definite type. The peculiarities of the selection of escort aptamers are discussed in this review. The methods used in selection of escort aptamers via the SELEX technique are considered, including selection against isolated cell-surface proteins, cell fragments, living eukaryotic cells, and bacteria. Particular attention is given to the design and chemical modification of escort aptamers. The different fields of application of escort aptamers are described, including the targeted delivery of siRNAs, nanoparticles, toxins, and photoagents, as well as the identification of specific cell markers and the detection or isolation of cells of a definite type. The potential for the application of escort aptamers in the development of new therapeutic agents and diagnostic systems is also discussed.

KEYWORDS SELEX method; NA aptamers; escort aptamers; specific cell binding; addressed cell delivery; detection of cells.

ABBREVIATIONS dsDNA – double-stranded DNA; ssDNA – single-stranded DNA; siRNA – small interfering RNA; PSMA – prostate-specific membrane antigen; IC_{50} – therapeutical concentration required to suppress the growth of 50% cells; K_d – apparent constant of dissociation of the aptamer–target complex; LNA – locked nucleic acids; SELEX – Systematic Evolution of Ligands by EXponential Enrichment.

INTRODUCTION

Aptamers (Latin *aptus* – suitable) are single-stranded DNA and RNA molecules that are capable of specific recognition of definite types of compounds, thanks to their unique spatial structure. In the 1990s, methods for *in vitro* selection, enabling one to obtain nucleic acids with predetermined properties, were described by three independent research groups. A. Ellington and J. Szostak [1] obtained an RNA molecule that was capable of specifically binding to an organic dye. C. Tuerk and L. Gold described the selection of RNA molecules that were capable of binding to phage 4 DNA polymerase and called the developed method SELEX (Systematic Evolution of Ligands by Exponential Enrichment) [2]. D. Robertson and G. Joyce used *in vitro* selection to convert a group I ribozyme from a ribonuclease into a deoxyribonuclease [3]. Throughout the subsequent two decades, this field has developed rapidly; methods for the selection of aptamers and approaches to their design have been further refined. A large number of aptamers capable of binding to various targets with high specificity have already been obtained (see Re-

views [4–7]). Aptamers find broad application across a wide range of research fields, thanks to their unique properties (namely their high affinity and selectivity in binding to a target molecule). In particular, aptamers can be used to obtain highly efficient and specific inhibitors of target proteins that can be applied in the design of new drugs. A number of aptamers are currently in different stages of clinical trials [8]. Macugen (*Eyetech Pharmaceuticals* and *Pfizer*), which is based on aptamer binding a human vascular endothelial growth factor (VEGF), has been certified as an efficient drug for the treatment of age-related macular degeneration [9, 10].

One of the most interesting and promising aspects in the field is designing aptamers that are capable of specific recognition of cells of a definite type through binding with certain dominants on their surface. In the review by B. Hicke *et al.* [11], these compounds were referred to as *escort aptamers*. The use of escort aptamers as an addressing fragment opens wide possibilities for the targeted delivery of agents of different nature to cells of definite types. Today, a large number of

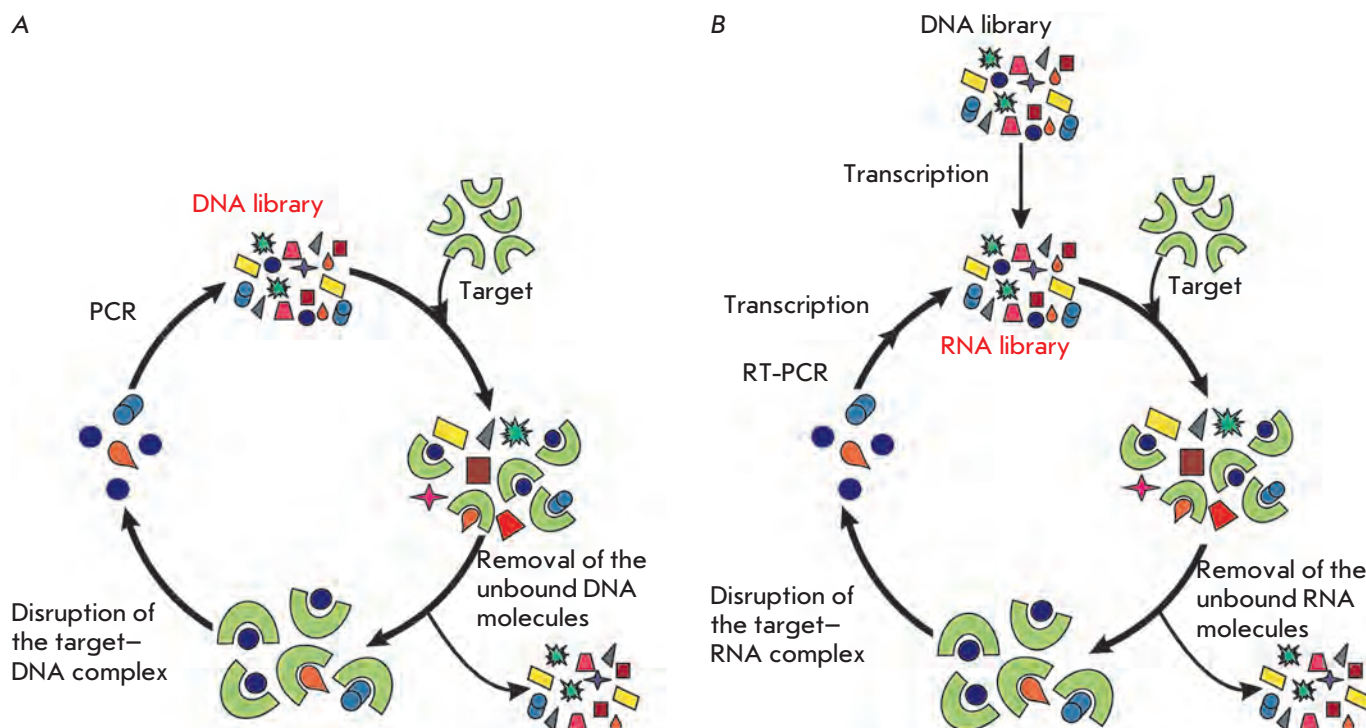


Fig. 1. The general scheme of the SELEX method using DNA (A) and RNA (B) libraries.

escort aptamers directed toward various target cells have been obtained, and a wide range of applications for these aptamers for specific action on cells, diagnostics, and cell isolation have been described. The present review is devoted to the selection, design, and different aspects in the use of escort aptamers.

OBTAINMENT OF APTAMERS BY *in vitro* SELECTION

The general principle of the SELEX method

DNA and RNA aptamers are obtained via *in vitro* selection from combinatorial libraries of nucleic acid molecules. A conventional library is a set of oligonucleotides with the randomized region consisting of 20–60 nucleotides flanked with the constant regions that are required for binding to primers and the PCR amplification of DNA. Currently, libraries containing both ssDNA and RNA molecules are widely used for the selection of aptamers. RNA aptamers are capable of forming a greater variety of spatial structures as compared with DNA aptamers, as a result of the presence of 2'-OH groups. However, RNA aptamers are more sensitive to the action of cell nucleases and require the introduction of additional protective groups [12].

The ssDNA libraries are obtained via the conventional methods for the chemical synthesis of oligodeoxyribonucleotides using a mixture of all four monomers

when synthesizing a randomized fragment. In order to obtain an RNA library, the chemical synthesis of an ssDNA library containing the promoter sequence for T7 RNA polymerase at its 5'-terminal region is first performed. The ssDNA matrix is then used to obtain a dsDNA, which is subsequently applied for the synthesis of RNA via *in vitro* transcription. The general scheme of the SELEX method for DNA libraries comprises the following stages: incubation of a library with a target, separation of oligonucleotide–target complexes from the unbound oligonucleotides, disruption of the oligonucleotide–target complexes, and amplification of the bound molecules (Fig. 1A). For the selection of RNA aptamers, SELEX also comprises the following additional stages: production of the RNA library on the DNA matrix, reverse transcription of the bound RNA molecules to produce DNA, and DNA amplification (Fig. 1B).

During the selection process, the library is enriched in sequences possessing increased affinity to the target. Five to fifteen rounds of selection are typically performed to obtain aptamers, depending on the values of the dissociation constant of the aptamer–target complex. After the dissociation constant ceases to decrease (i.e., the affinity of the library to the target stops rising), the enriched library is cloned, and the sequences of the individual aptamers are determined. The homology be-

Table 1. Comparison of the properties of NA aptamers and monoclonal antibodies

	Aptamers	Monoclonal antibodies
Selection method	<i>In vitro</i> selection	Hybridoma technology, including immunization of animals
Synthesis method	Chemical or enzymatic synthesis	Produced using cell cultures or laboratory animals
Limitations imposed on the target molecules	No limitations	Antibodies against non-immunogenic or toxic substances cannot be obtained
Affinity to the target	$K_d \approx 10^{-10}$ – 10^{-7} M	$K_d \approx 10^{-10}$ – 10^{-7} M
Specificity	High	High
Stability	Can re-naturate after heat treatment; long-term storage is possible	Irreversible denaturation after heat treatment; higher sensitivity to storing conditions
Immunogenicity	Not shown	High
Possibility of chemical modification	Wide	Limited

tween the individual aptamers is then analyzed. On the basis of the results obtained, the aptamers are classified into several groups; their capability to interact with the target is assessed. The sequences with the maximum affinity to the target are selected for further studies. The secondary structure of aptamers is studied by analyzing their conserved motifs, by computer simulation, and chemical and enzymatic probing. The minimal size of an aptamer required for specific recognition of a target is determined at the next stage. For this purpose, a series of truncated variants of the aptamer is synthesized and the ability of these aptamers to bind to the target is determined.

Aptamers are usually characterized by high affinity to their targets. The characteristic values of the dissociation constant (K_d) for protein targets lie in the nanomolar and subnanomolar ranges (1×10^{-10} – 1×10^{-7} M). In terms of their affinity and specificity, aptamers are similar to monoclonal antibodies; however, aptamers have a number of distinct characteristics (*Table 1*). Among these characteristics, the possibilities to produce an aptamer via chemical synthesis and to modify them chemically are the ones most worthy of note.

Chemical modifications of aptamers

The introduction of different modifications into escort aptamers enables one to considerably increase their stability in biological media, as well as their functionality. The introduction of different substituents at the 2' position of ribose (*Fig. 2*) (the most common modification used to increase an aptamer's stability) helps to prevent the cleavage of aptamers by endonucleases. This type of modification is typically used to protect escort RNA

aptamers, whereas escort DNA aptamers are more frequently used without any additional modifications. The major pathway of degradation of RNA aptamers in biological media is cleavage by pyrimidine endoribonucleases; therefore, as early as at the stage of construction of combinatorial RNA libraries for selecting escort aptamers, the pyrimidine nucleosides within them are substituted for their 2'-fluoro- and 2'-amino analogues by using the corresponding modified nucleoside triphosphates for synthesizing a library. It is possible to use T7 RNA polymerase [13] or its mutant version (capable of inserting these 2'-modified nucleoside triphosphates into RNA with higher efficiency) to integrate them into a growing RNA strand [14]. There is also mutant RNA polymerase inserting 2'-O-methyl analogues of nucleoside triphosphates [15, 16]; however, due to the problems associated with the reaction of reverse transcription of 2'-O-methyl-containing RNAs, the use of 2'-O-methyl-RNA libraries directly during the selection process has not yet become common practice [4].

In order to obtain 2'-O-methyl-containing aptamers, a quantity of ribonucleotides within a RNA aptamer are substituted for their 2'-O-methyl analogues, after the aptamers have been selected and their nucleotide sequences determined. The introduction of 2'-O,4'-C-methylene-linked bicyclic nucleotides (LNA – locked nucleic acids) is another way of increasing the stability of aptamers of a known sequence. This modification is used both in RNA [17] and DNA aptamers [18]. A number of nucleotides can be substituted for a flexible linker based on ethylene glycol for the purpose of minimizing the aptamer's length and simultaneously increasing its resistance to endonucleases [18, 19]. Cap-

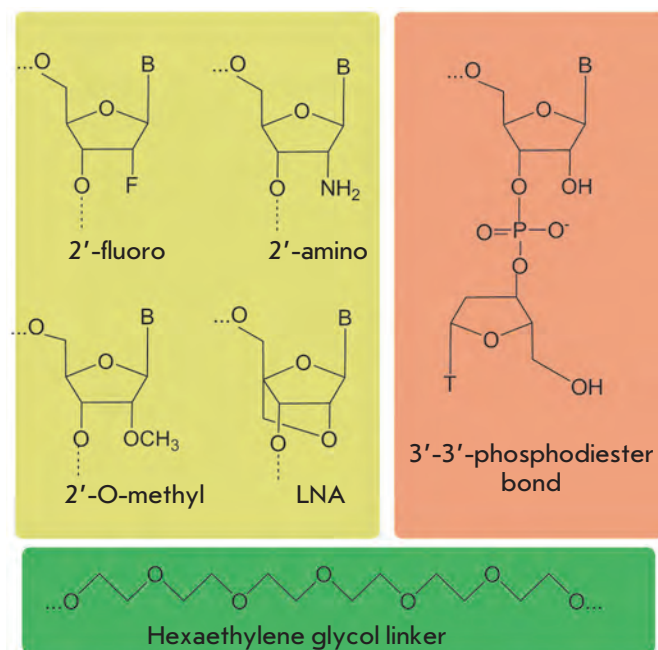


Fig. 2. Chemical modifications of sugar-phosphate backbone increasing the resistance of escort aptamers in biological media.

ping of the 3'-terminus with an additional thymidine residue linked via the 3'-3'-phosphodiester bond is used to prevent the cleavage of aptamers [17, 19].

Researchers either use the modified nucleoside triphosphates or modify the “ready-made” aptamers in order to introduce additional functional groups into an aptamer during the selection (see Review [4]). In the case of escort aptamers, the introduction of an aliphatic amino or sulfhydryl group to the 5'- or 3'-terminus of an aptamer is the most common. It allows one to synthesize the various conjugates of aptamers with toxins, antibiotics, fluorescent or photoreactive groups, nanoparticles, etc. (see Section Application of escort aptamers).

It must be kept in mind that the introduction of modifications into a “ready-made” aptamer may result in considerable changes in its molecular conformation, as well as a decrease in the aptamer’s affinity to its target. Therefore, in each case one must thoroughly select the type and position of these modifications. In addition, one must study the effect they have on the aptamer’s affinity to its target.

OBTAINMENT OF ESCORT APTAMERS

When selecting escort aptamers *in vitro*, the individual proteins from the cell surface or whole cells are used as targets. The use of cells as targets has a number of advantages over using purified proteins:

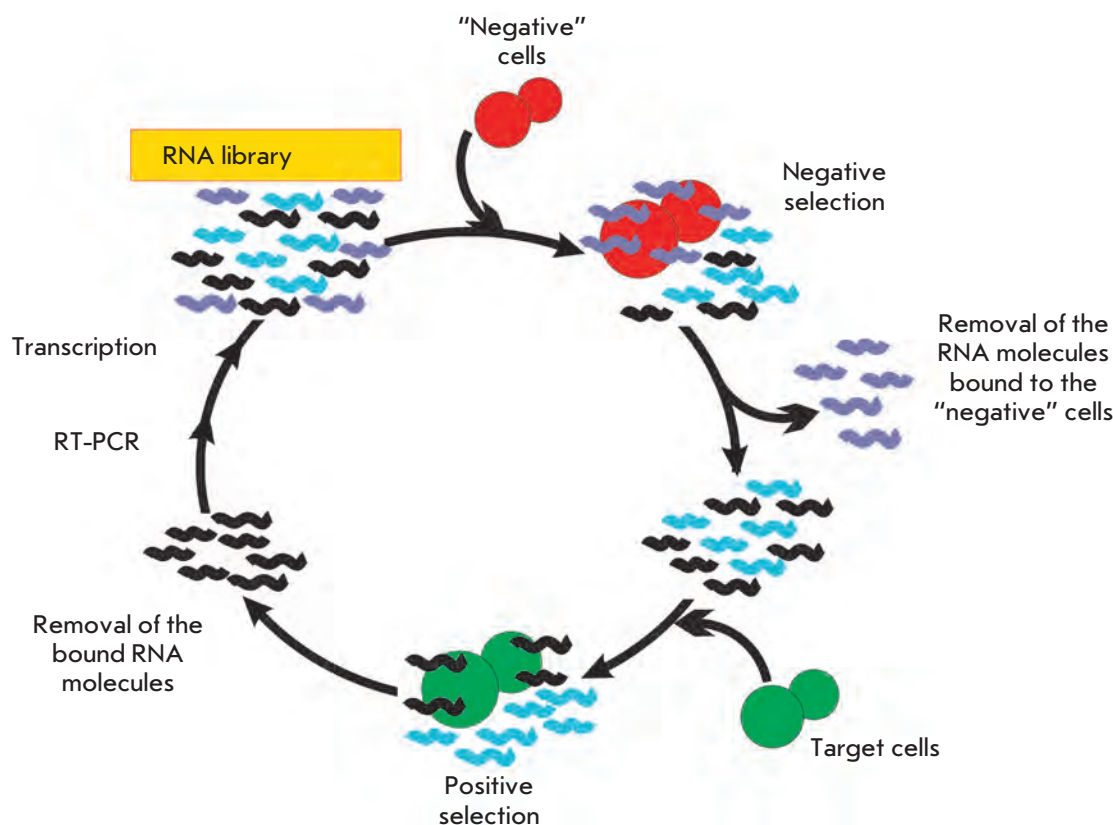
- No need for producing a pure protein to act as a target;
- The obtained aptamers possess high affinity to the target cells;
- The selection can be performed for the entire cell, even if a particular surface target protein is not known *a priori*; and
- The possibility to identify new, previously unknown specific markers on the cell surface emerges.

The protocol for cell selection of escort aptamers has specific features. The high number of surface dominants, which can either be unique for a definite cell type or be common to cells of various types, is one of the key problems that arise when using cells as targets. In order to eliminate the nonspecific aptamers binding to the molecular targets that are common to many cell types from the selection, an additional stage of counter-selection, or negative selection, is added to SELEX. Thus, to select aptamers that can bind to a certain protein on the cell surface, two cell lines are used: one of these cell lines (target cells) expresses the desired protein, whereas the second cell line (control “negative” cells) is represented by cells of the same type that do not express this protein. Sequential incubation of the nucleic acid library with the control cells and target cells enables one to select particular sequences that bind only to the desired protein on the cell surface.

The general scheme of cell selection of escort aptamers (by the example of an RNA library) is provided in Fig. 3. The initial oligonucleotide library is incubated with control cells, and the unbound molecules are isolated. They are then incubated with the target cells, and the unbound molecules are isolated again. After the cells have been disintegrated, the bound aptamers are extracted, amplified, and subsequently used in the next round of selection.

The usage of cells as targets for *in vitro* selection was first described by K. Morris *et al.* [20]. DNA aptamers recognizing ghosts of human erythrocytes (haemoglobin-free cells that retain the same shape of the membrane as native erythrocytes) were obtained in that study. In order to produce aptamers, the ssDNA library was incubated with target cells. Then, the bound sequences were isolated via filtration through nitrocellulose filters. The resulting set of DNA molecules was amplified and used in the subsequent round of selection. After 25 selection rounds, two aptamer motifs comprised 25% of the total number of clones. Photoactivatable phenyl azide groups introduced into these two aptamers were used to demonstrate that they bind to the cell surface of various molecular targets. The study was the first example of using combinatorial libraries of nucleic acids for the selection of aptamers targeted at such complex objects as the cell membrane.

Fig. 3. The scheme of *in vitro* cell selection (including the negative selection stage) by the example of the RNA library.



Aptamers recognizing malignant cells

The overwhelming majority of studies devoted to the selection of aptamers targeting living cells have focused on the search for sequences that can specifically bind to malignant cells. To this end, S. Lupold *et al.* [21] described the obtainment of 2'-F-modified RNA aptamers capable of binding to prostate-specific membrane antigen (PSMA). This protein is located on the cell membrane's surface and is the marker of tumor cells of the prostate gland. The cells of healthy tissues are characterized by a very low level of PSMA, which considerably increases with the development of malignant tumors. A recombinant protein corresponding to the extracellular domain of PSMA, rather than whole tumor cells, was used as a target. After six rounds of selection, two RNA sequences (**A9** and **A10**) comprised 95% of the enriched library. A 56-nt aptamer **A10-3** was obtained via minimization of the length of the **A10** aptamer; an additional thymidine residue was linked to the 3'-terminus of **A10-3** via a 3'-3'-phosphodiester bond for the purpose of protection from exonucleases. This aptamer was shown to specifically bind to PSMA-expressing LNCaP cells, and not to bind to PC-3 prostate cancer cells, which do not express this protein.

C. Ferreira *et al.* [22–24] also described the use of the fragments of individual surface proteins in studies de-

voted to the selection of DNA aptamers against the tumor marker surface glycoprotein mucin (MUC1). Mucin hyperexpression is typical of cancer cells. Immunogenic synthetic peptides (mucin fragments immobilized on a column with functionalized sepharose) were used as targets for the selection. After 10 rounds of selection, 12 aptameric sequences were obtained, one of which (aptamer **S1.3/S2.2**) was capable of binding to mucin-producing tumor cells [23]. The same method was used to produce an additional four DNA aptamers, although recombinant mucin was used as a target [22]. The third variant selected against the mucin mimetic compound, O-glycosylated peptide, proved to be the most successful [24]. The DNA aptamer **5TRG2**, which was obtained via this method, is characterized by the highest affinity to the target peptide ($K_d = 18.6$ nM) and is capable of not only selective binding to mucin on the cell surface, but also of penetrating into the cells via receptor-mediated endocytosis.

It is noteworthy that the selection against whole cells is considered to be the most reliable and efficient method for aptamer production. Thus, D. Daniels *et al.* [25] described the selection of DNA aptamers capable of binding to the surface of glioblastoma U251 cells. After 21 selection rounds, the resulting **GBI-10** aptamer, together with its homologues, comprised ap-

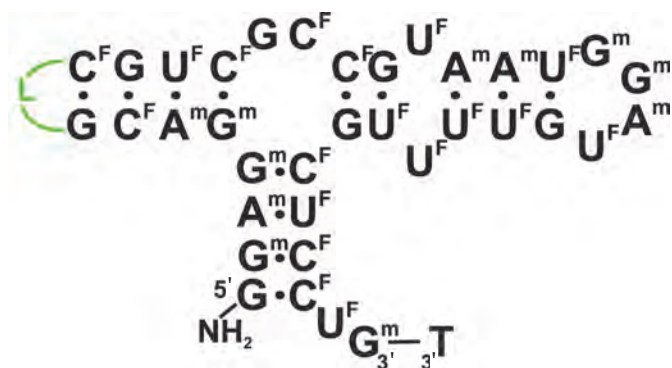


Fig. 4. The proposed secondary structure of the modified **TTA1** aptamer binding to tenascin C [19]. Designations: N^F – 2'-fluoro-2'-deoxyribonucleotide, N^m – 2'-O-methyl-ribonucleotide, NH₂ – aminohexanol residue, L – hexaethylene glycol phosphate linker.

proximately 10% of the entire quantity of the selected sequences. It was ascertained via affinity purification of the cell extract using the **GBI-10** aptamer immobilized on magnetic particles that this aptamer is targeted against tenascin C (TN-C), the protein located mostly in the extracellular matrix. Hyperexpression of this protein is typical of a wide range of tumors. Selection was carried out at 4°C in order to prevent the penetration of aptamers inside the cells and to reduce the degree of aptamer degradation. The apparent dissociation constant of the aptamer–tenascin C complex was equal to 150 nM under the said conditions, whereas the K_d value increased by an order of magnitude as the temperature rose from 4 to 37°C.

The considerably more stable complexes of 2'-F-RNA aptamers against tenascin C were obtained using three *in vitro* simultaneous selection protocols. In the first and second cases, a recombinant protein and glioblastoma U251 cells, respectively, were used as targets. In the third case, cross-selection was performed, which comprised two additional selection rounds with respect to the TN-C protein following the 9 rounds of selection with respect to glioblastoma cells [19]. All pyrimidine nucleosides within the RNA library were replaced by their 2'-F-analogues, in order to enhance their stability in biological media. The aptamers selected via all three methods had an appreciably high affinity to TN-C ($K_d = 1-10$ nM). The aptamers obtained by selection against the individual protein and the aptamers obtained by selection against the cells contained similar sequences. The 55-nt aptamer **TN-9** was truncated by 16 nucleotides; it also underwent several additional chemical modifications. Namely, several nucleotides were substituted for a hexaethylene glycol linker; most purine residues were substituted for their 2'-O-methyl

analogues; the 3'-terminus was capped with a thymidine residue linked via a 3'-3'-phosphodiester bond; and amino groups were added to the 5'-terminus to produce bioconjugates. The resulting modified **TTA1** aptamer (Fig. 4) retained a high level of affinity to the target protein ($K_d = 5$ nM) and was characterized by high biological stability.

W. Tan *et al.* obtained DNA aptamers capable of binding to T-cell leukaemia CCRF-CEM cells [26]. Burkitt lymphoma B-cells (the so-called 'Ramos cells') were used as controls at the counter-selection stage. The resulting, highly affine aptamers were capable of not only selective binding to the CCRF-CEM target cells, but also of recognizing these cells in a mixture containing other cancer cell lines and cells from the medullary fluid of healthy individuals [27]. It turned out that the 88-nt **sgc8** aptamer with the highest affinity to the target cells ($K_d = 0.8$ nM) binds to protein tyrosine kinase 7 (PTK7) on its surface [28]. PTK7 participates in signal transduction during the development and metastatic spread of malignant tumors. Moreover, the **sgc8** aptamer is capable of penetrating into CCRF-CEM cells, where it localizes in endosomes [29]. The **C8FL** aptamer containing 33 nucleotides and a linker and possessing exceptional stability to serum nucleases and high affinity to target cells ($K_d = 1.53$ nM) was obtained via minimization of the nucleotide sequence of the **sgc8** aptamer and the introduction of chemical modifications into its structure (Fig. 5) [18].

In 2009, A. Ellington *et al.* [30] studied the specificity of the binding of a number of cell aptamers. In particular, they demonstrated that aptamers targeted at CCRF-CEM cells were capable of recognizing other types of malignant cells, which are typically capable of forming a monolayer. The authors assumed that

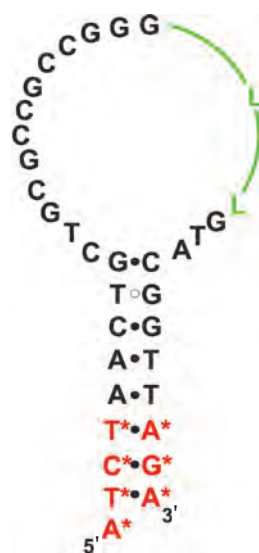


Fig. 5. The proposed secondary structure of the modified **C8FL** aptamer against CCRF-CEM cells [18]. Designations: L – hexaethylene glycol phosphate, N^{*} – LNA nucleotides.

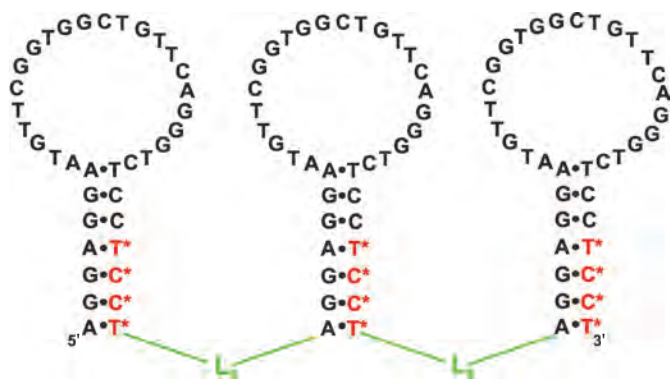


Fig. 6. The proposed secondary structure of the trimer formed by the modified **TD05.17** aptamer against Ramos cells [33]. Designations: **L** – hexaethylene glycol phosphate, **N*** – LNA nucleotides.

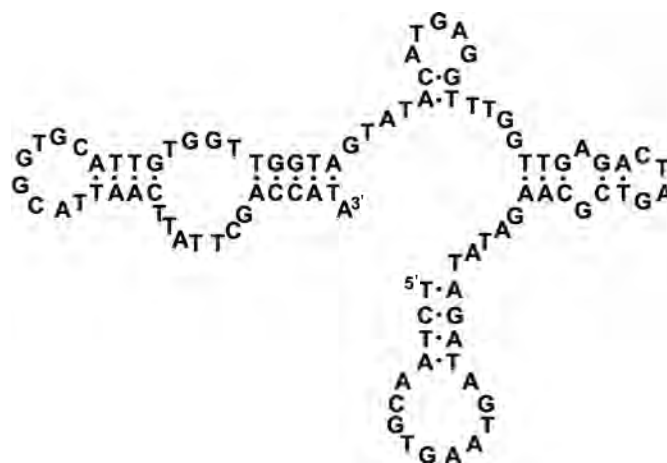


Fig. 7. The proposed secondary structure of DNA aptamer **III.1** against microvessels of rat brain tumor [37].

the aptamers obtained in the studies conducted by W. Tan *et al.* [26–29] could specifically recognize not a definite type of leukaemia cells, but cells capable of adhesion. The following arguments are given to support this assumption: 1) protein tyrosine kinase 7 participates in cell adhesion, 2) the CCRF-CEM cells capable of monolayer formation were used as targets during the selection, whilst the Ramos cells, which do not form a monolayer, were used as a negative control. In other words, it was possible to select aptamers against the cells capable of adhesion. However, it should be noted that it was the homologous **sga16** aptamer, and not the **sgc8** aptamer, that was used in the experiments described above. The affinity of the **sga16** aptamer to the target cells is lower than that of **sgc8** by an order of magnitude. Hence, one cannot unequivocally claim that all the aptamers obtained by W. Tan *et al.* [26–29] are nonspecific to CCRF-CEM cells.

W. Tan *et al.* [31, 32] used Ramos cells not only as control cells, but also as selection targets; in the latter case, the SELEX cycle did not comprise the counter-selection stage [31]. It was demonstrated that the immunoglobulin M heavy chain bound to the membrane acted as a molecular target for aptamers on the surface of Ramos cells [32]. The tendencies of these aptamers to bind to the target cells only at low temperatures (the selection was carried out at 4°C) and their potential to bind not only to the cell surface of IgM, but also to the soluble IgM in blood plasma were their significant drawbacks. To solve this problem, the minimization of the structure of **TD05** aptamer (truncation of the nucleotide sequence from 48 to 37 nucleotides), combined with the substitution of four deoxyribonucleotides at the 3'-terminus for their LNA analogues, was performed [33]. The truncated modified aptamers **TD05.17**

were then used to design tri- and tetrameric constructs in which the aptameric sequences were linked by non-nucleotide polyethylene glycol insertions (e.g., see *Fig. 6*). The resulting multimers were specifically bound to Ramos cells at 37°C ($K_d = 256$ nM for the trimer and 272 nM for the tetramer); they recognized heavy IgM chains and did not interact with soluble IgM.

W. Tan *et al.* also obtained DNA aptamers capable of distinguishing between two closely related acute myeloid leukaemia cell lines [34], between small-cell and nonsmall-cell lung cancer cells [35], and between hepatic cancer cells and normal hepatocytes [36].

M. Blank *et al.* [37] obtained DNA aptamers which can selectively recognize brain tumor micro-vessels in rats and do not bind to healthy vessels. During the study, the DNA library was first incubated with the control cells represented by N9 microglial cells (brain monocytes), followed by incubation with the target cells represented by rat YPEN-1 immortalized endothelial cells transformed with the SV40 hybrid virus. Following the *in vitro* selection, the specificity of the binding of the target and control cells to each clone was determined and the histochemical staining of tumor vessels was performed. It turned out that the endothelial protein pigpen, whose synthesis increases in migrating and actively dividing endothelial cells, is the molecular target for the most active **III.1** aptamer (*Fig. 7*). The authors believe that this protein can be considered both as a new diagnostic angiogenesis marker and as a potential molecular target to block tumor angiogenesis.

In 2011, E. Zueva *et al.* published a study [38] devoted to the search for aptamers capable of distinguishing between highly mobile metastatic cells and malignant cells with low mobility. Two lines of transformed Syrian hamster fibroblasts (the control line with low

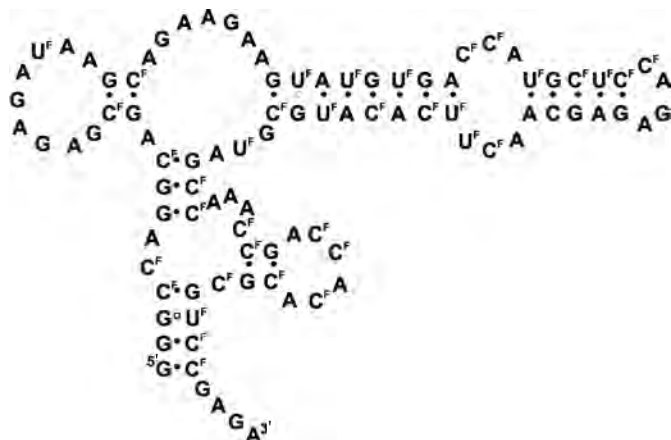


Fig. 8. The proposed secondary structure of RNA aptamer **A07** against the human transforming growth factor receptor [44]. Designations: N^F – 2'-fluoro-2'-deoxyribonucleotide.

mobility and the target cells with high mobility) were used to select 2'-F-containing RNA aptamers. Aptamers **E10** and **E37** were capable of binding to metastatic cells with high affinity and selectivity (K_d values were 37 and 50 nM, respectively), and they were capable of suppressing cell migration at a concentration of 100 nM. The **E10** aptamer was also capable of suppressing cell invasion.

J. Mi *et al.* [39] described the selection of aptamers against colorectal cancer cells with metastasis to the liver. It is noteworthy that model animals, rather than a cell culture, were used for the selection: a 2'-F-containing RNA library was intravenously injected into mice with a previously grafted liver tumor, followed by the extraction of the bound 2'-F-RNA from the liver. After it was intravenously injected to mice, the **14-16** aptamer was selectively bound to intraliver tumors. This aptamer was capable of penetrating into tumor cells and binding with helicase p68 in the nucleus and cytoplasm (hyper-expression of helicase p68 being typical of colorectal cancer). Thus far, this study is the only example of aptamer selection using multicellular organisms.

Aptamers binding to the surface receptors of cells

Cell receptors are considered to be an attractive therapeutic target. They can be neutralized by the action of aptamers blocking ligand-induced activation. Designing aptamers capable of specific blockade of certain receptors and the subsequent “switching-off” of the corresponding signal pathways provides the opportunity both to study the molecular mechanisms of their function and to investigate the diagnostics and therapy of different diseases. Several research groups have managed to obtain aptamers capable of binding to cell receptors.

Recombinant proteins corresponding to the extracellular domains of receptors have been used as targets to obtain receptor-recognizing aptamers. The method was used to obtain 2'-fluoro-containing RNA aptamers capable of recognizing rat CD4 receptors [40], human CD4 receptors [41], and mouse CTLA-4 receptors [42]. C. Chen *et al.* [43] described the production of aptamers against the mouse transferrin receptor. Fluorescently labelled RNA and DNA aptamers conjugated to streptavidin were used to demonstrate the ability of aptamers to penetrate into cells via endocytosis. Meanwhile, aptamer binding to the transferrin receptor had no effect on the interaction between this receptor and transferrin, since these aptamers can be used for the delivery of therapeutics without blocking the functions of the receptor necessary for the vital activity of the cells.

Using the cell-SELEX method with a counter-selection stage, 2'-F-containing RNA aptamers against the human transforming growth factor β (TGF- β) receptor type III (TbRIII)(expressed on the surface of Chinese hamster ovary (CHO) cells) were selected [44]. In the study, parent CHO cells that do not express this protein were used at the negative selection stage. The **A07** aptamer (*Fig. 8*) that is capable of selective binding to the receptor TbRIII and forms with it a stable complex ($K_d = 2.47$ nM) was obtained via selection. This aptamer was also shown to be capable of inhibiting association between the receptor TbRIII and its ligand, TGF- β_2 .

L. Cerchia *et al.* [45] described the selection of 2'-F-RNA aptamers that bind to the mutant dimeric form of the human receptor tyrosine kinase RET^{C634Y}, which is typically present upon multiple endocrine neoplasia type 2. During the selection, the library was incubated with cells expressing the mutant form of receptor RET^{C634Y} (PC12/MEN2A). At the counter-selection stage, the oligonucleotide library was incubated with two types of control cells, the “parent” cells PC12 that did not express the target protein and the PC12/MEN2B cells that had a morphology similar to that of PC12/MEN2A but expressed the monomeric form of receptor tyrosine kinase RET^{M918T}. The **D4** and **D24** aptamers obtained after 15 selection rounds were capable of efficiently binding to the target cells ($K_d = 40$ nM) and suppressing the activity of RET by 70% at a concentration of 200 nM. It should be noted that the **D4** aptamer was also capable of binding to PC12/MEN2B cells, although the degree of binding was considerably lower (by a factor of approximately 2.5 as compared with that of the target cells PC12/MEN2A).

Unfortunately, the use of cross-selection to obtain aptamers against the receptor RET^{C634Y} (seven rounds of selection for PC12/MEN2A cells and four rounds of selection for the purified recombinant protein [46])

failed to yield better results. The obtained **E38** aptamer had a considerably different structure in comparison with that of the aptamers against the target cells and was characterized by lower affinity to PC12/MEN2A cells ($K_d = 100$ nM). It was also incapable of inhibiting the activity of the receptor tyrosine kinase.

Aptamers capable of recognizing undifferentiated cells

The production of aptamers that can bind to undifferentiated cells is challenging. C. Wang *et al.* [47] selected DNA aptamers capable of distinguishing between differentiated PC12 cells and the undifferentiated “parent” cells that were used as the control cells at the counter-selection stage. Six selection rounds were sufficient to obtain aptamers that were capable of recognizing the differentiated cells and did not bind to the undifferentiated cells. Aptamers against undifferentiated cells types, e.g., against stem cells, can be used for cell isolation and purification in regenerative medicine, which is a rapidly developing field of medicine. The studies conducted by K. Guo *et al.* [48, 49] were devoted to the creation of DNA aptamers for cell isolation and immobilization. In particular, DNA aptamers capable of binding to mature mesenchymal stem cells were obtained [49]. After 12 selection rounds without counter-selection, aptamers capable of selectively recognizing the target cells, among other medullary cells, were obtained; the possibility of using them to isolate stem cells from bone marrow was demonstrated. J. Hoffmann *et al.* [50] produced DNA aptamers capable of binding to the precursors of porcine endothelial cells, which were subsequently used to immobilize the cells on the surface of polytetrafluoroethylene or polydimethylsiloxane disks (see Section Application of escort aptamers).

Identification of new biomarkers via the cell selection of aptamers

The *in vitro* selection of aptamers using living cells enables to identify new biomarkers typical for cells of a definite type, after the aptamers have been selected and the surface proteins binding to these aptamers have been revealed. Existing methods for searching for biomarkers (Western blotting, screening of mRNAs using quantitative PCR or chips, 2D electrophoresis coupled with mass spectroscopy) are not sufficiently efficient; their common drawback being the possibility of false positive and false negative results, which often occurs. The general strategy for the search for biomarkers using aptamers (AptaBiD, Aptamer-facilitated Biomarker Discovery) formulated by M.V. Berzovski *et al.* [51] enables to overcome these difficulties. The probability of obtaining false positive results

decreases through multiple selection rounds, which eliminate the impact of such random factors as the stochastic differences between cells of the same type and unintended variations at all stages of cell treatment. Meanwhile, the exponential enrichment of the library during the selection allows to reveal even insignificant distinctions between the control cells and the target cells, if they are retained from round to round. This reduces the probability of obtaining false negative results. To confirm the high potential of the AptaBiD strategy, it was used to search for biomarkers determining the differences between mature and immature dendritic cells. As a result, both previously known biomarkers of dendritic cells and six new biomarkers of immature dendritic cells were revealed. A significant feature of this method worth noting is that it does not involve the cloning and sequencing stages; the enriched libraries, rather than individual aptamers, are used for the search for biomarkers. Thus, the process becomes both quicker and cheaper.

Aptamers recognizing the surface proteins of microorganisms

In addition to cultured cells, pathogenic microorganisms can also be used as targets for cell selection. The aptamers obtained via this method can be subsequently used in the diagnostics and therapy of infectious diseases, as well as for the quantitative determination of microorganisms.

M. Homann and H. Göringer [52] obtained RNA aptamers capable of binding to the living trypanosomes *Trypanosoma brucei*, parasitic protozoans causing the sleeping sickness. Two *Tr. brucei* strains were used as targets for the selection. The RNA library was incubated with parasitic organisms that were present at the bloodstream stage; the unbound molecules were removed via centrifugation. The resulting aptamers were capable of binding to the organisms of both strains at the bloodstream stage ($K_d = 60$ nM), whilst being incapable of recognizing *Tr. brucei* at other stages of development. The methods of photoaffinity modification and fluorescent microscopy with the fluorescent-labelled aptamer **2-16** were used to ascertain that the protein with a molecular weight of 42 kDa located in the trypanosome flagellar pocket acts as a target for this aptamer. After binding to this protein, the aptamer penetrates into the trypanosome via receptor-mediated endocytosis and is subsequently located in endosomes. As shown by the example of the **2-16** aptamer conjugated with biotin, these aptamers can be used to deliver other substances into trypanosomes [53]. Pyrimidine nucleosides were replaced by their 2'-amino or 2'-fluoro analogues in order to increase the stability of the **2-16** aptamer in biological media. As a result

of the modification, the aptamer containing 2'-NH₂ groups lost its ability to bind to trypanosomes; in contrast, the 2'-F-modified aptamer retained its affinity to these organisms ($K_d = 70$ nM) and was characterized by high resistance to serum nucleases [54]. The use of modified RNA libraries containing 2'-fluoro or 2'-amino pyrimidine nucleotides during the selection was more successful. Living trypanosomes were used as targets when selecting 2'-amino-containing RNA aptamers. The resulting aptamer possessed affinity to trypanosomes, being virtually equal to that of the **2-16** aptamer ($K_d = 70$ nM), and bound to these organisms within the limited area around the flagellum [55]. Selection against the purified surface protein sVSG was used to obtain 2'-F-containing RNA aptamers capable of binding to the entire trypanosome surface [56, 57].

2'-F-RNA aptamers against another type of trypanosomes (*Tr. cruzi*, the agent of Chagas disease) were also obtained [58]. At the trypomastigote stage, *Tr. cruzi* bind to the host cells and penetrate into them through interaction with the extracellular matrix proteins of the host cells. 2'-F-pyrimidine-containing RNA aptamers at a concentration of 1 μM blocked the penetration of these parasitic organisms into the cells by 50–80%.

Aptamers capable of binding to different types of bacteria generate significant interest. Thus, the selection of DNA aptamers with respect to the causative agent of tuberculosis *Mycobacterium tuberculosis* was performed [59]. A single introduction of 0.8 μg of the resulting **NK2** aptamer resulted in a decrease in the numbers of microbacteria in tuberculosis-infected mice, alleviated disease presentations, and also increased the lifetime [59]. The potential use of the **NK2** aptamer in tuberculosis therapy is assumed. Aptamers capable of specific binding to the spore surface of the causative agent of anthrax *Bacillus anthracis* [60] and crystal-forming bacteria *B. thuringiensis* [61], salmonellae *Salmonella enterica* [62] and *S. typhi* [63], staphylococci *Staphylococcus aureus* [64], lactic acid bacteria *Lactobacillus acidophilus* [65], *Escherichia coli* [66, 67], and *Campylobacter jejuni* bacteria [68] have also been obtained.

Escort aptamers capable of binding to “foreign” proteins located on the surface of infected cells should be considered separately. A. Barfod *et al.* [69] obtained aptamers against the PfEMP1 protein, which is expressed on the surface of erythrocytes infected with the malaria parasite *Plasmodium falciparum*. This protein facilitates erythrocyte aggregation (formation of the so-called ‘rosettes’) and adhesion of the infected erythrocytes to the walls of minute blood vessels. The recombinant DBL1α protein (the semi-conserved N-terminal domain of the PfEMP1 protein responsible for rosettes formation) was used as a target for the se-

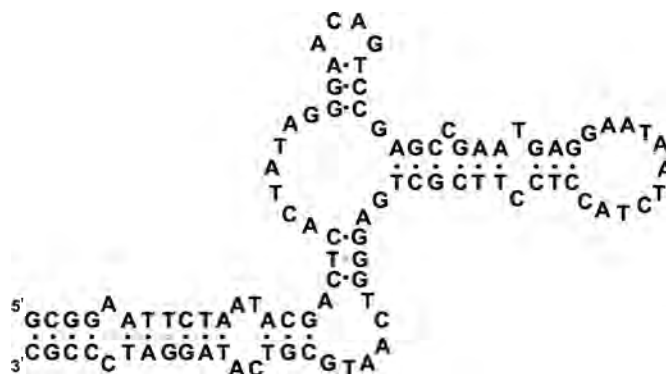


Fig. 9. The proposed secondary structure of DNA aptamer **ZE2** against the hepatitis C virus coat protein [70].

lection of 2'-F-pyrimidine-containing RNA aptamers. The resulting aptamers at a concentration of 387 nM (12 μg/ml) caused the almost complete disintegration of rosettes in a cell culture, which allows one to view them as potential anti-malaria agents.

2'-F-RNA aptamers against gp120, the human immunodeficiency virus type 1 (HIV-1) coat protein, were obtained by selection with respect to the recombinant protein; these aptamers were capable of binding to gp120 on the surface of the infected cells (see Review [7]).

F. Chen *et al.* [70] described a procedure for obtaining DNA aptamers against the E2 protein expressed on the cell surface (the hepatitis C virus coat protein). The same cell line incapable of expressing this protein was used for counter-selection. Among the resulting series of aptamers, the **ZE2** aptamer possessed the highest affinity to the surface protein ($K_d = 1$ nM) (Fig. 9). At a concentration of 100 nM, this aptamer was both capable of binding to viral particles, as well as blocking their fusion with cells. These results enable one to assume that the **ZE2** aptamer can potentially be used both for the diagnostics of hepatitis C and for the treatment of patients suffering from this disease, as well as for studying the virus-cell interactions.

The following section describes the design of systems centred on the cell delivery of therapeutic agents, diagnosing various diseases, and determining the pathogenic microorganisms in the environment and food products based on escort aptamers.

APPLICATION OF ESCORT APTAMERS

Numerous multifunctional constructs have been designed on the basis of escort aptamers, where an aptamer acts as a directing component ensuring the specific recognition of cells or target tissues. The aptamers that

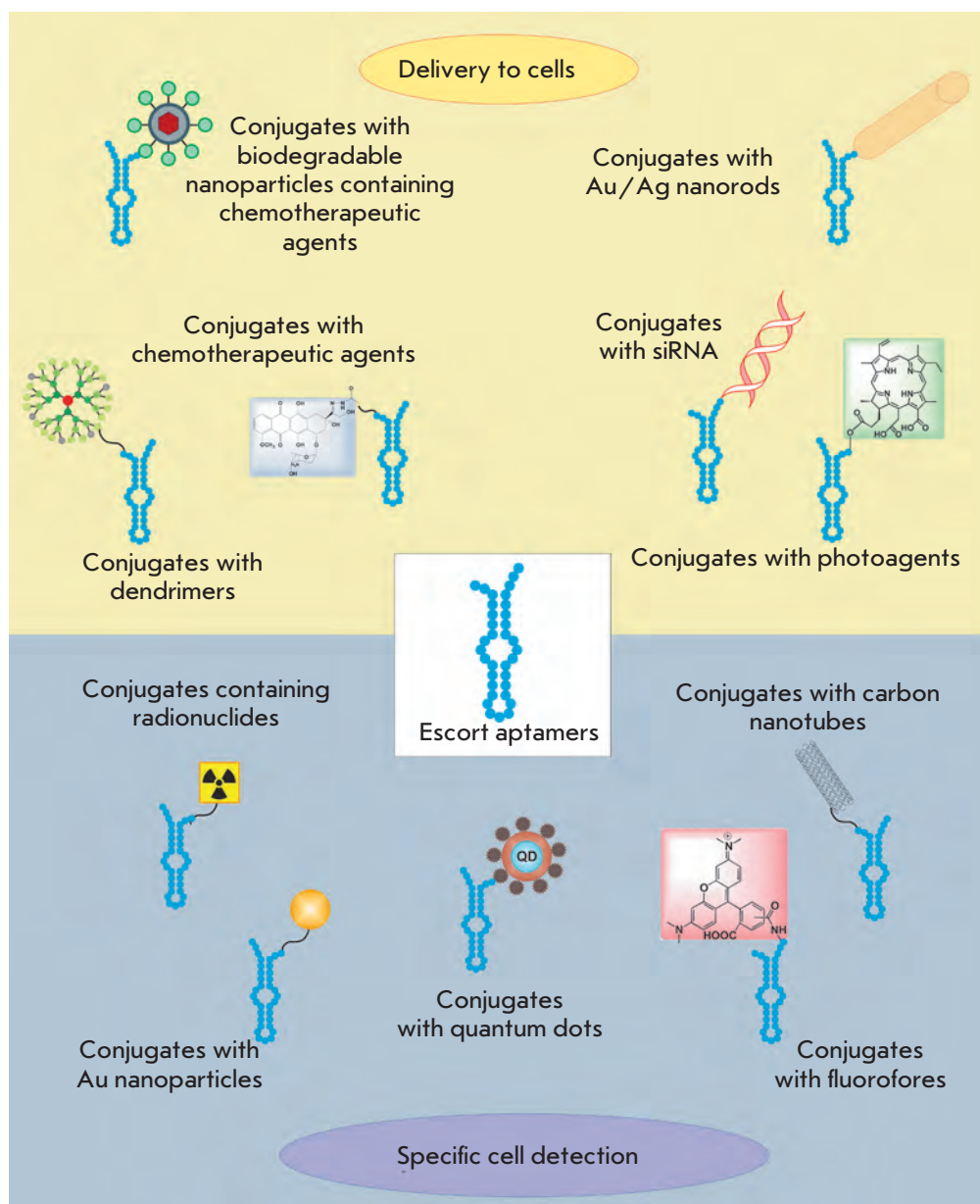


Fig. 10. The main types of conjugates of escort aptamers used for targeted cell delivery and specific cell detection.

are capable of penetrating into cells via receptor-mediated endocytosis after they bind to the surface proteins can be used as a platform to design highly specific therapeutic agents that can impose targeted action on cells of a definite type. Another actively developing direction in the application of escort aptamers is their use in the design of a highly precise diagnostic system enabling the detection of target cells, among other cells, in the organism. The schematic presentation of the major types of conjugated escort aptamers that are currently being used to deliver therapeutic agents to cells and perform specific cell detection is provided in *Fig. 10*. The data on the application of escort aptamers are briefly summarized in *Table 2*.

The use of escort aptamers to deliver various therapeutic agents to cells

The anti-PSMA-aptamers **A9** and **A10**, which bind to the prostate-specific membrane antigen, are among the most popular candidates for the design of a delivery systems [20]. PSMA is capable of penetrating into cells via clathrin-mediated internalization [97]; hyper-expression of this protein is a characteristic feature of many tumors. It was a combination of these factors that led to the significant interest pertaining to the use of anti-PSMA-aptamers as an addressing fragment in the delivery of various anti-tumor agents into cells. Thus, the conjugation of anti-PSMA-aptamer A9 with the protein toxin gelonin resulted in a ~180-fold increase

Table 2. Escort aptamers and their use for the delivery of various therapeutics into cells and for specific cell detection

Aptamer	Target	Selection method	Application
2'-F-RNA	Prostate-specific membrane antigen (PSMA)	Selection against recombinant protein – extracellular domain of PSMA [21]	Delivering gelonin [71] and doxorubicin [72] into LNCaP tumor cells. Delivering siRNA into LNCaP cells [74–77]. Delivering nanoparticles containing antitumor therapeutic docetaxel into LNCaP cells [82–84]. Imaging of LNCaP cells using aptamer-conjugated gold nanoparticles [92] or aptamer-conjugated luminescent CdSe–CdTe crystals [90]. Electrochemical detection of prostate cancer cells using an aptamer immobilized on an Au-electrode [91]. Detection of PSMA on LNCaP cell surface via proximity ligation assay [96]
DNA	Protein tyrosine kinase 7 (PTK7)	Selection against the CCRF-CEM cells (the precursors of T-cell acute myeloid leukaemia cells) [26]	Delivering doxorubicin [73], Au/Ag nanorods [80, 81], and poly(amidoamine)-based dendrimers [87] into CCRG-CEM cells. Investigation of the distribution of PTK7 receptors over the cell surface using aptamer–fluorescein conjugates [93]. Reversible fluorescent labelling of CCRF-CEM cells using aptamer-conjugated quantum dots Qdot525 [94]
2'-F-RNA	Rat CD4 receptor	Selection against recombinant protein [40]	Delivering siRNA into cells [78]
2'-F-RNA	HIV-1 coat protein	Selection against recombinant protein gp120 [79]	Delivering siRNA into HIV-1-infected cells [7, 79]
DNA	Mucin (MUC1)	Selection against synthetic peptides (mucin fragments) [23, 24]	Photodynamic therapy using photoreactive conjugates of the aptamer and chlorine e6 [24]. Tumor imaging using radioactive isotopes (⁹⁹ Tc) [88]
DNA, RNA	Mouse transferrin receptor (TfR)	Selection against recombinant protein – extracellular domain of TfR	Delivering lysosomal enzymes into cells to treat lysosomal storage diseases [43]
2'-F-RNA	Tenascin C	Cross-selection using a recombinant protein and U251 cells [19]	Tumor imaging using radioactive isotopes (⁹⁹ Tc) [89]
DNA	Membrane-bound IgM heavy chain	Selection against Burkitt lymphoma B-cells (Ramos cells) [31]	Micelles for delivering various pharmaceuticals into cells [86]. Test strips based on TD05 and TE02 aptamers for the detection of Ramos cells in blood samples [95]
DNA	<i>B. thuringiensis</i> bacteria	Selection against <i>B. thuringiensis</i> spores	Detection of <i>B. thuringiensis</i> spores using aptamer-conjugated CdSe–ZnS quantum dots [61]
RNA	<i>E. coli</i> bacteria	Selection against <i>E. coli</i> DH5α strain [67]	Potentiometric detection of <i>E. coli</i> using aptamers-conjugated carbon nanotubes [67]. Detection of <i>E. coli</i> via quantitative RT-PCR of RNA aptamers bound to the bacteria [98]
RNA	<i>S. typhi</i> bacteria	Selection against the major protein of <i>S. typhi</i> microvilli [63]	Potentiometric detection of <i>S. typhi</i> using aptamer-conjugated carbon nanotubes [97]
DNA	Mesenchymal stem cells	Selection against porcine mesenchymal stem cells [49]	Isolation of stem cells from bone marrow using aptamers immobilized on magnetic particles; cell sorting using fluorescent aptamer conjugates [49]
DNA	Precursors of porcine endothelial cells	Selection against CD31-positive cells from porcine blood [50]	Immobilization, growth, and differentiation of the precursors of endothelial cells on the surface of disks with immobilized aptamers (a model of vascular implants) [50]

in cytotoxicity with respect to the target cells, in comparison with that for unbound gelonin ($IC_{50} = 27 \text{ nM}$ for the conjugate and $5 \text{ }\mu\text{M}$ for gelonin) [71]. Meanwhile, in the case of control cells incapable of expressing the PSMA protein, the cytotoxicity of the aptamer-gelonin conjugate was lower than that of the unbound gelonin ($IC_{50} = 15 \text{ }\mu\text{M}$), which attests to the fact that this conjugate is highly selective. V. Bagalkot *et al.* [72] used the **A10** anti-PSMA-aptamer to deliver doxorubicin into cells. The anthracycline antibiotic agent doxorubicin is used for the therapy of a wide range of diseases, such as leukaemia, malignant lymphomas, sarcomas, and cancers of various etiologies. However, the drawbacks include toxic side effects, in particular, cardiotoxicity. The ability of doxorubicin to intercalate between the base pairs of double-stranded nucleic acids was used to obtain the conjugates [72]. The intercalation of doxorubicin into a double-stranded fragment of the **A10** aptamer yielded non-covalent conjugates. The cytotoxicity of these conjugates with respect to LNCaP target cells was comparable to that of unbound doxorubicin of the same concentration ($IC_{50} = 5 \text{ }\mu\text{M}$). The cytotoxicity of conjugates with respect to PC3 control cells was significantly lower. The **sgc8c** escort aptamer (“truncated” variant of the **sgc8** aptamer) was used to deliver doxorubicin into human leukemic lymphoblasts (CCRF-CEM cells). Y. Huang *et al.* [73] obtained the doxorubicin-**sgc8c** aptamer conjugate, with doxorubicin bound to the 5'-terminus of the aptamer via an acid-labile hydrazone bond that was hydrolyzed after the conjugate had penetrated into the cell. It has been shown that these conjugates can selectively penetrate into CCRF-CEM cells via receptor-mediated endocytosis; their cytotoxicity with respect to CCRF-CEM cells being comparable to that of unbound doxorubicin ($IC_{50} = 0.3 \text{ }\mu\text{M}$). As opposed to unbound doxorubicin, the aptamer-doxorubicin conjugate showed no toxicity with respect to the control Ramos cells. Thus, binding of escort aptamers to chemotherapeutic agents makes it possible to reduce their toxic effects on tumor cells only. It can be anticipated that these conjugates will be used to design novel agents for anti-tumor chemotherapy with minimum adverse effects.

Escort aptamers were also used to deliver small interfering RNA (siRNA) into cells. Several types of constructs to deliver siRNA were designed on the basis of anti-PSMA-aptamers. The tetrameric biotin-streptavidin complex containing two biotinylated strands of the **A9** aptamer and two biotinylated siRNA molecules targeted against mRNAs of the lamin A/C or GADPH genes (*Fig. 11A*) was used to deliver siRNAs into PSMA-positive tumor cells [74]. These complexes could penetrate into cells without the use of transfectants. At a concentration of 22.5 nM, they suppressed

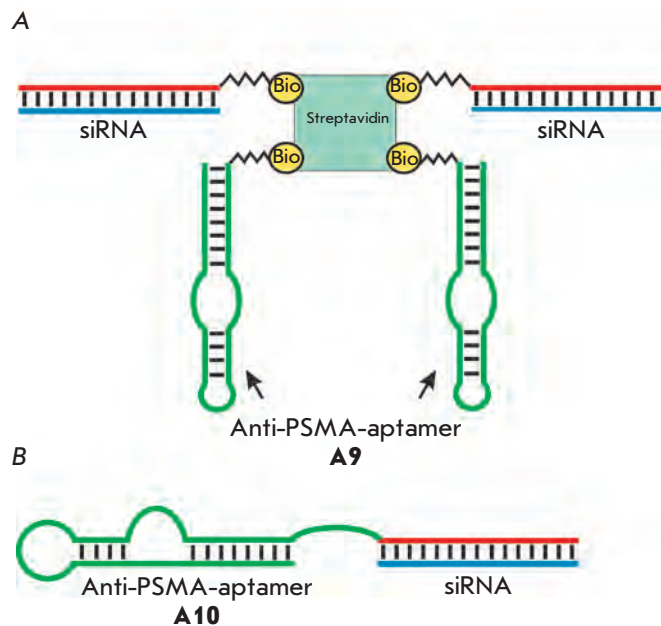


Fig. 11. Schematic representation of chimeric constructs for siRNA delivery into PSMA-positive cells. A. The conjugate of biotinylated anti-PSMA aptamer and siRNA connected via streptavidin [74]. B. Chimeric RNA built from an anti-PSMA aptamer and siRNA [75]. Bio – biotin residue.

target gene expression by 50–80%; the efficiency of the suppression was identical to that of the corresponding siRNAs delivered into cells using Oligofectamine. The chimeric constructs were designed which consisted of a joint nucleotide sequence containing the **A10** aptamer and one of the siRNA strands with the complementary second siRNA strand (*Fig. 11B*) [75]. At a concentration of 400 nM, these constructs can penetrate into PSMA-positive cells without transfectants and almost completely suppress the expression of the *bcl2* and *plk1* target genes. With the aim of optimizing the structure of chimeric constructs, the targeting aptamer was truncated from 71 down to 39 nucleotides, which simplified the chemical synthesis of both components of the construct. A number of modifications increasing the specificity and efficiency of the interaction with the mRNA target were introduced into the siRNA structure. A polyethylene glycol residue with a molecular weight of 20 kDa was bound to the siRNA passenger strand, which increased the half-circulation time of the chimeric constructs in mouse blood from 35 min to 30 h. The obtained preparation resulted in a considerable regression of the PSMA-positive tumor in mice after the injection of five 0.25 nmol doses [76].

Another variant of a chimeric construct containing two molecules of anti-PSMA-aptamer **A10-3** was

described in [77]. In this construct, one of the siRNA strands targeted against mRNA of the eukaryotic elongation factor 2 (eEF2) is inserted between two aptameric sequences, the second strand being complementary [77]. At a concentration of 2 μM , these conjugates caused suppression of the growth of the target cells by 95%, with no impact on the growth of PSMA-negative control cells.

An interesting construct containing the “addressing” aptamer and siRNAs was described in [78]. Phage $\phi 29$ RNA capable of multimeric complex formation via interaction between RNA loops was used to design these constructs. A phage RNA fragment was bound to each component of the construct, i.e., to the aptamer recognizing the CD4 receptor [40], to siRNAs targeted against the mRNAs of various apoptotic factors, and to the fluorescent dye. At a concentration of 100 nM, the resulting trimers containing an aptamer, siRNA, and a reporter group were able to penetrate into the CD4-positive cells and inhibit the expression of the target genes.

Chimeric constructs [7, 79] designed according to the principle proposed by J. McNamara *et al.* [75] and consisting of a 2'-F-RNA-aptamer recognizing the viral protein gp120 on the cell surface and siRNA targeted against the *Tat/Rev* of HIV-1 RNA were used to act upon HIV-1 infected cells. These constructs (at a concentration of 400 nM) have the ability to inhibit HIV-1 replication in a cell culture [79]. The use of these constructs to suppress HIV-1 replication in mice has also been reported [7].

The **sgc8c** aptamer conjugated with Au-Ag nanorods was used to impose photothermal action on leukaemia cells [80, 81]. The nanorods are heated to 50°C under laser irradiation, which results in cell death through thermal shock. Aptamers conjugated with nanorods (approximately 80 aptameric molecules were bound to a nanorod) were capable of selective penetration into the target cells; approximately 90% of the cells died after exposure to radiation [81].

Reactive agents for photodynamic therapy (aptamers covalently conjugated to chlorine e6) have been designed on the basis of aptamers capable of binding to the surface protein mucin [24]. These conjugates can selectively penetrate into mucin-expressing tumor cells and cause their death after exposure to radiation; the efficiency of the conjugates was 500-fold higher than that of unbound chlorine. Meanwhile, the conjugates showed no toxicity towards healthy cells.

The DNA aptamer against mouse transferrin receptor was used to deliver the lysosomal enzyme α -L-iduronidase into cells [43]. It was demonstrated that the aptamer-enzyme conjugates penetrated into mouse fibroblasts deficient in this enzyme and were further

transported to lysosomes, where the introduced enzyme was capable of both functioning and facilitating the recovery of the cell metabolism. The results obtained make aptamers against the transferrin receptor conjugated with lysosomal enzymes promising therapeutic agents for the treatment of diseases associated with the lysosomal function disorder.

Various carriers bound to the addressing aptamers are also used to ensure specific delivery of therapeutic agents. Thus, nanoparticles composed of the copolymer of lactic acid and glycolic acid (PLGA) with encapsulated docetaxel were covalently bound to the molecule of anti-PSMA-aptamer **A10** [82–84]. The resulting conjugate was capable of specific binding to LNCaP cells expressing the PSMA protein and penetrating into them [82, 85]. Mice with a grafted prostate tumor were used to demonstrate that anti-PSMA-aptamers conjugated with nanoparticles based on PLGA containing docetaxel can efficiently suppress tumor growth and can even result in complete remission [83].

The construction of micelles based on the **TD05** aptamer with the stearic acid bound to it was described in [86]. These micelles were characterized by increased affinity to the target cells in comparison with that of the individual **TD05** aptamer, and they were capable of specific penetration into the cells. It is not anticipated that these micelles will be used further to deliver therapeutics into cells.

J. Zhou *et al.* [87] proposed using polyamidoamine (PAMAM) dendrimers as carriers for therapeutic delivery [87]. **Sgc8c** aptamer-conjugated dendrimers proved capable of selective and efficient binding to CCRF-CEM cells and penetrating into them. The size of the aptamer-dendrimer conjugate is approximately 8 nm, the optimal size for using these conjugates as a platform for the delivery of therapeutic agents.

Thus, the use of aptamers for targeted delivery of nanoparticles with anti-tumor agents into tumor tissues is a promising avenue in the development of novel anti-tumor therapeutic strategies.

The use of escort aptamers for specific cell detection

The capability of escort aptamers to selectively recognize cells of a definite type enables one to use them to design highly specific detection systems. The introduction of different types of labels into aptamers allows one to use them for cell detection in cultures, biological samples, and in living multi-cellular organisms. Thus, radio-labeled aptamers have been used for tumor imaging in mice. Conjugates of the anti-tenascin aptamer **TTA1** and anti-mucin aptamers with chelating agents capable of binding to ^{99}Tc were used for the imaging of glioblastoma and breast cancer xenografts in mice [88, 89].

Various systems for detecting prostate cancer have been designed on the basis of anti-PSMA-aptamers. T. Chu *et al.* [90] obtained the anti-PSMA-aptamer **A9** conjugated with luminescent CdSe/CdTe crystals (the so-called quantum dots) for the imaging of PSMA-positive cells. These conjugates could bind to LNCaP cells distributed over the model tissue (3D collagen matrix) with high levels of efficiency and specificity. “Double” constructs consisting of the anti-PSMA-RNA-aptamer **A10** and the peptide aptamer against PSMA-negative cells immobilized on a gold electrode were used for the electrochemical detection of two types of prostate cancer cells: those that contained PSMA on their surface

(PSMA-positive) and those that did not contain the protein (PSMA-negative) [91]. D. Javier *et al.* [92] introduced additional oligonucleotide fragments, which were complementary to 24-membered oligonucleotides covalently bound to gold nanoparticles, into anti-PSMA-aptamers in order to perform the imaging of PSMA-positive cells. The binding of these complexes to PSMA on the cell surface was observed by reflected light detection using a confocal microscope.

DNA-aptamer **sgc8** conjugated to fluorescein was used to study the distribution of the receptors of PTK7 over the cell surface via fluorescence correlation microscopy [93]. A new method for the reversible fluorescent labelling of live cells was proposed in [94] and was illustrated by the example of CCRF-CEM cells. Aptamer **sgc8** conjugated with the quantum dot Qdot525 selectively bound to cells; after treatment with DNase, the conjugates were completely removed from the cell surface, whereas the cells retained their viability. Fluorescence-activated cell sorting, enabling the rapid and efficient isolation of cells of a definite type, is a promising application of this method. Fluorescence-activated sorting of stem cells using aptamer–fluorescein conjugates was also described by K. Guo *et al.* [49]

Aptamers **TD05** and **TE02** targeted against Ramos lymphoma cells were used when designing biosensor test strips for the rapid determination of malignant cells circulating in the blood stream [95]. The test zone of the biosensor contains the **TD05** aptamer conjugated with gold nanoparticles. These conjugates form coloured complexes with Ramos cells, which subsequently migrate along the strip until they are captured in the indicator zone of the biosensor through the binding of Ramos cells to the immobilized **TE02** aptamer. As a result, a characteristic red band is generated. These biosensors can be used for cell detection directly in blood samples; a visual qualitative assessment or quantitative determination can be performed using a portable scanner.

The use of a so-called ‘proximity ligation assay’ was proposed as means to detect the PSMA protein on the cell surface (*Fig. 12*) [96]. The system is composed of **A9** aptamers containing additional oligonucleotide fragments on their 3'- or 5'-termini, DNA probes that are complementary to each fragment, and the splint oligodeoxyribonucleotide, which is partially complementary to each DNA probe. Since PSMA is a dimer, when aptamers bind to PSMA on the cell surface, DNA probes become sufficiently close that they can be bound by a splint oligomer via the formation of a complementary complex. The DNA probes within this complex are then ligated; subsequently, real-time PCR is used to detect the resulting dsDNA. This method is highly sensitive and enables the detection of 10 LNCaP cells

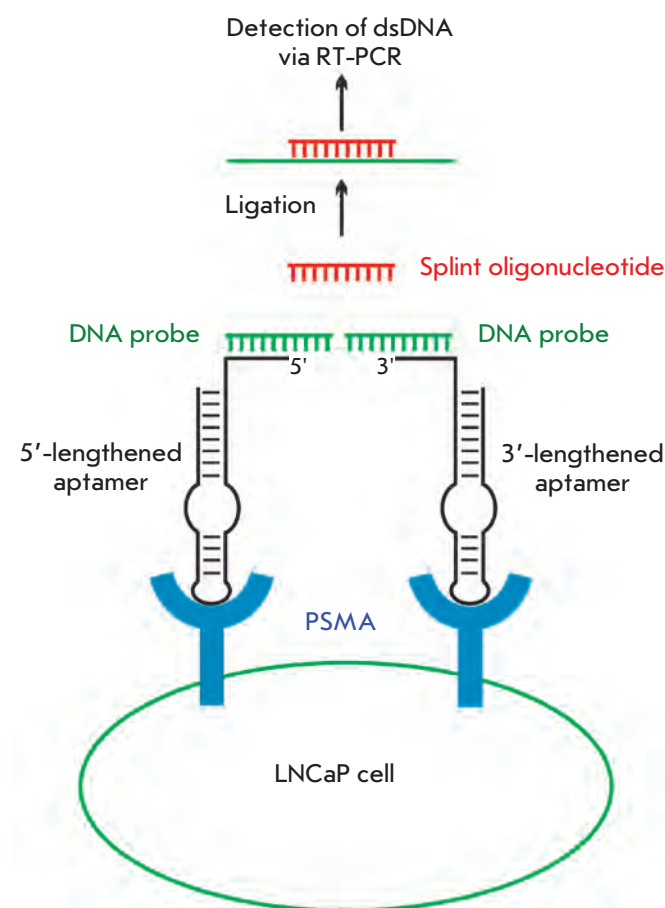


Fig. 12. Detection of prostate-specific membrane antigen using anti-PSMA aptamers by the proximity ligation assay [96]. The method includes the following stages: 1) formation of the complementary complexes of aptamers with DNA probes; 2) binding of aptamers to the adjacent sites on the cell surface, thus positioning DNA probes closer to each other; 3) hybridization of both DNA probes with the splint oligonucleotide; 4) ligation of DNA probes in the resulting complex; 5) detection of dsDNA via real-time PCR.

(prostate cancer) in the presence of 10^5 HeLa cells that do not contain the PSMA protein on their surface.

It was recently suggested that the aptamers binding to bacteria can be used for the design of biosensors for use in the detection of pathogenic microorganisms. DNA aptamers with bound CdSe-ZnS quantum dots were used for the fluorescent detection of *B. thuringiensis* [61]. RNA aptamers immobilized on the surface of single-walled carbon nanotubes were used to design potentiometric biosensors to determine *E. coli* [67] and *S. typhi* [97] and to demonstrate that they can be used for selective detection of these bacteria. A method based on the quantitative RT-PCR of RNA aptamers bound to bacteria immobilized on magnetic particles was developed for the detection of *E. coli* [98]. Novel aptamer-based biosensors could be used for highly selective determination of bacteria in the environment and food products and for diagnosing infectious diseases.

Another promising direction in the use of escort aptamers is the selective isolation of cells and cell immobilization. Thus, a system for the selective isolation of stem cells from bone marrow was designed on the basis of magnetic particles conjugated with aptamers capable of binding to porcine stem cells [49]. DNA aptamers capable of binding to the precursors of porcine endothelial cells were immobilized on the surface of polytetrafluoroethylene or polydimethylsiloxane disks [50]. It turned out that aptamer-coated disks can be used to selectively isolate endothelial precursor cells, which can be subsequently differentiated into vascular

endothelial cells while remaining bound to the disks. The assumption is that this approach could be used for the epithelialization of vascular implants, thus reducing the risk of implant rejection.

CONCLUSIONS

A number of escort aptamers capable of specific and efficient binding to cells of a definite type were recently obtained and approaches have been developed aimed at enhancing the stability of escort aptamers. It has been demonstrated that escort aptamers can be used to design efficient and highly specific systems for the delivery of therapeutic agents into cells, for the detection of cells of a definite type, for cell sorting, and for the selective blockage of surface proteins. Year after year, the number of studies devoted to the selection and application of escort aptamers against various cell targets (from bacteria to stem cells) steadily increases. It should be noted that the selection of aptamers against living cells has remained a more laborious and delicate process than the selection of aptamers against individual compounds. However, the increasing interest in this field and the advances in the selection methods are reasons to be hopeful that a greater variety of escort aptamers and aptamer-based therapeutic and diagnostic agents will appear in the near future. ●

This work was supported by the Russian Foundation for Basic Research (grant № 11-04-01014-a) and the Grant for Young Researchers provided by the Novosibirsk Region Administration, 2011.

REFERENCES

1. Ellington A.D., Szostak J.W. // *Nature*. 1990. V. 346. P. 818–822.
2. Tuerk C., Gold L. // *Science*. 1990. V. 249. P. 505–510.
3. Robertson D.L., Joyce G.F. // *Nature*. 1990. V. 344. P. 467–468.
4. Mayer G. // *Angew. Chem. Int. Ed.* 2009. V. 48. P. 2672–2689.
5. Stoltenburg R., Reinemann C., Strehlitz B. // *Biomol. Eng.* 2007. V. 24. P. 381–403.
6. Shamah S.M., Healy J.M., Cload S.T. // *Acc. Chem. Res.* 2008. V. 41. P. 130–138.
7. Zhou J., Rossi J.J. // *Oligonucleotides*. 2011. V. 21. P. 1–10.
8. Syed M.A., Pervaiz S. // *Oligonucleotides*. 2010. V. 20. P. 215–224.
9. Chapman J.A., Beckey C. // *Ann. Pharmacother.* 2006. V. 40. P. 1322–1326.
10. Ng E.W., Shima D.T., Calias P., Cunningham E.T., Guyer D.R., Adamis A.P. // *Nat. Rev. Drug. Discov.* 2006. V. 5. P. 123–132.
11. Hicke B.J., Stephens A.W. // *J. Clin. Invest.* 2000. V. 106. P. 923–928.
12. Breaker R.R. // *Curr. Opin. Chem. Biol.* 1997. V. 1. P. 26–31.
13. Fitzwater T., Polisky B. // *Meth. Enzymol.* 1996. V. 267. P. 275–301.
14. Sousa R. // *Meth. Enzymol.* 2000. V. 317. P. 65–74.
15. Chelliserrykattil J., Ellington A.D. // *Nat. Biotechnol.* 2004. V. 22. P. 1155–1160.
16. Burmeister P.E., Lewis S.D., Silva R.F., Preiss J.R., Horwitz L.R., Pendergrast P.S., McCauley T.G., Kurz J.C., Epstein D.M., Wilson C., et al. // *Chem. Biol.* 2005. V. 12. P. 25–33.
17. Schmidt K.S., Borkowski S., Kurreck J., Stephens A.W., Bald R., Hecht M., Friebe M., Dinkelborg L., Erdmann V.A. // *Nucl. Acids Res.* 2004. V. 32. P. 5757–5765.
18. Shangguan D., Tang Z., Mallikaratchy P., Xiao Z., Tan W. // *ChemBiochem.* 2007. V. 8. P. 603–606.
19. Hicke B.J., Marion C., Chang Y.F., Gould T., Lynott C.K., Parma D., Schmidt P.G., Warren S. // *J. Biol. Chem.* 2001. V. 276. P. 48644–48654.
20. Morris K.N., Jensen K.B., Julin C.M., Weil M., Gold L. // *Proc. Natl. Acad. Sci. USA.* 1998. V. 95. P. 2902–2907.
21. Lupold S.E., Hicke B.J., Lin Y., Coffey D.S. // *Cancer Res.* 2002. V. 62. P. 4029–4033.
22. Ferreira C., Papamichael K., Guilbault G., Schwarzacher T., Garipey J., Missailidis S. // *Anal. Bioanal. Chem.* 2008. V. 390. P. 1039–1050.

23. Ferreira C.S., Matthews C.S., Missailidis S. // *Tumour Biol.* 2006. V. 27. P. 289–301.
24. Ferreira C.S., Cheung M.C., Missailidis S., Bisland S., Garipey J. // *Nucl. Acids Res.* 2009. V. 37. P. 866–876.
25. Daniels D.A., Chen H., Hicke B.J., Swiderek K.M., Gold L. // *Proc. Natl. Acad. Sci. USA.* 2003. V. 100. P. 15416–15421.
26. Shangguan D., Li Y., Tang Z., Cao Z.C., Chen H.W., Mallikaratchy P., Sefah K., Yang C.J., Tan W. // *Proc. Natl. Acad. Sci. USA.* 2006. V. 103. P. 11838–11843.
27. Shangguan D., Cao Z. C., Li Y., Tan W. // *Clin. Chem.* 2007. V. 53. P. 1153–1155.
28. Shangguan D., Cao Z., Meng L., Mallikaratchy P., Sefah K., Wang H., Li Y., Tan W. // *J. Proteome Res.* 2008. V. 7. P. 2133–2139.
29. Xiao Z., Shangguan D., Cao Z., Fang X., Tan W. // *Chemistry.* 2008. V. 14. P. 1769–1775.
30. Li N., Ebright J.N., Stovall G.M., Chen X., Nguyen H.H., Singh A., Syrett A., Ellington A.D. // *J. Proteome Res.* 2009. V. 8. P. 2438–2448.
31. Tang Z., Shangguan D., Wang K., Shi H., Sefah K., Mallikaratchy P., Chen H.W., Li Y., Tan W. // *Anal. Chem.* 2007. V. 79. P. 4900–4907.
32. Mallikaratchy P., Tang Z., Kwame S., Meng L., Shangguan D., Tan W. // *Mol. Cell. Proteom.* 2007. V. 6. P. 2230–2238.
33. Mallikaratchy P.R., Ruggiero A., Gardner J.R., Kuryavyi V., Maguire W.F., Heaney M. L., McDevitt M.R., Patel D.J., Scheinberg D.A. // *Nucl. Acids Res.* 2011. V. 39. P. 2458–2469.
34. Sefah K., Tang Z.W., Shangguan D.H., Chen H., Lopez-Colon D., Li Y., Parekh P., Martin J., Meng L., Phillips J.A., et al. // *Leukemia.* 2009. V. 23. P. 235–244.
35. Chen H.W., Medley C.D., Sefah K., Shangguan D., Tang Z., Meng L., Smith J.E., Tan W. // *ChemMedChem.* 2008. V. 3. P. 991–1001.
36. Shangguan D., Meng L., Cao Z.C., Xiao Z., Fang X., Li Y., Cardona D., Witek R.P., Liu C., Tan W. // *Anal. Chem.* 2008. V. 80. P. 721–728.
37. Blank M., Weinschenk T., Priemer M., Schluesener H. // *J. Biol. Chem.* 2001. V. 276. P. 16464–16468.
38. Zueva E., Rubio L.I., Ducongé F., Tavitian B. // *Int. J. Cancer.* 2011. V. 128. P. 797–804.
39. Mi J., Liu Y., Rabbani Z.N., Yang Z., Urban J.H., Sullenger B.A., Clary B.M. // *Nat. Chem. Biol.* 2010. V. 6. P. 22–24.
40. Kraus E., James W., Barclay A.N. // *J. Immunol.* 1998. V. 160. P. 5209–5212.
41. Davis K.A., Lin Y., Abrams B., Jayasena S.D. // *Nucl. Acids Res.* 1998. V. 26. P. 3915–3924.
42. Santuli-Marotto S., Nair S.K., Rusconi C., Sullenger B., Gilboa E. // *Cancer Res.* 2003. V. 63. P. 7483–7489.
43. Chen C.-H.B., Dellamaggiore K.R., Ouellette C.P., Sedano C.D., Lizadjohry M., Chernis G.A., Gonzales M., Baltasar F.E., Fan A.L., Myerowitz R., et al. // *Proc. Natl. Acad. Sci. USA.* 2008. V. 105. P. 15908–15913.
44. Ohuchi S.P., Ohtsu T., Nakamura Y. // *Biochimie.* 2006. V. 88. P. 897–904.
45. Cerchia L., Duconge F., Pestourie C., Boulay J., Aissouni Y., Gombert K., Tavitian B., de Franciscis V., Libri D. // *PLoS Biol.* 2005. V. 3. e123.
46. Pestourie C., Cerchia L., Gombert K., Aissouni Y., Boulay J., De Franciscis V., Libri D., Tavitian B., Duconge F. // *Oligonucleotides.* 2006. V. 16. P. 323–335.
47. Wang C., Zhang M., Yang G., Zhang D., Ding H., Wang H., Fan M., Shen B., Shao N. // *J. Biotechnol.* 2003. V. 102. P. 15–22.
48. Guo K., Wendel H.P., Scheideler L., Ziemer G., Scheule A.M. // *J. Cell Mol. Med.* 2005. V. 9. P. 731–736.
49. Guo K.T., Schafer R., Paul A., Gerber A., Ziemer G., Wendel H.P. // *Stem Cells.* 2006. V. 24. P. 2220–2231.
50. Hoffmann J., Paul A., Harwardt M., Groll J., Reeswinkel T., Klee D., Moeller M., Fischer H., Walker T., Greiner T., et al. // *J. Biomed. Mater. Res. A.* 2008. V. 84A. P. 614–621.
51. Berezovski M.V., Lechmann M., Musheev M.U., Mak T.W., Krylov S.N. // *J. Am. Chem. Soc.* 2008. V. 130. P. 9137–9143.
52. Homann M., Göringer H.U. // *Nucl. Acids Res.* 1999. V. 27. P. 2006–2014.
53. Homann M., Göringer H.U. // *Bioorg. Med. Chem.* 2001. V. 9. P. 2571–2580.
54. Göringer H.U., Homann M., Zacharias M., Adler A. // *Handb. Exp. Pharmacol.* 2006. V. 173. P. 375–393.
55. Homann M., Lorger M., Engstler M., Zacharias M., Göringer H. // *Comb. Chem. High Throughput Screen.* 2008. V. 9. P. 491–499.
56. Göringer H.U., Homann M., Lorger M. // *Int. J. Parasitol.* 2003. V. 33. P. 1309–1317.
57. Lorger M., Engstler M., Homann M., Göringer H.U. // *Eukaryot. Cell.* 2003. V. 2. P. 84–94.
58. Ulrich H., Magdesian M.H., Alves M.J., Colli W. // *J. Biol. Chem.* 2002. V. 277. P. 20756–20762.
59. Chen F., Zhou J., Luo F., Mohammed A.B., Zhang X.L. // *Biochem. Biophys. Res. Commun.* 2007. V. 357. P. 743–748.
60. Torres-Chavolla E., Alcolija E.C. // *Biosens. Bioelectron.* 2009. V. 24. P. 3175–3182.
61. Ikanovic M., Rudzinski W., Bruno J., Allman A., Carrillo M., Dwarakanath S., Bhaadigadi S., Rao P., Kiel J., Andrews C. // *J. Fluoresc.* 2007. V. 17. P. 193–199.
62. Joshi R., Janagama H., Dwivedi H.P., Senthil Kumar T.M.A., Jaykus L.-A., Schefers J., Sreevatsan S. // *Mol. Cell. Probes.* 2009. V. 23. P. 20–28.
63. Pan Q., Zhang X.-L., Wu H.-Y., He P.-W., Wang F., Zhang M.-S., Hu J.-M., Xia B., Wu J. // *Antimicrob. Agents Chemother.* 2005. V. 49. P. 4052–4060.
64. Cao X., Li S., Chen L., Ding H., Xu H., Huang Y., Li J., Liu N., Cao W., Zhu Y., et al. // *Nucl. Acids Res.* 2009. V. 37. P. 4621–4628.
65. Hamula C.L.A., Zhang H., Guan L.L., Li X.-F., Le X.C. // *Anal. Chem.* 2008. V. 80. P. 7812–7819.
66. Bruno J., Carrillo M., Phillips T., Andrews C. // *J. Fluoresc.* 2010. V. 20. P. 1211–1223.
67. So H.-M., Park D.-W., Jeon E.-K., Kim Y.-H., Kim B.S., Lee C.-K., Choi S.Y., Kim S.C., Chang H., Lee J.-O. // *Small.* 2008. V. 4. P. 197–201.
68. Dwivedi H., Smiley R., Jaykus L.-A. // *Appl. Microbiol. Biotechnol.* 2010. V. 87. P. 2323–2334.
69. Barfod A., Persson T., Lindh J. // *Parasitol. Res.* 2009. V. 105. P. 1557–1566.
70. Chen F., Hu Y., Li D., Chen H., Zhang X.-L. // *PLoS One.* 2009. V. 4. P. e8142.
71. Chu T.C., Marks J.W., 3rd, Lavery L.A., Faulkner S., Rosenblum M.G., Ellington A.D., Levy M. // *Cancer Res.* 2006. V. 66. P. 5989–5992.
72. Bagalkot V., Farokhzad O.C., Langer R., Jon S. // *Angew. Chem. Int. Ed. Engl.* 2006. V. 45. P. 8149–8152.
73. Huang Y.F., Shangguan D., Liu H., Phillips J.A., Zhang X., Chen Y., Tan W. // *ChemBiochem.* 2009. V. 10. P. 862–868.
74. Chu T.C., Twu K.Y., Ellington A.D., Levy M. // *Nucl. Acids Res.* 2006. V. 34. P. e73.
75. McNamara J.O., Andrechek E.R., Wang Y., Viles K.D., Rempel R.E., Gilboa E., Sullenger B.A., Giangrande P.H. // *Nat. Biotechnol.* 2006. V. 24. P. 1005–1015.

REVIEWS

76. Dassie J.P., Liu X.-Y., Thomas G.S., Whitaker R.M., Thiel K.W., Stockdale K.R., Meyerholz D.K., McCaffrey A.P., McNamara J.O., Giangrande P.H. // *Nat. Biotechnol.* 2009. V. 27. P. 839–846.
77. Wullner U., Neef I., Eller A., Kleines M., Tur M.K., Barth S. // *Curr. Cancer Drug Targets.* 2008. V. 8. P. 554–565.
78. Khaled A., Guo S., Li F., Guo P. // *Nano Lett.* 2005. V. 5. P. 1797–1808.
79. Zhou J., Swiderski P., Li H., Zhang J., Neff C.P., Akkina R., Rossi J.J. // *Nucl. Acids Res.* 2009. V. 37. P. 3094–3109.
80. Huang Y.F., Chang H.T., Tan W. // *Anal. Chem.* 2008. V. 80. P. 567–572.
81. Huang Y.F., Sefah K., Bamrungsap S., Chang H.T., Tan W. // *Langmuir.* 2008. V. 24. P. 11860–11865.
82. Farokhzad O.C., Jon S., Khademhosseini A., Tran T.N., Lavan D.A., Langer R. // *Cancer Res.* 2004. V. 64. P. 7668–7672.
83. Farokhzad O.C., Cheng J., Teply B.A., Sherifi I., Jon S., Kantoff P.W., Richie J.P., Langer R. // *Proc. Natl. Acad. Sci. USA.* 2006. V. 103. P. 6315–6320.
84. Cheng J., Teply B., Sherifi I., Sung J., Luther G., Gu F.X., Levy-Nissenbaum E., Radovic-Moreno A.F., Langer R., Farokhzad O.C. // *Biomaterials.* 2007. V. 28. P. 869–876.
85. Farokhzad O.C., Khademhosseini A., Jon S., Hermmann A., Cheng J., Chin C., Kiselyuk A., Teply B., Eng G., Langer R. // *Anal. Chem.* 2005. V. 77. P. 5453–5459.
86. Wu Y., Sefah K., Liu H., Wang R., Tan W. // *Proc. Natl. Acad. Sci. USA.* 2010. V. 107. P. 5–10.
87. Zhou J., Soontornworajit B., Martin J., Sullenger B.A., Gilboa E., Wang Y. // *Macromol. Biosci.* 2009. V. 9. P. 831–835.
88. Perkins A.C., Missailidis S. // *Q. J. Nucl. Med. Mol. Imaging.* 2007. V. 51. P. 292–296.
89. Hicke B.J., Stephens A.W., Gould T., Chang Y.-F., Lynott C.K., Heil J., Borkowski S., Hilger C.-S., Cook G., Warren S., et al. // *J. Nucl. Med.* 2006. V. 47. P. 668–678.
90. Chu T.C., Shieh F., Lavery L.A., Levy M., Richards-Kortum R., Korgel B.A., Ellington A.D. // *Biosens. Bioelectron.* 2006. V. 21. P. 1859–1866.
91. Min K., Song K.-M., Cho M., Chun Y.-S., Shim Y.-B., Ku J. K., Ban C. // *Chem. Commun.* 2010. V. 46. P. 5566–5568.
92. Javier D.J., Nitin N., Levy M., Ellington A., Richards-Kortum R. // *Bioconjugate Chem.* 2008. V. 19. P. 1309–1312.
93. Chen Y., Munteanu A.C., Huang Y.-F., Phillips J., Zhu Z., Mavros M., Tan W. // *Chem. Eur. J.* 2009. V. 15. P. 5327–5336.
94. Terazono H., Anzai Y., Soloviev M., Yasuda K. // *J. Nanobiotechnol.* 2010. V. 8. P. 8.
95. Liu G., Mao X., Phillips J.A., Xu H., Tan W., Zeng L. // *Anal. Chem.* 2009. V. 81. P. 10013–10018.
96. Pai S.S., Ellington A.D. // *Meth. Mol. Biol.* 2009. V. 504. P. 385–398.
97. Zelada-Guillén G.A., Jordi R., Düzgün A., Rius F.X. // *Angew. Chem. Int. Ed.* 2009. V. 48. P. 7334–7337.
98. Lee H.-J., Kim B.C., Kim K.-W., Kim Y.K., Kim J., Oh M.-K. // *Biosens. Bioelectron.* 2009. V. 24. P. 3550–3555.

Mesenchymal Stem Cells in Tissue Growth and Repair

N. I. Kalinina, V. Yu. Sysoeva, K. A. Rubina, Ye. V. Parfenova, V. A. Tkachuk

Department of Fundamental Medicine, Lomonosov Moscow State University

*E-mail: n_i_kalinina@mail.ru

Received 14.07.2011

Copyright © 2011 Park-media, Ltd. This is an open access article distributed under the Creative Commons Attribution License, which permits unrestricted use, distribution, and reproduction in any medium, provided the original work is properly cited.

ABSTRACT It has been established in the recent several decades that stem cells play a crucial role in tissue renewal and regeneration. Mesenchymal stem cells (MSCs) are part of the most important population of adult stem cells. These cells have hereby been identified for the very first time and subsequently isolated from bone marrow stroma. Bone marrow-derived MSCs have been believed to play the role of a source of cells for the renewal and repair of connective tissues, including bone, cartilage and adipose tissues. Cells similar to bone marrow-derived MSCs have now been identified in all postnatal tissues. Data on the distribution and function of MSCs *in vivo* collected using novel approaches pertaining to the identification of MSCs *in situ*, to their isolation from tissues, and finally to the determination of their biological properties have enabled successful revision of the role of MSCs in various organs and tissues. This review summarizes our own, as well as others', data concerning the role of MSCs in the regulation processes of tissue repair and regeneration. In our opinion, MSCs provide the connection between the blood-vascular, immune, endocrine, and nervous systems and tissue-specific stem cells in the body.

KEYWORDS mesenchymal stem cells; tissue regeneration; differentiation; cell therapy.

ABBREVIATIONS HSC – hematopoietic stem cell; MSC – mesenchymal stem cell; MMSC – multipotent mesenchymal stromal cell; TSC – tissue-specific stem cell.

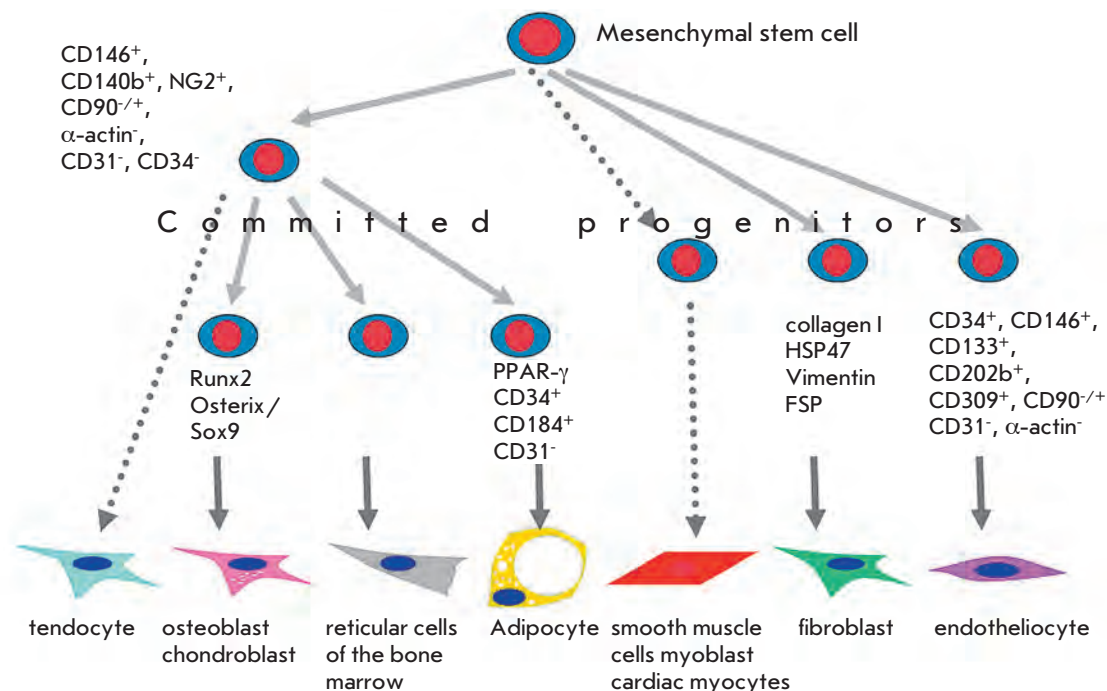
The conception of tissue renewal being facilitated by a self-sustaining pool of stem cells was first formulated in the study of hematosis over a century ago [1]. However, the existence of hematopoietic stem cells (HSCs) from which all blood cell types stem was confirmed experimentally only in the middle of the 20th century [2]. Until then, it was believed that the cellular composition of postnatal tissues was replenished as a result of the division of specific (differentiated) cells. The concept that the renewal occurs as a result of the activity of stem cells was considered a mechanism limited only to blood cells; a unique, rapidly renewing tissue containing a great number of functionally heterogeneous cell types. It has now been proven that the maintenance and replenishment of the cellular composition in almost all tissues of the human body (including skin and intestinal epithelium, liver, skeletal muscles, and myocardium) occur through the proliferation and differentiation of the corresponding tissue-specific stem cells (TSCs). However, along with the tissue-specific stem cells, other stem cells, known as mesenchymal stem cells (MSCs), have been identified in mammalian tissues.

The first body of data indicating the presence of postnatal stem cells, along with hematopoietic stem cells, in bone marrow was obtained by means of sev-

eral approaches. The first indication was the occurrence of osteogenesis in experimental models following the intraperitoneal transplantation of cultivated bone marrow stromal cells [3]. The second indication was the isolation of a cell population from the bone marrow that differs from hematopoietic stem cells but exhibits properties typical of stem cells. During cultivation, these cells cloned (the colonies of fibroblast) [4], maintaining their ability to differentiate into a variety of cell types (osteoblasts, adipocytes, and chondrocyte) [5].

The assumption was, by analogy with HSCs, that bone marrow-derived MSCs were at the top of the mesenchymal hierarchy [6, 7] (*Fig. 1*). It was suggested that, throughout life, descendants of these cells undergo several discrete stages of differentiation, thereby spawning the various cells found in connective tissues, i. e.: in bone and adipose tissues, tendons, cartilages, and smooth muscles [8]. Later, the cells with phenotypic characteristics and differentiation potential similar to bone marrow-derived MSCs were isolated from almost all the embryonal and postnatal tissues of mammals, birds, and amphibians [9, 10]. On the basis of these observations, a theory emerged, postulating that bone marrow is a deposit of both hematopoietic and mesenchymal stem cells. However, the suggestion that the renewal of connective tissues over the whole

Fig. 1. Model of mesenchymal hierarchy. The hypothetical scheme, according to which MSCs undergoes several discrete stages of differentiation, thereby producing various types of connective tissue cells for the entire life.



body depends on the activity of bone marrow-derived MSCs as yet remains unconfirmed [11].

CULTIVATED MULTIPOTENT MESENCHYMAL STROMAL CELLS

Identifying MSCs and analyzing them directly in tissues are very complicated tasks. Hence, most conclusions relating to the biological properties of MSCs are made on the basis of a study of stromal cell populations isolated from various tissues; these stromal cells possess the ability to attach culture plastic and to differentiate in osteogenic, adipogenic, and chondrogenic directions *in vitro* [12]. Despite the fact that, by their ability to renew and differentiate in various directions, these cells form a rather heterogenic population [13], they are also referred to as MSCs. The International Society for Cellular Therapy (ISCT, Vancouver, Canada) has suggested using the term “multipotent mesenchymal stromal cell” (MMSC) in order to separate such cultivated cells from MSCs *in situ*. According to the minimal criteria developed by the ISCT, MMSCs should have the ability to attach to plastic during cultivation in ambient conditions, to express CD105, CD73, and CD90 marker antigens on the surface, but they should not contain CD45, CD34, CD14 or CD11b, CD79α or CD19, and HLA-DR, and they also should differentiate into osteoblasts, adipocytes, and chondroblasts *in vitro* [14]. At present, bone marrow and adipose tissues are considered to be the most promising sources of MMSCs for use in the study of the biological properties of these cells and for

their application in regenerative medicine. However, multipotent mesenchymal stromal cells have also been isolated from other tissues, including skin, thymus, spleen, and endometrium [15]. It should be taken into account that MMSCs isolated from different postnatal and embryonal tissues differ from each other in the following ways: by their ability to form colonies, by gene expression, and by their differentiation potential even if they had been cultivated under the same conditions [9, 15–18]. From these distinctions, questions as to the extent to which the cells (selected based on their ability to attach to plastic and grow in ambient conditions of cultivation) are biologically equivalent to one another and whether or not these differences are the result of various biological functions of MSCs in the corresponding tissues arise [12].

MULTIPOTENCY OF MMSCs

In addition to their ability to differentiate into osteoblasts, chondroblasts, and adipocytes *in vitro* [7], MMSCs give rise to bone or cartilage after ectopic transplantation *in vivo* in animal models [3], as well as mediate the regeneration of bone tissue following injuries [11] and when genetic defects occur in osteogenesis (osteogenesis imperfecta) [19]. Moreover, many investigations have shown that MMSCs have the ability to differentiate into a variety of cells having mesodermal, ectodermal, and endodermal origins, including endothelial cells [20], cardiac myocytes [21], hepatocytes [22], and neural cells [23]. A number of authors, however,

conceding the ability of MMSCs to differentiate into osteoblasts, chondroblasts and adipocytes, continue to doubt the ability of MMSCs to differentiate into cells of other germ layers (endodermal and ectodermal) both *in vitro* and *in vivo* [12]. It has thus been shown that, post transplantation, bone marrow-derived MMSCs can integrate into the tissues of a recipient by fusion with resident cells [24] rather than through differentiation into the cells typical of the particular tissue.

The differences in the assessment of the differentiation potential of cultivated MMSCs can be explained by the dissimilar quantitative and qualitative compositions of progenitor cells in tissues from which they were obtained. Firstly, the isolated population of MSCs is heterogenic and includes cells with differing morphologies and cells exhibiting different proliferative and differentiation abilities *in vitro* and *in vivo* [25, 26]. Furthermore, the multipotency of MMSCs could disappear as they are being cultivated [25]. Thus, the clones of umbilical-cord-derived MMSCs, which differ from each other by their degree of self-renewal and by their differentiation potential *in vitro*, produce daughter clones that gradually lose their multipotency [25].

Secondly, it is possible that the newly isolated populations of MMSCs can contain progenitor cells already committed in various differentiation directions. Thus, according to the results of a cytometric analysis, adipose tissue contains at least five progenitor cells differing in the expression of marker antigens: sub-endothelial progenitor cells (CD146⁺, CD140b⁺, NG2⁺, α -actin⁻, CD31⁻, CD90^{+/+}, and CD34⁻), supra-adventitial progenitor cells (NG2⁺, CD90⁺, CD34⁺, CD146⁻, CD31⁻, and α -actin⁻), and transient progenitor cells (CD146⁺, CD34⁺, NG2⁺, CD90⁺, and CD31⁻), preadipocyte progenitor (CD34⁺, CD184⁺, and CD31⁻), and endothelial progenitor cells (CD34⁺, CD146⁺, CD133⁺, CD202b⁺, CD309⁺, CD31⁻, CD90^{+/+}, and α -actin⁻) [26]. In this author's opinion, the fact outlined above explains the frequent presence of endothelial islands (which disappear with cultivation) in a primary culture of MMSCs and explains the spherical shape of the colonies that are formed by small, and rapidly dividing rounded cells and large, very slowly dividing spread cells [27].

Thirdly, along with MSCs, all tissues contain minor subpopulations of pluripotent cells that have a wider spectrum of differentiation abilities, such as minute embryonic-like (VSEL) cells [28], multipotent adult progenitor cells (MAPCs) [29], and multilineage differentiating stress-enduring (MUSE) cells [30]. Our data indicate the presence of very small embryonic-like cells in a newly isolated population of MMSCs; but the contribution of these minor populations to the differentiation potential of the MMSC culture remains unclear, since it is unknown whether they retain their growth and dif-

ferentiation ability under cultivation conditions.

The disagreement in the analysis of the multipotency of MMSCs can also be attributed to the use of different techniques for isolation and cultivation, as well as the various assessment criteria of differentiation.

MMSCs AND TISSUE GROWTH

Transplantation of MMSCs stimulates the regeneration of tissues, including bone, skeletal muscles, myocardium, skin, liver, and peripheral nerves. According to our data, this occurs owing to both the integration of transplanted MMSCs into the recipient's tissues and the secretory activity of these cells [31]. It was demonstrated that transplanted MSCs integrate the endothelial lining of growing capillaries and the periendothelial space of newly formed blood vessels, thereby stabilizing them.

MSCs are an important source of growth factors and cytokines, which participate in the regulation of tissue regeneration. Thus, MSCs produce factors in the bone marrow that are necessary for the self-sustenance of hematopoietic stem cells and keep them in a niche; we can refer to such factors as SDF-1 α (the stromal factor-1 α), SCF (stem cell factor), angiopoietin -1, and interleukin-7 [32]. It was established in our laboratory that MSCs produce angiogenic and neurotrophic growth factors, including VEGF (vascular endothelial growth factor), bFGF (basic fibroblast growth factor), HGF (hepatocyte growth factor), angiopoietin, NGF (nerve growth factor), BDNF (brain-derived neurotrophic factor), and GDNF (glial cell line-derived neurotrophic factor) [33, 34]. The angiogenic growth factors produced by MMSCs in the transplantation region stimulate the division of endothelial cells, their migration, and the formation of blood vessels. In addition, the factors produced by MMSCs promote the mobilization of endothelial progenitors from the bone marrow, which participate in the formation of new blood vessels [34, 35]. Simultaneously, the neurotrophic factors produced by MMSCs stimulate both the growth and renewal of nerve endings [33]. Thus, MSCs can mediate the coordinated regulation of the growth of blood vessels and nerves during regeneration and remodeling of tissues (*Fig. 2*).

According to our data, MMSCs produce the following factors necessary for the functional maturation of blood vessels and their stabilization: bFGF, PDGF-BB (platelet-derived growth factor BB), and TGF- β (transforming growth factor beta) [18, 34, 36]. PDGF-BB initiates branching to them of growing blood vessels and migration of pericytes, smooth muscular cells, and mesenchymal cells; while TGF- β stimulates the differentiation of the smooth muscular cells and the production of the extracellular matrix components of the vascular wall [37].

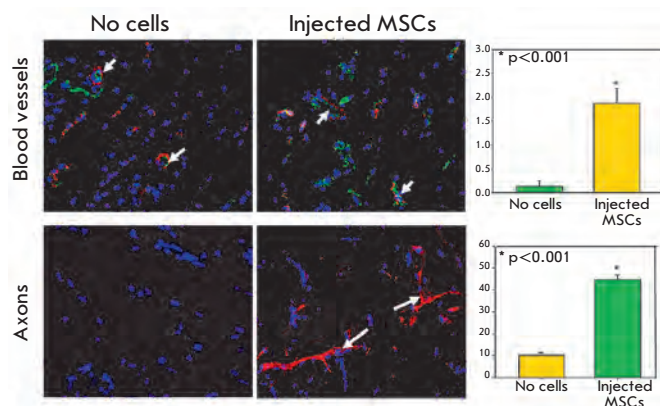


Fig. 2. Stimulation of growth of blood vessels and axons under the action of MSCs. Adipose tissue-derived MSCs were transplanted as subcutaneous matrigel implants in syngeneic mice. Blood vessel (upper panels) and axon (lower panels) densities were evaluated by immunofluorescent staining of frozen sections with antibodies against the markers of endothelium (CD31, green fluorescence) and pericytes (NG2, red fluorescence), or axonal cytoskeleton protein (NF200, red fluorescence). Cell nuclei are counterstained by DAPI. Short arrows indicate mature blood vessels, long arrows indicate axons. The diagrams represent the results of morphometry for the total length of blood vessels (upper diagram) and axons (lower diagram) [33, 34].

The amount of growth factors and cytokines produced in MSCs significantly increases when organs and tissues are damaged. Hypoxia causes coordinated changes in the expression of genes in MMSCs: the level of mRNA for the proangiogenic factors, such as VEGF, PlGF, HGF, bFGF, PDGF-BB, and TGF- β , increases by a factor of 2–4; and the mRNA level for anti-angiogenic factors, such as PAI-a, angiostatin, and thrombospondin, decreases more than twofold [34]. Furthermore, MMSCs secrete neurotrophic factors, including NGF, BDNF, and GDNF, which are responsible for the stimulation of growth and regeneration of the nerve filaments that are a result of the transplantation of MMSCs [33, 38].

The secretory activity of MMSCs also affects their immunomodulating properties. In several animal models, it was revealed that the injection of cultivated MMSCs causes immunosuppression *in vivo* [39]. The immunosuppressive effect of MMSCs is based on the suppression of the function of immune cells by means of the following: through the activation of T cells, via the differentiation of dendrite cells, through the proliferation of B cells, and by means of the cytolytic activity of natural killers. The immunosuppressive properties of these cells are mediated by the secretion of soluble

factors, including interleukin-10, prostaglandin-E2, nitric oxide, TGF- β , galectin-1 and galectin-3, as well as by the indirect intercellular contact of MMSCs with immune cells [40]. Moreover, MMSCs can promote the differentiation of naive T helpers into regulatory T cells and the migration of mature regulatory T cells [39, 40]. The colocalization of bone marrow-derived MSCs with dendrite cells and circulatory B cells in the perisinusoid space [41, 42] enables the reasonable assumption that MSCs are involved in the regulation of the functional activity and maturation of immune cells.

MMSCs AND TUMOR GROWTH

Tumor growth and angiogenesis are examples of pathologic remodeling of tissues. Mesenchymal cells are known to interact with tumor cells, both sustaining and inhibiting tumor growth *in vitro* and *in vivo*. It has thus been revealed that, *in vitro*, bone marrow-derived MMSCs stimulate the proliferation of pancreatic cancer cells [43], while MMSCs from the subcutaneous adipose tissue suppress the proliferation of primary leukemia cells [44]. In animal models, it was found that MMSCs stimulate the retention and growth of tumor cells when they are injected in conjunction with melanoma cells [45–47], breast cancer [48], prostate cancer [49], as well as bowel cancer [50, 51]. In addition, they also increase the probability of metastasis formation [52]. In all likelihood, the stimulating effect of MMSCs occurs owing to the secretion of chemokines (CCL5, SDF-1 α) and angiogenic growth factors (VEGF) and to their anti-apoptotic influence on tumor cells. In addition, MMSCs have the ability to migrate to tumor tissue and participate in the formation of its stroma. Thus, in tumors, MMSCs differentiate into fibroblasts, endothelial cells, and pericytes, thereby stimulating tumor growth [46, 53]. MMSCs are also capable of secreting cytokines, growth factors, and angiogenic factors [34, 43]; this stimulates tumor growth through increasing their vascularization.

It should be noted, however, that in these and other models, MMSCs can actually suppress tumor growth under particular conditions. There are several underlying processes for this MMSCs effect, such as the stimulation of the inflammatory reaction in the recipient's body in the case of colorectal cancer [50]; the activation of the Akt and Wnt signaling pathways in Kaposi's sarcoma cells, hepatoma cells, and breast cancer cells [54–56]; cell cycle arrest in G1-phase occurring in pancreatic cancer cells, hepatoma cells, and lymphoma cells [44, 57]; induction of apoptosis in tumor and endothelial cells in hepatoma and non-Hodgkin's lymphoma [44, 58]; and the suppression of angiogenesis in melanoma of B16F10 mice [57]. The systematic injection of MMSCs to experimental animals suffering from induced ma-

ture mancreatic cancer led to the apoptosis of tumor cells *in vitro* and to the suppression of tumor growth *in vivo* [57].

The data obtained during the study of the effect of MSCs on tumor growth indicate that the activation of MSCs, their directed migration, and their differentiation into the cells of connective tissue and blood vessels, as well as their interaction with immune cells, are important processes in oncogenesis.

IDENTIFICATION OF MSCs *in vivo*

The distribution of MSCs in tissues has remained unclear for a considerable period of time [13, 32], since the fraction of such cells in tissues is rather small, and the unique immunophenotype distinguishing them from other cells had not been determined. New marker antigens of MSCs were determined via the assessment of the ability of cells, which were isolated from tissues in accordance with their ability to express particular proteins, for self-renewal and differentiation *in vivo*.

It was recently revealed that in the bone marrow of mice, the following cells satisfy the criteria for MSCs: cells expressing Sca-1 (stem cell antigen-1) and PDGFR α (platelet-derived growth factor receptor α). These cells formed bone tissue and the functional stroma for HSCs during their heterotopic transplantation under the skin and osteoblasts, reticular cells, and adipocytes in the bone marrow after their systematic transplantation to an exposed recipient [13]. It was established using the same approach, that nestin can also be a marker of bone marrow-derived MSCs [32]; this conclusion was drawn since the cells expressing nestin possessed the ability to self-renew *in vitro* and *in vivo*, differentiated into osteoblasts and chondrocytes in the bone marrow *in vivo*, and formed a hematopoietic microenvironment when transplanted under the skin [59].

By using new marker antigens (CD146, Sca-1, and PDGFR α), it was shown that, *in situ*, MSCs accumulate in the immediate vicinity of blood vessels; in particular in the adventitia of the arteries supplying blood to the bone marrow. Moreover, the cells, which were isolated in accordance with their perivascular localization and the ability to express pericyte markers (NG2 [chondroitin sulfate proteoglycan], CD146, and PDGFR β) from various human organs and tissues, including the fetal and postnatal skin, the pancreas, the heart, the lungs, the bone marrow, and placenta, had the ability to self-maintain and also possessed differentiation potential and expression profiles that are typical of MSCs [60].

It is now widely believed that the cells producing the marker antigens of MSCs and pericytes *in vivo* are

found in close proximity to blood vessels, in adipose tissue, and in dental pulp [61, 62].

Despite the similarities in the localization and ability to express surface markers, the ability to differentiate into osteoblasts, chondrocytes, adipocytes, myocytes, and smooth muscle cells *in vitro* and form the foci of ectopic osteogenesis *in vivo* [60], the problem of the biological equivalence of MSCs and pericytes remains unresolved.

It remains thus unclear whether MSCs incorporate all of the functions of pericytes *in vivo*: e. g., the stabilization of capillaries, phagocytosis, and the regulation of the permeability and tonus of blood vessels, including those functions that are controlled through the reception of signals from the sympathetic nervous system [63]. The periendothelial space of blood vessels in all likelihood contains heterogenic cell populations. Apparently, only a portion of pericytes can belong to MSCs *in vivo*. The perivascular localization is a typical feature of not only MSCs; it has been noted in resident stem cells (or progenitor cells), HSCs, preadipocytes, and stem cells in the skeletal muscles of the bone marrow, in adipose tissues, and skeletal muscles [64–67]. The presence of MSCs in the periendothelial space indicates that endothelium is an important component of the MSC niche, which can regulate their functional activity.

MSCs ARE COMPONENTS OF THE TISSUE-SPECIFIC CELL NICHE

Studying the functions of MSCs in various tissues has become a topical research task. In the bone marrow, MSCs provide not only the renewal of stroma, but they are also an important regulator of hematosis and the functions of HSCs. HSCs in the bone marrow have a particular microenvironment (niches), which is comprised of non-hematopoietic cells, soluble factors and proteins of the territorial matrix, which regulate the process of hemopoiesis [69]. At the beginning of studies of the role of MSCs, these cells *in vivo* were found to be a source of osteoblasts, adipocytes, and reticular cells; altogether, these cells make up the niche for HSCs, which participate in hemopoiesis [3]. In addition, MSCs are the first to populate the sites of fetal hemopoiesis, transmitting the regulatory signals causing the migration of HSCs to those sites [70]. Cultivated bone marrow-derived MMSCs are also capable of maintaining the survival and proliferation of HSCs *ex vivo* [70].

Osteoblasts are necessary components of the hematopoietic microenvironment [71–72]. The number of osteoblasts in the bone marrow positively correlates with the number of HSCs [73]; i. e., around 14% of HSCs are located in the immediate vicinity of the

osteoblast-lined endosteum [65]. The ability of osteoblasts to regulate the self-maintenance and activation of HSCs has not yet been confirmed unequivocally. However, data showing that these cells regulate the differentiation of HSCs into granulocytes and B lymphocytes through the secretion of soluble growth factors and cytokines, such as LIF-1 (leukemia inhibitory factor-1), GM-CSF (granulocyte macrophage colony-stimulating factor), SDF-1, and interleukin-6 has been obtained *in vitro* [69]. Along with osteoblasts, the stroma of the bone marrow contains adipocytes, which also originate from MSCs. It is of interest that adipocytes function in the bone marrow as negative regulators of hemopoiesis, acting through a mechanism that is still unknown [74]. Consequently, bone-marrow MSCs play the role of a source for two types of cells (osteoblasts and adipocytes), which exhibit antagonist activity in the regulation of HSCs. It remains unclear what is the deciding factor concerning the direction in which MSCs differentiate, and how the balance between the production of osteoblasts and adipocytes would affect hemopoiesis. [12].

MSCs can also regulate the hemopoietic microenvironment by arranging a vasculature in the bone marrow; the latter is a necessary structural and functional component of HSC niches [69]. The existence of dual stem-cell niches containing two types of stem cells, HSCs and MSCs, which directly interact in the perivascular spaces of the brain marrow, was confirmed in two independent studies. In particular, it was established that the majority of HSCs are located at a distance of below 30 μm (~5 diameters of a HSC) from the reticular cells which produce a large amount of SDF-1 α and nestin [13, 32]. As was mentioned above, these cells are MSCs or their closest descendants, since they are capable of both self-maintenance and differentiation in the osteogenic and adipogenic directions both *in vitro* and *in vivo*.

Nestin-positive MSCs express factors are required to keep HSCs in their niche and for them to self-maintain; accordingly, their number should be 50–700 times higher than that of the other stromal cells of the bone marrow. In addition, nestin-positive MSCs maintain the growth of HSC colonies *in vitro*, and their removal causes a drastic fall in the amount of HSCs *in vivo*.

The distinctive features of nestin-expressing MSCs from the bone marrow are the expression of β 3-adrenoreceptors and their ability to respond to signals from the nervous system. The agonists of β 3- and β 2-adrenoreceptors induce suppression in the expression of SDF-1 α , SCF, angiopoetin-1, and interleukin-7 by nestin-expressing MSCs; the latter, in turn, leads to the mobilization of HSCs. Thus, hemopoiesis is regulated by the nervous system in this manner.

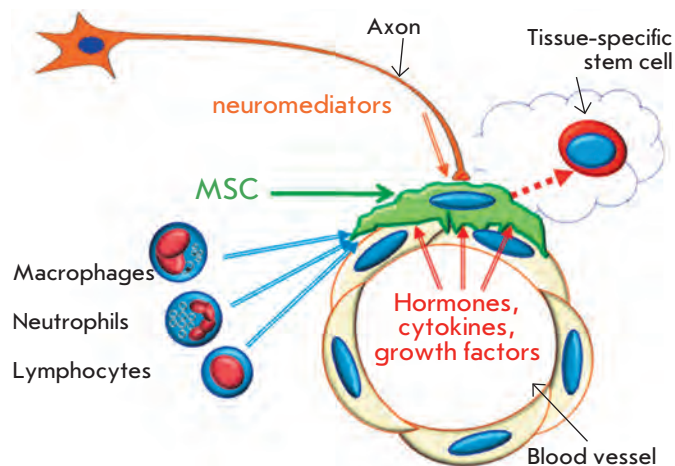


Fig. 3. Hypothetic scheme showing the interaction of MSCs with axons, endothelial cells, leukocytes, and tissue-specific stem cells (see details in the text).

It has been well-known since the time of Virchow that pericytes with periendothelial localization can be targets for axon endings, thereby playing a key role in the transmission of signals from the nervous system to the vascular system [75]. As was noted above, part of pericytes belong to MSCs. Therefore, the MSC function of connecting the compartment of HSCs and the nervous system is in good agreement with their perivascular localization (*Fig. 3*).

Bone-marrow-derived MSCs are also targets for innate immunity cells, such as macrophages. In contrast to the nervous system stimulating mobilization, bone-marrow-derived macrophages promote the retention of HSCs in the niche [76].

It remains unclear whether MSCs from other tissues are part of the niches for tissue-specific resident stem cells, and if they mediate the action of the nervous system in these niches. Thus, MSCs isolated from myocardium were found to be capable of stimulating the survival and proliferation of cardiac stem cells *in vitro* [77]; however, the questions of whether and how these cells interact with tissue-specific stem cells *in vivo* remains unanswered [78]. In both the small intestine and skin, the populations of MSCs responsible for the renewal of these tissues after injury were identified. However, the degree of importance of their interaction with tissue-specific stem cells for the processes of tissue renewal has yet to be studied. It is at least known, however, that bone-marrow MSCs are a necessary component of the perivascular niche for the tissue-specific resident stem cells (in this case HSCs) which enable integration between signals from the nervous and immune systems and the peripheral blood flow.

CONCLUSIONS

The results presented in this review allow us to suggest that there are two types of MSCs in the body: bone-marrow-derived MSCs circulating in the blood, which participate in tissue repair upon injury, and resident MSCs, which are located in the perivascular region of all organs and tissues of the body and regulate physiological tissue renewal and the maintenance of tissue homeostasis. MSCs are important participants in the processes of tissue renewal and regeneration. Firstly, they regulate the self-maintenance and differentiation

of tissue-specific stem cells. Secondly, MSCs stimulate growth, as well as stabilize blood vessels and nerves in the processes of tissue repair. Thirdly, the interaction between MSCs and lymphocytes, endothelial cells and axons facilitates the integration of the neurohumoral signals which regulate tissue renewal and repair. ●

This work was performed in the framework of Government Contract № 16.512.12.2005 and supported by the Russian Foundation for Basic Research (grant № 11-04-12107-ofi-m-2011).

REFERENCES

- Maximov A.A. // *Folia Haematologica*. 1909. V. 8. P. 125–134.
- Becker A.J., Mc C.E., Till J.E. // *Nature*. 1963. V. 197. P. 452–454.
- Friedenstein A.J., Piatetzky S., Petrakova K.V. // *J. Embryol. Exp. Morphol.* 1966. V. 16. P. 381–390.
- Friedenstein A.J., Chailakhjan R.K., Lalykina K.S. // *Cell Tissue Kinet.* 1970. V. 3. P. 393–403.
- Weissman I.L. // *Cell*. 2000. V. 100. P. 157–168.
- Caplan A.I. // *Clin. Plast Surg.* 1994. V. 21. P. 429–435.
- Prockop D.J. // *Science*. 1997. V. 276. P. 71–74.
- Caplan A.I. // *J. Orthop. Res.* 1991. V. 9. P. 641–650.
- da Silva Meirelles L., Chagastelles P.C., Nardi N.B. // *J. Cell Sci.* 2006. V. 119. P. 2204–2213.
- Young H.E. // *Curr. Top. Microbiol. Immunol.* 2004. V. 280. P. 71–109.
- Giannoudis P.V., Goff T., Roshdy T., Jones E., McGonagle D. // *Injury*. 2010. V. 41. P. 1099–1102.
- Nombela-Arrieta C., Ritz J., Silberstein L.E. // *Nat. Rev. Mol. Cell Biol.* 2011. V. 12. P. 126–131.
- Morikawa S., Mabuchi Y., Kubota Y., Nagai Y., Niibe K., Hiratsu E., Suzuki S., Miyauchi-Hara C., Nagoshi N., Sunabori T., et al. // *J. Exp. Med.* 2009. V. 206. P. 2483–2496.
- Dominici M., Le Blanc K., Mueller I., Slaper-Cortenbach I., Marini F., Krause D., Deans R., Keating A., Prockop D., Horwitz E. // *Cytotherapy*. 2006. V. 8. P. 315–317.
- Mosna F., Sensebe L., Krampera M. // *Stem Cells Dev.* 2010. V. 19. P. 1449–1470.
- Panepucci R.A., Siufi J.L., Silva W.A., Jr., Proto-Siquiera R., Neder L., Orellana M., Rocha V., Covas D.T., Zago M.A. // *Stem Cells*. 2004. V. 22. P. 1263–1278.
- Lee R.H., Kim B., Choi I., Kim H., Choi H.S., Suh K., Bae Y.C., Jung J.S. // *Cell Physiol. Biochem.* 2004. V. 14. P. 311–324.
- Rubina K.A., Kalinina N.I., Efimenko A., Lopatina T.V., Melikhova V.S., Tsokolaeva Z.I., Sysoeva V., Tkachuk V.A., Parfenova E.V. // *Kardiologia*. 2010. V. 50. P. 51–61.
- Li F., Wang X., Niyibizi C. // *Bone*. 2010. V. 47. P. 546–555.
- Konno M., Hamazaki T.S., Fukuda S., Tokuhara M., Uchiyama H., Okazawa H., Okochi H., Asashima M. // *Biochem. Biophys. Res. Commun.* 2010. V. 400. P. 461–465.
- Tan G., Shim W., Gu Y., Qian L., Chung Y.Y., Lim S.Y., Yong P., Sim E., Wong P. // *Differentiation*. 2010. V. 7. P. 260–271.
- Banas A., Teratani T., Yamamoto Y., Tokuhara M., Takeshita F., Osaki M., Kato T., Okochi H., Ochiya T. // *J. Gastroenterol. Hepatol.* 2009. V. 24. P. 70–77.
- Park B.W., Kang D.H., Kang E.J., Byun J.H., Lee J.S., Maeng G.H., Rho G.J. // *J. Tissue Eng. Regen. Med.* 2011, in press, doi: 10.1002/term.404.
- Alvarez-Dolado M., Pardal R., Garcia-Verdugo J.M., Fike J.R., Lee H.O., Pfeffer K., Lois C., Morrison S.J., Alvarez-Buylla A. // *Nature*. 2003. V. 425. P. 968–973.
- Muraglia A., Cancedda R., Quarto R. // *J. Cell Sci.* 2000. V. 113 (Pt 7). P. 1161–1166.
- Tallone T., Realini C., Bohmler A., Kornfeld C., Vassalli G., Moccetti T., Bardelli S., Soldati G. // *J. Cardiovasc. Transl. Res.* 2011. V. 4. P. 200–210.
- Haasters F., Prall W.C., Anz D., Bourquin C., Pautke C., Endres S., Mutschler W., Docheva D., Schieker M. // *J. Anat.* 2009. V. 214. P. 759–767.
- Ratajczak J., Wysoczynski M., Zuba-Surma E., Wan W., Kucia M., Yoder M.C., Ratajczak M.Z. // *Exp. Hematol.* 2011. V. 39. P. 225–237.
- Jiang Y., Jahagirdar B.N., Reinhardt R.L., Schwartz R.E., Keene C.D., Ortiz-Gonzalez X.R., Reyes M., Lenvik T., Lund T., Blackstad M., Du J., Aldrich S., Lisberg A., Low W.C., Largaespada D.A., Verfaillie C.M. // *Nature*. 2002. V. 41. P. 41–49.
- Kuroda Y., Kitada M., Wakao S., Nishikawa K., Tanimura Y., Makinoshima H., Goda M., Akashi H., Inutsuka A., Niwa A., et al. // *Proc. Natl. Acad. Sci. USA*. 2010. V. 107. P. 8639–8643.
- Tolar J., Le Blanc K., Keating A., Blazar B.R. // *Stem Cells*. 2010. V. 28. P. 1446–1455.
- Mendez-Ferrer S., Michurina T.V., Ferraro F., Mazloom A.R., Macarthur B.D., Lira S.A., Scadden D.T., Ma'ayan A., Enikolopov G.N., Frenette P.S. // *Nature*. 2010. V. 466. P. 829–834.
- Lopatina T., Kalinina N., Karagyaur M., Stambolsky D., Rubina K., Revischin A., Pavlova G., Parfyonova Y., Tkachuk V. // *PLoS One*. 2011. V. 6. P. e17899.
- Rubina K., Kalinina N., Efimenko A., Lopatina T., Melikhova V., Tsokolaeva Z., Sysoeva V., Tkachuk V., Parfyonova Y. // *Tissue Eng. Part A*. 2009. V. 15. P. 2039–2050.
- Kinnaird T., Stabile E., Burnett M.S., Lee C.W., Barr S., Fuchs S., Epstein S.E. // *Circ. Res.* 2004. V. 94. P. 678–685.
- Efimenko A., Starostina E.E., Rubina K.A., Kalinina N.I., Parfenova E.V. // *Tsitologia*. 2010. V. 52. P. 144–154.
- Semenza G.L. // *J. Cell Biochem.* 2007. V. 102. P. 840–847.
- Cai L., Johnstone B.H., Cook T.G., Tan J., Fishbein M.C., Chen P.S., March K.L. // *Stem. Cells*. 2009. V. 27. P. 230–237.
- Uccelli A., Moretta L., Pistoia V. // *Nat. Rev. Immunol.* 2008. V. 8. P. 726–736.
- Sioud M. // *Scand. J. Immunol.* 2011. V. 73. P. 79–84.

REVIEWS

41. Pillai S., Cariappa A. // *Immunol. Cell. Biol.* 2009. V. 87. P. 16–19.
42. Sapoznikov A., Pewzner-Jung Y., Kalchenko V., Krauthgamer R., Shachar I., Jung S. // *Nat. Immunol.* 2008. V. 9. P. 388–395.
43. Beckermann B.M., Kallifatidis G., Groth A., Frommhold D., Apel A., Mattern J., Salnikov A.V., Moldenhauer G., Wagner W., Diehlmann A., et al. // *J. Cancer.* 2008. V. 9. P. 622–631.
44. Zhu Y., Sun Z., Han Q., Liao L., Wang J., Bian C., Li J., Yan X., Liu Y., Shao C., Zhao R.C. // *Leukemia.* 2009. V. 23. P. 925–933.
45. Djouad F., Bony C., Apparailly F., Louis-Pence P., Jorgensen C., Noel D. // *Transplantation.* 2006. V. 82. P. 1060–1066.
46. Djouad F., Pence P., Bony C., Tropel P., Apparailly F., Sany J., Noel D., Jorgensen C. // *Blood.* 2003. V. 102. P. 3837–3844.
47. Kucerova L., Matuskova M., Hlubinova K., Altanerova V., Altaner C. // *Mol. Cancer.* 2010. V. 9. P. 129.
48. Karnoub A.E., Dash A.B., Vo A.P., Sullivan A., Brooks M.W., Bell G.W., Richardson A.L., Polyak K., Tubo R., Weinberg R.A. // *Nature.* 2007. V. 449. P. 557–563.
49. Prantl L., Muehlberg F., Navone N.M., Song Y.H., Vykoukal J., Logothetis C.J., Alt E.U. // *Prostate.* 2010. V. 70. P. 1709–1715.
50. Torsvik A., Rosland G.V., Svendsen A., Molven A., Immervoll H., McCormack E., Lonning P.E., Primon M., Sobala E., Tonn J.C., et al. // *Cancer Res.* 2010. V. 70. P. 6393–6396.
51. Zhu W., Xu W., Jiang R., Qian H., Chen M., Hu J., Cao W., Han C., Chen Y. // *Exp. Mol. Pathol.* 2006. V. 80. P. 267–274.
52. Shinagawa K., Kitadai Y., Tanaka M., Sumida T., Kodama M., Higashi Y., Tanaka S., Yasui W., Chayama K. // *Int. J. Cancer.* 2010. V. 127. P. 2323–2333.
53. Spaeth E.L., Dembinski J.L., Sasser A.K., Watson K., Klopp A., Hall B., Andreeff M., Marini F. // *PLoS One.* 2009. V. 4. P. e4992.
54. Khakoo A.Y., Pati S., Anderson S.A., Reid W., Elshal M.F., Rovira I.I., Nguyen A.T., Malide D., Combs C.A., Hall G., et al. // *J. Exp. Med.* 2006. V. 203. P. 1235–1247.
55. Qiao L., Xu Z., Zhao T., Zhao Z., Shi M., Zhao R.C., Ye L., Zhang X. // *Cell Res.* 2008. V. 18. P. 500–507.
56. Qiao L., Xu Z.L., Zhao T.J., Ye L.H., Zhang X.D. // *Cancer Lett.* 2008. V. 269. P. 67–77.
57. Cousin B., Ravet E., Poglio S., De Toni F., Bertuzzi M., Lulka H., Touil I., Andre M., Grolleau J.L., Peron J. M., et al. // *PLoS One.* 2009. V. 4. P. e6278.
58. Secchiero P., Zorzet S., Tripodo C., Corallini F., Melloni E., Caruso L., Bosco R., Ingraio S., Zavan B., Zauli G. // *PLoS One.* 2010. V. 5. P. e11140.
59. Sacchetti B., Funari A., Michienzi S., Di Cesare S., Piersanti S., Saggio I., Tagliafico E., Ferrari S., Robey P.G., Riminucci M., Bianco P. // *Cell.* 2007. V. 131. P. 324–336.
60. Crisan M., Yap S., Casteilla L., Chen C.W., Corselli M., Park T.S., Andriolo G., Sun B., Zheng B., Zhang L., et al. // *Cell Stem Cell.* 2008. V. 3. P. 301–313.
61. Shi S., Gronthos S. // *J. Bone Miner. Res.* 2003. V. 18. P. 696–704.
62. Corselli M., Chen C.W., Crisan M., Lazzari L., Peault B. // *Arterioscler. Thromb. Vasc. Biol.* 2010. V. 30. P. 1104–1109.
63. Dore-Duffy P. // *Curr. Pharm. Des.* 2008. V. 14. P. 1581–1593.
64. Tang W., Zeve D., Suh J.M., Bosnakovski D., Kyba M., Hammer R.E., Tallquist M.D., Graff J.M. // *Science.* 2008. V. 322. P. 583–586.
65. Kiel M.J., Yilmaz O.H., Iwashita T., Terhorst C., Morrison S.J. // *Cell.* 2005. V. 121. P. 1109–1121.
66. Dellavalle A., Sampaoli M., Tonlorenzi R., Tagliafico E., Sacchetti B., Perani L., Innocenzi A., Galvez B.G., Messina G., Morosetti R., et al. // *Nat. Cell Biol.* 2007. V. 9. P. 255–267.
67. Traktuev D.O., Merfeld-Clauss S., Li J., Kolonin M., Arap W., Pasqualini R., Johnstone B.H., March K.L. // *Circ. Res.* 2008. V. 102. P. 77–85.
68. Saleh F.A., Whyte M., Ashton P., Genever P.G. // *Stem Cells Dev.* 2010. V. 20. P. 391–403.
69. Garrett R.W., Emerson S.G. // *Cell Stem Cell.* 2009. V. 4. P. 503–506.
70. Mendes S.C., Robin C., Dzierzak E. // *Development.* 2005. V. 132. P. 1127–1136.
71. Lo Celso C., Fleming H.E., Wu J.W., Zhao C.X., Miake-Lye S., Fujisaki J., Cote D., Rowe D.W., Lin C.P., Scadden D.T. // *Nature.* 2009. V. 457. P. 92–96.
72. Xie Y., Yin T., Wiegraebe W., He X.C., Miller D., Stark D., Perko K., Alexander R., Schwartz J., Grindley J.C., et al. // *Nature.* 2009. V. 457. P. 97–101.
73. Calvi L.M., Adams G.B., Weibrecht K.W., Weber J.M., Olson D.P., Knight M.C., Martin R.P., Schipani E., Divieti P., Bringham F.R., et al. // *Nature.* 2003. V. 425. P. 841–846.
74. Naveiras O., Nardi V., Wenzel P.L., Hauschka P.V., Fahey F., Daley G.Q. // *Nature.* 2009. V. 460. P. 259–263.
75. Armulik A., Genove G., Mae M., Nisancioglu M.H., Wallgard E., Niaudet C., He L., Norlin J., Lindblom P., Strittmatter K., et al. // *Nature.* 2010. V. 468. P. 557–561.
76. Chow A., Lucas D., Hidalgo A., Mendez-Ferrer S., Hashimoto D., Scheiermann C., Battista M., Leboeuf M., Prophet C., van Rooijen N., et al. // *J. Exp. Med.* 2011. V. 208. P. 261–271.
77. Lushaj E.B., Anstadt E., Haworth R., Roenneburg D., Kim J., Hematti P., Kohmoto T. // *Cytotherapy.* 2011. V. 13. P. 400–406.
78. Mazhari R., Hare J.M. // *Nat. Clin. Pract. Cardiovasc. Med.* 2007. V. 4. Suppl 1. P. S21–26.

NAD⁺-dependent Formate Dehydrogenase from Plants

A.A. Alekseeva^{1,2,3}, S.S. Savin^{2,3}, V.I. Tishkov^{1,2,3,*}

¹Chemistry Department, Lomonosov Moscow State University

²Innovations and High Technologies MSU Ltd

³Bach Institute of Biochemistry, Russian Academy of Sciences

*E-mail: vitishkov@gmail.com

Received 05.08.2011

Copyright © 2011 Park-media, Ltd. This is an open access article distributed under the Creative Commons Attribution License, which permits unrestricted use, distribution, and reproduction in any medium, provided the original work is properly cited.

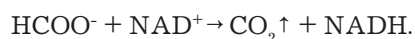
ABSTRACT NAD⁺-dependent formate dehydrogenase (FDH, EC 1.2.1.2) widely occurs in nature. FDH consists of two identical subunits and contains neither prosthetic groups nor metal ions. This type of FDH was found in different microorganisms (including pathogenic ones), such as bacteria, yeasts, fungi, and plants. As opposed to microbiological FDHs functioning in cytoplasm, plant FDHs localize in mitochondria. Formate dehydrogenase activity was first discovered as early as in 1921 in plant; however, until the past decade FDHs from plants had been considerably less studied than the enzymes from microorganisms. This review summarizes the recent results on studying the physiological role, properties, structure, and protein engineering of plant formate dehydrogenases.

KEYWORDS plant formate dehydrogenase; physiological role; properties; structure; expression; *Escherichia coli*; protein engineering.

ABBREVIATIONS FDH – formate dehydrogenase; PseFDH, CboFDH – formate dehydrogenases from bacteria *Pseudomonas* sp. 101 and yeast *Candida boidinii*, respectively; SoyFDH, AthFDH – plant formate dehydrogenases from soybean *Glycine max* and *Arabidopsis thaliana*, respectively.

INTRODUCTION

NAD⁺-dependent formate dehydrogenases (FDHs) [EC 1.2.1.2] belong to the family of enzymes catalyzing the oxidation of the formate ion to carbon dioxide, coupled with NAD⁺ reduction to NADH:



It is possible to distinguish two major FDH groups based on the differences in structure of these enzymes. The first group is comprised of formate dehydrogenases from anaerobic microorganisms and archae. FDHs in this group are heterooligomers with a complex quaternary structure and a high molecular weight. They are generally characterized by the presence of various prosthetic groups (iron–sulphur clusters, molybdenum and tungsten ions) in the active site and high sensitivity to oxygen [1, 2].

The second group is comprised of NAD⁺-dependent formate dehydrogenases consisting of two identical subunits, both having two active sites and containing neither metal ions nor prosthetic groups in the protein globule. FDHs of this group belong to the superfamily of D-specific dehydrogenases of 2-oxyacids [3]. The reaction of formate oxidation catalyzed by a FDH from

this group is the simplest example of dehydrogenation of carbonyl compounds, since there is neither the stage of proton transfer in the catalytic mechanism nor other stages of acid–base catalysis. The reaction rate is generally limited by the rate of hydride ion transfer from the substrate to the C4 atom of the nicotinamide ring [4]. Thus, FDH can be used as a model enzyme for studying the mechanism of hydride ion transfer in the active site of dehydrogenases that belong to this superfamily.

The active and systematic study of FDHs began in the early 1970s and was primarily devoted to enzymes from microorganisms. The physiological role of microbial FDHs is different. Thus, in methanol-utilizing bacteria and yeast, this enzyme participates in the supply of energy to a cell, whereas in pathogenic bacteria and fungi FDH is a stress protein. The properties and protein engineering of FDH were thoroughly discussed in [5, 6].

NAD⁺-dependent formate dehydrogenases from plants also belong to the second FDH group. Recent studies have revealed that FDH also belongs to stress proteins in plants, similar to those found in pathogenic microorganisms. FDH synthesis strongly increases under the following conditions: drought, with abrupt changes in temperature, irradiation with hard ultraviolet

let light, through the action of chemical agents [7–9], hypoxia [10], and action of pathogenic microorganisms [11]. The significance of the physiological role of this enzyme gives rise to the necessity of studying plant FDHs. Till now, there are no publications in which the data on plant FDHs are systematized. The major features of plant formate dehydrogenases, as well as their kinetic properties and stability, are summarized in this review; a detailed description of the physiological role of FDH is also presented.

DISCOVERY HISTORY, LOCALIZATION, AND PHYSIOLOGICAL ROLE OF PLANT FDHS

Plant FDH was first found in beans (*Phaseolus vulgaris*) in 1921 [12].

The first attempt to provide a detailed description of FDH and to assess the role of this enzyme in plant metabolism was made by Davison in 1951 [13], by the example of formate dehydrogenases from pea and bean seeds. The role of FDH was believed to consist in the production of NADH, which was subsequently consumed for the formation of ethanol, succinate, and glutamate in coupled reactions. Thus, the role of FDH as a “supplier” of NADH molecules to fit the various needs of a cell was first defined. An assumption concerning the mechanisms of the emergence of formate in a plant cell was made in the same study. According to the first hypothesis, formate could be formed along with ethanol and acetic acid as a result of anaerobic respiration. According to an alternative hypothesis, formate could be formed during the oxidation of glycolic acid; however, no unambiguous data that would corroborate a certain metabolic pathway, during which formate is formed, have been obtained thus far.

The first experiments for determining the localization of FDHs in plant cells were carried out in 1956. It was revealed that formate dehydrogenase activity was primarily present in mitochondria [14]. However, due to the fact that the samples under study were contaminated with other organelles, it couldn't be unequivocally proven that FDH is localized in mitochondria. In 1960, it was demonstrated that FDH was localized not only in seeds, but also in other plant parts. Formate dehydrogenase activity was revealed in cabbage and spinach leaves, roots of garden radish and turnip, cauliflower buds, and pumpkin fruits [15]. It was demonstrated using spinach leaves that there were at least two pathways for formate oxidation in a plant cell: by FDH in mitochondria and by peroxidase in peroxisomes [16]. It was ascertained in separate experiments that formate was oxidized by FDH in mitochondria at $\text{pH} > 6$, while peroxidase in peroxisomes plays the major role in formate oxidation at lower pH values. Later, it was shown that FDH in mitochondria was a component of a pro-

tein complex with a molecular weight of approximately 200 kDa rather than being an individual molecule [17]. These complexes can potentially be formed by glycine decarboxylase and fumarase; their concentration increasing synchronically with rising FDH activity [9].

It was shown in systematic studies that formate dehydrogenase activity was strongly dependent both upon a plant and upon a particular plant organ containing the enzyme [18]. The dependence of enzymatic activity on the rate of oxygen consumption by a plant was also revealed. Thus, in plants with high oxygen consumption (spinach, tobacco, etc.), formate dehydrogenase activity was higher than that in a plant with low oxygen consumption (the Leguminosae, lettuce, etc.) [18]. In this study, the hypothesis was postulated that in oxidation of NADH obtained via the formate dehydrogenase reaction, the accumulated energy was consumed for ATP formation via the electron transport chain, thus satisfying the energy demand of the cell [18]. Unfortunately, high variation of FDH activity in different plants prevents the unambiguous answering of the question concerning the role of this enzyme in the metabolism. The relationship between formate metabolism and plant response to stress was first noted in 1978 [19], the increased formation of labelled carbon dioxide from formate was observed in barley, which was grown under overwatering conditions.

In 1992, research into the physiological role of formate dehydrogenase from plants was raised to a new level [20]. It was revealed that the mitochondria of non-photosynthesizing tissues of potato contained an unknown peptide with a molecular weight of approximately 40 kDa, which composed up to 9% of all mitochondrial proteins. cDNA of this polypeptide was cloned in 1993; the analysis of the amino acid sequence encoded by this cDNA demonstrated 55% homology with FDH from *Pseudomonas* sp. 101 [21]. Comparison of the N-terminal sequences of natural FDH and polypeptide translated from cDNA revealed that the theoretical protein contained an additional signal peptide consisting of 23 amino acid residues, which provided the transport of pro-enzyme from cytoplasm inside mitochondria. Polypeptides of the same molecular mass were found in pea, tomato, and onion; the FDH content in the mitochondria of non-photosynthetic tissues (tubers and roots) was approximately eightfold higher than that in leaves [20]. Moreover, FDH concentration sharply increased in plants which were grown in the dark (pea stems, chicory leaves, carrot roots, sweet potato tubers, etc.) [20].

Actually, numerous data have been published supporting the fact that FDH is synthesized at a high concentration under conditions that are unfavourable to plant growth, e.g.: drought, low temperature, hard

ultraviolet radiation, exposure chemical agents, deficiency of both light and iron, and low oxygen concentration. However, the response rate strongly depended on the type of interaction. Thus, the fastest response of potato plants, which manifests itself by mRNA synthesis, was observed upon direct damage to plant tissue (~20 min), whereas the average response time for other types of impacts was equal to 8 h [7]. Under conditions of iron deficiency, the amount of formate dehydrogenase mRNA in barley roots began to increase after 1 day, attaining the maximum value after 14 days [8, 22], whereas the synthesis of formate dehydrogenase in leaves did not change. Under anaerobic stress, the concentration of FDH mRNA in barley roots increased as early as after 12 h, attaining the maximum value by the 48th hour. In maritime pine, the biosynthesis of FDH is enhanced during a drought [23]. An increase in the level of FDH mRNA was also observed in *Lotus japonicus* plants cultivated under conditions of hypoxia [10].

The gene expression in moss *Physcomitrella patens* responding to stress was studied in [24]. Moss plants were treated with abscisic acid (hormone inducing the transfer of plants to the rest period and being capable of decelerating stem growth, which is accumulated in seeds and buds in Autumn) followed by cooling to +4°C. It was found that abscisic acid induced an increase in resistance of moss to low temperatures; it also altered the set of expressed genes. FDH is one of the enzymes whose gene is expressed under the action of abscisic acid. It turned out that the level of FDH gene expression increased during several hours following treatment with abscisic acid and when the plants were stored in cold temperature for 24 h. In the absence of abscisic acid, the response to the impact of low temperatures occurs much more slowly. Treatment with sodium chloride at high concentrations (0.125 and 0.25 M) and mannitol (0.25 and 0.5 M) enhanced both the resistance of the moss to low temperatures and the expression of a number of genes, including the FDH gene. It was thus demonstrated that formate dehydrogenase was a stress protein both in higher plants and in mosses; the level of its biosynthesis could be regulated by hormones. Other plant hormones, such as auxin and cytokinin, also have an effect on FDH activity in higher plants [25].

The synthesis of FDH was also studied in *Arabidopsis thaliana*, being exposed to various factors. It was the first plant for which the complete nucleotide sequence of the genome was determined; therefore, in many cases *A. thaliana* is used as a model plant. The plants were sprayed with various C1-compounds (methanol, formaldehyde, and formate) followed by the Northern blot analysis using FDH cDNA as a probe. The most intensive expression of the FDH gene was observed for treatment with formaldehyde or methanol. A lower

level of expression was observed in the samples sprayed with formate and deionized water. An increase in the expression of the FDH gene was not recorded, neither in plants with their leaves pruned nor in the control sample. These data enabled one to reasonably conclude that the synthesis of FDH was induced to a larger extent not by the formate substrate, but by its reduced form (formaldehyde) [26]. It was also demonstrated [27] that one-carbon compounds (methanol, formaldehyde, and formate) induced the synthesis of FDH in plant leaves. Methanol has a direct effect on the synthesis of FDH transcripts, while its oxidized modifications (formaldehyde, formate) can act as signalling molecules. An analysis of the N-terminal region of the enzyme allowed one to assume that FDH can also be transported to chloroplasts. The dual localization of FDH, both in mitochondria and chloroplasts, was shown in transgenic *A. thaliana* and tobacco plants containing the AthFDH gene [28].

The origin of formate in cells of the plants exposed to stress remains unknown. The hypothesis has been put forward suggesting that formate may be synthesized during photorespiration, in the methanol metabolism, or from glyoxylate formed from different products of the Krebs cycle [7]. The formation of formate by the serine pathway as it takes place in bacteria [1] has been discussed, since the introduction of serine resulted in the increase in FDH concentration in potato plants. In further experiments [29], the transgenic potato with suppressed synthesis of FDH was obtained. It was revealed that formate that does not undergo further oxidation to carbon dioxide was accumulated in the tissues of transgenic plants. It was also shown that proline and its precursor glutamate were formed at a high concentration in transgenic potato under conditions of drought.

The metabolism of formate and its physiological role have been well studied [30]. In photosynthesizing potato tissues, formate is the major precursor of all other carbon-containing compounds; it is basically synthesized via ferredoxin-dependent fixation of carbon dioxide. In other tissues, formate is a side product of photorespiration and some enzymatic processes; its formation seems to result from the direct reduction of carbon dioxide in chloroplasts. In potato plants, the metabolism of formate is associated with the synthesis of serine.

A close relationship between the biosynthesis of formate and serine also exists in *A. thaliana* [31]. Three lines of transgenic plants with enhanced expression of FDH were obtained. Formate concentration in transgenic plants was almost identical to that in wild-type *A. thaliana*. Following the introduction of labelled formate, the intensity of formation of radioactively labelled carbon dioxide in transgenic plants was much

higher, whereas serine accumulation remained at the same level. Transgenic *A. thaliana* plants with an enhanced level of FDH gene expression were also obtained in [32].

Phosphorylation is the most important method of metabolism regulation. 14 proteins of potato mitochondria, which can be presented in the phosphorylated form, have been discovered [33]; among them FDH can also be found. The amino acid residues of mitochondrial FDH of potato, which undergo phosphorylation (Thr76 and Thr333) have been identified [34]. An analysis of the FDH structure demonstrated that these two threonine residues were located on the surface of a protein globule and could be easily accessible for kinases catalyzing the phosphorylation process. A high phosphorylation level is observed in the E1- α subunit of pyruvate dehydrogenase (PDH). The phosphorylation of both FDH and pyruvate dehydrogenase is regulated by the variation of concentrations of NAD⁺, formate, and pyruvate, which attests to the similarity in the mechanisms of regulation of the function of these enzymes. The level of phosphorylation of the enzyme is considerably reduced with increasing concentrations of NAD⁺, formate, and pyruvate. It is assumed that pyruvate can be converted into formate in the reaction catalyzed by pyruvate formate lyase (PFL) followed by the oxidation of formate with the participation of FDH.

Formate ion takes part in a great number of metabolic processes with complicated regulation, as can clearly be seen from the data provided. The most complete scheme of participation of formate in plant metabolism can be found in [11].

Recent studies have attested to the fact that FDH content in plant mitochondria increases in response not only to physical and chemical factors, but also as a result of a “biological attack”. The activation of biosynthesis of FDH was observed following infection of the English oak with the pathogenic fungus, *Piloderma croceum* [35]; wheat, with fungus *Blumeria graminis f. sp. tritici* [36]; and the common bean, with fungus *Colletotrichum lindemuthianum* [11]. The common bean genome contains three FDH genes; their expression is regulated by the type of exposure factor. It is assumed that synthesis of FDH in wheat is induced by methanol as a result of the impact of pectin methyltransferase on pectin. In plants of the common tobacco *Nicotiana attenuata* damaged by *Manduca sexta* caterpillars, fatty acid conjugates initiating the synthesis of a number of proteins, including FDH, are released [37].

Summarizing this section, let us note that formate dehydrogenase is a universal enzyme involved in the cell stress response caused by both exogenic (negative ambient impact) and endogenic (deficiency of essential microelements, exposure to pathogens) processes. This

fact attests to the key role of FDH in metabolism processes of higher plants. The production of mutant forms of FDH characterized by an enhanced catalytic activity and the insertion of their genes into the plant genome instead of wild-type enzyme genes represents a fundamentally new approach to the design of plants with an enhanced resistance to stress.

THE FEATURES OF THE PRIMARY STRUCTURE OF PLANT FDH

Due to the active development of mega-sequencing methods, a new genome structure of various organisms, including plants, is published almost every day. Searching in GenBank (GB), EMBL, and KEGG (<http://www.genome.jp/>) databases enabled us to find nucleotide sequences of genes (complete or as cDNA) of plant FDH from over 70 sources. Moreover, study [11] presents a number of sequences that are not present in the databases. *Table 1* lists the names of the plants and the contracted notations of FDHs. FDHs that are characteristic of various microorganisms, such as enzymes from methylotrophic bacteria *Pseudomonas* sp. 101 (the most well studied FDH to this moment), *Moraxella* sp. C2, pathogenic bacteria *Burkholderia stabilis* and *Bordetella bronchiseptica* RB50 (*Alcaligenes bronchisepticus*), uncultured marine alpha proteobacteria and nitrogen-fixing bacteria *Sinorhizobium meliloti*, yeasts *Saccharomyces cerevisiae* and *Candida boidinii*, were used for comparison.

The presence of a signal peptide, which is responsible for FDH transport from the cytoplasm to mitochondria, at the N-terminus of the synthesized proenzyme is the distinctive feature of plant FDHs [21]. Bacterial and yeast FDHs contain no signal peptides. The genes of FDHs from a number of pathogenic fungi also contain the nucleotide sequence encoding the signal peptide. However, depending on the condition of a host cell, the RNA synthesized from the FDH gene undergoes alternative splicing, resulting in the formation of different mRNAs encoding proteins both with and without the signal peptide [49].

Figure 1 shows the signal sequences of formate dehydrogenases from various sources. The potential specific sequences providing the transport of an enzyme to mitochondria are underlined. The residue, after which the cleavage of the signal peptide occurs, is shown in green italics. In the majority of formate dehydrogenases, it is the arginine residue. Serine residue (FDH from sorghum SbiFDH1, castor bean tree RcoFDH1), lysine (grape VviFDH1), proline (FDHs from soybean SoyFDH1 and SoyFDH2, isoforms 1 and 2) can also be found in this position. The signal sequence of FDH is enriched in amino acid residues containing hydroxyl or positively charged groups and is capable of form-

REVIEWS

Table 1. The sources and contracted notations of formate dehydrogenases considered in the present study

Organism		FDH	Reference
Latin name	English name		
PLANTS			
<i>Antirrhinum majus</i>	Common Snapdragon	AmaFDH1	KEGG: EST 2545
<i>Aquilegia formosa x Aquilegia pubescens</i>	Buttercup	ApuFDH1	KEGG: EST 273
		ApuFDH2	[11]
<i>Arabidopsis thaliana</i>	Mouse-ear cress	AthFDH	EMBL AF208029
<i>Brachypodium distachyon</i>	Purple false brome	BdiFDH1	[11]
<i>Brassica napus</i>	Rapeseed	BnaFDH1	[11]
		BnaFDH2	KEGG: EST 21261
<i>Brassica oleracea</i>	Cabbage	BolFDH1	[11]
<i>Cryptomeria japonica</i>	Japanese cedar	CjaFDH1	KEGG: EST 5066
<i>Carica papaya</i>	Papaya	CpaFDH1	KEGG: EST 3924
<i>Citrus reticulata</i>	Tangerine	CreFDH3	KEGG: EST 11052
<i>Citrus sinensis</i>	Sweet orange	CsiFDH1	[11]
<i>Coffea canephora</i>	Coffea canephora	CcaFDH1	KEGG: EST 1007
<i>Festuca arundinacea</i>	Tall fescue	FarFDH1	KEGG: EST 5855
<i>Glycine max</i>	Soybean	SoyFDH1	GB AK244764, [38]
		SoyFDH2	GB Bt094321
		SoyFDH3	GB AK243932, [38]
		SoyFDH4	GB BT095613
		SoyFDH5	KEGG: EST 19520
<i>Gossypium arboreum</i>	Tree cotton	GarFDH1	KEGG: EST 1085
<i>Gossypium hirsutum</i>	Tree cotton	GhiFDH1	KEGG: EST 19680
<i>Gossypium raimondii</i>	Tree cotton	GraFDH1	KEGG: EST 213
<i>Helianthus annuus</i>	Common sunflower	HanFDH1	[11]
<i>Hordeum vulgare</i>	Barley	HvuFDH1	GB D88272, [8]
<i>Ipomoea batatas</i>	Sweet potato	IbaFDH	EMBL BM878811
<i>Lactuca saligna</i>	Willowleaf lettuce	LsaFDH1	KEGG: EST 1616
<i>Lotus japonicus</i>	–	LjaFDH1	GB FM865900, [10]
<i>Lycopersicon esculentum</i>	Tomato	LesFDH1	GB AJ849378
<i>Malus domestica</i>	Apple	MdoFDH	EMBL CN496368
<i>Manihot esculenta</i>	Cassava	MesFDH1	KEGG: EST 2788
<i>Medicago truncatula</i>	Barrel Medic	MtrFDH1	KEGG: EST 1503
<i>Mesembryanthemum crystallinum</i>	Common ice plant	McrFDH	GB BE035085
<i>Nicotiana tabacum</i>	Common tobacco	NtaFDH1	[11]
<i>Oryza sativa Japonica group</i>	Japanese rice	OsaFDH_Ja	GB AK065872, [39]
<i>Oryza sativa indica cultivar-group</i>	Indian rice	OsaFDH_In	GB CT832868, [40]
<i>Oryza sativa</i>	Rice	OsaFDH1	AB019533, [41]
<i>Panicum virgatum</i>	Switchgrass	PviFDH1	KEGG: EST 8602
<i>Phaseolus vulgaris</i>	Common bean	PvuFDH1	GB ACZ74695, [42]
<i>Phyllostachys edulis</i>	Moso bamboo	PedFDH	GB FP093692
<i>Physcomitrella patens</i>	Moss <i>Physcomitrella patens</i>	PpaFDH	GB XM001768721, [43]
<i>Picea glauca</i>	White spruce	PglFDH1	KEGG: EST 2327
<i>Picea sitchensis</i>	Sitka spruce	PsiFDH	GB EF085163, [44]
<i>Pinus pinaster</i>	Maritime pine	PpiFDH1	KEGG: EST 174

REVIEWS

<i>Pinus taeda</i>	Loblolly pine	PtaFDH1	[11]
		PtaFDH2	KEGG: EST 2972
		PtaFDH3	KEGG: EST 15504
<i>Populus nigra</i>	Lombardy poplar	PniFDH2	KEGG: EST 7989
<i>Populus tremula</i>	Aspen	PtmFDH1	KEGG: EST 4757
<i>Populus trichocarpa</i>	Western balsam poplar	PtrFDH1	PtrFDH1 GB XM002320465, [45]
<i>Prunus persica</i>	Peach tree	PpeFDH1	KEGG: EST 4281
<i>Quercus robur</i>	English oak	QroFDH1	GB AJ577266.2, [35]
<i>Raphanus raphanistrum</i> subsp. <i>raphanistrum</i>	Wild radish	RraFDH1	KEGG: EST 15157
<i>Ricinus communis</i>	Castor bean tree	RcoFDH1	GB XM_002517292
<i>Saccharum officinarum</i>	Sugarcane	SofFDH1	KEGG: EST 18227
<i>Solanum tuberosum</i>	Potato	StuFDH1	GB Z21493, [21]
<i>Sorghum bicolor</i>	Sorghum	SbiFDH1	GB XM002438363, [46]
		SbiFDH2	GB XM002454363, [46]
<i>Taraxacum officinale</i>	Common dandelion	TofFDH1	[11]
<i>Theobroma cacao</i>	Cacao tree	TcaFDH1	KEGG: EST 10274
<i>Triphysaria pusilla</i>	Dwarf owl's-clover	TpuFDH1	KEGG: EST 5550
<i>Triticum aestivum</i>	Common wheat	TaeFDH1	TaeFDH1 GB AK332605, [47]
<i>Vigna unguiculata</i>	Cowpea	VunFDH1	KEGG: EST 6491
<i>Vitis vinifera</i>	Grape	VviFDH1	GB XM002278408
<i>Yucca filamentosa</i>	Bear grass	YfiFDH1	YfiFDH1 [11]
<i>Zea mays</i>	Maize	ZmaFDH	GB EU967680, [48]
<i>Zingiber officinale</i>	Ginger	ZofFDH1	KEGG: EST 5316
FUNGI			
<i>Aspergillus oryzae</i>	Fungus <i>Aspergillus oryzae</i>	AorFDH1	NCBI XM001827498
<i>Mycosphaerella graminicola</i>	Fungus <i>Mycosphaerella graminicola</i>	MgrFDH	GB AW180713 180985
<i>Penicillium marneffeii</i>	Fungus <i>Penicillium marneffeii</i>	PmaFDH1	GB XM002153251
<i>Ajellomyces capsulatus</i>	Darling's disease fungus	AjcFDH1	[49]
		AjcFDH3	
YEASTS			
<i>Candida boidinii</i>	Methylotrophic yeast <i>Candida boidinii</i>	CboFDH	EMBL AF004096
<i>Saccharomyces cerevisiae</i>	Baker's yeast	SceFDH	EMBL Z75296
BACTERIA			
<i>Pseudomonas</i> sp. 101	Methylotrophic bacterium <i>Pseudomonas</i> sp. 101	PseFDH	[50]
<i>Moraxella</i> sp. C2	Methylotrophic bacterium <i>Moraxella</i> sp.	MorFDH	EMBL Y13245
<i>Burkholderia stabilis</i>	Bacterium <i>Burkholderia stabilis</i>	BstFDH	[51]
<i>Bordetella bronchiseptica</i> RB50 (<i>Alcaligenes bronchisepticus</i>)	Bacterium <i>Bordetella bronchiseptica</i> RB50 (<i>Alcaligenes bronchisepticus</i>)	BbrFDH	EMBL BX640441
Uncultured marine alpha proteobacterium	Uncultured marine alpha proteobacterium	BbrFDH	EMBL BX640441
<i>Sinorhizobium meliloti</i>	Nitrogen-fixing <i>Sinorhizobium meliloti</i>	SmeFDH	Ae006469, [52]

REVIEWS

BdiFDH1-----MAMWRAAARQLVDRALVGSRAAHTSAG-SKKIVGVF
 PedFDH1-----MAMWRAAARQLVDRALGSRRAAHTSAG-SKKIVGVF
 FarFDH1-----MWRAAARHLVDRALGSRRAAHTSAG-SKKIVGVF
 HvuFDH1-----MAAMWRAAARQLVDRAVGSRRAAHTSAG-SKKIVGVF
 TaeFDH1-----MAAMCRAAARQLVDRAVGSRRAAHTSAG-SKKIVGVF
 SbiFDH1-----MAMWRAAARQLVDRALGSSAAHTSAG-SKKIVGVF
 SofFDH1-----MAMWRAAARQLVDRALGSRRAAHTSAG-SKKIVGVF
 ZmaFDH1-----MAMWRAAARQLVDRALGSRRAAHTSTG-SKKIVGVF
 PviFDH1-----MAMWRAAARQLVDRALGARAHTSAG-SKKIVGVF
 OsaFDH1-----MAMWRAAAGHLLGRALGSRRAAHTSAG-SKKIVGVF
 SbiFDH2-----MAMWRAAARQLVDRALGSRRAAHTSAG-SKKIVGVF
 LjaFDH1-----MAMKRAASSAVRSLLTAPTNPSSSIFSRNLHASGG-KKKIVGVF
 MtrFDH1-----MAMKRAASTLITASSKISSLSPPSSITRDLHASGG-KKKIVGVF
 PvuFDH1-----MAMKRAASSAFRSLSSSTFSRNLH-----KKIVGVF
 VunFDH1-----MAMRRAAGSSAIRSLFSSSTFSRNLHVSAGE-KKKIVGVF
 SoyFDH3-----MAMMKRAASSVRSLSSSSSTFTRNHLHASEG-KKKIVGVF
 SoyFDH4-----MAMMKRAASSALRSLSSSTFTRNHLHASEG-KKKIVGVF
 SoyFDH1--MSNFTLKMSDPTLAQOHLVKVHTTTHETVVTTHNNHQTPSINASGE-KKKIVGVF
 SoyFDH2--MLNFTLKMSDPTLAQPHLVKHTT-LETVVTTHNNHNRPSINASGE-KKKIVGVF
 SoyFDH5-----MAMKRAVQSLSSSTFTRNHLHASEG-KKKIVGVF
 TofFDH1-----MAIAMKRAAAAATRAISSANSIGSIFTRHLHASSG-KKKIVGVF
 LsaFDH1-----MAIAMKSDSGSILTRHLHASSG-KKKIVGVF
 HanFDH1-----MAMSMAMKRSAAAATRALSSATSSLLTRDLHSSGG-KKKIVGVF
 AmaFDH1-----MAMKRAAVTAVRALTSSAPSSVLTRELHASP-G-KKKIVGVF
 TpuFDH1-----MAMKRAVASTVGAITSSGNPASSVLARYLHASP-G-KKKIVGVF
 LesFDH1-----MAMRRVASTAARAIASPSLVTRELQASPG-KKKIVGVF
 StuFDH1-----MAMSRVASTAARAITSPSSLVTRELQASPG-PKKIVGVF
 NtaFDH1-----MAMRRVASTAARAFASSSPSSLVTRELQASPG-KKKIVGVF
 VviFDH1-----MAMMKRVAESAVRAFALGSTSGALTTRHLHASEG-KKKIVGVF
 MesFDH1-----MKRAATSARAFSSSFGISGSSALGRHLHASEG-KKKIVGVF
 GraFDH1-----MKQVANSAIKAIANSNGSSLLTRQLHASP-G-KKKIVGVF
 GarFDH1-----MKQVANSAIKAIANSNGSSLLTRQLHASP-G-KKKIVGVF
 GhiFDH1-----MKQVANSAIKAIANSNGSSLLTRQLHASP-G-KKKIVGVF
 TcaFDH1-----MKQVASSAIKALANSNGSSVLTRELHASP-G-KKKIVGVF
 CcaFDH1-----MAMKRVAASALRAFTSSNGSTSSLLTRQLHASP-G-KKKIVGVF
 IbaFDH1-----MAMRRVAASGLRAFASYGNPS--LLTRQLHASP-G-KKKIVGVF
 ApuFDH1-----MATRKAVVLGAQSLRRSSSTSSPSIRNLHASSE-KKKIVGVF
 ApuFDH2-----MKKAALSTVQSVLSSSSSTSSLLTRHLHASEG-KKKIVGVF
 YfiFDH1-----MAMLRRAAKQAIQTLGSRIPSSSTFSRHLHASP-G-KKKIVGVF
 ZofFDH1-----MAMLRRAAKHAMRALGSRAPDASPFAARMLHASTG-KKKIVGVF
 QroFDH1-----MAGAATSIAIKSVLTRHLHASP-G-KKKIVGVF
 RcoFDH1-----MKSYSKRIALWLQRIEDGASDVTEELGVSINASAG-SKKIVGVF
 BnaFDH2-----MAMRRVTRAAIRASCVSSSSSGYFARKFNASSGDSKKIVGVF
 BolFDH1-----MAMRRVIRASCVSSSSSGYFARKFNASSGDSKKIVGVF
 CsiFDH1-----MAMKRVAASAINAFASSGYLRSRSSFRRHY-ASSG-RKKIVGVF
 MdoFDH1-----MASKGVIASAVRALASSGSSASSTFTTRHLHASSG-KKKIVGVF
 PpeFDH1-----MKGVIASAVRTLASSGSSASSTFTTRHLHASP-G-KKKIVGVF
 CpaFDH1-----MKRAATSARAFASSTQTSFGLSTNFAARNLHASP-G-KKKIVGVF
 CreFDH3-----MKRVASSAINAFASSGYLRSRSSFRRHY-ASSG-SKKIVGVF
 BnaFDH1-----MAMRRTGAIASCVSSSSSGYFARQFNASSGDSKKIVGVF
 AthFDH1-----MAMRQAATKATIRACSSSSSGYFARQFNASSGDSKKIVGVF
 RraFDH1-----MAMQAARACVSSNSGFLSRHLHASSGDSKKIVGVF
 PpiFDH1-----MASRRAVISAFRAASRRPICSPVSSIASSVRELHAPAG-SNKIVGVF
 PtaFDH2-----MASRRSVISAFRAASRRPICSPVSSIASSVRELHAPAG-SNKIVGVF
 PtaFDH3-----MASKRAVISAFRAASRRPICSPVSSIASSVRELHAPAG-SNKIVGVF
 PtaFDH1-----MASRRSVISAFRAASRRPICSPVSSIASSVRELHAPAG-SNKIVGVF
 PsiFDH1-----MASKRAVISTFRAASRRPICSPVSSIASSVRELHAPAG-SNKIVGVF
 PglFDH1-----MASKRAVISTFRAASRRPICSPVSSIASSVRELHAPAG-SNKIVGVF
 CjaFDH1-----MASKRAVKS--AAQ-----AFSPL-SSIRALHAPAG-PNKIVGVF
 PtrFDH1-----MAMKRAATSARAFSSSSPASSVSSGSSSTRLLHASAE-SKKIVGVF
 PtmFDH1-----MAMKRAATSARAFSSSSPASSVSSGSSSTRLLHASAE-SKKIVGVF
 PniFDH2-----MAMKRAATSARAFSSSPASSVSSGSSSTRLLHASAE-SKKIVGVF
 McrFDH1-----MKRATASAIRAMVASSSTNSSTILSRNLHASSD-SKKIVGVF
 AorFDH1-----MTFARSITRAALKASPLSRASRTFSSSSSAQS~~KVLMVL~~
 MgrFDH1--MVFARSSLRMARPASSLLSQRTASFTQRGANLARAGGV~~RTLTSTSSRQGVLLVL~~
 PmaFDH1-----MVFSRSIPRALQRPATSLLAIPARQWRAPVFS~~GVRTLTASAPRQGVLLVL~~
 AjcFDH3-----MGRGLPRSSSAPFPQYNTQSYGLPLRPLPSL~~TRVITLTASPKLQGVLLVL~~
 AjcFDH1-----MGRGLPRSSSAPFPQYNTQSYGLPLRPLPSL~~TRVITLTASPKLQGVLLVL~~
 PseFDH1-----MAKVL~~CVL~~

Fig. 1. Signal sequences of plant formate dehydrogenases. Here and in Figs. 2,3, abbreviations of enzymes are those from Table 1. Plant enzymes are highlighted in green; fungi enzymes are highlighted in magenta; FDHs from bacteria are highlighted in blue. Specific sequences that are responsible for the transport of the enzyme to mitochondria are underlined. The residue, after which the signal peptide is eliminated, are highlighted in green italics.

ing an amphiphilic α -helix. The signal sequence is highly conserved. Thus, the deletion of only two N-terminal amino acids blocks the transport of the enzyme to the mitochondria [53]. It was ascertained that the N-terminal MAM motif enabled swift transport of the enzyme to mitochondria to be performed. Figure 1 shows the N-terminal sequences of 63 plant FDHs; 35 enzymes of those have the MAM motif at position 1–3. A number of plant FDHs have similar motifs at their N-terminal fragments: MAAM (in two plant FDHs) and MAS (in eight plant FDHs). The N-terminal amino acid sequences of isoenzymes 1 and 2 of soybean FDHs are significantly different from those of other plant formate dehydrogenases, both in terms of their composition (it starts with MSN an MLN) and size, which attests to the possible specific function of these FDH isoforms. The N-terminal sequences of FDHs from fungi *Aspergillus oryzae*, *As. flavus*, *Penicillium marneffei*, *Mycosphaerella graminicola*, and *Ajellomyces capsulatus* are also shown in Fig. 1 (the names are highlighted in pink). Two enzyme isoforms from *Aj. capsulatus* (AjcFDH1 and AjcFDH3) are also given, which result from the alternative splicing of mRNA [49]. Some sequences also contain an arginine residue, at which the cleavage of the signal peptide may occur (the residue is highlighted in pink italics). A similar mechanism of the FDH transport to different cell organelles seems to exist in fungi. The Lys and Val residues that are totally conserved in all formate dehydrogenases are shown in red in Fig. 1. The N-terminal sequence of formate dehydrogenase from *Pseudomonas* sp. 101 that is highly homologous to the N-terminal region AjcFDH3 without the signal peptide is shown for comparative purposes. As can be seen in Fig. 1, signal peptide sequences in enzymes from the plants belonging to one family (the family Solanaceae: tomatoes, potato; the family Gramineae: rice, barley, rye, etc.) have a high degree of homology.

In most plants, FDH is located in the mitochondria; however, the thorough

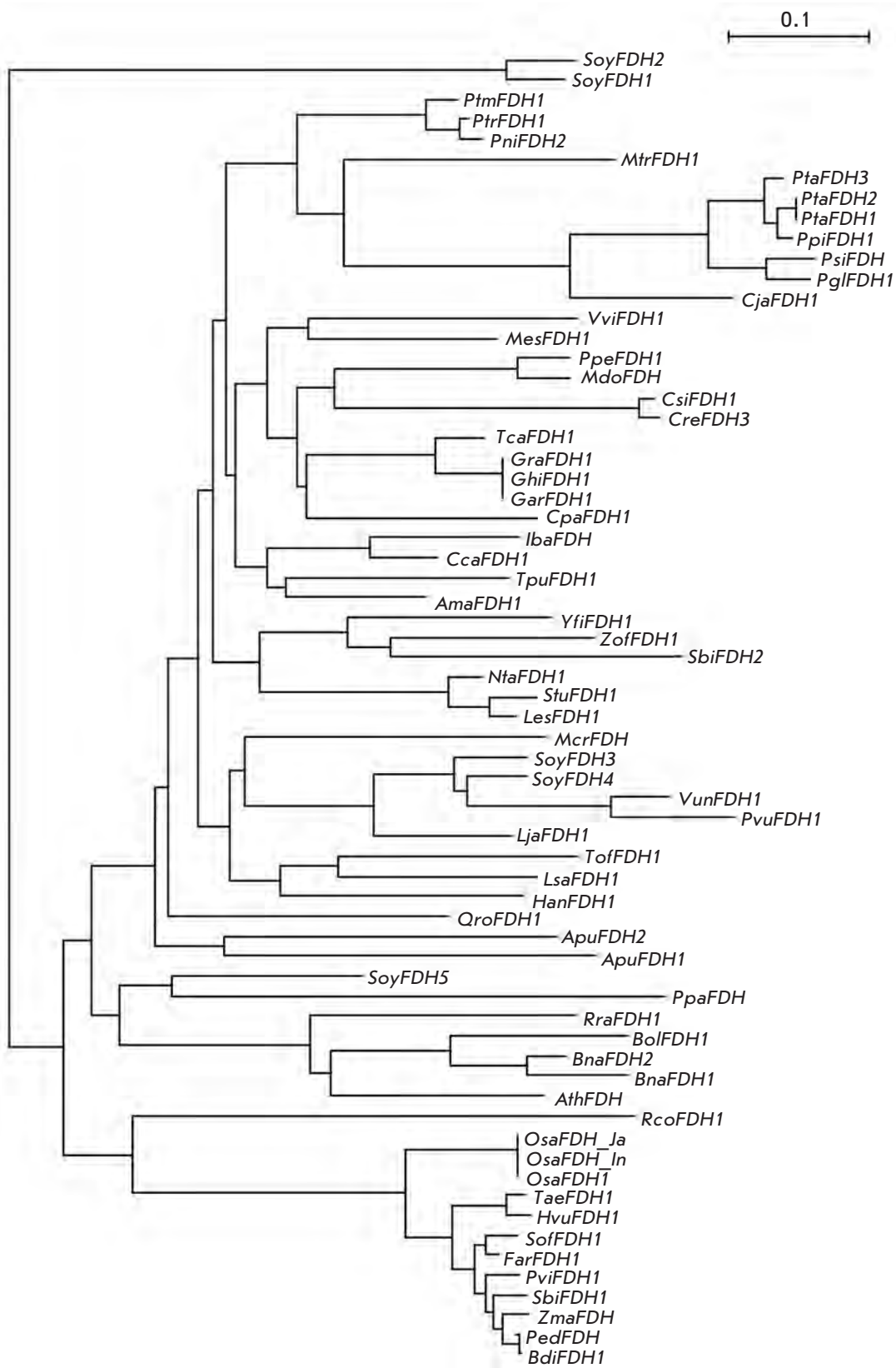


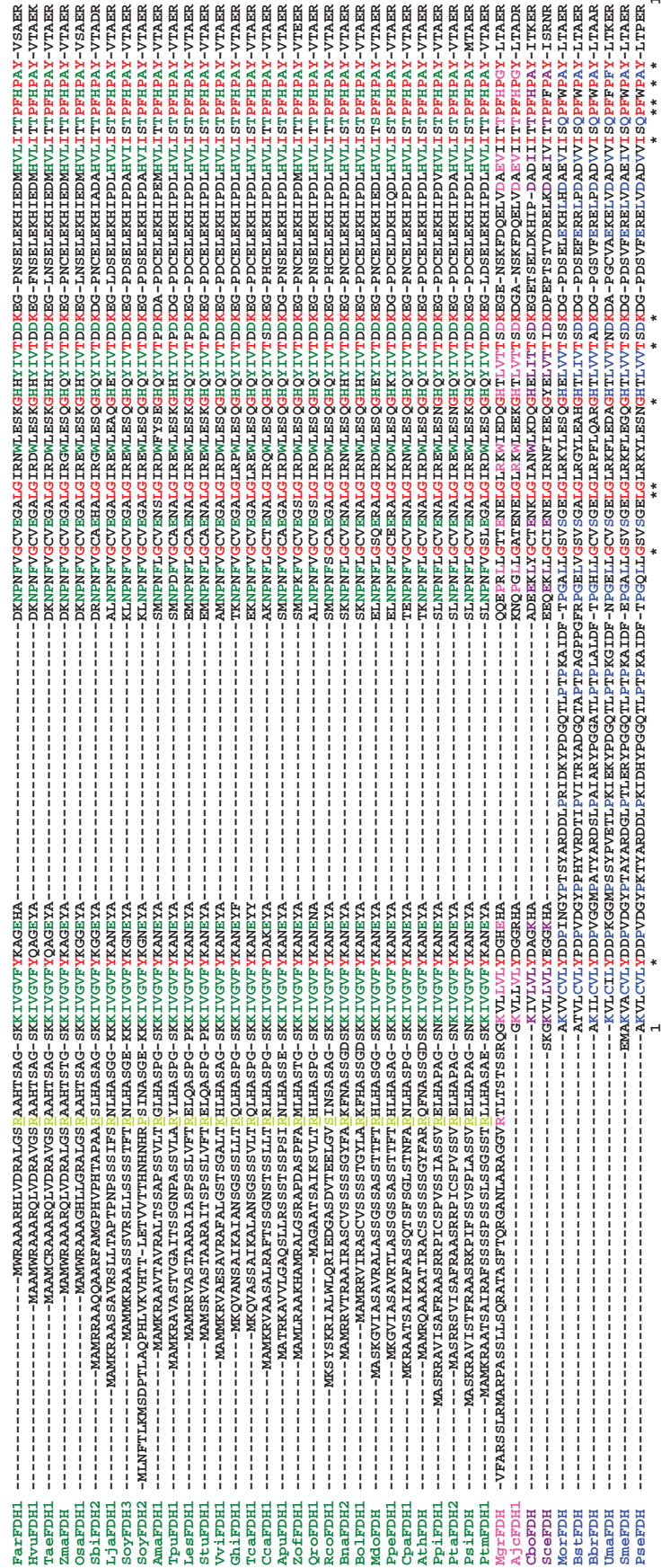
Fig. 2. Phylogenetic tree of N-terminal sequences for plant formate dehydrogenases.

study of the signal peptide of the enzyme from *A. thaliana* has shown that the enzyme can also be transported to chloroplasts. The N-terminal fragment of this enzyme strongly differs from the signal sequences of FDHs from potato, barley, and rice. There is a hypothesis that under certain conditions AthFDH localizing in chloroplasts is capable of catalyzing the reverse reaction, i.e., the conversion of carbon dioxide into formate [27]. It was shown by using another algorithm to compare the signal peptides of FDHs that all the enzymes, with the exception of FDH from tomato plants, were capable of being transported both to mitochondria and chloroplasts [28]. An analysis of signal sequences carried out using the Predotar, TargetP, and Mitoprot software [11] confirmed the fact that FDH is basically localized in mitochondria.

In plants, formate dehydrogenase is often represented by several isoforms, also known as isoenzymes, whose synthesis is determined by the condition of a plant. The differences in the isoenzyme composition of FDHs in healthy and affected palms *Pericopsis mooniana* are used to select trees when selective cutting is performed [54]. Polymorphism is also typical for FDH from the almond tree *Prunus dulcis* [55] or *P. amygdalus* [56]. Based on the data of the analysis of isoforms of FDHs and several other dehydrogenases, a method for identifying plant genotype was proposed. As previously mentioned above, phosphorylation may be the reason for the formation of different FDH isoforms [34]. Depending on the modification degree, the formation of numerous forms of the enzyme with pI varying from 6.75 to 7.19 was observed. Moreover, it was ascertained that the additional isoforms of potato FDH emerged as a result of post-translational deamidation of Asn329 and Gln330 residues [34].

The differences in sequences of signal peptides are more strongly

Fig. 3. Alignment of formate dehydrogenases from different sources. Abbreviations of enzymes are highlighted in green; fungi enzymes are highlighted in magenta; FDHs from bacteria are highlighted in blue. Specific sequences that are responsible for transport of the enzyme to mitochondria are underlined. The numeration of residues is the same as for the FDH from *Pseudomonas* sp. 101 (PseFDH). The asterisk and red font mark the conserved amino acid residue.



pronounced when compared with those in plant FDHs; the homology level between which is ~80%. It is most clearly demonstrated in the case of isoenzymes of soybean FDH. Homology of the sequences of isoenzymes is 98%, whereas for the signal sequences, it is lower than 40%. *Figure 2* shows a phylogenetic tree of the signal peptides of plant FDHs. As can be seen, two isoenzymes of FDH from soybean *Glycine max*, SoyFDH1 and SoyFDH2, form an individual group. The N-terminal fragment of these enzymes is much longer than that in FDHs from other plants (*Fig. 1*) and strongly differs in terms of its amino acid composition. Next, there is a large branch of the family Gramineae, which includes the enzymes of rice (OsaFDH), wheat (TaeFDH), barley (HvuFDH), sugarcane, moso bamboo, etc. A large group is represented by the enzymes of plants belonging to the family Brassicaceae (Cruciferae), namely, wild radish (RraFDH), cabbage (BolFDH), rapeseed (BnaFDH), and *A. thaliana* (AthFDH). The other groups are formed of proteins from Asteroideae, Leguminosae, Solanaceae, Malvaceae, Pinaceae, and Salicaceae. As previously mentioned, five isoenzymes of soybean FDH do not form a separate group. Since the signal peptide is basically responsible for the transport of the enzyme inside the cell, an assumption can be made that different isoenzymes of soybean FDH are transported into different organelles.

Figure 3 shows the alignment of some complete sequences of plant FDHs that are known at the present time; the sequences of a number of similar enzymes from microorganisms are provided for the purposes of comparison. The absolutely conserved regions are highlighted in red; the residues repeating only in plant FDHs are highlighted in green. A significant difference of bacterial enzymes from the plant ones is an N-terminal rigid loop. This region embraces a considerable part of the enzyme subunit. Its interaction with other amino acid residues is likely to be accounted for by a higher thermal stability of bacterial enzymes as compared with the plant ones. In addition, in FDHs of microbial origin, the C-terminal region is longer than that in plant enzymes. Meanwhile, the differentiation of FDH into two groups on the basis of its homology is clearly observed in the remaining part of the amino acid sequence. The first group contains bacterial and plant enzyme, whereas the second group consists of the enzymes from yeasts and fungi.

Plant enzymes are highly homologous (approximately 80%); the similarity between the bacterial and plant FDHs is ~50%.

OBTAINMENT OF PLANT FORMATE DEHYDROGENASES

In plants, FDHs are localized in mitochondria; they therefore constitute a small part of all soluble proteins

within a cell, and the isolation of an enzyme directly from plants is a labour-intensive and time-consuming procedure. Plant FDHs are mostly not very stable, which results in an appreciably significant inactivation of the enzyme during the extraction. Therefore, the specific activity of the resulting FDH specimens is much lower than one may expect (*Table 2*). The purified plant FDH was first obtained in 1951 from pea and French bean [13]. In 1983, FDH was extracted from soybean *G. max* in appreciably large amounts; this enabled the determination of the amino acid composition of plant formate dehydrogenase [57].

Since 1993 several cDNA of plant FDH have been cloned: in 1993 – from potato [21], in 1998 – from barley [8], in 2000 – from rice [41] and *A. thaliana* [26, 27]. Transgenic *A. thaliana* and tobacco plants expressing AthFDH were developed [28]; however, the yield of the enzyme was not very high. The expression of full size cDNA of potato FDH in *Escherichia coli* cells yielded insoluble inclusion bodies [21].

The active and soluble recombinant formate dehydrogenase from plants was first obtained in *E. coli* cells, [41]; however, the protein content was very low, approximately 0.01% of all soluble proteins within the cell. In our laboratory, we obtained *E. coli* strains, which are superproducers of active FDHs from *A. thaliana* (AthFDH) and soybean *G. max* (isoenzyme SoyFDH2) with an enzyme content attaining 40% of all soluble proteins in the cell [58] (the gene of soybean FDH was kindly provided by Professor N. Labrou from the Agricultural University of Athens (Greece); the FDH gene from *A. thaliana*, by Professor J. Markwell from the University of Nebraska (Lincoln, USA)). There is no system of transport to mitochondria in *E. coli* cells; therefore, in order to obtain the “natural enzyme”, we deleted the sequences encoding the signal peptide from the cDNA [58]. After the optimization of the cultivation conditions, the yield of recombinant FDH from *A. thaliana* and soybean *G. max* reached 500–600 mg/l of the medium [6]. A procedure was developed which enabled the obtaining of several hundred milligrams of homogenous FDH specimen via a single chromatographic stage per extraction run. Thus, all necessary conditions for the performance of systematic studies of FDHs from *A. thaliana* and soybean *G. max* were provided, including genetic engineering experiments and X-ray diffraction determination of the structure. The experiments were successfully carried out for the expression of FDH from *L. japonicas* in *E. coli* cells [10].

KINETIC PROPERTIES OF PLANT FORMATE DEHYDROGENASE

Table 2 summarizes the kinetic properties of natural and recombinant plant FDHs. The characteristics of the

REVIEWS

Table 2. Kinetic parameters of formate dehydrogenases from different sources

FDH specimen	Specific activity, U/mg	k_{cat}^1 , $\frac{U}{mg \cdot s}$	K_M (NAD ⁺), μM	K_M (formate), mM	K_M (NADP ⁺), mM	$\frac{k_{cat}^{NADP^+}}{K_M^{NADP^+}} / \frac{k_{cat}^{NAD^+}}{K_M^{NAD^+}}$	Reference
<i>Arabidopsis thaliana</i> , native, after affinity chromatography	NA*	NA	65	10	NA	NA	[27]
<i>A. thaliana</i> , native, from mitochondria	NA	NA	76	11	NA	NA	[59]
<i>A. thaliana</i> , recombinant from transgenic tobacco	1.3	0.87	78	11	NA	NA	[59]
<i>A. thaliana</i> , recombinant from transgenic tobacco + thermal treatment for 5 min at 60°C	0.1	0.07	35	3.3	ND	ND	[59]
<i>A. thaliana</i> , from mitochondria from leaves	1.9	1.27	34	1.4	NA	NA	[60]
<i>A. thaliana</i> , recombinant from <i>E. coli</i>	6.5	3.8	20	2.8	10	5.0×10^{-5}	[58]
Pea (seeds) <i>Pisum sativum</i>	NA	NA	22	2 [61] 1.67; 6.25 [62]	NA	NA	[61, 62]
Mung bean, <i>Phaseolus aureus</i> , native	NA	NA	7.2	1.6	NA	NA	[63]
Soybean, <i>G. max</i> , native	NA	NA	5.7	0.6	NA	NA	[57]
Soybean, <i>G. max</i> , recombinant	4.0	2.83 [64]	13.2	1.5	1	8.7×10^{-4}	[58, 64, 76]
Lotus japonicus	NA	1.2 (NAD ⁺) 0.005 (NADP ⁺)	29.5	6.1	29.5	3.7×10^{-6}	[10]
Spinach, <i>Spinacia oleracea</i> L., from leaves	NA	NA	NA	1.7	NA	NA	[16]
Potato <i>Solanum tuberosum</i>	NA	NA	19	0.54	NA	NA	[29]
<i>C. boidinii</i> , wild-type	6.3	3.7	37	5.9	NA	NA	[65]
<i>C. metillica</i> , wild-type	2.1	1.4	55	NA	NA	$< 4 \times 10^{-6}$	[66]
<i>Saccharomyces cerevisiae</i> , recombinant	10	6.5	36	5.5	NA	$< 3.3 \times 10^{-10}$	[67, 68]
Burkholderia stabilis	NA	1.66 (NAD ⁺) 4.75 (NADP ⁺)	1430	55.5	0.16	25.0	[51]
<i>Moraxella</i> sp. C2, recombinant	10.0	7.3	80	7.5	NA	NA	[6]
<i>Pseudomonas</i> sp. 101	10.0	7.3	60	7	> 200	4.2×10^{-4}	[6]

* NA – Data not available.

most thoroughly studied bacterial and yeast enzymes are provided for comparative purposes. Several major conclusions can be drawn from the data in Table 2:

1. It is clearly visible that in case of FDH from *A. thaliana* the multistage extraction of the natural enzyme is accompanied by a considerable loss in activity. The specific activity of the specimens, even those obtained from transgenic plants, is several times lower than the activity of recombinant AthFDH expressed in *E. coli* cells. It is noteworthy that AthFDH belongs to stable FDHs. In terms of thermal stability, it is even superior to FDH from *Moraxella* sp. C2 and yeast *C. boidinii* (Table 3). It is obvious that the degree of inactivation of less stable, FDHs (in particular, in the case of SoyFDH) being extracted from natural sources will be higher. This fact should be taken into consideration when analysing formate dehydrogenase activity in plants.

2. The specific activity of recombinant AthFDH and SoyFDH is comparable with that of formate dehydrogenases from microorganisms; although it is inferior to FDHs from methylotrophic bacteria and baker's yeast. As previously mentioned, a partial inactivation of enzymes may occur during the extraction; therefore, calculation of the catalytic constant based on the values of specific activity and molecular weight may give underestimated k_{cat} values. This fact is of particular significance for SoyFDH, the thermal stability of which is much lower than that of other FDHs (see the thermal stability section below). Therefore, we developed a procedure for determining the concentration of active sites of recombinant SoyFDH based on the quenching of the intrinsic fluorescence of the enzyme as it is titrated with azide ion in the presence of coenzyme NAD^+ [64]. The azide ion is a strong competitive inhibitor of SoyFDH ($K_i = 3.6 \times 10^{-7}$ M). Therefore, a linear dependence of quenching of FDH fluorescence on the azide concentration is observed under the conditions ensuring the equimolar binding of enzyme and inhibitor. The k_{cat} value determined from these experiments actually coincided with that calculated using the specific activity and molecular weight. The obtained data attest to the fact that despite the low thermal stability, SoyFDH extracted using the designed procedure is not inactivated. Today, this procedure is being actively used for determining the k_{cat} values of the mutant forms of SoyFDH.

3. Plant FDHs are characterized by significantly lower values of the Michaelis constants with respect to both formate and coenzyme NAD^+ in comparison with the bacterial and yeast enzymes. It is very important for the practical application of FDH. Today, recombinant FDHs from *Pseudomonas* sp. 101 and *C. boidinii*, whose chemical and thermal stability have been enhanced by protein engineering methods, are used for the regeneration of the reduced coenzyme (NADH or

NADPH) in the synthesis of chiral compounds using dehydrogenases [6].

4. Almost all FDH that have been studied are highly specific to the coenzyme NAD^+ . Their catalytic activity in the reaction with NAD^+ is higher than that in the reaction with NADP^+ by a factor of 2500 (PseFDH) to 3×10^9 . The exception is the recently described FDH from pathogenic bacteria *Burkholderia stabilis*, which is twenty-six-fold more efficient in the reaction with NADP^+ in comparison with NAD^+ [51]. It should be noted that the mutant PseFDH, whose coenzyme specificity changed from NAD^+ to NADP^+ , was obtained as early as in 1993 [6, 68]; this enzyme has been successfully used for NADPH regeneration [69, 70]. Having the lowest K_m value with respect to NADP^+ among all NAD^+ -specific wild-type FDHs, SoyFDH has a huge potential for obtaining the NADP^+ -specific enzyme [58] (Table 2).

THERMAL STABILITY OF PLANT FORMATE DEHYDROGENASES

Prior to obtaining recombinant AthFDH and SoyFDH in *E. coli* cells, no systematic studies on the thermal stability of plant FDHs were performed. According to [59], the values of K_m with respect to formate and NAD^+ decrease after the incubation of transgenic AthFDH for 5 min at 60°C ; however, the specific activity value decreased by 13 times. We performed systematic studies of the thermal stability of recombinant AthFDH and SoyFDH using two approaches: determining the kinetics of thermal inactivation and the differential scanning calorimetry [71, 72]. It was revealed that the thermal inactivation of plant FDHs occurred via a monomolecular mechanism, similar to the FDHs from bacteria and yeasts. Time dependences of decrease in the activity of AthFDH and SoyFDH are described by the kinetics of the first-order reaction, the observed constant of inactivation rate was independent of enzyme concentration. The thermal stabilities of AthFDH and SoyFDH strongly differ. AthFDH lost 50% of its activity after 20 min at 59.5°C , whereas SoyFDH lost 50% of its activity at 52.8°C . The difference by almost 7°C corresponds to a difference in the inactivation rate constants of more than 1000 times. AthFDH is actually inferior in terms of its thermal stability only to FDH from *Pseudomonas* sp. 101 (63.0°C , the most stable FDH among the known ones) [6] and *Staphylococcus aureus* (62.0°C) and is superior to all known microbial formate dehydrogenases. In contrast, SoyFDH is inferior in terms of stability to all known FDHs, with the exception of the enzyme from baker's yeast that is characterized by another inactivation mechanism. The temperature dependences of the rate constants of inactivation of AthFDH and SoyFDH are described by the transition state

Table 3. Parameters of thermal inactivation of formate dehydrogenases from different sources

FDH source	Kinetics of thermal inactivation*		Differential scanning calorimetry* [72]		
	ΔH^\ddagger , kJ/mol	ΔS^\ddagger , J/(mol·K)	C_p , kJ/mol	T_m , °C	$T_{1/2}$, °C
<i>Pseudomonas sp. 101</i>	540 [6]	1320 [6]	2060	67.6	5.4
<i>Moraxella sp. C2</i>	NA**	NA**	1830	63.4	4.9
<i>Candida boidinii</i>	480 [77]	1250 [77]	1730	64.4	5.3
<i>Saccharomyces cerevisiae</i>	420 [67]	NA	820	46.4	3.2
<i>Arabidopsis thaliana</i>	490 [6]	1200 [6]	1330	64.9	5.9
<i>Glycine max</i>	370 [76]	860 [76]	820	57.1	7.5

* All measurements were carried out in the 0.1 M phosphate buffer, pH 7.0

** Data not available

theory. The calculated values of activation enthalpy ΔH^\ddagger and activation entropy ΔS^\ddagger are listed in *Table 3*. It can be noticed that thermal stability of formate dehydrogenases correlates well with the ΔH^\ddagger and ΔS^\ddagger values. The highest values are typical of the most stable PseFDH, whereas the lowest ones refer to SoyFDH.

The results of experiments studying the thermal stability of plant FDHs using differential scanning calorimetry are in close agreement with the data of inactivation kinetics. In *Table 3* the values of the temperature and heat of the phase transition are shown. All investigated FDHs are characterized by their high cooperativity of the denaturation process. PseFDH is characterized by the highest melting point, whereas this value is lower by a factor of 2.5 for SoyFDH. The melting point of AthFDH is higher than that of CboFDH and MorFDH.

Experiments on enhancing the thermal stability of recombinant SoyFDH using genetic engineering techniques are currently being performed.

CHEMICAL STABILITY OF PLANT FORMATE DEHYDROGENASES

FDH has been actively used in the process of synthesizing optically active compounds catalyzed by dehydrogenases. In these processes, the operational stability (the operating time of an enzyme) plays the greatest role. Under conditions of biocatalytic process, the inactivation of FDH is associated with either oxidation with oxygen or chemical modification of sulfhydryl groups of the enzyme. The operational stability of PseFDH and CboFDH was enhanced by site-directed mutagenesis of two Cys residues [6, 65]. As previously mentioned,

the synthesis of FDHs in plants increased under various stress factors. The concentration of active forms of oxygen (superoxide radicals, hydrogen peroxide, etc.) is likely to increase in a cell under the same conditions. It should be expected that in order to ensure high activity under stress, plant FDHs should be far more resistant to the action of these agents than formate dehydrogenases functioning under non-stress conditions. In order to verify this hypothesis, the kinetics of inactivation of recombinant AthFDH, SoyFDH, PseFDH, FDH from wild-type *S. aureus* (SauFDH) and three mutant PseFDH, where one or two Cys residues were replaced, under the action of hydrogen peroxide was studied. FDH from *S. aureus* is a stress protein as well, since the biosynthesis of this enzyme increases by 20 times when staphylococci pass from planktonic growth to biofilm formation [73]. It was revealed that the inactivation rate of AthFDH and SoyFDH under the action of H_2O_2 is virtually equal and is 18 times lower than that in wild-type PseFDH. Under the same conditions, the stability of SauFDH was sixfold higher than that in plant enzymes [74]. PseFDH with the stability identical to that of SoyFDH was successfully obtained only after double Cys145Ser/Cys255/Ala replacement. It was thus demonstrated that plant and bacterial FDHs synthesized under stress impact indeed possess a higher chemical stability than formate dehydrogenases, whose synthesis is induced by other factors. Moreover, studying the thermal inactivation of formate dehydrogenase in the presence of hydrogen peroxide can be used to comparatively assess the *in vivo* chemical stability of FDHs.

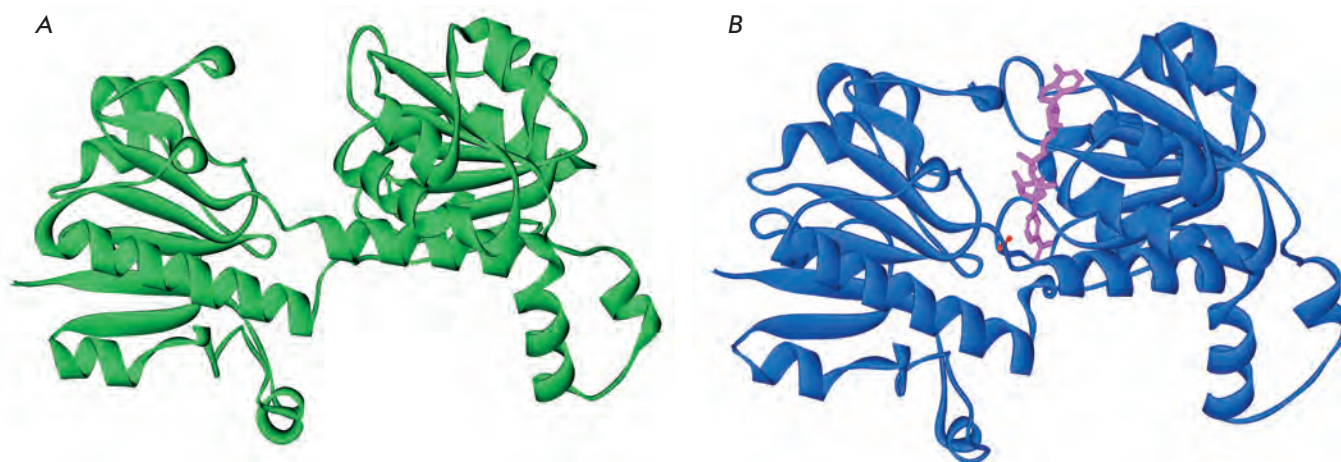


Fig. 4. The structures of apo-(A) and holo-(B) forms of FDH from *A. thaliana*. Figures were obtained using PDB structures 3JTM and 3N7U, respectively. In the structure of the holo-form, the molecules of NAD⁺ and azide ion are highlighted in magenta and red, respectively.

STRUCTURAL STUDIES OF PLANT FORMATE DEHYDROGENASES

FDH has not been well studied from a structural perspective. Until recently, only the FDH structures from three sources, namely, bacteria *Pseudomonas* sp. 101 and *Moraxella* sp. C2 (unbound enzyme, and the enzyme–NAD⁺–azide ternary complex) and *C. boidinii* yeast (structures of two mutant forms of an apoenzyme) were deposited into the protein data bank (PDB). In case of formate dehydrogenases, free enzyme is in its «open» conformation. When the FDH–NAD⁺–azide ternary complex is formed (its structure being considered similar to that of the enzyme in the transition state), a considerable compacting of the protein globule occurs, and FDH is transformed into the «closed» state. The development of a highly efficient system of expression of AthFDH and SoyFDH in *E. coli* cells enabled the transition to their crystallization and identification of their structure. Nowadays AthFDH structures both in open and closed conformations (3NAQ and 3N7U, with resolution of 1.7 and 2.0 Å, respectively) have been identified. Enzyme crystals were produced in space [75] in order to obtain AthFDH structure in open conformation with higher resolution (3JTM, 1.3 Å), Fig. 4 shows the structures of apo- and holoFDHs (the open and closed conformations, respectively). A more detailed analysis of these structures will be provided in individual articles. The crystals of the SoyFDH–NAD⁺–azide ternary complex of FDH from soybean *G. max* have been obtained both on the Earth and in space. The structures of these complexes were identified with resolution of 1.9 Å; the deposition of these structures into the PDB data bank is in progress.

CONCLUSIONS

Both our own and the published data attest to the fact that plant FDHs are extremely significant, in particular when responding to stress factors. Biosynthesis regulation and the physiological role of FDHs are diverse and complex; they have not been completely elucidated thus far. The systematic investigation of the structure and function of these enzymes is still in its infancy. The results of these studies are of significant interest to fundamental science and are of great practical importance. Production of mutant forms of FDH with a high activity opens a new approach for the design of plants with an enhanced resistance to unfavourable factors. More active mutant enzymes will supply the cell with the energy required to more efficiently overcome unfavourable effects of stress with the same expression level of FDH. Soybean FDH is also considered to be an exceptionally promising FDH for the design of a highly efficient biocatalyst for NAD(P)H regeneration in the synthesis of optically active compounds using dehydrogenases. The natural enzyme is notable for its high operational stability and has one of the lowest values of the Michaelis constant with respect both to NAD⁺ and formate among all of the known FDHs. However, in order to practically implement SoyFDH, its catalytic activity and thermal stability need to be enhanced. We are currently performing active research in this direction. ●

This study was supported by the Ministry of Education and Science of the Russian Federation (State Contract № 16.512.11.2148) and the Russian Foundation for Basic Research (grant № 11-04-00920).

REFERENCES

1. Rodionov Yu.V. // *Uspekhi microbiologii*. 1982. V. 16. P.104-138 (rus).
2. Ferry J.G. // *FEMS Microbiol. Rev.* 1990. V. 7. P. 377-382.
3. Vinals C., Depiereux E., Feytmans E. // *Biochem. Biophys. Res. Commun.* 1993. V. 192. P. 182-188.
4. Tishkov V.I., Galkin A.G., Egorov A.M. // *Biochimie*. 1989. V. 71. № 4. P. 551-557.
5. Tishkov V.I., Popov V.O. // *Biochemistry (Mosc.)* 2004. V. 69. P. 1252-1267.
6. Tishkov V.I., Popov V.O. // *Biomol. Eng.* 2006. V. 23. P. 89-110.
7. Hourton-Cabassa C., Ambard-Bretteville F., Moreau F., Davy de Virville J., Remy R., Colas des Francs-Small C. // *Plant Physiol.* 1998. V. 116. P. 627-635.
8. Suzuki K., Itai R., Suzuki K., Nakanishi H., Nishizawa N.-K., Yoshimura E., Mori S. // *Plant Physiol.* 1998. V. 116. P. 725-732.
9. Thompson P., Bowsher C.G., Tobin A.K. // *Plant Physiol.* 1998. V. 118. P. 1089-1099.
10. Andreadeli A., Flemetakis E., Axarli I., Dimou M., Urdvardi M.K., Katinakis P., Labrou N.E. // *Biochim. Biophys. Acta.* 2009. V. 1794. P. 976-984.
11. David P., Colas des Francs-Small C., Seignac M., Thareau V., Macadre C., Langin T., Geffroy V. // *Theor. Appl. Genet.* 2010. V. 121. P. 87-103.
12. Thunberg T. // *Arch. Physiol. Biochem.* 1921. V. 18. P. 601-606.
13. Davison D.C. // *Biochem. J.* 1951. V. 49. P. 520-526.
14. Davies D.D. // *J. Exp. Bot.* 1956. V. 7. P. 203-218.
15. Mazelis M. // *Plant Physiol.* 1960. V. 35. P. 386-391.
16. Halliwell B. // *Biochem. J.* 1974. V. 138. P. 77-85.
17. Jansch L., Krufft V., Schmitz U.K., Braun H.-P. // *Plant J.* 1996. V. 9. № 3. P. 357-368.
18. Oliver D.J. // *Plant Physiol.* 1981. V. 68. P. 703-705.
19. Hanson A.D., Nelsen C.E. // *Plant Physiol.* 1978. V. 62. P. 305-312.
20. Colas des Francs-Small C., Ambard-Bretteville F., Darpas A., Sallantin M., Huet J.-C., Pernollet J.-C., Remy R. // *Plant Physiol.* 1992. V. 98. P. 273-278.
21. Colas des Francs-Small C., Ambard-Bretteville F., Small I.D., Remy R. // *Plant Physiol.* 1993. V. 102. P. 1171-1177.
22. Herbig A., Giritch A., Horstmann C., Becker R., Balzer H.-J., Baumlein H., Stephan U.W. // *Plant Physiol.* 1996. V. 111. P. 533-540.
23. Dubos C., Plomion C. // *Plant Mol. Biol.* 2003. V. 51. P. 249-262.
24. Minami A., Nagao M., Arakawa K., Fujikawa S., Takezawa D. // *J. Plant Physiol.* 2003. V. 160. P. 475-483.
25. Yin L., Lan Y., Zhu L. // *Plant Mol. Biol.* 2008. V. 68. P. 597-617.
26. Fukusaki E., Ikeda T., Shiraishi T., Nishikawa T., Kobayashi A. // *J. Biosci. Bioeng.* 2000. V. 90. P. 691-693.
27. Olson B.J., Skavdahl M., Ramberg H., Osterman J.C., Markwell J. // *Plant Sci.* 2000. V. 159. P. 205-212.
28. Herman P.L., Ramberg H., Baack R.D., Markwell J., Osterman J.C. // *Plant Sci.* 2002. V. 163. P. 1137-1145.
29. Ambard-Bretteville F., Sorin C., Rebeille F., Hourton-Cabassa C., Colas des Francs-Small C. // *Plant Mol. Biol.* 2003. V. 52. P. 1153-1168.
30. Igamberdiev A.U., Bykova N.V., Kleczkowski L.A. // *Plant Physiol. Biochem.* 1999. V. 37. № 7-8. P. 503-513.
31. Li R., Moore M., King J. // *Plant Cell Physiol.* 2003. V. 44. № 3. P. 233-241.
32. Perales M., Eubel H., Heinemeyer J., Colaneri A., Zabalata E., Braun H.P. // *J. Mol. Biol.* 2005. V. 350. P. 263-277.
33. Bykova N.V., Egsgaard H., Miller I.M. // *FEBS Lett.* 2003. V. 540. P. 141-146.
34. Bykova N.V., Stensballe A., Egsgaard H., Jensen O.N., Moller I.M. // *J. Biol. Chem.* 2003. V. 278. P. 26021-26030.
35. Kruger A., Peskan-Berghofer T., Frettinger P., Herrmann S., Buscot F., Oelmuller R. // *New Phytol.* 2004. V. 163. P. 149-157.
36. Bruggmann R., Abderhalden O., Reymond P., Dudler R. // *Plant Mol. Biol.* 2005. V. 58. P. 247-267.
37. Giri A.P., Wunsche H., Mitra S., Zavala J.A., Muck A., Svatos A., Baldwin I.T. // *Plant Physiol.* 2006. V. 142. P. 1621-1641.
38. Umezawa T., Sakurai T., Totoki Y., Toyoda A., Seki M., Ishiwata A., Akiyama K., Kurotani A., Yoshida T., Mochida K., et al. // *DNA Res.* 2008. V. 15. P. 333-346.
39. Kikuchi S., Satoh K., Nagata T., Kawagashira N., Doi K., Kishimoto N., Yazaki J., Ishikawa M., Yamada H., Ooka H., et al. // *Science.* 2003. V. 301. P. 376-379.
40. Liu X., Lu T., Yu S., Li Y., Huang Y., Huang T., Zhang L., Zhu J., Zhao Q., Fan D., et al // *Plant Mol. Biol.* 2007. V. 65. P. 403-415.
41. Shiraishi T., Fukusaki E., Kobayashi A. // *J. Biosci. Bioeng.* 2000. V. 89. P. 241-246.
42. David P., Chen N.W.G., Pedrosa-Harand A., Thareau V., Seignac M., Cannon S.B., Debouck D., Langin T., Geffroy V. // *Plant Physiol.* 2009. V. 151. P. 1048-1065.
43. Rensing S.A., Lang D., Zimmer A.D., Terry A., Salamov A., Shapiro H., Nishiyama T., Perroud P.-F., Lindquist E.A., Kamisugi Y., et al. // *Science.* 2008. V. 319. № 5859. P. 64-69.
44. Ralph S.G., Chun H.J., Kolosova N., Cooper D., Oddy C., Ritland C.E., Kirkpatrick R., Moore R., Barber S., Holt R.A., et al. // *BMC Genomics.* 2008. V. 9. P. 484.
45. Tuskan G.A., Difazio S., Jansson S., Bohlmann J., Grigoriev I., Hellsten U., Putnam N., Ralph S., Rombauts S., Salamov A., et al. // *Science.* 2006. V. 313. P. 1596-1604.
46. Paterson A.H., Bowers J.E., Bruggmann R., Dubchak I., Grimwood J., Gundlach H., Haberger G., Hellsten U., Mitros T., Poliakov A., et al // *Nature.* 2009. V. 457. № 7229. P. 551-556.
47. Kawaura K., Mochida K., Enju A., Totoki Y., Toyoda A., Sakaki Y., Kai C., Kawai J., Hayashizaki Y., Seki M., et al. // *BMC Genomics.* 2009. V. 10. P. 271.
48. Alexandrov N.N., Brover V.V., Freidin S., Troukhan M.E., Tatarinova T.V., Zhang H., Swaller T.J., Lu Y.P., Bouck J., Flavell R.B., et al. // *Plant Mol. Biol.* 2009. V. 69. P. 179-194.
49. Hwang L., Hocking-Murray D., Bahrami A.K., Andersson M., Rine J., Sil A. // *Mol. Biol. Cell.* 2003. V. 14. P. 2314-2326.
50. Tishkov V.I., Galkin A.G., Egorov A.M. // *Dokl Acad. Nauk USSR.* 1991. V. 317. P. 745-748 (rus).
51. Hatrongjit R., Packdibamrung K. // *Enz. Microb. Technol.* 2010. V. 46. P. 557-561.
52. Barnett M.J., Fisher R.F., Jones T., Komp C., Abola A.P., Barloy-Hubler F., Bowser L., Capela D., Galibert F., Gouzyet J., et al. // *Proc. Natl. Acad. Sci. USA.* 2001. V. 98. № 17. P. 9883-9888.
53. Ambard-Bretteville F., Small I., Grandjean O., Colas des Francs-Small C. // *Biochem. Biophys. Res. Commun.* 2003. V. 311. P. 966-971.
54. Weerasinghe P.A., Weerasekera M.L.M.C., van Holm L.H.J. // *Biologia Plantarum.* 1999. V. 42. P. 541-547.
55. Colic S., Milatovic D., Nikolic D., Zec G. // *Hort. Sci. (Prague).* 2010. V. 37. P. 56-61.

REVIEWS

56. Colich S., Milatovich D., Nikolich D., Zec G. // *Bulgarian J. Agricul. Sci.* 2009. V. 15. P. 552–556.
57. Farinelli M.P., Fry D.W., Richardson K.E. // *Plant Physiol.* 1983. V. 73. P. 858–859.
58. Sadykhov E.G., Serov A.E., Yasnyi I.E., Voinova, N.S., Alexeeva, A.A., Petrov A.S., Tishkov V.I. // *Moscow University Chemistry Bulletin*, 2006, V. 47. № 1. P. 31–34.
59. Baack R.D., Markwell J., Herman P.L., Osterman J.C. // *J. Plant Physiol.* 2003. V. 160. P. 445–450.
60. Li R., Ziola B., King J. // *J. Plant Physiol.* 2000. V. 157. P. 161–167.
61. Uotila L., Koivusalo M. // *Arch. Biochem. Biophys.* 1979. V. 196. P. 33–45.
62. Ohyama T., Yamazaki I. // *J. Biochem.* 1975. V. 77. P. 845–852.
63. Peacock D., Boulter D. // *Biochem. J.* 1970. V. 120. P. 763–769.
64. Romanova E.G., Alekseeva A.A., Pometun E.V., Tishkov V.I. // *Moscow University Chemistry Bulletin*. 2010. V.65. N3. P. 127–130.
65. Slusarczyk H., Felber S., Kula M.R., Pohl M. // *Eur. J. Biochem.* 2000. V. 267. P. 1280–1289.
66. Karaguler N.G., Sessions R.B., Clarke A.R., Holbrook J. // *Biotechnol. Lett.* 2001. V. 23. P. 283–287.
67. Serov A.E. / Structure – properties relationships in recombinant fromate dehydrogenases from bakery yeasts and methylotrophyc bacteria. // Ph.D. Disseration. Moscow, Lomonosov Moscow State University, 2002.
68. Serov A.E., Popova A.S., Fedorchuk V.V., Tishkov V.I. // *Biochem. J.* 2002. V. 367. P. 841–847.
69. Seelbach K., Riebel B., Hummel W., Kula M.-R., Tishkov V.I., Egorov A.M., Wandrey C., Kragl U. // *Tetrahedron Lett.* 1996. V. 37. № 9. P. 1377–1380.
70. Rissom S., Schwarz-Linek U., Vogel M., Tishkov V.I., Kragl U. // *Tetrahedron: Assymetry.* 1997. V. 8. № 15. P. 2523–2526.
71. Sadykhov E.G., Serov A.E., Voinova N.S., Uglanova S.V., Petrov A.S., Alekseeva A.A. Kleimenov S.Yu., Popov V.O., Tishkov V.I. // *Appl. Biochem. Microbiol.* 2006. V. 42. № 3. P. 236–240.
72. Sadykhov E.G. Preparation, thermal stability and structural studies of recombinant formate dehydrogenases from different sources : Ph.D. Dissertation, Moscow, A.N.Bach Institute of Biochemistry RAS, 2007.
73. Resch A., Rosenstein R., Nerz C., Gotz F. // *Appl. Environ. Microbiol.* 2005. V. 71. № 5. P. 2663–2676.
74. Savin S.S., Tishkov V.I. *Acta Naturae.* 2010. V. 2. N (4). P. 78–82.
75. Shabalin I.G., Serov A.E., Skirgello O.E., Timofeev V.I., Samygina V.R., Popov V.O., Tishkov V.I., Kuranova I.P. // *Crystallography Reports.* 2010. V.55. N 5. P. 806–810.
76. Alekseeva A.A., Shabalin I.G., Polyakov K.M., Tishkov V.I. // *J. Biotechnol.* 2010. V. 150. № S1. P. 476.
77. Tishkov V.I., Uglanova S.V., Fedorchuk V.V., Savin S.S. // *Acta Naturae.* 2010. V. 2. N 2(5). P. 82–87.

Screening of Potential HIV-1 Inhibitors/ Replication Blockers Using Secure Lentiviral *in Vitro* System

M.M. Prokofjeva¹, P.V. Spirin¹, D.V. Yanvarev¹, A.V. Ivanov¹, M.S. Novikov², O.A. Stepanov¹, M.B. Gottikh³, S.N. Kochetkov¹, B. Fehse⁴, C. Stocking⁵, V.S. Prassolov^{1*}

¹Engelhardt Institute of Molecular Biology, Russian Academy of Sciences

²Volgograd State Medical University

³Belozersky Institute of Physico-Chemical Biology, Lomonosov Moscow State University

⁴Research Department Cell and Gene Therapy, Department for Stem Cell Transplantation University Medical Center Hamburg-Eppendorf

⁵Heinrich-Pette-Institute for Experimental Virology and Immunology

*E-mail: prassolov45@mail.ru

Received 08.07.2011

Copyright © 2011 Park-media, Ltd. This is an open access article distributed under the Creative Commons Attribution License, which permits unrestricted use, distribution, and reproduction in any medium, provided the original work is properly cited.

ABSTRACT The development and usage of safe cell systems for testing agents which possess anti-HIV activity is a very important factor in the design of new drugs. We have described in detail a system we designed that is based on lentiviral vectors (Prokofjeva et al., *Antiviral Therapy*, in print) for swift and completely safe screening of potential HIV-1 replication inhibitors. The system enables one to test the efficiency of the inhibitory activity of compounds whose action is directed towards either wild-type HIV-1 reverse transcriptase or integrase, or mutant enzymes corresponding to the drug-resistant virus form. Testing results of a number of already known drugs, which correlate well with published data as well as data on newly synthesized compounds, were obtained. Application of this system substantially broadens the possibilities of preclinical anti-HIV drugs testing.

KEYWORDS HIV; lentiviral vectors; pseudo-HIV-1 particles; nucleoside reverse transcriptase inhibitors; non-nucleoside reverse transcriptase inhibitors; integrase inhibitors.

ABBREVIATIONS HIV – human immunodeficiency virus; RT – reverse transcriptase; VSV – vesicular stomatitis virus; eGFP – enhanced green fluorescent protein; AZT – 3-azido-3- deoxythymidine; IC₅₀ – half maximal (50%) inhibitory concentration (IC) of a substance.

INTRODUCTION

The human immunodeficiency virus type 1 (HIV-1), which belongs to the lentivirus genus of the retrovirus family, is responsible for one of the most common and life-threatening diseases known as the acquired immunodeficiency syndrome (AIDS). According to the World Health Organization (WHO), by the end of 2008, the number of HIV-1-infected people topped 33 million [1]. In 2010, official records put the number of HIV-1-infected people in Russia at 520,000 [2]. It should be noted that in reality the actual number of infected people can be two or even three times higher. It follows from the prognoses of the WHO and non-governmental organizations that even if all the initiatives to control AIDS propagation were implemented and anti-HIV therapy was used, the number of HIV-infected people may still exceed 48 million in the next several years.

Despite great efforts, no efficacious preventive or therapeutic vaccine has as yet been designed. The use of low-molecular inhibitors of different stages of the

replicative cycle of the virus remains the only therapeutic approach upon HIV infection. Thus far, approximately 30 substances of varying structures have been designed and certified as anti-HIV drugs. The majority of these substances inhibit three HIV-1 enzymes: reverse transcriptase (RT), integrase, and protease; the so-called fusion blockers (blocker of viral penetration into the cell) were recently added to this list [3]. The simultaneous use of several substances of different types in cases of highly active antiretroviral therapy (HAART) enables to achieve a relatively long-term and noticeable decrease in virus titer in the blood; hence, a patient's life is prolonged considerably [4, 5]. Nevertheless, all the aforementioned substances have several limitations. Firstly, long-term administration of drugs is required because of the lifetime HIV infection, resulting in the emergence of new mutant forms of the virus, which are resistant to the drugs used and can further spread in the virus population. As a consequence, viral forms that are insusceptible to one or even all classes

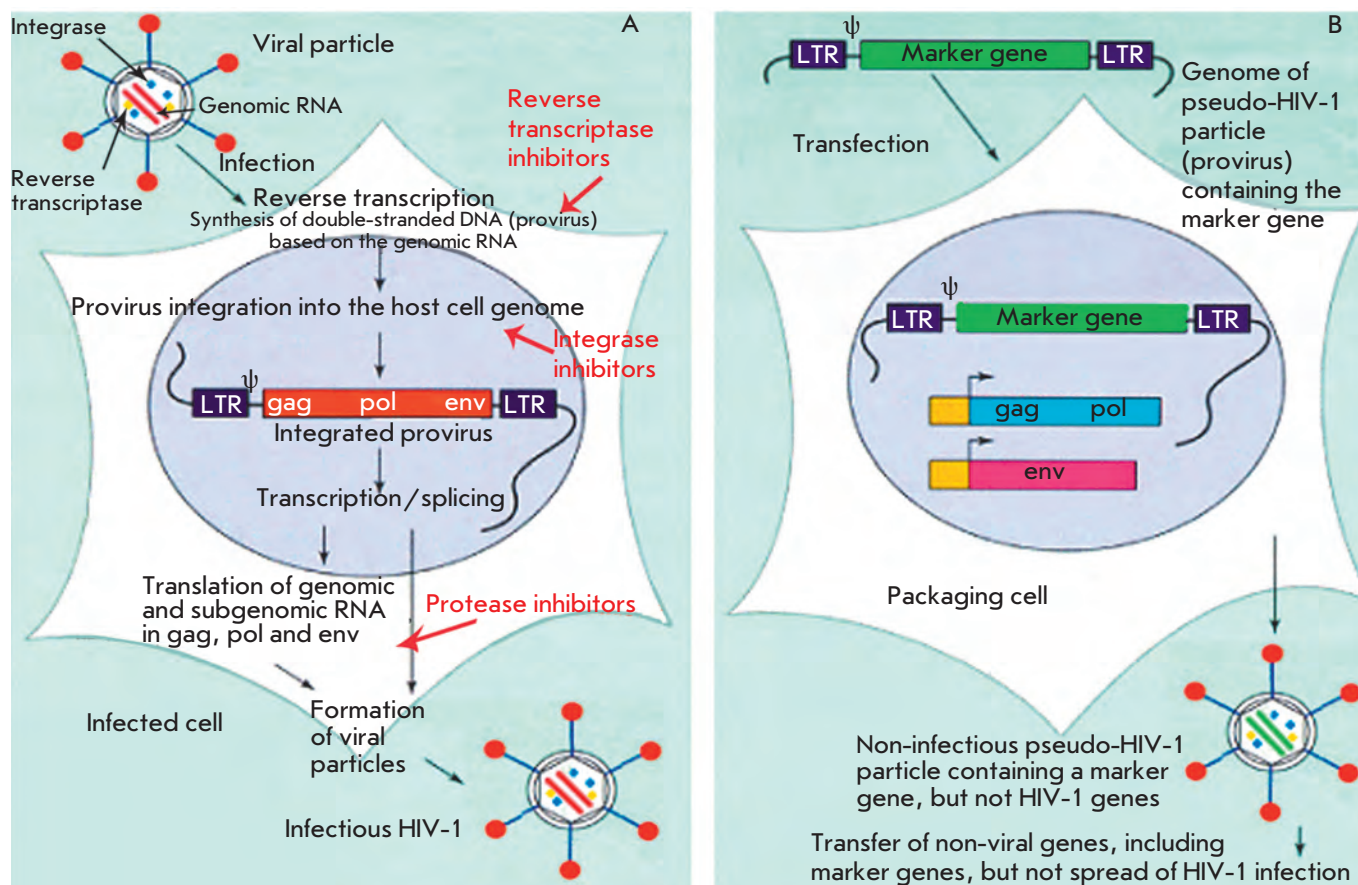


Fig. 1. The life cycle of infectious HIV-1 (A) and production of recombinant pseudo-HIV-1 particles in packaging cells (B).

of the above-listed anti-HIV-1 drugs have been detected in approximately 10% of the U.S. and European patients who had never been exposed to antiretroviral therapy [6]. Secondly, the need for long-term therapy often increases the possibility of adverse effects from antiretroviral agents [7, 8]. Thus, the search for new compounds with anti-HIV-1 activity is an extremely important issue in modern virology and medicinal chemistry. Moreover, it appears necessary to develop new agents that can be both relatively safe for patients and at the same time active towards both the wild-type virus and its drug-resistant forms.

An important stage in the development of new antiretroviral agents is testing their efficacy. Most laboratories involved in the search for new anti-HIV agents do not have the opportunity to work directly with the infectious replication-competent virus. This kind of research, which involves personnel coming into direct contact with the natural virus, can be performed only in certified laboratories that provide conditions that ensure operational safety and have permission to deal with class III hazard infectious substances. In this regard, the development and use of safe cell systems to

test antiviral activity is of quite high significance in the design process of new therapeutic agents. Lentiviral vectors, whose functional activity manifests itself as a result of the activity of all HIV-1 enzymes, are of particular interest for expeditious and safe screening of potential inhibitors of HIV-1 replication.

Since the early 1980s, vectors based on simple and complex retroviruses have been intensively used as powerful universal tools, including those for designing efficient transfer systems and for the expression of different genes and interfering RNAs in human and animal cells both *in vitro* and *in vivo* [9–13].

Lentiviral vectors have been used in our laboratory, as well as in other laboratories, in order to design safe systems for the screening of inhibitors of wild-type HIV-1 replication [14–18]. These systems are represented by a recombinant lentivirus carrying a fragment of the HIV-1 genome, without the regions that encode virus peptides and contain the gene of a reporter (marker) protein (e.g., green fluorescent protein). Moreover, pseudoviral particles are composed of the enzymes that are required for HIV-1 replication (reverse transcriptase, integrase, and protease), which provides the potential to synthe-

size a DNA copy of this genome, as well as the possibility to integrate it into the host cell genome via the same mechanism as the one at play in the infectious HIV-1. It is essential that these pseudo-HIV-1 particles can carry coat proteins of HIV-1 or other enveloped viruses (e.g., G-protein from vesicular stomatitis virus) on their surface, depending on researchers' choice. This provides the possibility of using certain lines of eukaryotic cells (target cells) and sufficiently high infection efficiency. The assembly of HIV-1-like particles occurs in this system according to the modified procedure that was developed for constructing virus-like particles on the basis of the murine leukemia virus that is related to HIV-1 [19] (Fig. 1). This procedure consists in individual introduction of plasmids containing a) the *gag-pol* gene of HIV-1 that encodes the structural proteins for the formation of the capsid of a viral particle and HIV-1 enzymes, b) the *env* gene that encodes glycoproteins of the HIV-1 envelope or the gene of the envelope protein of another virus, and c) antiviral DNA that encodes the recombinant RNA genome containing the marker gene of the fluorescent protein to the cultivated human embryonic kidney cells (the so-called packaging cells). After all the components listed are introduced into the packaging cells, viral proteins and recombinant RNA ensuring the formation of the HIV-1-like particles that are released into the environment are synthesized in the aforementioned cells. The addition of these particles to the target cells induces the synthesis of the DNA of a provirus that contains a marker gene, whose integration into the target cell genome renders it capable of fluorescing on the recombinant RNA genome in target cells. It should be stressed that the use of plasmid DNAs expressing individual virus-specific proteins enables to construct any variants of pseudo-HIV-1 particles with one or several mutations in any enzyme of viral replication which correspond to the drug-resistant HIV-1 strains.

Thus far, published investigations still contain an insufficient number of examples of successful use of these systems to study the antiretroviral activity of substances that differ in their nature; this makes it unclear just how universal the described systems are. In this regard, our study mainly endeavoured to verify the adequacy of the cell system proposed for screening potential anti-HIV-1 agents. The activity of a number of inhibitors of HIV-1 reverse transcriptase and integrase were tested, both of which have found application in medical practice and have undergone various stages of laboratory research.

EXPERIMENTAL

Cell cultivation

The following cell lines were used in this study: HEK293 (human embryonic kidney cells), SC-1 (mouse

embryonic fibroblasts), Jurkat (human T-lymphoblastic leukemia), CEM-SS (human T-lymphoblastic leukemia), and Kasumi-1 (human acute myeloid leukemia). The HEK293 and SC-1 cell lines were cultured in DMEM containing 10% fetal calf serum (FCS), 4 mM of *L*-glutamine, 100 U/ml of penicillin, and 100 µg/ml of streptomycin. The Jurkat, CEM-SS, and Kasumi-1 cell lines were cultured in RPMI-1640 containing 20% FCS, 4 mM of *L*-glutamine, 100 U/ml of penicillin, and 100 µg/ml of streptomycin. The cells were grown at 37°C in humid air containing 5% of CO₂.

Obtainment of pseudo-HIV-1 particles

HEK293 cells seeded in Petri dishes with a diameter of 100 mm in the amount of $3.0\text{--}3.5 \times 10^6$ cells per dish 12–14 h prior to the transfection onset were used as packaging cells, in which the assembly of recombinant lentiviral (pseudo-HIV-1) particles occurs.

DNA of the lentiviral vector containing the marker gene of green fluorescent protein (GFP) and the plasmids directing the synthesis of the proteins that are required for the formation of pseudo-HIV-1 particles were introduced into HEK293 cells via calcium phosphate transfection. The infectious pseudo-HIV-1 particles were collected 24 h following transfection with a 12 h interval [13].

The virus was titrated on HEK293 cells seeded to 24-well plates 24 h prior to infection. The level of cell fluorescence was measured on an Epics 4XL Beckman Coulter flow cytofluorimeter (USA) 48 h following the infection. The virus titer was calculated using the formula $T = NP/V$, where N is the amount of seeded cells, P is the share of the infected cells in the population, V is the amount of the added supernatant containing pseudo-HIV-1 particles, and T is virus titer. The samples with virus titer of $5 \times 10^5\text{--}5 \times 10^6$ were used in this study.

Investigation of the viral activity of compounds

In order to assess the anti-HIV-1 activity, a solution of the analyzed substances in water or dimethylsulfoxide (DMSO, the final concentration in the medium was no higher than 0.1%), was added to the cells; after 2–8 h (depending on the inhibitor), the cells were infected with pseudo-HIV-1 particles. The relative level of infection was determined by flow cytofluorimetry on an Epics 4XL Beckman Coulter instrument (USA) 48 h following the infection.

RESULTS AND DISCUSSION

Construction of pseudo-HIV-1 particles and using them to infect different eukaryotic cell lines

Efficiency of transduction of target cells with pseudo-HIV-1 particles, and thus the fluorescence level of the

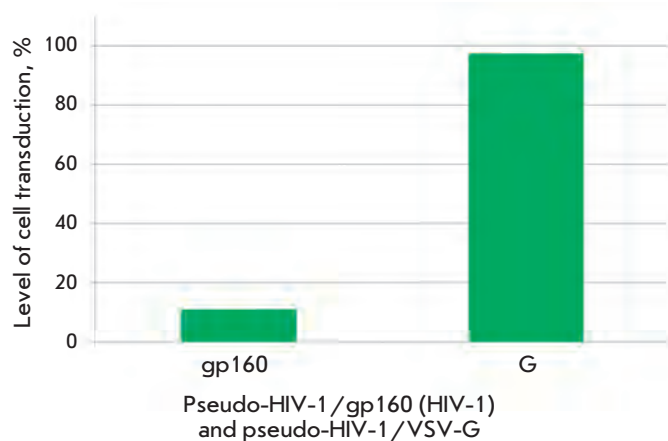


Fig. 2. The level of transduction of the Jurkat cell line with pseudo-HIV-1 particles containing glycoprotein gp160 of HIV-1 or glycoprotein G of the vesicular stomatitis virus (VSV-G) as an envelope protein.

resulting transgenic cells, is the most significant parameter of a lentiviral system. This parameter depends on the structure of pseudoviral particles (the type of coat proteins) and the particular line of infected target cells. The transplantable human lymphoblastic cells Jurkat and CEM-SS (T-lymphoblastic leukemia contain specific HIV-1 receptors), Kasumi-1 (acute myeloid leukemia), and mouse embryonic fibroblasts SC-1 were used as target cells.

Two types of pseudo-HIV-1 particles differing in coat proteins were obtained and subjected to study. Particles of the first type contain the HIV-1 coat protein gp160 (SUgp120 + TMgp41); particles of the second type contain the vesicular stomatitis virus (VSV) G

protein. The use of particles of the first type resulted in a comparatively low transduction efficiency and a weaker fluorescence signal (the data are not presented) from the infected cells (Fig. 2). In the case of pseudo-HIV-1 particles carrying the VSV G protein, the share of infected cells and the level of expression of the green fluorescent marker protein (eGFP) were considerably higher (Fig. 2). Moreover, the particles pseudo-typed with the VSV G protein can be used to transfer marker genes to the cells with wide type and tissue specificity. This procedure enables one to perform the search for retroviruses affecting tissues other than blood. Therefore, pseudo-HIV-1 particles with the VSV G protein were the ones used in most experiments devoted to the study of the properties of inhibitors of HIV-1 reverse transcriptase and integrase.

Nucleoside inhibitors of HIV-1 reverse transcriptase

Modified nucleosides and nucleotides have found broad application in the therapy of various viral diseases, including the HIV-1 infection [3]. Their mechanism of action includes conversion of these compounds, in a cell, into the corresponding nucleoside triphosphates, which act as terminating substrates for viral DNA and RNA polymerases. The integration of nucleotides into the growing chain of viral DNA/RNA blocks viral replication and slows the spread of the infection. The first and most well-known anti-HIV-1 agent of this class is 3'-azido-3'-deoxythymidine (AZT), which can inhibit viral replication even at a nano-molar concentration. The antiviral activity of AZT was studied with respect to pseudo-HIV-1 particles carrying the HIV-1 coat protein gp160 or the VSV protein G on their surface. Figure 3 shows the effect of AZT on the efficiency of cell transduction with HIV-1-like particles containing

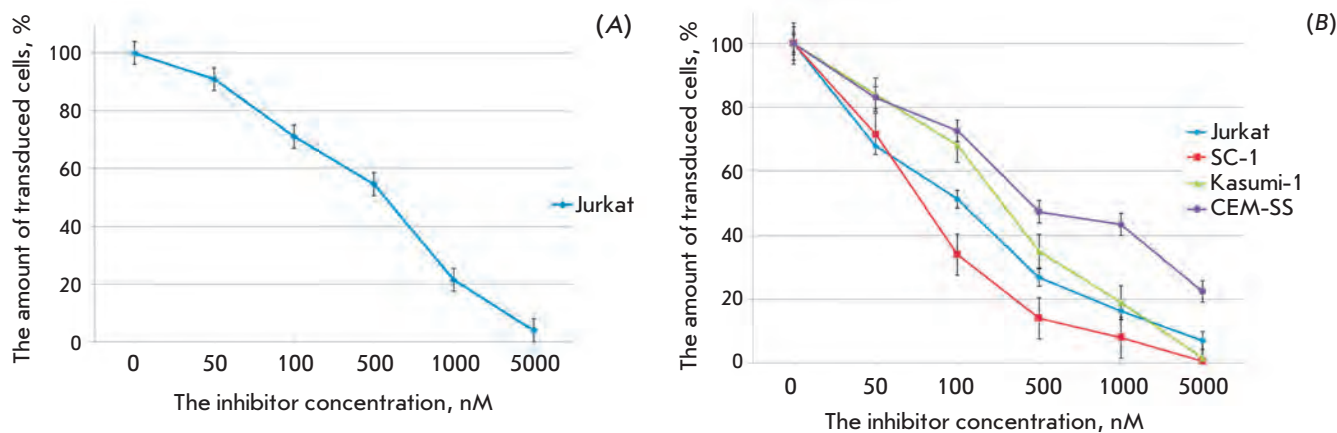


Fig. 3. The action of AZT on the transduction efficiency of different cell lines with pseudo-HIV-1 particles containing the envelope protein gp160 (A), or the envelope protein VSV-G (B). The level of transduction is shown with respect to the positive control.

Antiviral activity of the investigated agents with respect to pseudo-HIV-1 particles pseudotyped with vesicular stomatitis virus G protein

Agent	Cell line	ID ₅₀ , μm	
		Experimental data	Published data [20–29]
AZT	Jurkat	0.1 ± 0.01	0.004–0.1
	SC-1	0.08 ± 0.005	
	Kasumi-1	0.3 ± 0.02	
	CEM-SS	0.46 ± 0.05	
3TC	Jurkat	0.7 ± 0.05	0.02–0.35
	CEM-SS	0.85 ± 0.05	
d4T	Jurkat	7 ± 0.5	0.43–1.67
	SC-1	10 ± 0.5	
ddC	Jurkat	7 ± 0.5	0.067–0.316
	SC-1	5 ± 0.5	
ddI	Jurkat	> 20	1.79–12
	SC-1	> 20	
Nevirapine	Jurkat	0.1 ± 0.005	0.0072–0.22
	SC-1	0.15 ± 0.005	
	Kasumi-1	0.08 ± 0.005	
	CEM-SS	0.2 ± 0.01	
Non-nucleoside inhibitor of RT 1	Jurkat	0.95 ± 0.005	0.13
Non-nucleoside inhibitor of RT 2	Jurkat	0.08 ± 0.001	0.016
Non-nucleoside inhibitor of RT 3	Jurkat	0.085 ± 0.001	0.018
Raltegravir	Jurkat	0.009 ± 0.0005	0.0022–0.0037
	SC-1	0.006 ± 0.0005	
	CEM-SS	0.009 ± 0.0005	
L-731988	Jurkat	12 ± 0.1	1
	SC-1	8 ± 0.1	

reverse transcriptase, wild-type integrase, and HIV-1 coat protein gp160 (A) or the vesicular stomatitis virus G protein (B). It is clear that AZT suppresses the infection of eukaryotic cells with both types of pseudoviral particles, although the concentration of the particles is higher than that of infectious HIV-1 (Table) [20–22]. In the Jurkat cell culture, the activity of the agent was higher with respect to the particles pseudotyped with the VSV G protein. The antiviral activity of the nucleoside depended not only on the particle type, but also on the line of target cells. Thus, the maximum effect was observed on mouse SC-1 fibroblasts, whereas the minimum effect was observed when using CEM-SS cells. The reasons for these differences may be due to the different intracellular contents of nucleoside and nucleotide kinases [30], i.e., the enzymes required for the conversion of a nucleoside into the corresponding triphosphate, and the differences in the levels of expression of the specific transporters that are responsible for the transport of an agent into the cell, or its elimination [31].

Other well-known and commonly used antiretroviral agents are 2',3'-dideoxy-3'-thiocyridine (3TC) and 2',3'-2',3'-didehydrothymidine (d4T); similar to AZT, they are nucleoside inhibitors of HIV-1 reverse transcriptase [3]. 3TC was synthesized in 1989 and certified for clinical use in 1995. It is currently being used in combination with other drugs. The efficiency of joint use of 3TC and AZT has been demonstrated. We assessed the antiviral activity of 3TC on Jurkat and CEM-SS cell lines (Fig. 4). Drug activity in our system was somewhat lower than recorded in published data [20, 24]. The activity of other nucleoside analogues, including d4T, was also lower for our system, in comparison with that shown for infectious HIV-1 (Table) [20, 21, 24].

Non-nucleoside inhibitors of HIV-1 reverse transcriptase

Nevirapine is the most commonly used non-nucleoside blocker of HIV-1 replication and reverse transcriptase inhibitor [3]. This compound was certified as a drug in

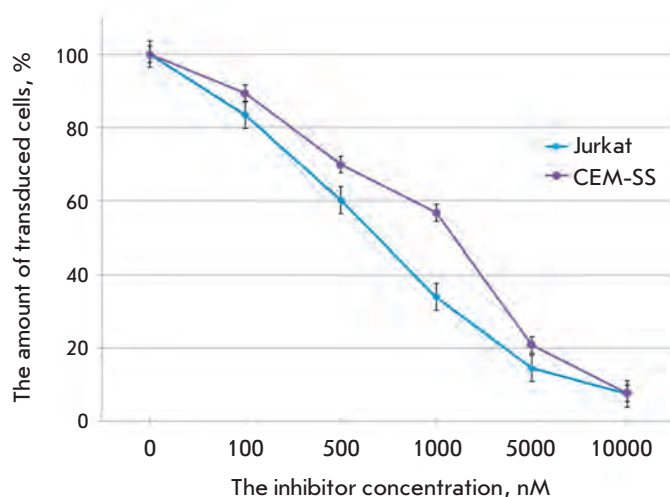


Fig. 4. The action of 3TC on the transduction efficiency of the cell lines Jurkat and CEM-SS with pseudo-HIV-1 particles containing the envelope protein VSV-G. The level of transduction is shown with respect to the positive control.

1996; at a concentration of 10^{-8} – 10^{-7} M, it can slow the development of the HIV-1 infection in cells infected with the natural virus. We studied the ability of nevirapine to prevent the transduction of target cells using the above-described pseudo-HIV-1 particles. In similar fashion to AZT, nevirapine exhibited a higher antiviral activity towards pseudoviral particles carrying the VSV G protein on their surface (Fig. 5). Again, similarly to AZT, nevirapine was most efficient in the SC-1 fibroblast culture, and less efficient in the CEM-SS cell line. It should be emphasized that nevirapine activity in our system was comparable to its activity towards infectious HIV-1 [21, 25].

In addition to the commercially available drug nevirapine, we tested three non-nucleoside inhibitors (denoted with the numbers 1, 2, and 3) which were synthesized according to the procedure described in [27]. These compounds are N¹-substituted uracils carrying benzophenone-oxyethyl (2 and 3) or benzyl-phenoxyethyl fragments (1). These compounds have been shown to possess high levels of anti-HIV-1 activity in a cell culture infected with the wild-type virus [27]. It was demonstrated that all three compounds can prevent the transduction of SC-1 cells with pseudo-HIV-1 particles with the VSV G protein; the activity of benzophenone-containing compounds (2 and 3) was considerably higher than that of the benzyl-phenoxyethyl-uracil derivative (1) (Fig. 6) and was comparable to that of nevirapine. The data obtained are in good correlation with the results of the study of these compounds in the infectious cell system (Table).

HIV-1 integrase inhibitors

The commercially available drug raltegravir (certified for use in clinical practice in October 2007) and the well-known integrase inhibitor L-731988 were used to assess the potential of the designed system for screening integrase inhibitors [28]. Raltegravir and L-731988 block the second integration stage, the chain transfer, thus impeding integrase binding to cell DNA. The efficiency of cell transduction with pseudo-HIV-1 particles with wild-type integrase as a function of inhibitor concentration is shown in Fig. 7. It is clear that raltegravir activity is higher than that of L-731988 by approximately three orders of magnitude, a fact that correlates with the data obtained for the infectious system [28, 32]. A decrease in the amount of fluorescing cells in the presence of integrase inhibitors attests to the fact that an

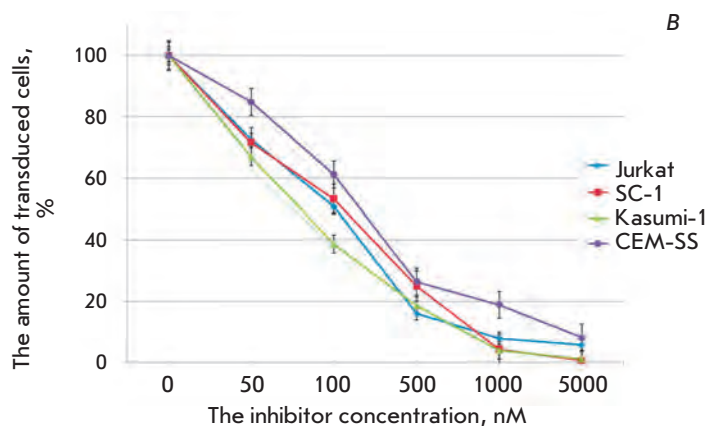
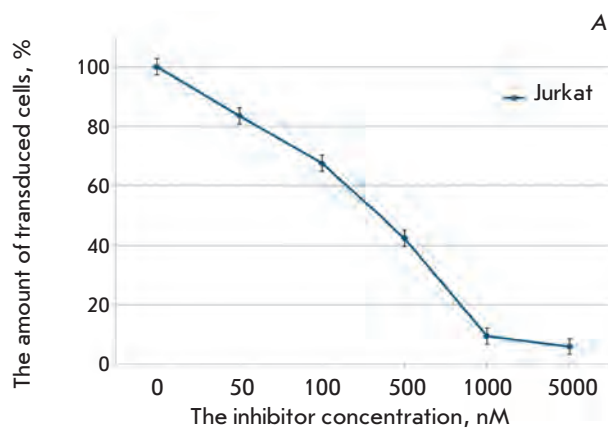


Fig. 5. The action of nevirapine on the transduction efficiency of different cell lines with pseudo-HIV-1 particles containing the envelope protein gp160 (A) or envelope protein VSV-G (B). The level of transduction is shown with respect to the positive control.

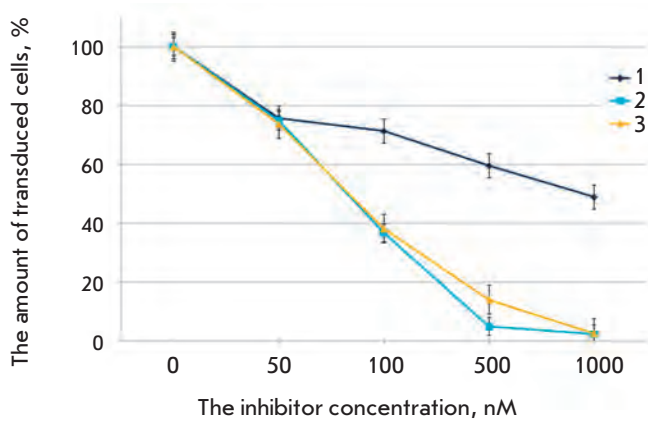


Fig. 6. The action of non-nucleoside reverse transcriptase inhibitors of HIV-1 1, 2 and 3 on the transduction efficiency of the Jurkat cell line with pseudo-HIV-1 particles containing the envelope protein VSV-G. The level of transduction is shown with respect to the positive control.

adequate integration of the synthesized DNA into the target cell genome takes place in the proposed pseudoviral system, and that pseudo-HIV-1 particles can indeed be used as a convenient tool for studying the antiviral activity of inhibitors of virus protease.

AZT-resistant pseudo-HIV-1 particles

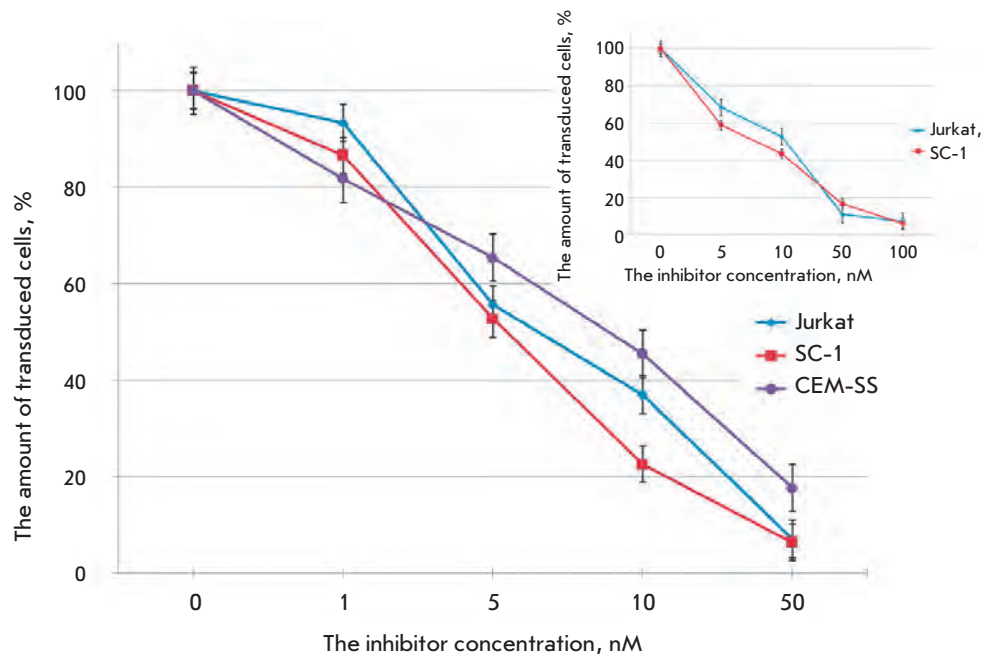
The search for potential inhibitors of the replication of drug-resistant HIV-1 strains is a very important task. However, such studies are often hampered not only by the need to use an infectious virus that is dan-

gerous for both personnel and the laboratory, but also by the complexity of obtaining strains that would be insensitive to this group of preparations. The proposed system allows one to easily construct variants of pseudo-HIV-1 particles that carry replication enzymes with the mutations determining their resistance to drugs. This fact was verified by constructing three types of pseudo-HIV-1 particles with the point substitutions D67N, K70R, T215F, and K219Q in reverse transcriptase, which are most typical of AZT-resistant HIV-1 strains [33, 34]. The antiviral activity of AZT was compared with that of these variants of pseudo-viral particles, demonstrating that AZT had a much weaker effect on the efficiency of transduction with mutant particles (*Fig. 8*). The decrease in the inhibiting effect correlated with an increase in the number of mutations (this effect was most clearly pronounced in SC-1 cells). Meanwhile, nevirapine, the non-nucleoside inhibitor of HIV-1 reverse transcriptase, retained its degree of activity towards all AZT-resistant types of pseudoviral particles (*Fig. 9*). This can be explained by the fact that the site of the binding to AZT is distant from the active site of the enzyme, which interacts with AZT triphosphate and contains all the aforementioned mutations. Thus, it is indeed pseudo-HIV-1 particles that allow one to study the ability of a substance to inhibit the drug-resistant forms of the virus.

Analogues of inorganic pyrophosphate

Another direction in approaches to the therapy of drug-resistant forms of HIV-1 consists in searching for compounds that would result in the recovery of virus

Fig. 7. The action of HIV-1 integrase inhibitors raltegravir (main figure) and L-731988 (inset) on the transduction efficiency of different cell lines with pseudo-HIV-1 particles containing the envelope protein VSV-G. The level of transduction is shown with respect to the positive control.



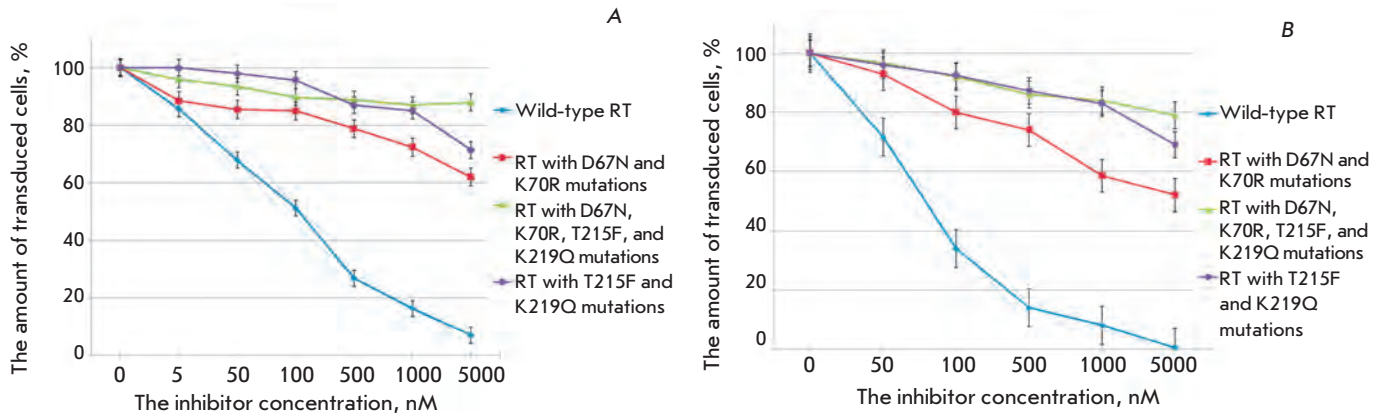


Fig. 8. The action of AZT on the transduction efficiency of cells with pseudo-HIV-1 particles containing envelope protein VSV-G and reverse transcriptase of wild-type or mutant form, shown for the Jurkat (A) and SC-1 (B) cell lines. The level of transduction is shown with respect to the positive control.

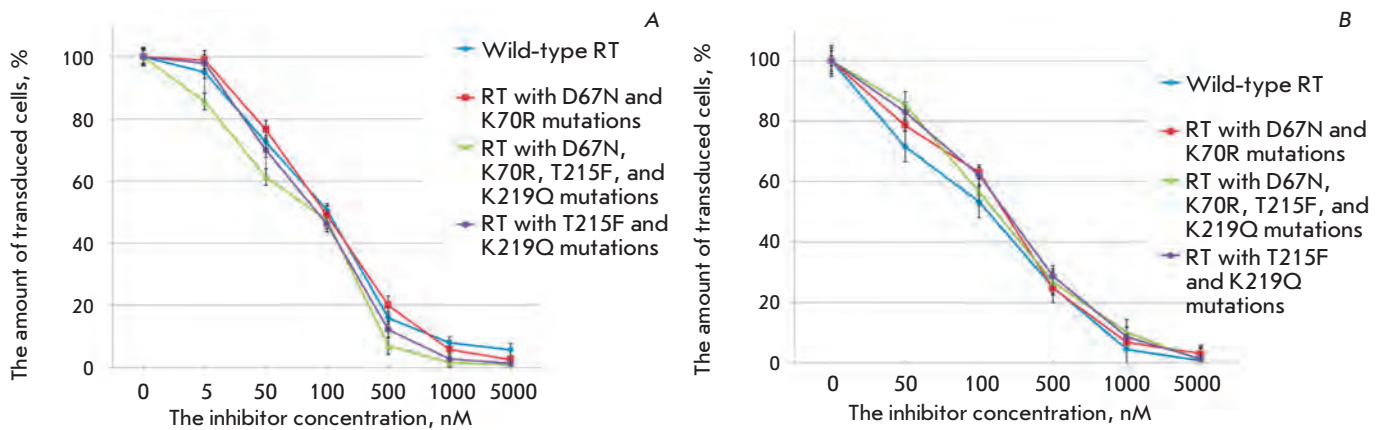


Fig. 9. The action of nevirapine on the transduction efficiency of cells with pseudo-HIV-1 particles containing envelope protein VSV-G and reverse transcriptase of wild-type or mutant form, shown on the Jurkat (A) and SC-1 (B) cell lines. The level of transduction is shown with respect to the positive control.

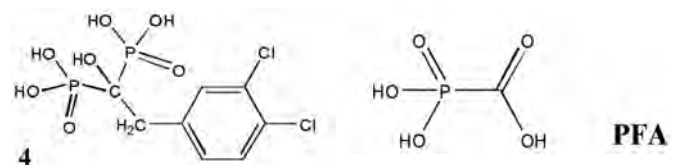
sensitivity to the earlier used antiretroviral agents, when used in conjunction with such agents. The modern concept holds that HIV-1 resistance to nucleoside reverse-transcriptase inhibitors can be achieved using two alternative mechanisms, which include the emergence of the following mutations in reverse transcriptase:

a) Mutations impeding the interaction between the enzyme and the corresponding nucleoside triphosphates (was described for 3TC) or:

b) Mutations facilitating the cleavage of the already-integrated terminating nucleotide from DNA during the pyrophosphorolysis reaction; after which synthesis of the growing DNA strand can continue (this mechanism is considered to be the major one for AZT) (Fig. 10).

Thus far, a number of mimetic compounds of inorganic pyrophosphate capable of suppressing nucleotide

cleavage upon pyrophosphorolysis have been described [35, 36]. One of these, foscarnet (PFA), has been successfully used in combination with AZT [37], a fact that supports the potential use of non-hydrolysable analogues of inorganic pyrophosphate in combination with nucleoside inhibitors in anti-AIDS therapy [37].



Derivatives of the hydroxymethylene diphosphonic acid, which are used in the therapy of bone-related diseases, are considered to be the most promising types of analogues of inorganic pyrophosphate. Contrary to foscarnet, this class of compounds do not be-

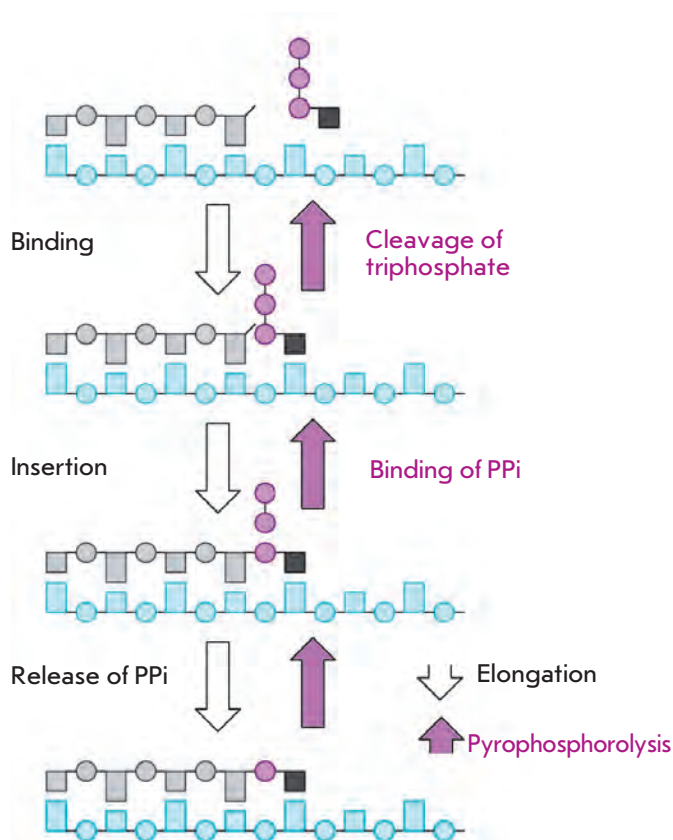


Fig. 10. Mechanism of the pyrophosphorolysis reaction catalyzed by reverse transcriptase.

have as substrates in the pyrophosphorolysis reaction. Nevertheless, they efficiently inhibit the pyrophosphorolytic cleavage of AZT from DNA, which is catalyzed by HIV-1 reverse transcriptase [36]. It should also be noted that no data on their activity in cell systems have been published. In this study, foscarnet (PFA) and the analogue of inorganic pyrophosphate, biphosphonate 4, were selected to assess the adequacy of the proposed cell system and study this type of compounds. Among its analogues, the dichlorobenzyl derivative of methylene diphosphonic acid 4 is the most active; it can suppress the cleavage of AZT monophosphate catalyzed by reverse transcriptase in the submicromolar concentration range [35]. The data on the joint action of azidothymine and the specified pyrophosphorolysis inhibitors are shown in Fig. 11. The degree of cell transduction inhibition with AZT-resistant pseudo-HIV-1 particles (carrying the point substitutions D67N, K70R, T215F, and K219Q in the reverse transcriptase) after the introduction of AZT combined with the selected pyrophosphorolysis inhibitor was determined in this experiment. The quantity of fluorescing cells in the individual presence of each

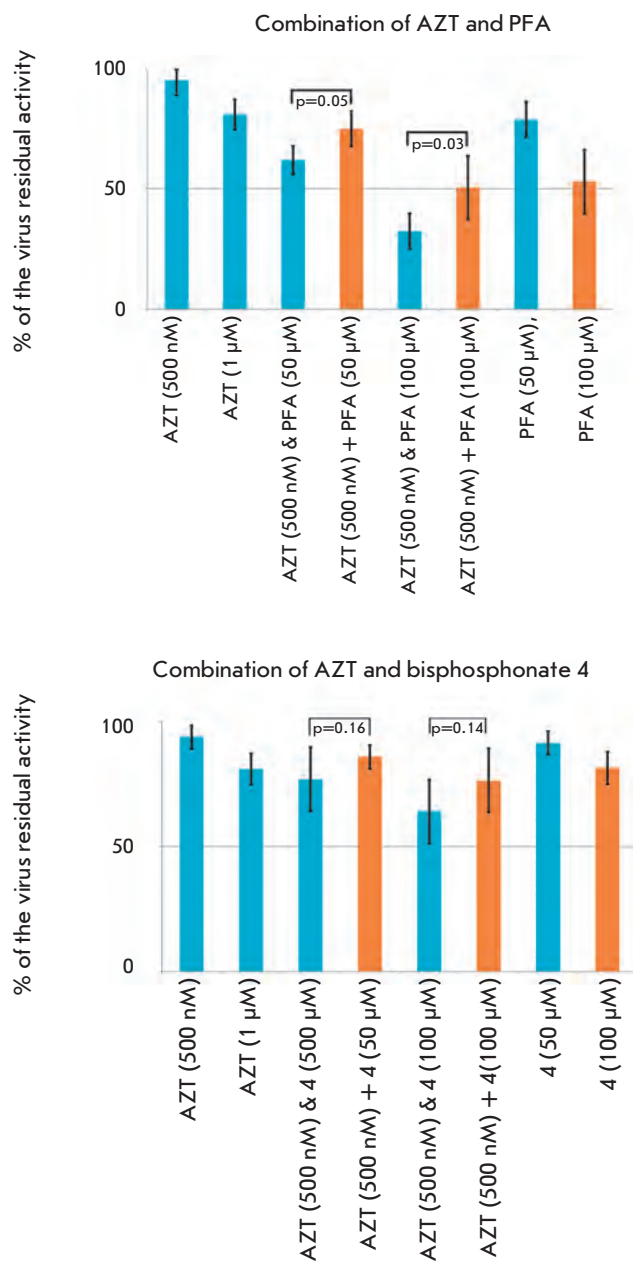


Fig. 11. The suppression of viral transduction via the combination of pyrophosphorolysis inhibitors and AZT. The data are represented as the average value of a series of five experiments \pm confidence interval ($P \leq 0.1$). The values of the series "AZT &" were obtained by simultaneous application of inhibitors at the concentrations indicated in brackets. The values of the series "AZT +" were calculated by multiplication of the residual activity of individual inhibitors. Concentrations are indicated in brackets. p – value of Paired Two Sample T-test of Student for indicated values.

of these substances was determined in the control experiment.

A conclusion concerning the additivity of the action of AZT and pyrophosphate analogues was made by comparing the degree of inhibition in the presence of two substances and the product of the degrees of inhibition by each substance (which attests to the independence of their action). As can be seen in *Fig. 11*, foscarnet and biphosphonate **4** suppressed cell infection with pseudoviral particles and provided a considerable and statistically significant enhancement of the action of AZT. Thus, the data obtained demonstrate, for the first time, that it is possible to recover the sensitivity of resistant forms of HIV-1 to nucleoside reverse transcriptase inhibitors in a cell culture. The data is also testament to the fact that analogues of inorganic pyrophosphate are promising agents for antiretroviral therapy.

CONCLUSIONS

A number of human and mouse cell lines were used to demonstrate that the described system for safe screening of potential HIV-1 replication inhibitors allows one to test the inhibitory activity of the compounds, whose action is directed both towards the reverse transcriptase and integrase of wild-type HIV-1 and towards their mutant forms corresponding to drug-resistant forms of the virus. It is important that the pseudo-HIV-1 particles used in this system are noninfectious. They are actually single-acting viruses (recombinant lentiviral vectors) that contain a complete set of viral enzymes ensuring the synthesis of the recombinant two-stranded DNA provirus and its integration into the genome of target cells. Next, the cell systems allow the expression of marker genes, which were integrated

into the cell genome, within the recombinant genome of pseudo-HIV-1 particles.

The absence of a complete set of HIV-1 in this recombinant genome on one hand ensures safety when testing the efficacy of new anti-HIV-1 compounds and, on the other hand, enables to adequately assess the action of these compounds on HIV-1 reverse transcriptase and integrase in the cells infected (transduced) with pseudo-HIV-1 particles. The possibility of forming pseudo-HIV-1 particles containing mutant drug-resistant reverse transcriptase and/or integrase allows one to perform the screening of potential inhibitors of drug-resistant forms of HIV-1.

Pseudotyping of a pseudo-HIV-1 particle with coat proteins of retroviruses of a different nature (including HIV-1 coat protein gp160) and those of other enveloped viruses considerably broadens the possibilities of the screening system by enabling the infection of cells of different types, and it also enables testing of the inhibitors of virus penetration into the cell. Finally, this system allows one to study the HIV-1 protease inhibitors, although this was beyond the scope of the present work. ●

This study was supported by the Programmes of Fundamental Research of the Presidium of the Russian Academy of Sciences “Molecular and Cell Biology” and “Foundations of Fundamental Research in Nanotechnologies and Nanomaterials”, Government Contracts with the Ministry of Education and Science of the Russian Federation № 16.512.11.2192, 16.512.11.2193, 16.512.12.2006, and 02.740.11.0706, and grants of the Russian Foundation for Basic Research № 09-04-01221-a, 11-04-12035-ofi-m, and 11-04-01365-a.

REFERENCES

- 2008 Report on the global AIDS epidemic, World Health Organization.
- <http://www.hivrussia.org/stat/2009/10.shtml>
- De Clercq E. // *Int. J. Antimicrob. Agents*. 2009. V. 33. № 4. P. 307–320.
- Kuritzkes D.R., Walker B.D. // *Fields Virology* / Eds Knipe D.M., Howley P.M. Philadelphia: Lippincott, Williams & Wilkins, 2007.
- Hengge U.R., Ruzicka T., Tying S.K., Stuschke M., Roggendorf M., Schwartz R.A., Seeber S. // *Lancet Infect. Dis*. 2002. V. 2. № 5. P. 281–292.
- Wittkop L., Günthard H.F., de Wolf F., Dunn D., Cozzi-Lepri A., de Luca A., Kücherer C., Obel N., von Wyl V., Masquelier B., et al. // *Lancet Infect. Dis*. 2011. V. 11. № 5. P. 363–371.
- Núñez M. // *Hepatology*. 2010. V. 52. № 3. P. 1143–1155.
- Izzedine H., Harris M., Perazella M.A. // *Nat. Rev. Nephrol*. 2009. V. 5. № 10. P. 563–573.
- Panyutich A.V., Prassolov V.S., Shydlovskaya E.A., Reznikov M.V., Chumakov P.M., Voitenuk N.N. // *Hybridoma*. 1990. V. 9. № 4. P. 401–406.
- Prassolov V.S., Meyer J., Brandenburg G., Hannemann J., Bergemann J., Ostertag W., Stocking C. // *Exp. Hematol*. 2001. V. 29. № 6. P. 756–765.
- Spirin P.V., Vilgelm A.E., Prassolov V.S. // *Mol. Biol. (Mosk)*. 2008. V. 42(5). P. 814–825.
- Spirin P.V., Baskaran D., Rubtsov P.M., Zenkova M.A., Vlassov V.V., Chernolovskaya E.L., Prassolov V.S. // *Acta Naturae*. 2009. V. 2. № 2 (2). P. 86–90.
- Spirin P.V., Baskaran D., Orlova N.N., Rulina A.V., Nikitenko N.A., Chernolovskaya E.L., Zenkova M.A., Vlassov V.V., Rubtsov P.M., Chumakov P.M., et al // *Mol. Biol. (Mosk)*. 2010. V. 44(5). P. 776–786.
- Kellam P., Larder B. // *Antimicrob. Agents Chemother*. 1994. V. 38. № 1. P. 23–30.
- Walter H., Schmidt B., Korn K., Vandamme A.M., Harrer T., Überla K. // *J. Clin. Virol*. 1999. V. 13. № 1–2. P. 71–80.
- Jármy G., Heinkelein M., Weissbrich B., Jassoy C., Reth-

RESEARCH ARTICLES

- wilm A. // *J. Med. Virol.* 2001. V. 64. № 3. P. 223–231.
17. Garcia-Perez J., Sanchez-Palomino S., Perez-Olmeda M., Fernandez B., Alcami J. // *J. Med. Virol.* 2007. V. 79. № 2. P. 127–137.
18. Cheresiz S.V., Grigoryev I.V., Semenova E.A., Pustyl'nyak V.O., Vlasov V.V., Pokrovsky A.G. // *Dokl. Biochem. Biophys.* 2010. V. 435. P. 295–298.
19. Prassolov V.S., Chumakov P.M. Vector pPS-1-neo for gene transfer and expression in cultivated somatic mammalian cells. Inventor's certificate № 1440036 from 26.06.1987. Application 4268094. (Russian).
20. Rosenblum L.L., Patton G., Grigg A.R., Frater A.J., Cain D., Erlwein O., Hill C.L., Clarke J.R., McClure M.O. // *Antivir. Chem. Chemother.* 2001. V. 12. № 2. P. 91–97.
21. Smith R.A., Gottlieb G.S., Miller A.D. // *Retrovirology.* 2010. V. 7. P. 70–81.
22. Bjerke M., Franco M., Johansson M., Balzarini J., Karlsson A. // *Biochem. Pharmacol.* 2008. V. 75. № 6. P. 1313–1321.
23. Perez-Bercoff D., Wurtzer S., Compain S., Benech H., Clavel F. // *J. Virol.* 2007. V. 81. № 9. P. 4540–4550.
24. Patick A.K., Boritzki T.J., Bloom L.A. // *Antimicrob. Agents Chemother.* 1997. V. 41. № 10. P. 2159–2164.
25. Grob P.M., Wu J.C., Cohen K.A., Ingraham R.H., Shih C.K., Hargrave K.D., McTague T.L., Merluzzi V.J. // *AIDS Res. Hum. Retroviruses.* 1992. V. 8. № 2. P. 145–152.
26. Witvrouw M., Arranz M.E., Pannecouque C., Declercq R., Jonckheere H., Schmit J.C., Vandamme A.M., Diaz J.A., Ingate S.T., Desmyter J., et al. // *Antimicrob. Agents Chemother.* 1998. V. 42. № 3. P. 618–623.
27. Novikov M.S., Ivanova O.N., Ivanov A.V., Ozerov A.A., Valuev-Elliston V.T., Gurskaya G.V., Kochetkov S.N., Pannecouque C., Balzarini J., Seley-Radtke K.L. // *Bioorg. Med. Chem.* 2011. V. 19. № 19. P. 5794–5802.
28. Hazuda D.J., Felock P., Witmer M., Wolfe A., Stillmock K., Grobler J.A., Espeseth A., Gabryelski L., Schleif W., Blau C., et al. // *Science.* 2000. V. 287. № 5453. P. 646–650.
29. Paprotka T., Venkatachari N.J., Chaipan C., Burdick R., Delviks-Frankenberry K.A., Hu W.S., Pathak V.K. // *J. Virol.* 2010. V. 84. № 11. P. 5719–5729.
30. Gröschel B., Höver G., Doerr H.W., Cinatl J., Jr. // *Nucleosides Nucleotides Nucleic Acids.* 2001. V. 20. № 4–7. P. 487–492.
31. Paintsil E., Dutschman G.E., Hu R., Grill S.P., Wang C.J., Lam W., Li F.Y., Ghebremichael M., Northrup V., Cheng Y.C. // *Antimicrob. Agents Chemother.* 2011. V. 55. № 2. P. 895–903.
32. Summa V., Petrocchi A., Bonelli F., Crescenzi B., Donghi M., Ferrara M., Fiore F., Gardelli C., Gonzalez Paz O., Hazuda D.J., et al. // *J. Med. Chem.* 2008. V. 51. № 18. P. 5843–5855.
33. Arion D., Parniak M.A. // *Drug Resist. Updat.* 1999. V. 2. № 2. P. 91–95.
34. Isaguliantis M.G., Belikov S.V., Starodubova E.S., Gizatullin R.Z., Rollman E., Zuber B., Zuber A.K., Grishchenko O.I., Rytting A.S., Källander C.F., et al. // *AIDS Res. Hum. Retroviruses.* 2004. V. 20. № 2. P. 191–201.
35. Cruchaga C., Ansó E., Rouzaut A., Martínez-Irujo J.J. // *J. Biol. Chem.* 2006. V. 281. № 38. P. 27744–27752.
36. Song Y., Chan J.M.W., Tovian Z., Secrest A., Nagy E., Krysiak K., Bergan K., Parniak M.A., Oldfield E. // *Bioorg. Med. Chem.* 2008. V. 16. P. 8959–8967.
37. Jacobson M.A., van der Horst C., Causey D.M., Dehlinger M., Hafner R., Mills J. // *J. Infect Dis.* 1991. V. 163. № 6. P. 1219–1222.

Behavior of Transplanted Multipotent Cells after *in Vitro* Transplantation into the Damaged Retina

S.A. Sergeev^{1*}, Y.V. Khranova¹, M.L. Semenova¹, I.N. Saburina², N.V. Kosheleva^{1,2}

¹Biology Faculty, Lomonosov Moscow State University

²Institute of General Pathology and Pathophysiology, Russian Academy of Medical Sciences

*E-mail: embryossa@gmail.com

Received 05.08.2011

ABSTRACT The use of stem cell technologies in retinal defect reparation therapy has produced beneficial results. Nowadays, numerous protocols exist which provide a neural differentiation of the stem cells transplanted into the retina. However, questions concerning the functional replacement of the missing retinal neurons by transplanted cells thus far remain unanswered. The organotypic culture protocol was used in this study in order to prove the possibility of transdifferentiation of bone marrow stromal cells (MMSCs) and neural stem/progenitor cells (NSPCs) from EGFP-positive mice and the functional integration of these cells. This technique enables a detailed characterization of cell behavior post-transplantation. Using atomic force microscopy, we reliably demonstrated the difference ($p < 0.01$) between the thickness of the outgrowths formed by glial and endothelial retina cells and the thickness of neurites and neuro-like transplanted MMSC outgrowths. MMSCs are also shown to form synapses up to $2.5 \pm 0.06 \mu\text{m}$ in diameter on day 4 after the transplantation. Following electrical stimulation (20V, 0.5Hz, 200ms), clear depolarization of retinal neurons and their outgrowths is detected. It is shown that some of these GFP+ MMSCs, which changed their morphology after the transplantation in retinal explants to neuro-like MMSCs, are capable of depolarizing after exogenous stimulation.

KEYWORDS stem cells; *in vitro* transplantation; retinal organotypic cultures; stem cell plasticity; retinal reparation.

ABBREVIATIONS MMSC – bone marrow-derived mesenchymal stem cells; NSPC – neural stem/progenitor cells; EGFP – enhanced green fluorescent protein.

INTRODUCTION

Retinal changes caused by various exogenous damaging factors often lead to a partial or total loss of vision. In order to provide efficient therapy for retinal pathologies it is necessary to understand the processes involved in the emergence and progression of these pathologies, as well as the processes leading to retinal reparation. Methods for the transplantation of cells of wide differentiation potential – neural stem/progenitor cells (NSPCs) or bone marrow-derived mesenchymal stem cells (MMSCs) – are currently being developed in order to curb the progression of irreversible neurodegenerative processes in the retina. It is believed that, after they are introduced into a recipient's organism, these cells not only actively migrate to the damaged site and replace the missing tissue elements with their differentiated descendants, but that they also secrete a broad range of trophic and regulatory factors that maintain the functionality of the damaged tissue and activate its own reparation systems [1].

Unfortunately, the theoretical and practical data thus far accumulated in the area of stem cell biology

remains insufficient in order to reliably predict how efficient cell transplantation therapy can be. We are still some way from a complete understanding of the mechanisms that initiate reparation in a recipient's tissue following the introduction of cells. Moreover, we still haven't figured out means to control this process. In this context, it seems reasonable to design adequate models that are as close as possible to *in vivo* conditions, thereby enabling one not only to perform easy detection of cell migration, differentiation, and death at any stage following transplantation, but also to adjust the behavior of the transplanted cells. An organotypic explant culture of rat retina is one of such models. This type of culture is used to obtain specimens that are capable of retaining *in vitro* their initial cytoarchitectonics and cell structure for a long time [2].

Laser-induced local damage to retinal explants in the *in vitro* system is considered to be the most appropriate experimental model of retinal damage. This approach allows to inflict a strictly defined level of damage: i.e., to obtain reproducible results in an entire series of experiments. The use of this approach in experimental

studies devoted to the simulation of neuronal network damage has a lot of potential, due to the fact that it allows to independently control the various parameters of laser radiation.

EXPERIMENTAL

Obtainment of retinal cultures

The retinal explant culture was obtained from 4-day-old male Wistar rats. Eyeball dissection was performed according to the modified protocol [3]. After isolation of the retina, it was then placed on the surface of a 35 mm diameter Petri dish with the photoreceptor layer on top.

Culturing was performed under standard conditions (+37 °C, 5% CO₂, 98% humidity) for 30 days in a DMEM/F12 medium (PanEco, C420/C600) containing glutamine (Sigma, G-8540) and insulin-transferrin-sodium selenite at 1 : 50 dilution (PanEco, F-065) supplemented with FCSTM 5% serum (HyClone, SH30109.03), the major fibroblast growth factor (10 ng/ml, Sigma, F0291), epidermal growth factor (10 ng/ml, Sigma, E9644), heparin, gentamicin at a concentration of 5 µl/ml (Sigma, G1264), additives N2 at 1 : 100 dilution (Gibco, 17502-048), and B27 at 1 : 50 dilution (Gibco, 17504044).

Damaging explant

A Zilos-tkTM infrared laser (Hamilton Thorne, 1480 nm, millisecond-long pulse duration, 300 mV intensity) heating the spot of laser focus to 150⁰ C was used as the damaging factor. A square with a 100 µm side length (within the average explant margin excrescence area) was selected as the object to be damaged. Damage was inflicted on the retina using 15 laser pulses (1000–3000 ms long) on day 14 of explant culturing.

Cell transplantation

Red bone marrow from EGFP-positive C57BL/6-Tg(ACTB-EGFP)/OsJ mice (1 month) was used to obtain the MMSC culture. Red bone marrow specimens were taken from the shinbones and thigh bones of the animals immediately prior to euthanasia, according to the protocol [4]. The stroma of the bone marrow was removed by washing the bone cavity with an insulin syringe filled with the DMEM medium supplemented with antibiotic agents. The resulting suspension was centrifuged for 7 min at 1000 g. The supernatant liquid was poured away; the precipitate was then re-suspended and diluted with the culture medium to attain a density of 1 × 10⁵ cells/ml. The primary suspension cell culture from the stroma of the bone marrow was placed into culture dishes (60 mm in diameter); after 24 h, the cells were sub-cultured at a significantly low cell density (1–5 cells within the field of vision, 200x

magnification). The cells were then cultured until colonies formed.

The material taken from the subventricular zone of the brain of a 14-day-old C57BL/6-Tg(ACTB-EGFP)/OsJ mouse embryo was used to culture NSPCs. After the brain was released from the meninges, it was placed into a DMEM medium supplemented with antibiotic agents and then subjected to mechanical deaggregation with a pipette until a homogeneous cell suspension was obtained. The cells were then centrifuged for 5 min at 1000 g. The supernatant liquid was poured away; the precipitate was subsequently re-suspended in the culture medium at a concentration of 1 × 10⁶–2 × 10⁶ cells/cm². The cells were cultured in the neuroepithelial stratum.

The cells were injected with a glass microcapillary on a Nikon TE2000S inverted microscope equipped with hydraulic micromanipulators and Narishige injectors (MMO-202ND, IM-9B, IM-H1, Narishige HD-21) into the zone of explant cell excrescence (0.1 µl of the culture medium) at a distance of 100, 1000, and 3000 µm from the damaged area. The efficiency of the protocols of cell transplantation into the retina imitating the suprachoroidal injection was assessed by placing the suspension of cells to be transplanted onto the external (photoreceptor) explant surface using a microinjector (medium volume being less than 5 µl).

Immunohistochemical analysis

The immunohistochemical analysis of the differentiation of the transplanted cells was performed by detecting neuronal and glial differentiation markers: βIII-tubulin – using anti-tubulin, beta III isoform antibody (Chemicon, MAB1637), and glial fibrillary acidic protein GFAP – using anti-glial fibrillary acidic protein antibody (Sigma, G9269), respectively. The expression of the neurite outgrowth markers GP-45 was also assessed using a G protein-regulated inducer of neurite outgrowth 2 antibody (Abcam, ab110898) and the capillary endothelial cell marker GSL-IB4 – isolectin from *Griffonia simplicifolia* IB4 (Sigma, L1509).

Cell imaging

The images of living cells were obtained using a Nikon TE2000S inverted microscope; the fluorescence images were taken using an Axiovert 25 inverted fluorescence microscope. The spatial pattern of distribution of the transplanted cells in an explant was obtained via confocal laser scanning microscopy (Axiovert 200LSM 510Meta Carl Zeiss microscope).

Statistical analysis

The reliability analysis of the results and statistical processing were performed using the STATISTICA 6.0

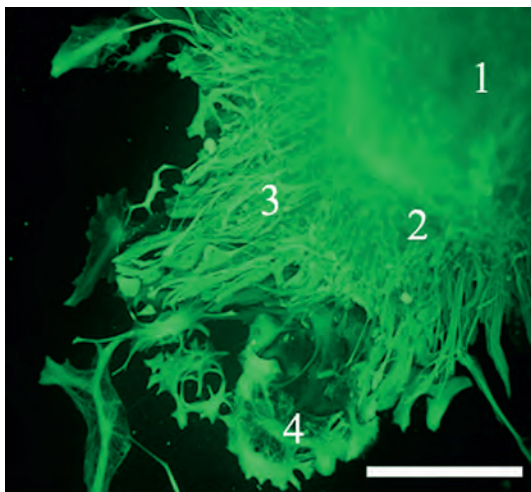


Fig. 1. Migration of retinal explant cells (1) with the formation of multicellular close-in (2), middle (3), and monolayer distant (4) areas of explant margin excrescence. The scale bar is 300 μm .

software. The existence and reliability of differences between the sample values of independent samplings was assessed using the nonparametric Kruskal–Wallis H test. The statistical significance of differences between the injected cell groups (MMSCs, NSPCs) was determined using the Student–Newman–Keuls test (ANOVA).

Atomic force microscopy (AFM)

AFM images were obtained on a Solver BIO Olympus atomic force microscope (NT-MDT, Russia) with a scanning range of $100 \times 100 \times 7 \mu\text{m}^3$, equipped with a system of capacity sensors and cantilever Veeco MSCT-AUHW (Veeco Instruments, USA) with a rigidity of 0.01–0.03 N/m. A laser operating at 650 nm was used to record the cantilever bending. The instrument was integrated into the inverted optical microscope in order for the cantilever to be close enough to the sample and establish the scanning sites. The images were processed using the Nova software (NT-MDT, Russia).

RESULTS AND DISCUSSION

Organotypic retinal explant cultures capable of surviving long-term *in vitro* were obtained during the first stage of our study. Tissue architectonics was retained during the entire culturing period (up to 30 days); the major cell types typical of an intact retina *in vivo* were present within the tissue [5] (Fig. 1). Thus, this explant culture is an adequate model of the developing neuroretina, enabling the retention of the micro-surrounding neural cells within.

The tissue macrostructure within the beam focus changed distinctly after damage with a laser pulse. This was accompanied by the darkening of the cell cytoplasm, an intense vacuolization of the cells, and the coagulation of the intercellular matrix. A delayed effect of laser irradiation (mass cell death in the area of retinal explant damage) was observed on days 2–3 after the injury. A zone of mass cell death with a radius of up to 500 μm formed around the immediate area of laser impact ($100 \times 100 \mu\text{m}$). Thus, the laser-induced damage (irreversible) could clearly be visualized, manifesting itself in an essential reorganization of the intercellular matrix (coagulation), thus resulting in the loss of cellular interactions and in changes to the cell morphology, finally culminating in cell death.

NSPCs and MMSCs from EGFP-positive mice were injected into the centre of explant cell location in order to simulate repair of the area of the retina damaged by the laser pulse. After the transplanted cells reached their new micro-surrounding, they actively migrated and changed in morphology, sprouting long branching outgrowths, and acquiring neuron-like phenotypes.

The distribution of EGFP-positive cells within the damaged area and the injection area over their migration vector was analyzed during the first 24 h and on day 3 and day 7 after the transplantation. It was established via a comparison of the distribution of the EGFP-positive cells that the most active cell migration occurs from the transplantation site to the damaged area (Fig. 2A, B). It was shown by daily registration of cell migration by confocal microscopy that the migration was most intense during the first 24 h, followed by a considerable decrease as the cells underwent morphological differentiation on day 3 following the injection. The first cells that migrated to the laser-influenced area were detected 1 h after the transplantation, when they were introduced at a distance of 100 μm . When the cells were transplanted at a distance of 500 and 1000 μm away from the damaged site, they were detected after 12 h or 3–5 days, respectively. Cell migration to the damaged area was most active during the first 3 days after the retinal defect, followed by an abrupt decrease in the level of cell migration. It appeared that 3 days after the transplantation, the injected cells actively migrated to distances of over 1000 μm from the injection site. It is notable that the cells moved towards the damaged area. The injected cells propagated in the explant along a vector directed toward the injured area at a distance of 5 mm, and in the opposite direction, at a distance not exceeding 1 mm (Fig. 2C, D). A significantly greater ($p < 0.01$) amount of the transplanted cells was detected in this region via statistical processing of the results of a count of EGFP+–NSPCs

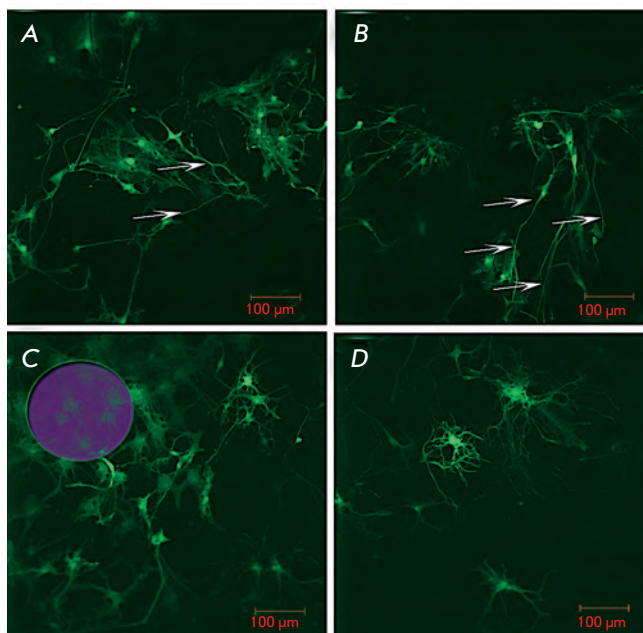


Fig. 2. NSPC taxis directed towards the laser-damaged retinal explant area. (A, B) – Neurite outgrowth (marked with arrows) from transplanted EGFP+ cells following the direction of the vector from the injection site to the laser-damaged area. (C, D) – Localization of the transplanted NSPCs in the laser-damaged area on day 7 after the transplantation and the development of the dense neurite net on day 14.

within one vision field in the damaged area and at the same distance along a vector passing through the injection site (*Fig. 3*).

The propagation of injected cells in the control explants subjected to cell transplantation without laser damaging was uniform in all directions; cell migration from the explant center along the migration routes was predominant. Thus, nonuniformity of the distribution of the transplanted NSPCs with respect to the injected site after the laser-induced damage (the taxis directed towards the defect area) was demonstrated. Similar data concerning the changes in the behavior of injected cells in the neuronal micro-surrounding were obtained after the *in vivo* transplantation of NSPCs [6].

After reaching the damaged area, cell migration ceased; formation of asynaptic dendrites propagating in all planes and aggregation of the transplanted cells were observed. The cells that migrated into the damaged area remained there throughout the entire experiment (up to 30 days after the transplantation) and formed a dense neurite network, thereby completely losing their migration activity.

The cell concentration upon transplantation had a considerable impact on the behavior of the transplanted cells. The introduction of single cells into the explant resulted in a rapid end to their migration within the retina and was accompanied by weak morphological differentiation. Single NSPCs acquired a glial phenotype and had glial differentiation markers (GFAP) starting from day 5 after the transplantation. The maximum time during which single MMSCs were retained in the explant was 24 h. The migration activity of cells was suppressed upon transplantation of 50–100 cells. Association was observed, and cell taxis occurred in opposite directions. Only single cells migrated to considerable distances. The situation was different with the transplantation of over 1,000 cells. In this case, most cells actively migrated towards the damaged area, where they formed long neurites, which facilitated the migration of other cells. The differentiation of NSPCs was also faster in comparison to that for the intact explant; the neuronal component was predominant, and the transplanted cells expressed β III-tubulin and GP-45. The injected cells within the explant not only remained viable for over 2 months, but also actively proliferated.

When studying the distribution of the transplanted NSPCs over the explant with several sequential laser-damaged areas located at different distances from the injection site (600, 1 000, and 3 000 μ m), we found that lodging of all damaged areas with the transplanted cells occurred throughout the 7 days immediately following the injection (*Fig. 3*). However, the amount of cells in the damaged areas decreased with increasing distance from the injection site. Thus, 56% of the cells detected in the area at a distance of 600 μ m were located in the damaged area at a distance of 1 000 μ m from the transplantation site, whereas the zone at a distance of 3 000 μ m contained only 27% of the cells.

Two methods of cell introduction were used for the transplantation of MMSCs and NSPCs: firstly, direct injection into the middle area of the explant excrescence margin; secondly, coating of the surface with cells. In the first case, the transplanted cells were in immediate contact with the neuronal component, whereas the *in vivo* suprachoroidal injection was simulated in the second case. After NSPCs were coated onto the surface of the retinal explant, they manifested an almost complete absence of migration activity and neuronal differentiation processes (negative β III-tubulin staining). This observation allows one to interpret the insignificant therapeutic effect of the transplanted NSPCs in clinical practice after suprachoroidal or retrobulbar injection [7]. After NSPCs were injected deep into neuroretinal layers, the transplanted cells actively migrated and changed their morphology. They sprouted long

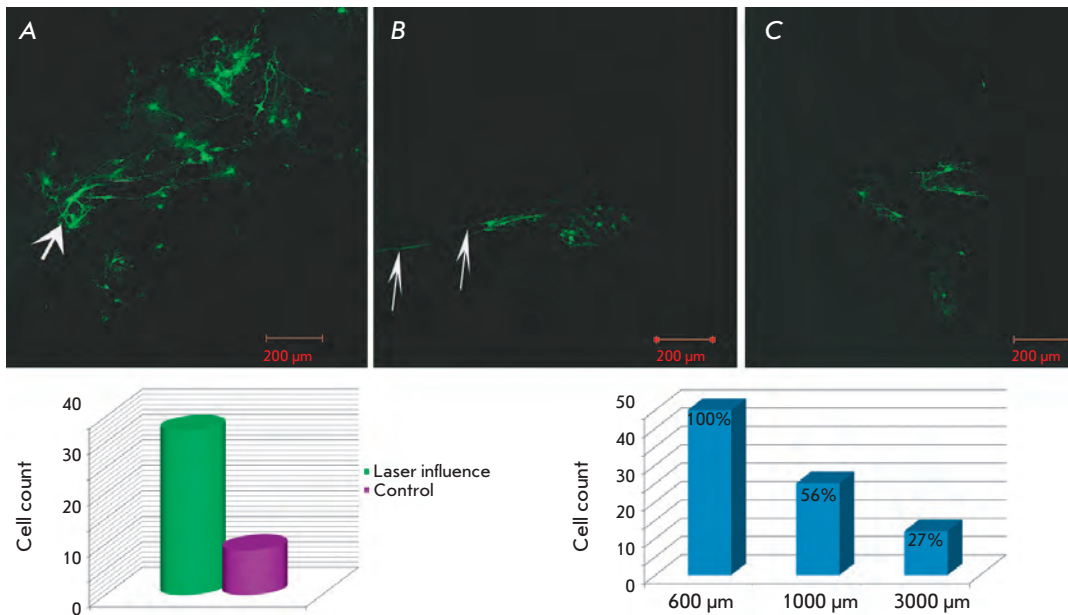


Fig. 3. Dynamics of NSPC fast migration to the laser-damaged retina area after the transplantation at a distance of 600 μm (A), 1000 μm (B), and 3000 μm (C) from the laser influence. The diagrams of quantitative differences between cell migration in the damaged and intact explants and the histogram of the percentage of cell count in laser-damaged areas at different distances from the damage site.

branching outgrowths, acquired a neuron-like phenotype, and were positively stained against β III-tubulin and GP-45.

Rapid migration of individual cells of small diameter (10–15 μm) and the formation of long neurite-like outgrowths and lamellopodia were observed when MMSCs were introduced using both methods. Thus, the transplanted cells were morphologically differentiated according to the new micro-surrounding; the transplanted cells acquired a neural cell phenotype (Fig. 4). When transplantation of at least 500 cells was performed, MMSCs remained intact within the explant for 30 days. The transplanted MMSCs acquired two characteristic phenotypes: the neuronal one (with long and thin branching outgrowths with ampullary dilations and a compact cell body) and glial one (with cytoplasmic outgrowths (lamellopodia) and a large nucleus with easily-observable nucleoli). Neurite-like MMSC outgrowths penetrated deep into the retinal explant, formed anastomoses, and were in contact with other transplanted cells and neurons of the explant; i.e., the behavior of MMSCs transplanted into the surrounding of the neuroretina was similar to that of the injected NSPCs. However, in contrast to NSPCs, the method of introduction of MMSCs had no effect on the migration activity of the transplanted cells. MMSCs migrated in all directions from the injection site during the first day, both after being coated onto the surface and after injection into the explant. The onset of cell differentiation resulted in the end of migration, attesting to the fact that the first hours after the transplantation are

significant for the migration of the injected cells and the occupation of new niches, as well as their proliferation and differentiation, with the subsequent possibility of defect repair [8].

When the explant was damaged, the changes in MMSC morphology were more rapid in comparison with those in the cells introduced into the control specimens that were not damaged by a laser. In this experimental series, the morphological changes in MMSCs manifested themselves 24 h after the injection, whereas the period for the control specimens was 3 days. These data allow one to assume that the regulatory factors releasing as a result of cell death in the damaged area are of extreme importance for the morphological differentiation of the transplanted cells, which satisfies the conditions of their new micro-surrounding.

By means of atomic force microscopy, it was possible to show the morphological transformation of MMSCs transplanted into the cells with a neuronal phenotype, their active migration during a period up to 3 days after the injection, and the formation of bipolar and multipolar neurite-like outgrowths. Cell migration from the retinal explant was preceded by lamellopodia formation. AFM was used to measure the heights of lamellopodia, to study their spatial distribution, and to estimate the roughness of their surface. According to the AFM data, the average length of the primary lamellopodia of the migrating cells was $10.1 \pm 2.0 \mu\text{m}$; the average diameter was equal to $3.6 \pm 0.5 \mu\text{m}$. An increase in the extent of synaptic dendrites sprouted by the migrating cells of the retinal explant was observed by day 7 of cell culturing. According to the AFM

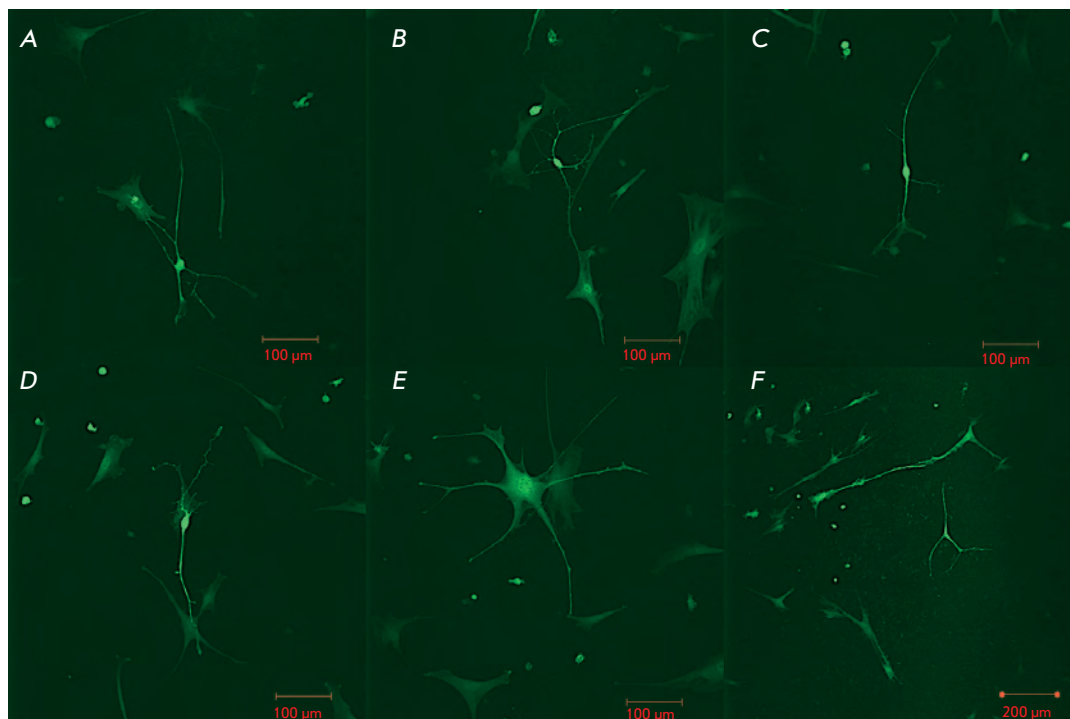


Fig. 4. Changes in the morphology of the transplanted MMSCs in laser-damaged retinal explants. (A–D) – The injected MMSCs acquired a neuronal morphology; (E, F) – Differentiation of the injected MMSCs according to the glial phenotype.

data, their average length was $21.7 \pm 5.0 \mu\text{m}$; the average diameter was equal to $0.8 \pm 0.23 \mu\text{m}$. The neurite-like outgrowths of MMSCs (being several millimeters long and up to $0.47 \mu\text{m}$ in diameter) propagated on the surface of glial (GFAP-positive) and endothelial (GSL-IB4-immunopositive, GFAP-immunonegative) cells (Fig. 5A, B).

The quantitative analysis of the distribution of outgrowth heights for the groups of glia-like cells and neuron-like MMSCs revealed a significant divergence ($p < 0.01$) in the heights of the outgrowths formed by glial and endothelial retinal components and the neuronal outgrowths and transplanted MMSCs (Fig. 5E). It was clear that no statistically significant differences existed ($p = 0.52$) between the root-mean-square roughness of the surface of the transplanted MMSCs (whose morphology changed to neuron-like) and retinal neurons. No statistically significant differences ($p = 0.26$) were revealed when comparing the asymmetry of distribution of the outgrowths of the transplanted cells and retinal explant neurons (Fig. 5F). When examining the images of the cell surface, no statistically significant differences in the range of outgrowth heights were detected between MMSCs and retinal neurons, whereas there were statistically significant differences ($p < 0.01$) between the heights of MMSC outgrowths and the heights of the outgrowths of glial and endothelial retinal cells. AFM images of synaptic dilatations formed by the transplanted

MMSCs on the ends of neurite-like outgrowths were obtained (Fig. 5C). The interaction between these synapses and explant cells was also studied. The morphometric parameters of the synapses between the transplanted MMSCs and retinal neurons did not differ from the parameters between the transplanted NSPCs and the recipient cells.

The retinal explant cells were stained with dye Di-I, which was used to demonstrate that no fusion of the transplanted EGFP-positive MMSCs and the retinal cells took place, since no cells carrying both labels were detected.

Based on the data obtained, it can be reasonably suggested that direct introduction of NSPCs into the neuroretina is the optimal method for efficient reparation of retinal damage using cell transplantation. MMSCs, which are capable of initiating and maintaining the reparation processes in the recipient tissue and of following the neuronal differentiation path, can be considered a similar and available alternative to these cells [9]. However, the questions regarding the functional replacement of the missing nerve cells with transplanted MMSCs and their descendants still remain open.

CONCLUSIONS

The obtained retinal explant cultures are equivalent to *in vivo* neuroretina.

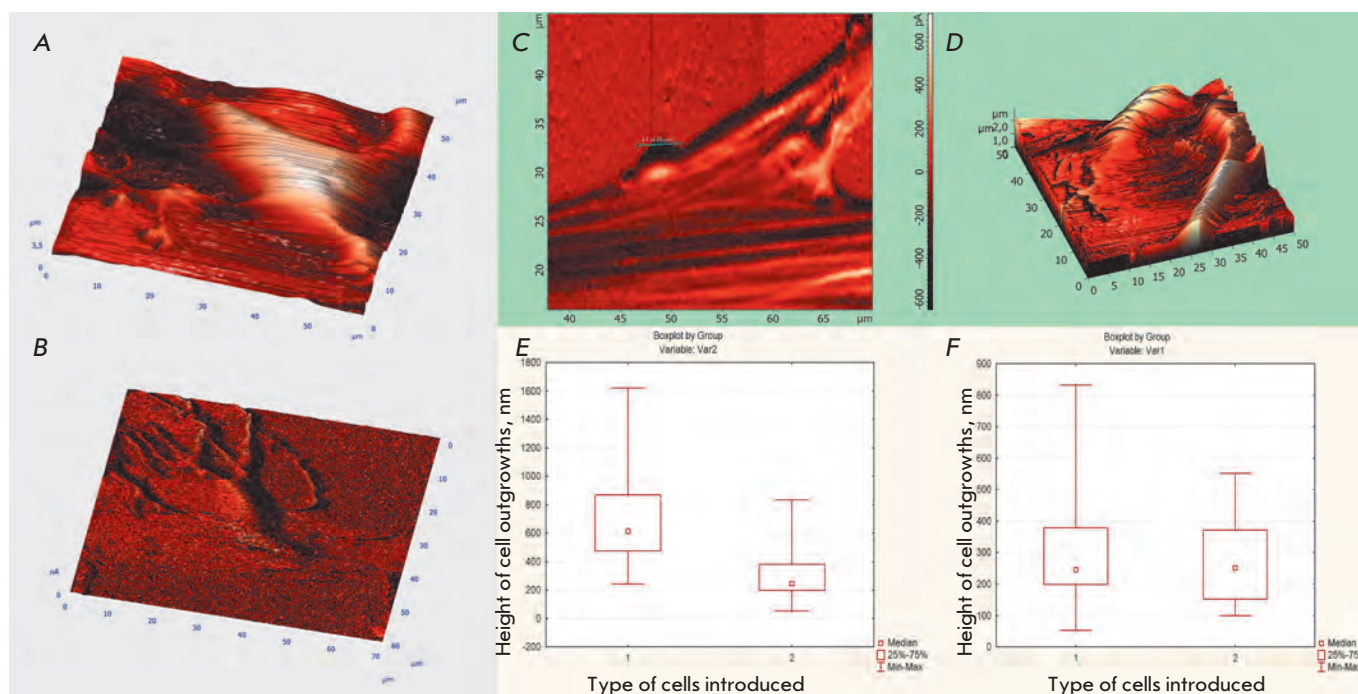


Fig. 5. AFM analysis of the surface of the injected MMSCs in the complete contact and semi-contact modes. (A) – Reconstruction of the MMSC surface after the changes in morphology. (B) – Early cell migration from the retina explant with lamellopodia formation. (C, D) – The formation of synaptic connections between the transplanted MMSCs and retinal cells. (E) – quantitative analysis of the distribution of outgrowth heights: group 1 – glial cells of the retinal explant, group 2 – outgrowth of the transplanted MMSCs ($p < 0.01$). (F) – quantitative analysis of the distribution of outgrowth heights: group 1 – neuronal explant cells, group 2 – outgrowths of the transplanted MMSCs ($p > 0.01$).

After MMSCs and NSPCs were injected, active migration of these cells was observed during the first hours after the transplantation. The migration rates were different in the case of injection deep inside the neuroretinal layers and upon application onto the explant surface.

The micro-surrounding of the introduced cells is the key factor for the differentiation of the transplanted cells. In some cases, MMSCs transplanted into the retina may acquire a neuronal phenotype.

A laser can be used to control *in vitro* retinal damage, which stimulates the migration of the transplanted cells towards the injured area and accelerates their differentiation, according to the niche they occupy. ●

This study was supported by the Federal Target-Oriented Program “Scientific and Scientific-Pedagogical Personnel of the Innovative Russia”, 2009–2013” (№ P113).

REFERENCES

1. Bull N.D., Martin K.R. // *Regenerative Medicine*. 2009. V. 4. № 6. P. 855–865.
2. Johansson K., Ehinger B. // *Vision Res*. 2005. V. 45. P. 3235–3243.
3. Kretz A., Hermening S.H., Isenmann S. // *J. Neurosci. Methods*. 2004. V. 136. P. 207–219.
4. Schrepfer S., Deuse T., Lange C., Katzenberg R., Reichen-spurner H., Robbins R.C., Pelletier M.P. // *Stem Cells Dev*. 2007. V. 1. P. 105–107.
5. Semenova M.L., Sergeev S.A., Saburina I.N., Kosheleva N.V. // *Cellular Transplantation and Tissue Engineering*. 2010. V. V. № 2. P. 55–61.
6. Aleksandrova M.A., Podgorniy O.V., Marey M.V., Pol-tavceva R.A., Citrin E.B., Gulyaev D.V., Cherkasova L.V., Revischin A.V., Korochkin L.V., Suhih G.T. // *Kletochnie Technologii v Biologii i Medicine*. 2005. № 1. P. 13–19.
7. Sergeev S.A., Pavlova G.V., Tahchidi H.P., Gavrilova N.A., Revischin A.V., Saburina I.N., Lanevskaya N.I., Ivanova Z.G., Bastakov V.A., Komova O.Y et al. // *Oftalmokhirurgia* 2010. № 3. P.33–38.8. Blong C.C., Jeon C.J., Yeo J.Y., Ye E.A., Oh J., Callahan J.M., Law W.D., Mallapragada S.K., Saka-guchi D.S. // *J. Neurosci. Res*. 2010. V. 88. P. 1445–1456.
9. Lei Z., Yongda L., Jun M., Yingyu S., Shaoju Z., Xinwen Z., Mingxue Z. // *Cell Biol. Internat*. 2007. V. 31. P. 916–923.

New Viral Vector for Superproduction of Epitopes of Vaccine Proteins in Plants

L. G. Tyulkina¹, E. V. Skurat¹, O. Yu. Frolova², T. V. Komarova², E. M. Karger², I. G. Atabekov^{1*}

¹Faculty of Biology, Lomonosov Moscow State University

²Belozersky Institute of Physico-Chemical Biology, Lomonosov Moscow State University

*E-mail: atabekov@genebee.msu.su

Received 20.06.2011

Copyright © 2011 Park-media, Ltd. This is an open access article distributed under the Creative Commons Attribution License, which permits unrestricted use, distribution, and reproduction in any medium, provided the original work is properly cited.

ABSTRACT The novel viral vectors PVX-CP AltMV and PVXdt-CP AltMV are superexpressors of the capsid protein (CP). These viral vectors were constructed on the basis of the potato virus X (PVX) genome and *Alternanthera* mosaic virus (AltMV) CP gene. The expression, based on the hybrid viral vectors, is genetically safe, since the systemic transport and formation of infective viral particles are blocked. CP AltMV can self-assemble into virus-like particles (VLPs) in the absence of genomic RNA. The vectors can be used for the presentation of foreign peptides (including epitopes of human pathogens) on the surface of the VLP. The N-terminal extracellular domain (M2e) of the influenza virus A M2 protein and its truncated variant (Δ M2e) were used as model heterologous peptides for the construction of the chimeric CP AltMV. Chimeric CP AltMV retains its ability to self-assemble into VLP. The epitopes of the M2 influenza virus protein were not eliminated during the process of accumulation, polymerization and purification of chimeric VLP AltMV, providing evidence of the stability of chimeric VLP with C-terminal heterologous epitopes. It appears that VLP produced by the vectors PVX-CP AltMV and PVXdt-CP AltMV can be used in the field of biotechnology for the presentation of the epitopes of vaccine proteins on their surfaces. The chimeric VLP AltMV with the presented foreign epitopes can be used as candidate vaccines.

KEYWORDS potexviruses; viral vector; foreign epitope; chimeric virus-like particles.

ABBREVIATIONS PVX – potato virus X; AltMV – *Alternanthera* mosaic virus; CP – capsid protein; dt – deletion of triple gene block; PVX-CP AltMV – hybrid viral vector based on PVX genome and CP AltMV; M2e – ectodomain of influenza A virus M2 protein; Δ M2e – truncated variant of M2e; CP-M2e AltMV, CP- Δ M2e AltMV – chimeric CP AltMV with epitope of M2 protein; VLP – virus-like particles; PCR – polymerase chain reaction; NTR – Non-translated region.

INTRODUCTION

The utilization of plants for the expression and accumulation of foreign (target) proteins (TPs) used in medicine, veterinary science, agriculture, and industry is one of the most promising directions in bioengineering.

Plant cells are superior to those collected from animals or microorganisms in terms of both their technological simplicity and the possibility to simultaneously produce a large amount of inexpensive target products, and proteins produced from plants are completely safe, due to the absence of pathogens that are common to humans and plants. The presence of post-translational modification systems in plants typically ensures correct conformation formation of target proteins through disulfide bonds and glycosylation.

One of the most efficient methods for the rapid production of significant amounts of target proteins in the cytoplasm of infected cells is the use of autonomously replicating recombinant viral vectors. The high rate of viral genome replication allows to achieve

high copy numbers of transcripts from foreign genes in the infected cell's cytoplasm. Therefore, the average efficiency of a viral expression system is higher than the efficiency upon stable plant transformation or the transient expression using nonviral vectors by two orders of magnitude [1, 2]. Viral vectors constructed on the basis of plant RNA viruses (tobamo-, potex-, como-, bromo-, and potyvirus) are the most frequently used. [3].

There are two major strategies for producing target proteins using a viral vector:

1) The TP gene is expressed under the control of the viral promoter, yielding an individual protein. This can be based on the “gene insertion strategy,” when a TP gene is placed under the control of the duplicated sub-genomic promoter (e.g., the coat protein gene [2, 4–6]) or on the “gene substitution strategy,” when a viral gene (most frequently the coat protein gene and/or the genes responsible for viral transport) is substituted for the TP [7–11]. This approach facilitates the accumula-

tion of the target protein at quantities amounting to at least 10% of the total amount of soluble plant proteins, over a short period of time. Vectors based on the phytoviral genome have been successfully applied in the production of proteins for medical use (including vaccine proteins) in plants. This strategy was used to synthesize the hepatitis B virus core protein (HBcAg) and calicivirus capsid protein, which are capable of forming stable virus-like particles stimulating the humoral and cellular immune responses [12, 13];

2) The strategy of “fusion” of the nucleotide sequence of the TP gene, or its fragment, and the viral gene or its fragment. Here, the viral gene of the capsid protein and the TP gene are typically expressed as a single translational frame. However, there are limits to the size of the inserted foreign sequence. Extensive polypeptides are usually linked to the principal protein via a flexible bridge, via proteolysis sites, via the sequence of 2A peptide from the foot-and-mouth disease virus, etc. [14–17].

Studies of the molecular mechanisms of the activation of the adaptive immune response indicate that peptides, rather than entire proteins, are more likely to be responsible for the activation of T- and B-lymphocytes [18]. Both synthetic and recombinant peptides are unstable and possess weak antigenic activity [19]; however, binding to high-molecular weight supports with a high immunogenicity results in the enhancement of the immunogenicity and stability of these peptides [18].

An example of such supports are the capsid proteins (CP) of plant viruses, which are capable of forming viral and/or virus-like nanoparticles which can be used for the presentation of pathogen epitopes on their surface. These nanoparticles have a stable and regularly repeating structure that facilitates the induction of strong cellular and humoral immune responses [20–23].

The strategy was used to construct viral vectors that produce viruses with chimeric CP in plants. The epitopes of antigens of the *Staphylococcus aureus*, foot-and-mouth disease virus, hepatitis C virus, papillomavirus, human immunodeficiency virus, influenza virus [24–33], and many other viruses (see reviews [3, 34]) were presented on the surface of these virions.

However, viral vectors based on full-length genomes (capable of systemic transport and formation of infective viral particles) are considered unsafe for use in bio-engineering. When producing the target proteins, it is impossible to eliminate the probability of penetration of recombinant viruses into the environment, followed by uncontrolled propagation of the genetic material.

The capsid proteins of certain animal and plant viruses retain their ability to form stable capsids, virus-like particles (VLPs), in the absence of a viral genome. The use of VLPs for efficient presentation of epitopes

foreign to the immune system [21, 35–37] on their surface can resolve the problem of bio-safety as relates to vaccine protein production. Today, special attention is paid to the construction of vector systems that express capsid proteins forming VLPs free of any RNA impurities. Only such VLPs are believed permissible for application in bio- and nano-engineering [38, 39].

This study focuses on the construction of a system of genetically safe viral vectors based on potex virus genomes for the production of VLPs that present pathogen epitopes on their surface in plants.

EXPERIMENTAL

Media, reagents, enzymes, and synthetic oligonucleotides

In this study, we used *Escherichia coli* XL-1 Blue (Stratagene, USA) and *Agrobacterium tumefaciens* GV3101 from the collection of the Department of Virology, Moscow State University. The recombinant DNAs were cloned in *E. coli* XL-1 Blue cells through the conventional procedures [40] using restriction endonucleases, DNA ligase, and Taq and Pfu polymerases (Fermentas, Lithuania and SibEnzyme-M, Russia). The oligonucleotides were synthesized by Sintol (Russia). The following synthetic oligonucleotides were used for cloning: CP AltMV-XhoI-p (CTAGCTCGAGATGTCCACTC-CATTTCTCAA), CP AltMV-XbaI-m (CGTCTAGATTACTCCGGTGGTGGGAGGTATTGA), PVX-R-Avr2-p(TGCACAGATTTTCTAGGCAC), PVX-R-XhoI-m (AGCTCTCGAGCTTATTCAAATCTCTAAG-GTA), PVX-3ntr-XbaI-p (AGCTTCTAGACTACGTCTACATAACCGACGC), Oligo(dT)₂₄-Kpn-m (AGCTGGTACCTTTTTTTTTTTTTTTTTTTTTTTTTTTTTT), PVX-Kpn-(dT)₁₂-3ntr-m (AGCTGGTACCTTTTTTTTTTTTTTATATTATTCATACAATC), PVX-Xba-cpxho-3ntr-p (AGTCTCTAGTCGAGGCGTTCAGGAACA), CP AltMV-epet-pirn-XbaI-m (CGTCTAGATTAGTTTCTGATGGTGTTCACCTCCGGTGGTGGGAGGTA), CP AltMV-M2E-m (TTTCCACCTCTGTCAAGAGTGACTCCGGTGGTGGGAGGTA), M2E-XbaI-m (CGTCTAGATTAGTCGGATGAGTCGTTGCATCT), M2E-p (TCACTCTTGACAGAGGTGGAAACACAATCAGAAACGAGTGGG), and M2E-m (GTCG-GATGAGTCGTTGCATCTGCATCCCCACTCGTT-TCTGATT). The validity of the obtained constructs was verified by automatic sequencing plasmid DNA samples at GenoTekhnologiya (Russia).

PVX-CP AltMV and PVXdT-CP AltMV vector constructs

Binary hybrid vectors were constructed in several stages using intermediate constructs (ICs).

IC 1 – The fragment from the plasmid PVX-201 containing the 35S promoter, PVX replicon with the duplicated subgenomic promoter, but without the transcription terminator of the nopaline synthase gene (Tnos-terminator) at the HindIII/EcoRI sites, was transferred into the pBIN 19 binary vector.

IC 2 – The AltMV capsid protein gene was obtained by PCR on a matrix of cDNA-copy of the 3'-terminal region of the AltMV genomic RNA using primer pair CP AltMV-XhoI-p and CP AltMV-XbaI-m and subcloned into the Cambia 6963 vector at the XhoI/XbaI restriction sites.

IC 3 – For convenient cloning, the XbaI restriction site flanking the subgenomic promoter of 25 kDa protein PVX was substituted for the XhoI restriction site. For this purpose, the cDNA fragment of PVX encoding the C-terminal region of the viral polymerase was obtained by PCR on the PVX-201 matrix using the PVX-R-Avr2-p and PVX-R-XhoI-m primer pair. The synthesized fragment was cloned at the Avr2/XhoI sites into the pGEM3-11369(polio)x2 vector containing the subgenomic promoter of the 25 kDa protein gene; the sequence encoding the C-terminal region of PVX polymerase and the CP U1 tobacco mosaic virus (TMV) with a duplicated poliovirus epitope. The procedure was used to delete the sequence of the U1 TMV CP gene from the pGEM3-11369(polio)x2 vector and design the XhoI restriction site at the 3'-terminus of the subgenomic promoter of the 25 kDa protein.

IC 4 – Three variants of 3'-NTR were obtained by PCR on the PVX-201 matrix using three primer pairs: PVX-3ntr-XbaI-p and Oligo(dT)₂₄-Kpn-m were used to synthesize 3'-NTR of PVX (A)₂₄; primers PVX-3ntr-XbaI-p and PVX-Kpn-(dT)₁₂-3ntr-m, to synthesize 3'-NTR of PVX (A)₁₂; and primers PVX-Xba-cpxho-3ntr-p and PVX-Kpn-(dT)₁₂-3ntr-m, to synthesize 3'-NTR of PVX p/cp(A)₁₂.

Following cleavage by XbaI/KpnI restrictases, the synthesized DNA fragments corresponding to different variants of 3'-NTR were cloned into the pBlue-Script II SK⁺ plasmid at XhoI-(XbaI)-KpnI sites, simultaneously with the CP AltMV gene that had been removed at a preliminary stage from IC 2 at the XhoI/XbaI sites.

IC 5 – The DNA fragment corresponding to CP AltMV with the adjacent 3'-NTR was removed from IC 4 at the XhoI/KpnI restriction sites and cloned into IC 3 at the XhoI-(KpnI)-SacI sites, simultaneously with the DNA fragment that corresponded to the Tnos-terminator and had been removed at a preliminary stage at the KpnI/SacI sites from the pGEM subclone containing the Tnos-terminator.

At the last stage of cloning, the DNA fragment from IC 5 at the XhoI/SacI or AvrI/SacI site was transferred

into the IC 1 that had undergone prior treatment with SalI/SacI or AvrI/SacI restrictase.

Obtainment of vector constructs expressing chimeric capsid proteins of AltMV

IC 6 – The CP AltMV gene containing the sequence encoding the Δ M2e-variant was obtained by PCR on the matrix of a cDNA copy of the 3'-terminal region of AltMV genomic RNA using the CP AltMV-XhoI-p and CP AltMV-evetpirn-XbaI-m primer pair, and it was subcloned into the Cambia 6963 vector at the XhoI/XbaI restriction sites. The CP AltMV gene encoding the full-length M2e domain was obtained by PCR via three stages, using the pair of synthetic oligonucleotides M2E-p and M2E-m, and two primer pairs (CP AltMV-XhoI-p and CP AltMV-M2E-m, CP AltMV-XhoI-p and M2E-XbaI-m) and subcloned into the Cambia 6963 vector at the XhoI/XbaI restriction sites.

IC 7 – In IC 5, the sequence of the viral capsid protein was substituted at the XhoI/XbaI sites for the sequences of chimeric capsid proteins from IC 6.

At the final cloning stage, the DNA fragments from IC 7 at site XhoI/SacI or AvrI/SacI were transferred to the IC 1 that had been preliminarily treated with the restrictase SalI/SacI or AvrI/SacI.

Agroinjection

Agrobacteria *A. tumefaciens* (strain GV3101) were transformed by recombinant plasmids using the freeze-thawing procedure [41]. The agrobacteria containing recombinant binary vectors were cultivated overnight on a incubator shaker at 28°C in an LB medium containing 50 mg/l of rifampicin, 50 mg/l of kanamycin, and 25 mg/l of gentamicin. The cells were deposited by centrifugation at 4000 g for 5 min and then resuspended in an agroinjection buffer containing 10 mM of Mes (pH 5.5) and 10 mM of MgSO₄. *Nicotiana benthamiana* leaves were injected with an agrobacterial suspension ($OD_{600} = 0.2$) using a needle-free syringe. Following the agroinjection, the plants were grown under a daylight lamp subjected to 16 h of light per day at a temperature of 22°C. In order to suppress posttranscriptional gene silencing, the agroinjection of plants was performed in the presence of the p19 suppressor gene of the tomato bushy stunt virus.

Analysis of expression of the AltMV capsid protein upon agroinjection

The preparations from agroinjected *N. benthamiana* leaves were homogenized in three-five volumes of the extraction buffer (10 mM Tris, pH 8.0, containing 5 mM EDTA). The obtained suspension was clarified by centrifugation at 12000 g for 15 min. An equal volume of denaturing buffer for subsequent application onto

polyacrylamide gel was added to the supernatant. The buffer for applying the samples on SDS-PAGE gel contained 60% of glycerol, 20% of β -mercaptoethanol, 10% of sodium dodecyl sulfate, 250 mM Tris-HCl buffer, pH 6.8, and 1% bromophenol blue. The analyzed samples were heated at 95°C for 15 min and fractionated by electrophoresis in 12% SDS-PAGE gel using the Laemmli procedure [42], followed by Coomassie R-250 staining. The chimeric capsid viral proteins synthesized in *N. benthamiana* leaves were identified via Western blot analysis as previously described [43], using polyclonal antibodies to CP AltMV and/or M2e-epitope and secondary antibodies conjugated to horseradish peroxidase (Sigma). The reaction products were visualized via chemiluminescence, using the ECL system (Amersham Biosciences).

Extraction of AltMV capsid proteins from plant tissue

On the sixth - eighth day after agroinjection, the leaf material was ground in the extraction buffer (10 mM Tris, pH 8.0, 5 mM EDTA) in order to achieve a homogeneous suspension. The resulting mixture was centrifuged at 12000 g for 15 min, followed by the collection of the supernatant containing capsid proteins. For the polymerization of CP AltMV and formation of VLPs, a 0.5 M citrate buffer, pH 4.0, was added to the supernatant until a concentration of 25 mM was achieved, followed by incubation for 40 min at room temperature. The pseudovirions from the plant extract were deposited by ultracentrifugation at 100 000 g for 120 min, or using polyethylene glycol (8% PEG 6000, 2% NaCl, 25 mM citrate buffer, pH 4.0). The precipitates were suspended in a 25 mM citrate buffer (pH 4.0), incubated for 40 min for the correcting polymerization, and then clarified by centrifugation at 12000 g for 15 min. The resulting preparations of chimeric VLPs were subjected to an enzyme immune assay and electron microscopy analysis.

Electron microscopy

The samples prepared by the conventional negative contrast procedure using a 1% uranyl acetate solution were viewed on a JEM-1011 transmission electron microscope (JEOL, Japan). The images were made using a Gatan Erlangshen ES500W digital camera and Gatan Digital Micrograph software \times 250000.

RESULTS AND DISCUSSION

Hybrid viral vectors

Potato virus X and the *Alternanthera* mosaic virus belong to the genus *Potexvirus* (potexviruses), family Flexiviridae. The particles of typical PVX are flexible filamentous virions of helical structure with a length of 515 nm and a diameter of 13.5 nm. Approximately

1,300 identical capsid protein subunits form the polar PVX helix with a pitch of 3.6 nm. The viral RNA is located between the helix turns; each turn comprises 8–9 CP subunits. The particles have a hollow central axial channel with a diameter of 3 nm [44, 45]. An expression system based on potexvirus genomes was designed using the popular vector PVX-201 containing a complete cDNA copy of the PVX UK3 genome cloned between the 35S promoter of the cauliflower mosaic virus (CaMV) and the Tnos-terminator [4]. AltMV serologically close, but not identical, to the papaya mosaic virus (PMV) was used as a capsid protein donor [46]. CP PMV differs from the CP of the typical representative of potexviruses (PVX) in terms of the former's ability to form virus-like particles *in vitro* with helical symmetry, without the participation of RNA [47]. The data of the electron microscopy analysis of CP AltMV preparations indicate that the AltMV capsid protein is also capable of *in vitro* formation of VLPs.

Two types of hybrid viral vectors, PVX-CP AltMV (complete genome variant) and PVXdT-CP AltMV (minireplicon variant), were constructed on the basis of the PVX and AltMV genomes. The PVX-CP AltMV genome is controlled by the 35S promoter and Tnos-terminator and contains 5'- and 3'-untranslated regions of PVX RNA, the gene of RNA-dependent RNA polymerase of PVX, and the triple block of PVX transport genes. The CP AltMV gene is expressed under the control of the subgenomic promoter of CP PVX. The PVXdT-CP AltMV is also controlled by the 35S promoter and Tnos-terminator and contains 5'- and 3'-untranslated PVX RNA regions, and the gene of RNA-dependent RNA polymerase of PVX. However, it does not contain the triple gene block, like in the case of the construct described in [10]. In viral vectors PVXdT-CP AltMV, the gene of the AltMV capsid protein is controlled by the subgenomic promoter of the 25 kDa PVX protein.

It is known that, for efficient synthesis of the target protein, the viral vector needs to contain a certain set of *cis*-acting elements in the 3'-untranslated region, which determine the following: the affinity to replicase, to facilitate transcription and translation, and to provide a maximum expression level of foreign genes. Since the 3'-terminal CP PVX gene in hybrid viral vectors is substituted by the CP AltMV gene, three model variants of 3'-NTR were used to construct the vectors: 3'-NTR of PVX (A)₂₄; 3'-NTR of PVX (A)₁₂; and 3'-NTR of PVX p/cp (A)₁₂. The 3'-NTR of PVX (A)₁₂ corresponds to the 3'-terminal region of the full-length infectious cDNA copy of the PVX genome (PVX-201). The 3'-NTR of PVX (A)₂₄ does not contain an ATAAAT sequence; however, the poly(A) tract is increased from 12 to 24 A. The 3'-NTR of PVX p/cp (A)₁₂ contains the corresponding PVX-201 poly(A) tract; however, the 3'-NTR is in-

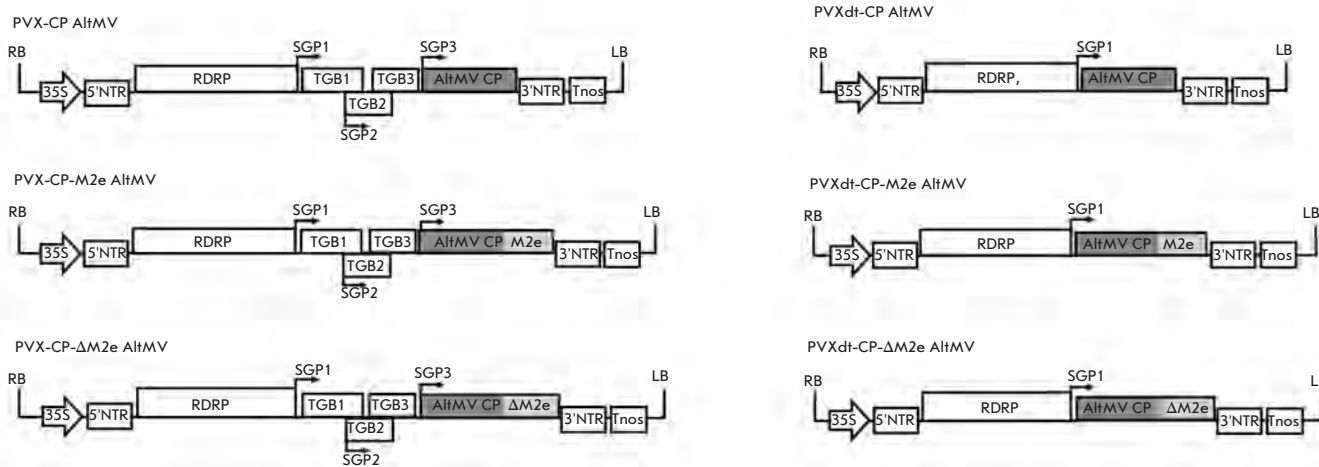


Fig. 1. Schematic representation of hybrid viral vectors constructed on the basis of the potato virus X (PVX) genome and *Alternanthera* mosaic virus (AltMV) CP gene. RDRP – gene of viral RNA-dependent RNA polymerase; TGB1, TGB2, TGB3 – triple gene block; sgp – sub-genomic promoter are indicated by arrows; CP AltMV – gene of *Alternanthera* mosaic virus capsid protein; M2e – N-terminal extracellular domain of the M2 protein of the influenza virus; Δ M2e – truncated variant of the M2e; 35S – promoter for the 35S RNA of CaMV; Tnos – terminator of nopaline synthase; NTR – non-translatable region; LB – left border and RB – right border of the T-DNA. The initial polygenomic vector PVX-CP AltMV and the truncated replicon vector PVXdt-CP AltMV contained DNA fragments encoding full-length native CP AltMV. The complete genome chimeric vectors (PVX-CP-M2e AltMV and PVX-CP- Δ M2e AltMV) and chimeric replicon vectors (PVXdt-CP-M2e AltMV, PVXdt-CP- Δ M2e AltMV) encoded chimeric coat proteins: CP-M2e AltMV and CP- Δ M2e AltMV. The above constructs were cloned into the binary vector and used to infect plants via agrobacteria.

created by 60 nucleotides at its 5'-terminus, due to the CP PVX gene that is adjacent to the 3'-NTR.

Thus, two types of hybrid viral vectors (*Fig. 1*) were constructed on the basis of the PVX genome at the first stage: PVX-CP AltMV and mini-vector-replicon PVXdt-CP AltMV, with three variants of 3'-NTR for each vector. All constructs were cloned into the binary pBIN19 vector for further infection of *N. benthamiana* plants with agrobacteria.

Replication of hybrid viral vectors in *N. benthamiana* leaves

The efficiency of the expression of the CP AltMV gene using various vectors was determined via the accumulation of the capsid protein in *N. benthamiana* leaves on the sixth – eighth day after agroinjection. It should be noted that, in all the constructs under discussion, the replication of the hybrid viral vector PVX-CP AltMV in *N. benthamiana* plants led to the accumulation of CP AltMV in approximately identical amounts as were determined for CP PVX upon mechanical inoculation of the virus to plants (over 1 mg per 1 g of green material). AltMV is typically accumulated in plants in lower concentrations (approximately 340 μ g per 1 g of green material).

No distinctions were detected in the efficiency of CP production when using different 3'-NTR. The

deletion of the 60 nucleotide 3'-terminal fragment from the CP PVX gene did not result in a reduction in the CP AltMV level, contrary to the data presented in [10]. It can reasonably be assumed that the existing homology between the 3'-terminal regions of the CP PVX and CP AltMV genes is sufficient to provide an efficient performance of PVX polymerase. Similar results, namely, the absence of preference for any 3'-NTR variant and a similar level of accumulation of the recombinant CP AltMV, were also obtained upon replication of PVXdt-CP AltMV viral vectors (*Fig. 2A*). Vector constructs with only a single 3'-NTR variant (3'-NTR of PVX (A)₁₂) were subsequently used (*Fig. 1*).

The mini-vectors PVXdt-CP AltMV were not superior to the PVX-CP AltMV vectors in terms of accumulation of the recombinant AltMV capsid protein in *N. benthamiana* leaves on days 6–8 following the agroinoculation in the presence of the gene-silencing suppressor (the p19 protein gene of the tomato bushy stunt virus) (*Fig. 2A*).

It is known that intercellular and systemic transport of PVX in plants is regulated by four genes, including the triple gene block (TGB) and CP [4]. No recombinant CP AltMV was detected in the systemic, non-agroinjected *N. benthamiana* leaves that were agroinoculated with hybrid viral PVX-CP AltMV vectors on days 16–

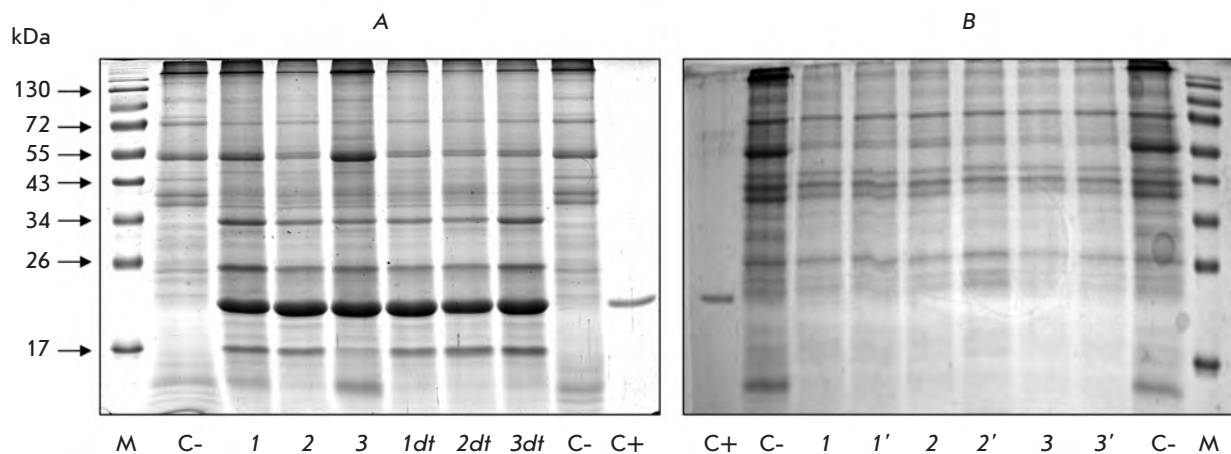


Fig. 2. AltMV capsid protein production in *N. benthamiana* leaves agroinjected with viral vectors PVX-CP AltMV and PVXdT-CP AltMV with differing 3'-NTR (1, 1dt, 3'-NTR PVX (A)₂₄; 2, 2dt, 3'-NTR PVX p/cp (A)₁₂; 3, 3dt, 3'-NTR PVX (A)₁₂). Coomassie stained 12% SDS-PAGE gel loaded with 2.5 mg of total protein extracted from agroinjected leaves; C+, CP AltMV, 0.5 µg; C-, non-inoculated leaf (negative control); M, protein molecular weight markers. (A) – agroinjected leaves, 8 dpa; (B) – upper systemic leaves, 16 dpa (1, 2, 3) and 20 dpa (1', 2', 3') after agroinjection of lower leaves

20 (Fig. 2B). Thus, the substitution of the CP PVX gene in recombinant hybrid viral vectors for the CP AltMV gene results in disruption of the systemic transport of the hybrid virus.

It was demonstrated via electron microscopy analysis of the extracts from *N. benthamiana* leaves agroinoculated with the hybrid viral vectors PVX-CP AltMV and PVXdT-CP AltMV that the recombinant capsid protein of AltMV can form extensive virus-like particles (see below), which can be used to present foreign epitopes on their surface. A UV absorption spectrum within 225–339 nm of the VLP-CP AltMV preparation isolated from the plant extract attests to the absence of RNA in it (the data are not presented).

When used for presentation of pathogen epitopes, it is noteworthy that VLPs with helical symmetry present a certain advantage over VLPs with icosahedral symmetry; specifically, they possess a greater number of subunits per VLP. Therefore, it is possible that they can present a larger number of pathogen epitopes by chimeric CP in VLP.

Construction of hybrid viral vectors expressing chimeric capsid proteins of AltMV

The N-terminal domain of the influenza A virus M2 (M2e) protein and its truncated variant (Δ M2e), which are responsible for the triggering of the protective immune response, were used as a model foreign peptide for construction of the chimeric CP AltMV [48]. The influenza A virus matrix (M2) protein is considered a promising candidate for the design of an antiviral vac-

cine, since the amino acid sequence of the ectodomain of this protein (M2e) is highly conserved and has remained almost unaltered since the human influenza A virus was first isolated in 1933 [49]. A consensus synthetic amino acid sequence of the M2 protein ectodomain was proposed on the basis of a computer analysis of 55 isolates of the human influenza A virus [50].

Since the conformational structure of CP AltMV is still as yet unknown, the search for the optimal insertion site (an insertion site which ensures the presentation of a heterologous epitope on the capsid protein surface whilst having a minimal effect on CP conformation without impeding the formation of polymeric structures) was carried out using the DNASTar software package. Finally, the C-terminal localization of the M2e-epitope and the Δ M2e variant within the chimeric CP AltMV were selected. The nucleotide sequence of the M2e-epitope and the Δ M2e variant was constructed on the basis of the corresponding consensus amino acid sequence of the N-terminal domain of the influenza A virus M2 protein, using the synonymous codons that occur most frequently in the genome of the PVX and AltMV capsid proteins.

The chimeric CP AltMV genes encoding the full-length M2 protein ectodomain (23 amino acid residues, M2e-epitope), SLLTEVETPIRNEWGCRCNDSSD, and the truncated variant, Δ M2e (8 amino acid residues, EVETPIRN) fused to the C-terminus of CP (CP-M2e AltMV and CP- Δ M2e AltMV), were obtained by PCR. Cloning sequences of chimeric capsid proteins in the hybrid viral vectors PVX-CP AltMV and PVXdT-

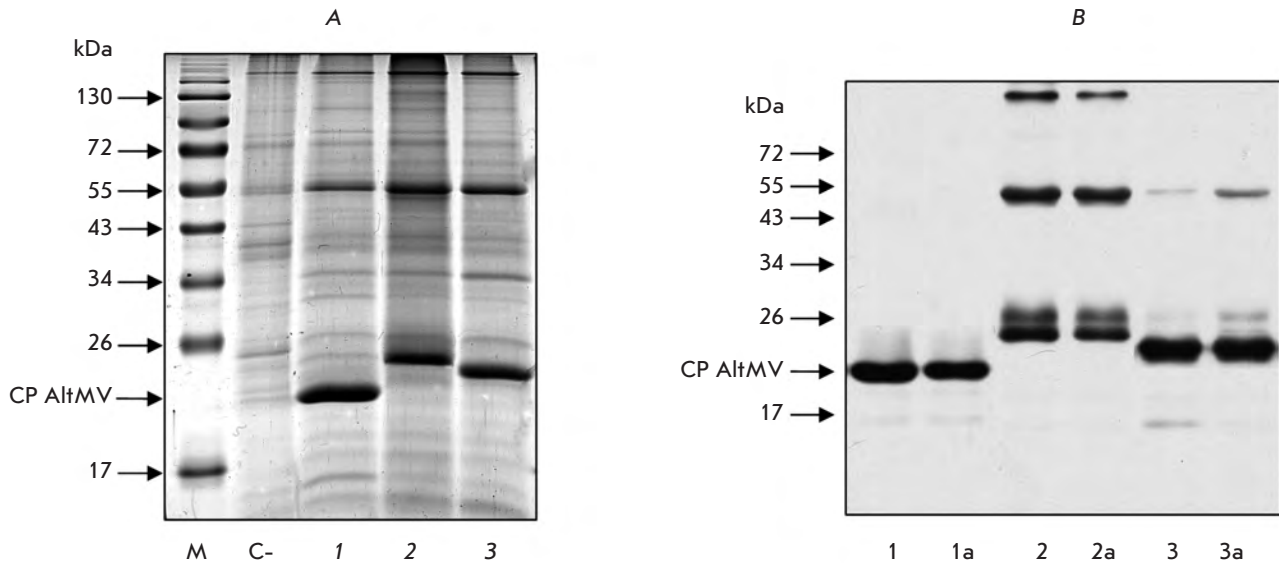


Fig. 3. Production of CP AltMV and chimeric AltMV capsid protein in *N. benthamiana* leaves agroinjected with viral vectors: PVX-CP AltMV (1) and PVXdT-CP AltMV (1a); PVX-CP-M2e AltMV (2) and PVXdT-CP-M2e AltMV (2a), PVX-CP- Δ M2e AltMV (3) and PVXdT-CP- Δ M2e AltMV (3a); 6 dpa. A – Coomassie stained 12% SDS-PAGE gel loaded with 1.5 mg of total protein extracted from agro-injected leaves. C-, no agro-injected leaf, negative control; B – Western blot analysis of CP AltMV and chimeric AltMV capsid protein production in agroinjected leaves using polyclonal antibodies to CP AltMV. M, protein molecular weight markers. The positions of CP AltMV are indicated by arrows.

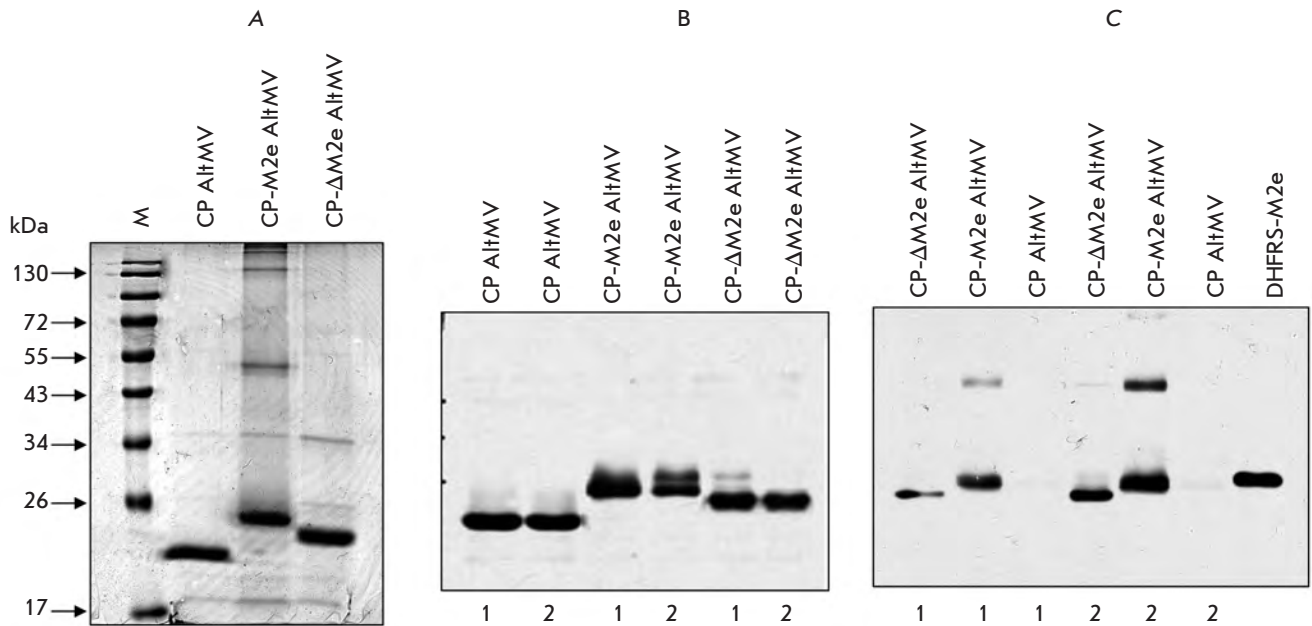


Fig. 4. Analysis of VLP preparations formed by CP AltMV and chimeric AltMV CP with M2 influenza virus protein epitopes (M2e and Δ M2e) obtained in *N. benthamiana* leaves and purified by PEG precipitation (1) or by ultracentrifugation (2). (A) – Laemmli electrophoresis of VLP preparations purified by ultracentrifugation. Coomassie stained 12% SDS-PAGE gel. (B) – Western blot analysis of VLP preparations using polyclonal antibodies to CP AltMV. (C) – Western blot analysis of VLP preparations using polyclonal antibodies to influenza A virus M2e-epitope. Recombinant protein DHFRS-M2e was used as a control for the M2e-epitope.

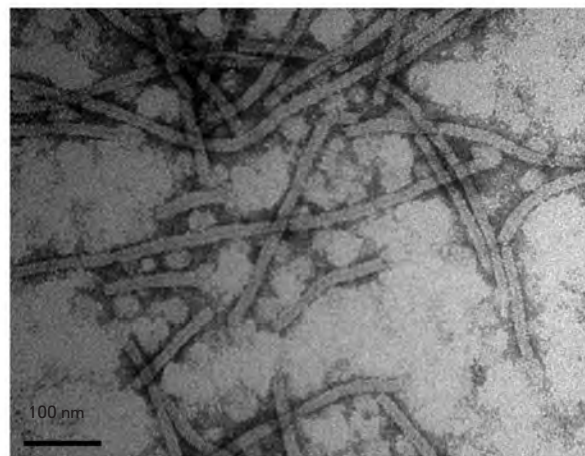
CP AltMV were performed to replace the sequences of the viral capsid proteins.

Thus, four hybrid viral vectors containing the genes of the chimeric capsid proteins of AltMV (Fig. 1) were constructed on the basis of the PVX genome: PVX-CP-M2e AltMV and its mini-variant PVXdt-CP-M2e AltMV; PVX-CP- Δ M2e AltMV and its mini-variant PVXdt-CP- Δ M2e AltMV. These constructs were used to transform competent cells of agrobacteria to infect *N. benthamiana* plants.

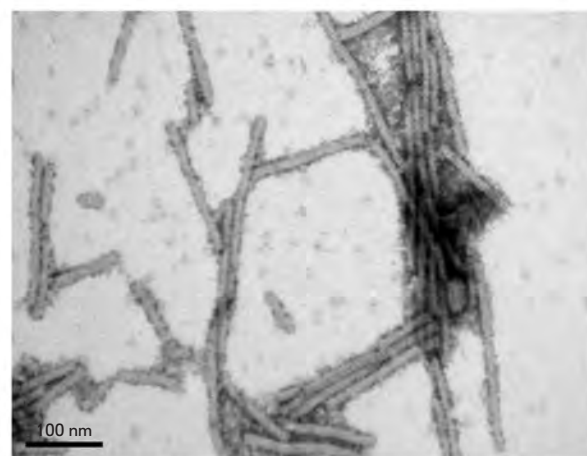
Expression of chimeric capsid proteins of AltMV in *N. benthamiana* leaves

Hybrid viral vectors based on the PVX genome which encode the genes of the chimeric capsid proteins of AltMV (CP-M2e and CP- Δ M2e) were agroinjected into *N. benthamiana* leaves. Six to eight days following the agroinjection, the synthesis of chimeric proteins was quantitatively assessed via fractionation of the soluble proteins in SDS-PAGE gel and Coomassie staining (Fig. 3A). The chimeric capsid viral proteins were identified via a Western blot analysis using polyclonal antibodies to CP AltMV or M2e-epitope (Fig. 3B). Same as for CP AltMV, no differences in the accumulation of chimeric capsid proteins were observed upon replication of the full-length hybrid viral vector or its mini-variant. The production of CP-M2e and CP- Δ M2e depended upon the individual features of the plant, the layer a leaf belonged to, and seasonal conditions. Nevertheless, it follows from the electrophoregrams shown in Fig. 3 that the level of accumulation of the chimeric capsid proteins of AltMV (CP-M2e and CP- Δ M2e) in plant leaves is comparable to the level of recombinant CP AltMV and is equal to over 1 mg (in some experiments, up to 3 mg) per 1 g of green material.

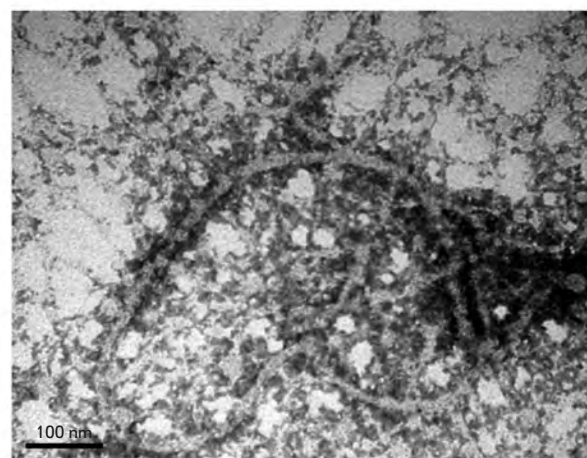
The chimeric capsid proteins of AltMV with M2e-epitope and the Δ M2e-variant, similar to the initial capsid protein of AltMV, form extensive virus-like particles with pH decreasing to 4.0–4.9 under conditions of low ionic strength of a solution. A chimeric VLP preparation can be isolated from the plant extract by ultracentrifugation or precipitation with polyethylene glycol. The results of the enzyme immune assay and electrophoretic and electron microscopy analyses of chimeric VLP preparations are shown in Figs. 4, 5. As follows from the presented data, epitopes of the influenza A virus M2 protein are not eliminated during the accumulation, polymerization, and purification, which attests to the stability of the chimeric CP AltMV when the foreign epitope localizes at the C-terminus. The fact that the foreign epitope does not impede the polymerization of the chimeric CP AltMV upon C-terminal localization indicates the conformational differences between the C-terminal regions CP AltMV and CP PVX [51].



CP AltMV



CP- Δ M2e AltMV



CP-M2e AltMV

Fig. 5. Electron micrographs of AltMV VLP and chimeric AltMV VLP preparations obtained in *N. benthamiana* leaves. Polymers of CP AltMV were negatively stained with a 1% uranyl acetate solution. The bar is 100 nm. $\times 250000$.

CONCLUSIONS

Our study aimed to design a system that could be used to present heterologous epitopes (pathogene epitopes) on the surface of the virus-like particles formed by the capsid protein of the phytovirus. The hybrid viral vectors PVX-CP AltMV and PVXdT-CP AltMV, with a number of advantages over the initial PVX and AltMV viruses, were constructed on the basis of the PVX genome and the CP AltMV gene.

1) The level of accumulation of the recombinant capsid protein of AltMV upon agroinjection of *N. benthamiana* leaves with hybrid viral vectors is as high as 1 mg/g of plant material, which considerably exceeds the accumulation upon mechanical inoculation of a natural host;

2) The substitution of the CP PVX gene in hybrid viral vectors for the CP AltMV gene results in the suppression of systemic transport of the hybrid virus and disruption of viral particle formation;

3) The ability to form VLPs is ensured by the feature of the AltMV capsid protein; CP PVX is incapable of forming VLPs.

The results presented point to the potential application of the viral vectors PVX-CP AltMV and PVXdT-CP AltMV in bioengineering in order to produce vaccine proteins in plants. The AltMV capsid protein that

is accumulated at a high concentration and forms virus-like particles in the absence of genomic RNA can be used for efficient presentation of epitopes of human and animal infectious agents on the VLP surface. Chimeric capsid proteins of AltMV with model heterologous peptides, epitopes of the influenza A virus M2 protein, are also capable of forming stable VLPs. The expression system based on the hybrid viral vectors PVX-CP AltMV and PVXdT-CP AltMV is genetically safe. The use of this vector system allows one to avoid both the spontaneous vertical and horizontal transmission of plant infection and the unregulated spread of genetic material into the environment. ●

The authors are grateful to P.A. Ivanov for providing the cDNA copy of the 3'-terminal region of AltMV genomic RNA, A. Mukhamedzhanova for providing the sample of mouse antibodies to CP AltMV, and T.V. Gasanova for providing the sample of mouse antibodies to the influenza A virus M2e epitope.

This study was supported by the Ministry of Education and Science of the Russian Federation (Government Contract № 02.527.11.0002) and the Seventh Framework Program of the European Union (PLAPROVA project).

REFERENCES

- Giddings G., Allison G., Brooks D., Carter A. // *Nat. Biotechnol.* 2000. V. 18. № 11. P. 1151–1155.
- Lindbo J.A. // *Biotechnology.* 2007. V. 7. P. 1–11.
- Yusibov V., Rabindran S., Commandeur U., Twyman R.M., Fischer R. // *Drugs.* 2006. V. 7. № 4. P. 203–217.
- Baulcombe D.C., Chapman S., Santa Cruz S. // *Plant J.* 1995. V. 7. № 6. P. 1045–1053.
- Shivprasad Sh., Pogue G.P., Lewandowski D.J., Hidalgo J., Donson J., Grill L.K., Dawson W.O. // *Virology.* 1999. V. 255. № 2. P. 312–323.
- Wagner B., Fuchs H., Adhami F., Ma Y., Scheiner O., Breiteneder H. // *Methods.* 2004. V. 32. № 3. P. 227–234.
- Takamatsu N., Ishikawa M., Meshi T., Okada Y. // *EMBO J.* 1987. V. 6. № 2. P. 307–311.
- Ravin N.V., Kuprianov V.V., ZamchuK L.A., Kochetov A.V., Dorokhov Yu.L., Atabekov J.G., Skryabin K.G. // *Biochemistry (Moscow).* 2008. V. 73. № 10. P. 1108–1113.
- Ravin N.V., Mardanov E.S., Kotyarov R.Y., Novikov V.K., Atabekov J.G., Skryabin K.G. // *Biochemistry (Moscow).* 2008. V. 73. № 1. P. 44–49.
- Komarova T.V., Skulachev M.V., Zvereva A.S., Schwartz A.M., Dorokhov Yu.L., Atabekov J.G. // *Biochemistry (Moscow).* 2006. V. 71. № 8. P. 646–650.
- Natilla A., Hammond R.W., Nemchinov L.G. // *Arch. Virol.* 2006. V. 151. № 7. P. 1373–1386.
- Huang Z., Santi L., LePore K., Kilbourne J., Arntzen Ch.J., Mason H.S. // *Vaccine.* 2006. V. 24. № 14. P. 2506–2513.
- Santi L., Barchelora L., Huang Z., Hjelm B., Kilbourne J., Arntzen Ch.J., Chen Q., Hugh S., Mason H.S. // *Vaccine.* 2008. V. 26. № 15. P. 1826–1824.
- Santa Cruz S., Chapman S., Roberts A.G., Roberts I.M., Prior D.A., Oparka K. // *Proc. Natl. Acad. Sci. USA.* 1996. V. 93. № 13. P. 6286–6290.
- Unde K., Fischer R., Commandeur U. // *Arch. Virol.* 2005. V. 150. № 2. P. 327–340.
- Werner S., Marillonner S., Hause G., Klimyuk V., Gleba Y. // *Proc. Natl. Acad. Sci. USA.* 2006. V. 103. № 47. P. 17678–17683.
- Zelada A.M., Calamante G., Santangelo M., Bigi F., Verna F., Mentaberry A., Cataldi A. // *Tuberculosis.* 2006. V. 86. № 3–4. P. 263–267.
- Molnar E., Dopfer E.P., Deswal S., Schamel W.W. // *Curr. Pharm. Des.* 2009. V. 15. № 28. P. 3237–3248.
- Lico C., Chen Q., Santi L. // *J. Cell Physiol.* 2008. V. 216. № 2. P. 366–377.
- Noad R., Roy P. // *Trends Microbiol.* 2003. V. 11. № 9. P. 438–444.
- Denis J., Majeau N., Acosta-Ramirez E., Savard Ch., Bedard M.C., Simard S., Lecours K., Bolduc M., Pare Ch., Willems B., et al. // *Virology.* 2007. V. 363. № 1. P. 59–68.
- Denis J., Acosta-Ramirez E., Zhao Y., Hamelin M.-E., Koukavica I., Baz M., Abed Y., Savard Ch., Pare Ch., Macias C.L., et al. // *Vaccine.* 2008. V. 26. № 27–28. P. 3395–3403.
- McCormick A.A., Palmer K.E. // *Expert. Rev. Vaccines.* 2008. V. 7. № 1. P. 33–41.
- Brennan F.R., Jones T.D., Longstaff M., Chapman S., Bellaby T., Smith H., Xu F., Hamilton W.D.O., Flock J.I. // *Vaccine.* 1999. V. 17. № 15–16. P. 1846–1857.
- Porta C., Spall V.E., Loveleand J., Johnson J.E., Barker P.J., Lomonosoff G.P. // *Virology.* 1994. V. 202. № 2. P. 949–955.

RESEARCH ARTICLES

26. Joelson T., Akerblom I., Oxelfelt P., Strandberg B., Tomenius K., Morris T.J. // *J. Gen. Virol.* 1997. V. 78. № 6. P. 1213–1217.
27. Natilla A., Piazzolla G., Nuzzaci M., Saldarelli P., Tortorella C., Antonaci S., Piazzolla P. // *Arch. Virol.* 2004. V. 149. № 1. P. 137–154.
28. MeshcheriaKova Iu.A., El'darov M.A., Migunov A.I., Stepanova L.A., Repko I.A., Kiselev O.I., Lomonosoff D.P., Skrjabin K.G. // *Mol. Biol. (Mosk).* 2009. V. 43. № 4. P. 741–750.
29. Wu L., Jiang L., Zhou Z., Fan J., Zhang Q., Zhu H., Han Q., Xu Z. // *Vaccine.* 2003. V. 21. № 27–30. P. 4390–4398.
30. Jiang L., Li Q., Li M., Zhou Z., Wu L., Fan J., Zhang Q., Zhu H., Xu Z. // *Vaccine.* 2006. V. 24. № 2. P. 109–115.
31. Lico Ch., Mancini C., Italiani P., Betti C., Boraschi D., Benvenuto E., Baschieri S. // *Vaccine.* 2009. V. 27. № 31. P. 5069–5076.
32. Palmer K.E., Benko A., Doucette S.A., Cameron T.I., Foster T., Hanley K.M., McCormick A.A., McCulloch M., Pogue G.P., Smith M.L., Christensen N.D. // *Vaccine.* 2006. V. 24. № 26. P. 5516–5525.
33. Fujiyama K., Sarjung W., Yanagihara I., Nakado J., Misaki R., Honda T., Watanabe Y., Seki T. // *J. Biosci. Bioengin.* 2006. V. 101. № 5. P. 398–402.
34. Komarova T.V., Baschieri S., Donini M., Marusic C., Benvenuto E., Dorokhov Yu.L. // *Expert. Rev. Vaccines.* 2010. V. 9. № 8. P. 859–876.
35. Nemchinov L.G., Natilla A. // *Protein Expr. Purif.* 2007. V. 56. № 2. P. 153–159.
36. Leclerc D., Beauseigle D., Denis J., Morin H., Pare Ch., Lamarre A., Lapointe R. // *J. Virol.* 2007. V. 81. № 3. P. 1319–1326.
37. Morin H., Tremblay M.-H., Plante E., Pare Ch., Majeau N., Hogue R., Leclerc D. // *J. Biotechnol.* 2007. V. 128. № 2. P. 423–434.
38. Saunders K., Sainsbury F., Lomonosoff G.P. // *Virology.* 2009. V. 393. №2. P. 329–327.
39. Kothyarov R.Y., Kuprianov V.V., Migunov A.I., Stepanova L.A., Tsybalova L.M., Kiselev O.L., Ravin N.V., Skryabin K.G. // *Acta Naturae.* 2010. V. 2. № 2(5). P. 71–76.
40. Sambrook J., Russel D. *Molecular Cloning: A Laboratory Manual.* N.Y.: CSHL Press, 2001.
41. Chen H., Nelson R.S., Sherwood J.L. // *Biotechniques.* 1994. V. 16. № 4. P. 664–668.
42. Laemmli U. // *Nature.* 1970. V. 227. № 5259. P. 680–685.
43. Tyulkina L.G., Karger E.M., Sheveleva A.A., Atabekov J.G. // *J. Gen. Virol.* 2010. V. 91. № 6. P. 1621–1628.
44. Tollin P., Wilson H. R. // *The Plant Viruses / Ed. Milne R.C.* N.Y.: Plenum Press, 1988. V. 4. P. 51.
45. Atabekov J.G., Dobrov E.N., Karpova O.V., Rodionova N.P. // *Molec. Plant Pathol.* 2007. V. 8. № 5. P. 667.
46. Geering A.D.W., Thomas J.E. // *Arch. Virol.* 1999. V. 144. № 3. P. 577–592.
47. Erickson J.W., Bancroft J.B. // *Virology.* 1976. V. 72. № 2. P. 514–517.
48. Liu W., Zou P., Chen Y.-H. // *Immunol. Lett.* 2004. V. 93. № 2–3. P. 131–136.
49. Liu W., Zou P., Jian D., Chen Y.-H. // *Microb. Infect.* 2005. V. 7. № 2. P. 171–177.
50. Fiers W., De Filette M., Birkett A., Neiryneck S., Min Jou W. // *Virus Res.* 2004. V. 103. № 1–2. P. 173–176.
51. Lukashina E., Badun G., Fedorova N., Ksenofontov A., Nemykh M., Serebryakova M., Mukhamedzhanova A., Rodionova N., Baratova L., Dobrov E. // *FEBS J.* 2009. V. 276. № 23. P. 7006–7015.

Triggering of Toll-like Receptor-2 in Mouse Myelomonocytic Leukaemia Cells WEHI-3B Leads to the Suppression of Apoptosis and Promotes Tumor Progression *in Vivo*

D.V. Shcheblyakov*, D.Y. Logunov, I.V. Rakovskaya, M.M. Shmarov, B.S. Naroditsky, A.L. Ginzburg

Gamaleya Research Institute of Epidemiology and Microbiology, Russian Academy of Medical Sciences

*E-mail: sdmitryv@yahoo.com

Received 26.08.2011

Copyright © 2011 Park-media, Ltd. This is an open access article distributed under the Creative Commons Attribution License, which permits unrestricted use, distribution, and reproduction in any medium, provided the original work is properly cited.

ABSTRACT Toll-like receptors are the essential components of innate immunity. It is shown that TLRs play an essential role in the immune resistance of an organism to bacterial and viral infections. The binding of TLR to its own ligands results in the activation of several adapter molecules and kinases, inducing the activation of the main pro-inflammatory transcriptional factors, which in turn induce the activation of the main pro-inflammatory transcriptional factors. This activation results in the development of both the innate immune response triggered by the enhanced expression of a number of pro-inflammatory cytokines and antimicrobial peptides and that of the adaptive immune response, via the activation of dendritic cells and enhancement of antigen presentation, etc. The ability of TLR agonists to bolster the immune reaction makes them promising for use in the therapy of infectious diseases and in the chemotherapy of malignant neoplasms. However, different TLR ligands may have either antitumor activity (lipopolysaccharide, imiquimod, CpG) or, conversely, could beef up the resistance of tumor cells to apoptosis, stimulating their proliferation under certain conditions (lipopolysaccharide, lipopeptide). It has been shown that the TLR2-dependent signalling pathway in the myelomonocytic mouse leukaemia cell line WEHI-3B leads to the constitutive activation of the transcriptional factor NF- κ B, suppression of apoptosis in tumor cells, and progression of myelomonocytic mouse leukaemia *in vivo*, upon the addition of TLR2 agonist (synthetic lipopeptide Pam2CSK4) or following the infection of tumor cells with *Mycoplasma arginini*.

KEYWORDS Toll-like receptor 2; synthetic diacylated lipopeptide Pam2CSK4; mouse myelomonocytic leukaemia cells WEHI-3B; transcription factor NF- κ B; apoptosis; tumor progression.

ABBREVIATIONS TLR2 – Toll-like receptor 2; NF- κ B – nuclear transcription factor- κ B; PAMP – pathogen-associated molecular pattern; DAMP – damage-associated molecular pattern; ssRNA – single-stranded ribonucleic acid; RT-PCR – reverse transcription polymerase chain reaction; TNF- α – tumor necrosis factor α ; IL – interleukin; MCP1 – monocyte chemoattractant protein 1.

INTRODUCTION

It is known that toll-like receptors (TLRs) are the crucial components of innate immunity and that they participate in the recognition of conserved pathogen-associated molecular patterns (PAMPs) and damage-associated molecular patterns (DAMPs) [1, 2]. The interaction between bacterial structures or DAMPs and specific Toll-like receptors initiates the development of reactions of both the innate and adaptive immune re-

sponses to induce the elimination of the causative agent from the organism [3, 4].

At the moment, thirteen human Toll-like receptors (TLR-13) are known. The majority of them are located on the surface of various immune cells (macrophages, dendritic cells and mast cells, neutrophils, B-cells and T-cells, natural killer cells) and on nonimmune cells, such as fibroblasts, epithelial cells, keratinocytes, etc. [5–7]. The interaction between TLR and specific ligands initiates a cascade of signals originating from

the cytoplasmic TIR domains of TLR [8]. The signal proceeds from the TIR domain through the adaptor molecules MyD88 (myeloid differentiation factor 88), TIRAP (TIR-domain-containing adaptors), TICAM1 (TRIF), TICAM2 (TIR-containing adaptor molecule) to the corresponding kinases (TAK, IKK, TBK, MAPK, JNKs, p38, ERK, Akt, etc.), providing differential activation of the transcription factors (NF- κ B, AP-1, and IRF) that are responsible for the expression of various pro-inflammatory and antimicrobial factors (IL-6, IL-8, TNF, IL-1 β), as well as for the activation of antigen-presenting cells [7, 9].

TLR have been shown to play a key role in the regulation of the adaptive immune response. Thus, the TLR-dependent activation of antigen-presenting dendritic cells is a crucial moment in several processes that are essential for the development of adaptive immunity, such as for the activation of mature T-cells; for the processing and presentation of microbial antigens; for boosting the expression of costimulatory molecules (CD80, CD86), which is required for the activation of naive CD4⁺-T-cells; and for the suppression of regulatory T-cells via IL-6 production [8, 10]. It was also discovered that TLR-dependent activation is essential for B-cell maturation during the infection process [11]. Thus, TLR play a significant role in the organism, a role that consists in the development of inflammatory reactions (activation of the innate immune system) in response to various pathogens (protozoa, fungi, bacteria, and viruses) entering the organism [12].

The impact the expression and activation of Toll-like receptors has on tumor progression is currently a subject of wide-ranging discussion. It has been demonstrated that TLR can have a dual effect on tumor cells, depending on the following factors: TLRs or their ligands type, tumor type, administration method, and ligand concentration [13]. On the one hand it has been shown that TLR can activate an anti-tumor immune response [14, 15]. Numerous TLR agonists are currently in clinical trials for prospective application as anti-tumor agents. Thus, the natural (ssRNA) and synthetic (imiquimod) TLR7 and TLR8 agonists have a demonstrable high activity with respect to chronic lymphocytic leukaemia and skin cancer [16]. The TLR9 – CpG ligand is capable of suppressing the development of lymphomas, as well as brain, kidney, and skin cancer [14]. The TLR3 – poly(IC) ligand possesses proapoptotic activity not only against tumor cells, but also against the cells surrounding the tumor (e.g., endothelial cells).

However, despite the existing data on the anti-tumor activity of TLR agonists, numerous studies have recently been published that demonstrate that TLR ligands can enhance the progression of different types

of tumors [15–17]. The TLR level is known to be high in various tumor cells; the frequency of induced tumor formation is decreased in TLR-knockout mice [18]. Furthermore, the boost in TLR expression on the cell surface of prostate tumors or head and neck tumors lead to an increase of the proliferation rate of these cells [19, 20]. Huang *et al.* [20] demonstrated that *Listeria monocytogenes* possesses a direct tumor-stimulating effect associated with its ability to activate TLR2-dependent signal pathways in ovarian cancer cells. In addition, the TLR2-dependent activation of NF- κ B induced by *L. monocytogenes* has been shown to increase the resistance of tumor cells to the action of chemotherapeutic agents [16]. The relationship between TLR2 and tumor progression was confirmed by Karin *et al.* [21], who proved that this receptor plays the key role in the metastasis of lung cancer.

Thus, the dual effect of TLR indicates that its functional role in tumor biology is most complex, and that it requires a systematic investigation based on various models.

An analysis of the TLR2 expression in various tumor cell lines was carried out in our laboratory. It was shown, using the model of the myelomonocytic mouse leukaemia cell line WEHI-3B, that the activation of the TLR2-dependent signalling pathway leads to apoptosis suppression and enhanced tumor growth *in vivo*, following the enjection of synthetic diacylated lipopeptide Pam2CSK4. A similar effect was observed for WEHI-3B cells infected with *Mycoplasma arginini*. It was revealed that micoplasma infection or the addition of the TLR2 agonist – diacylated lipopeptide Pam2CSK4 – to WEHI-3B cells results in the TLR2-dependent activation of the NF- κ B transcription factor in tumor cells and the suppression of apoptosis induced by the action of various anti-tumor agents. Moreover, it was demonstrated on a model of myelomonocytic mouse leukaemia *in vivo* that the intramuscular introduction of Pam2CSK4 results in greater tumor resistance to the action of 5-fluorouracil, enhancement of tumor growth, and a reduction in the survival rate of mice. An analysis of the mechanism of the previously described effect of the TLR2 agonist on WEHI-3B cells demonstrated that the activation of the NF- κ B factor, as well as the stimulation of the secretion of a number of pro-inflammatory cytokines (which are growth and development factors of myelomonocytic tumors), plays the key role in faster tumor progression.

EXPERIMENTAL

Cell lines

TLR2 expression was analyzed in the myelomonocytic mouse leukaemia cell line WEHI-3B, transformed

murine macrophages B10M, murine fibroblasts L929, human leukaemic monocyte lymphoma U937 cells, human lung cancer cells A549 and H460, human nonsmall cell lung cancer H1299 cells, human large intestine cancer HCT116 cells, and human breast cancer MCF-7 cells. The following were analyzed in WEHI-3B cells: the activity of NF- κ B, caspases-3/7, viability, the mitochondrial transmembrane potential, and the proliferation rate.

WEHI-3B cells were cultured in a RPMI medium with 10 vol % of fetal bovine serum (catalogue number SV30160.03, Hyclone, USA), 1 mg/ml glutamine (catalogue number F032, PanEco, Russia), 50 U/ml penicillin, and 50 μ g/ml streptomycin (catalogue number A065, PanEco, Russia) at 37°C in 5% CO₂. Cells were seeded at a 1 : 6 ratio on day 2.

Bacterial strains

The micoplasm strain *Mycoplasma arginini* used in this study was kindly provided by I.V. Rakovskaya (Laboratory of Mycoplasmas and Bacterial L-Forms, Gamaleya Research Institute of Epidemiology and Microbiology, Russian Academy of Medical Sciences). A flow cytometry kit (Bender Medsystems FlowCytomix, Austria) was used to determine the concentrations of chemokine and cytokine.

Reverse transcription reaction

The expression of *TLR2* genes in different human/murine cell lines was determined by RT-PCR. The total RNA was isolated using TRIZOL reagent (Invitrogen). The reverse transcription reaction was performed using an RT System kit (Promega). cDNA of the human/mouse *TLR2* and *GAPDH* genes were PCR-amplified using the following primers: mouse *TLR2* gene – upstream primer 5'-gttcctctgaccaggatc-3', downstream primer 5'-gcagcatcattgttctcttc-3'; human *TLR2* gene – upstream primer 5'-acctgtgtgactctccatcc-3', downstream primer 5'-gcagcatcattgttctcttc-3'; human *GAPDH* gene – upstream primer 5'-tctagacggcaggtcaggtccacc-3', downstream primer 5'-ccaccatggcaaattccatggca-3'; mouse *GAPDH* gene – upstream primer 5'-gcattctctgtgagtcagtgcc-3', downstream primer 5'-tcacacccatcacaaacatg-3'.

Measurement of β -galactosidase activity

The culture medium was removed 24 h after the specimens had been added to the cells, and a lysis solution with β -galactosidase substrate (1 mM MgCl₂; 0.25 M Tris-HCl pH 7.4; 0.02% NP40; 2 g/l *o*-nitrophenyl- β -*D*-galactopyranoside (catalogue number 102473, MP Biomedicals, USA) was then added. β -galactosidase activity was determined spectrophotometrically (414 nm) based on the conversion of

the substrate (*o*-nitrophenyl- β -*D*-galactopyranoside) into the colored product *o*-nitrophenol.

Cell viability analysis

Cell survival was assessed based on the ratio (%) between the intensity of the cells stained with methylene blue (pre-treated with cisplatin, taxol, and fluorouracil at varying concentrations) and the control, untreated cells (methylene blue was extracted with 0.1% SDS, its amount was determined chromatographically).

Caspases-3/7 activity measurement

The measurement of caspase activity was performed with the use of a specific to caspase-3/7 fluorogenic substrate Ac-DEVD-AMC (30 μ M in lysis buffer pH 7.0 containing 10 mM HEPES, 0.4 mM EDTA, 0.1% CHAPS, 2% glycerol, and 2 mM DTT). Cells were incubated for 16 h with apoptosis-inducing drugs. The fluorescence intensity was measured immediately (after 0 h) and 6h after additions of a substrate. The measurement was performed using a Wallac 1420 plate reader (Perkin Elmer).

Measurement of the level of mitochondrial transmembrane potential ($\Delta\psi_m$)

The level of the mitochondrial transmembrane potential ($\Delta\psi_m$) was assessed on the basis of the binding of the fluorogenic dye DioC6 (Sigma, USA), of which the degree of specific binding with mitochondrial membranes is dependent upon the $\Delta\psi_m$ value. The cells infected with *M. arginini* were placed into a 24-well plate (10⁵ cells per well). DioC6 at a concentration of 40 nM was added to the cells following apoptosis induction. The cells were incubated for 30 min at +37°C and washed twice with a phosphate buffer. The fluorescence was then measured using a Wallac 1420 plate reader.

Measurement of cytokine activity

BALB/c mice received 5 μ g of Pam2CSK4 intramuscularly. Blood samples were collected, and the concentrations of 14 chemokines and cytokines (IL-1, -2, -4, -5, -6, -10 and -12, TNF α , MCP-1 and -3, MIP-1a, -1b, RANTES, interferon- γ) were determined in serum by flow cytometry using a FlowCytomix BenderMedsystems kit (Austria).

Laboratory animals

Six-week-old (by the beginning of the experiment) female BALB/c mice and D2&I thymus-free mice were used for this study.

Analysis of the survival rate of BALB/c mice

In order to assess the effect of diacylated lipopeptide Pam2CSK4 on the rate of tumor progression, WEHI-3B

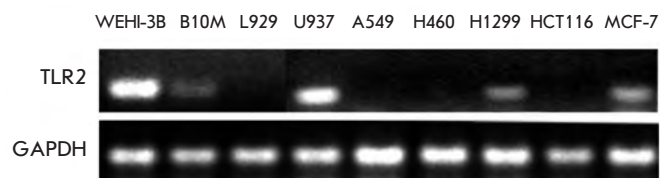


Fig. 1. Analysis of TLR2 expression in different tumor cell lines.

cells (2×10^6 cells per mouse) were introduced intraperitoneally to BALB/c mice, which had been divided into different groups. 5 μ g of Pam2CSK4 was introduced into each mouse at intervals of 1, 3, and 5 days post tumor transplantation. After 20 days, the mice were euthanized with diethyl ether; the liver and spleen were removed so as to be used for the macroscopic and histological analysis. In addition, the average weight of the spleen for each experimental group was determined.

The effect of the joint introduction of Pam2CSK4 and tumor cells on the animals survival rate was studied on BALB/c mice, to which WEHI-3B cells (2×10^6 cells per mouse) were intraperitoneally transplanted. Synthetic diacylated lipopeptide (Pam2CSK4) was systemically introduced at a dose of 5 μ g/mouse after 24 h. After 2 days, the mice also received Pam2CSK4 for a period of 3 days; the mice from the groups subjected to chemotherapy additionally received 0.6 mg of 5-fluorouracil. The control groups consisted of the animals that had received Pam2CSK4 and 5-fluorouracil only. Each group consisted of 10 mice. The animals were monitored until the death of the final mouse (32 days); the general condition of the mice was recorded.

RESULTS AND DISCUSSION

Analysis of the expression of the Toll-like receptors 2 and 6 in different tumor cell lines

The model we used to study the effect of TLR2 on the proliferation of tumor cells and on tumor progression *in vivo* was selected via an analysis of the expression of the Toll-like receptor 2 in different tumor cell lines (WEHI-3B, B10M, L929, U937, A549, H460, H1299, HCT116, and MCF-7) by reverse transcription followed by PCR against the *TLR2* gene (Fig. 1).

The Toll-like receptor 2 was expressed in five out of the nine cell lines analysed (WEHI-3B, B10M, U937, H1299 and MCF-7). The highest level of expression of this receptor was observed in the myelomonocytic mouse leukaemia cell line (WEHI-3B), which was subsequently selected for use as a model for the *in vitro* and *in vivo* experiments.

TLR2 agonist activates NF- κ B and suppresses apoptosis in tumor cells WEHI-3B expressing Toll-like receptor 2

Such parameters as the NF- κ B factor activity (Fig. 2), cell survival rate, caspases-3/7 level (Fig. 3), and the level of the mitochondrial transmembrane potential ($\Delta\psi_m$) (Fig. 4) were measured at the next stage of the assessment of the effect of TLR2 agonists on apoptosis induced by chemotherapy drugs in WEHI-3B cells expressing the Toll-like receptor 2. WEHI-3B cells were infected with *M. arginini*, or the TLR2 agonist (synthetic diacylated lipopeptide Pam2CSK4) was added followed by treatment with cisplatin, taxol or fluorouracil. The parameters mentioned above were measured after 16–18 h of incubation.

It was demonstrated that micoplasmal infection of the tumor cells WEHI-3B containing the Toll-like receptor 2 resulted in the activation of the transcription factor NF- κ B in these cells (Fig. 2). Similar results were obtained when synthetic diacylated lipopeptide was added to Pam2CSK4.

Figure 2A shows the data obtained by flow cytometry using specific antibodies to TLR2, which confirm the expression of TLR2, the major receptor of micoplasmal diacylated lipopeptides, and the data on the activation of NF- κ B in WEHI-3B cells via the TLR2-dependent pathway (Fig. 2B).

Figure 3 shows the survival rate and activity level of the major effector caspases-3/7 upon induction of apoptosis by chemotherapeutic drugs in WEHI-3B cells infected with *M. arginini*, or upon the addition of Pam2CSK4 to these cells. The level of caspases-3/7 was measured spectrophotometrically, using the specific fluorogenic substrate Ac-DEVD-AMC. As follows from these data, mycoplasma infection or the addition of lipopeptide Pam2CSK4 results in a statistically significant ($p < 0.005$) increase in the survival rate of WEHI-3B cells and a 25–30% decrease in the level of caspase-3/7 activation upon various intracellular damages in comparison with noninfected cells (white bars).

The mitochondrial transmembrane potential ($\Delta\psi_m$) was also measured in WEHI-3B cells; a decrease in this potential caused by various stress factors is the major apoptotic marker.

For this purpose, different concentrations of cisplatin were used to affect the infected or Pam2CSK4-treated cells; the level of the mitochondrial transmembrane potential ($\Delta\psi_m$) was measured after 16 h (Fig. 4).

The level of $\Delta\psi_m$ was assessed based on the binding of the fluorogenic dye DioC6, the degree of specific binding to mitochondrial membranes, which is dependent upon $\Delta\psi_m$.

As can be seen from the data presented, the level of mitochondrial transmembrane potential in cispla-

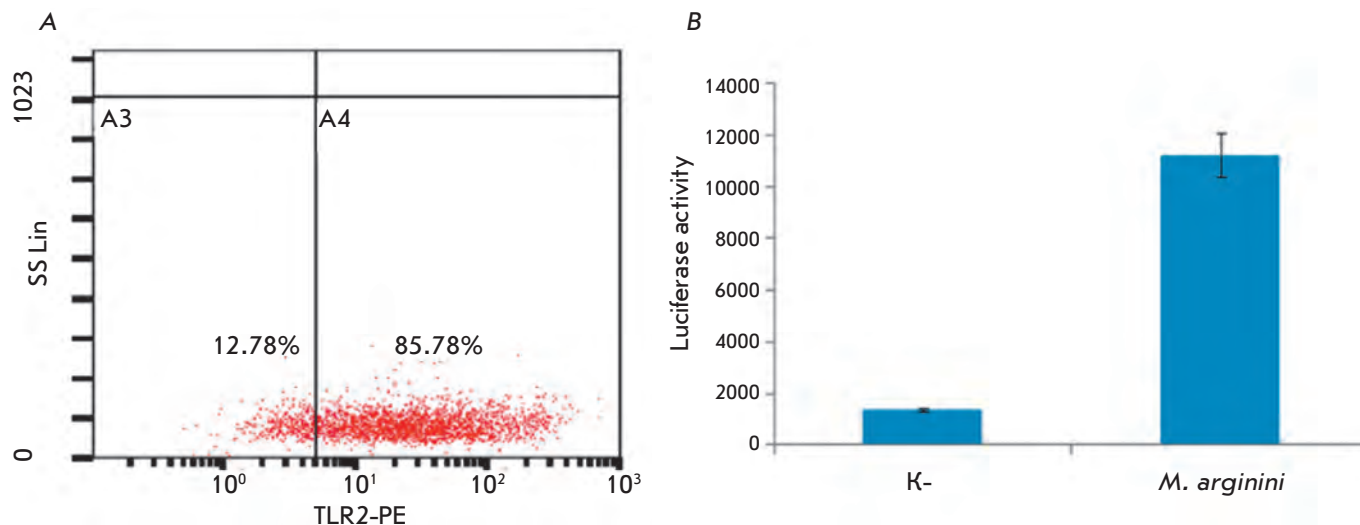


Fig. 2. Activation of NF- κ B in WEHI-3B cells in response to mycoplasmal infection or after treatment with diacylated lipopeptide Pam2CSK4. (A) – TLR2 expression in WEHI-3B cells. Expression of the specific for diacylated lipopeptides receptor TLR2 was additionally confirmed by flow cytometry. WEHI-3B cells were incubated with antibodies specific to mouse TLR2 (eBioscience, USA). Control cells were incubated with isotype control antibody (anti-IgG). The percentage of TLR2 positive cells was determined by phycoerythrin fluorescence (the assay was conducted according to the manufacture manual). (B) – NF- κ B-dependent expression of luciferase gene. Luciferase gene under NF- κ B – responsive promoter was introduced in WEHI-3B cells by lentiviral infection. NF- κ B-dependent luciferase expression was measured using the standard procedure after *M. arginini* infection or treating the cells with diacylated lipopeptide Pam2CSK4.

tin-treated WEHI-3B cells infected with *M. arginini* was higher by 25–30% than that of the noninfected cells (white bars), a point attesting to apoptosis suppression in the infected cells. Similar results were also obtained when using the synthetic diacylated peptide Pam2CSK4.

Thus, it was demonstrated in the first path of the *in vitro* experiment that micoplasmal infection or the addition of structural micoplasmal components to WEHI-3B cells expressing the Toll-like receptors 2 and 6 results in the activation of the transcription factor NF- κ B in them and apoptosis suppression upon different types of intracellular damage.

Kinetics of the growth of tumor cells WEHI-3B upon infection with *M. arginini*, or upon addition of diacylated lipopeptide Pam2CSK4 in the *in vitro* experiment

The transcription factor NF- κ B participates in the regulation of the expression of a number of proteins, including those controlling cell proliferation and apoptosis [19].

At the next stage of the study, we decided to observe the level of the impact that the micoplasmal infection or structural micoplasmal components, together with the anti-apoptotic activity, can have on both the kinetics and proliferation rates of the tumor cells WEHI-3B

under normal conditions and/or upon the induction of apoptosis in them.

For this purpose, *M. arginini* or Pam2CSK4 was added to the WEHI-3B cell line selected as a model; the activation of Nf- κ B in these cells was verified. The cells were then seeded into a 96-well plate (10^3 cells per well), and apoptosis-inducing drugs (cisplatin and taxol) were added. The kinetics of cell growth was determined based on the accumulation of cell biomass (methylene blue staining) for 72 h (with or without the apoptosis stimulus).

It follows from *Fig. 5* that apoptosis blockage was observed in micoplasmal-infected cells with and/or upon addition of Pam2CSK4. However, no increase in the proliferation rate was observed.

It was thus demonstrated that apoptosis suppression in micoplasmal-infected cells caused by the activation of the transcription factor NF- κ B does not result in an *in vitro* increase in the cell proliferation rate.

The effect of the TLR2 agonist – diacylated lipopeptide Pam2CSK4 – on the proliferation and resistance of WEHI-3B cells to chemotherapeutic agents in an *in vivo* experiment

The effect of the antigens circulating in the mouse's organism (TLR2 agonists) on the proliferation and resistance of the myelomonocytic mouse leukaemia cells

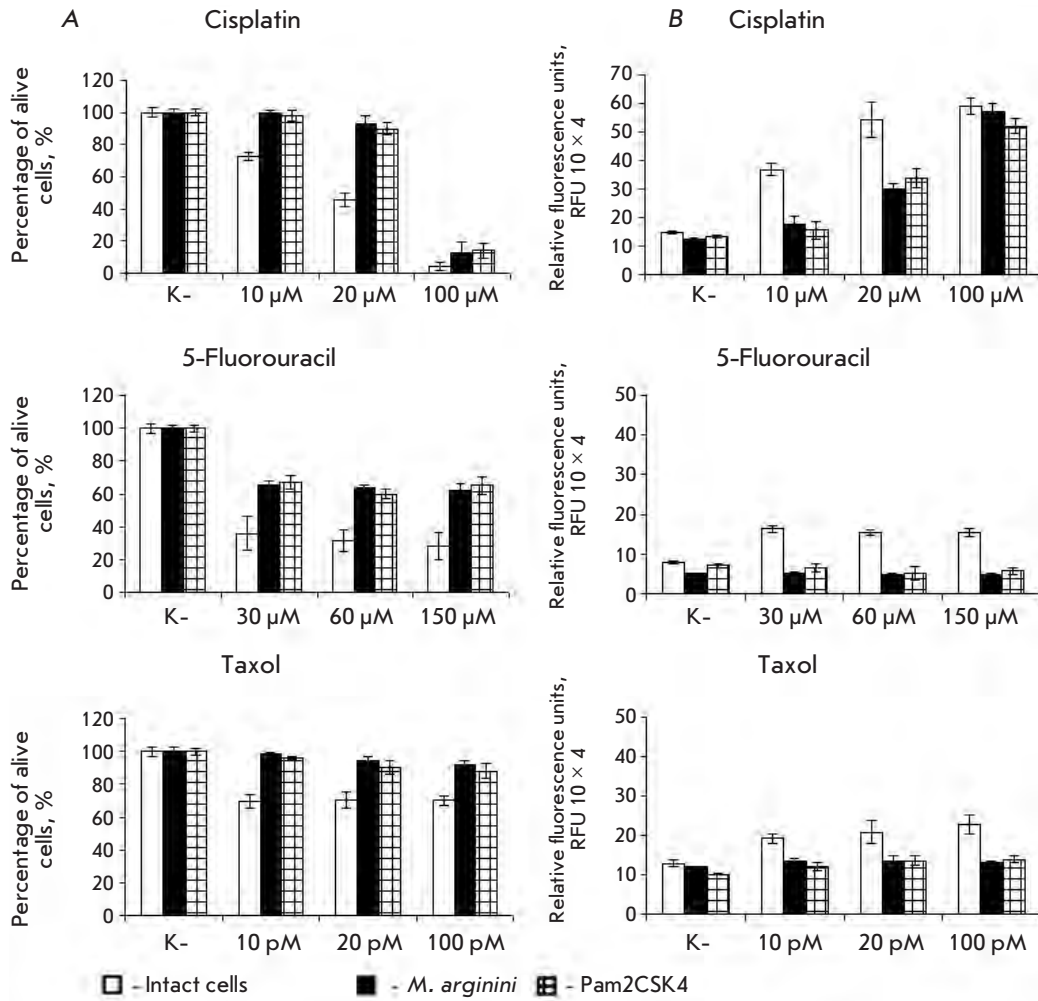


Fig. 3. Survival and caspases 3/7 activity in myelomonocytic leukaemia cells WEHI-3B following exposure to chemotherapeutic agents at different concentrations. (A) – survival of myelomonocytic leukaemia cells WEHI-3B; (B) – caspases 3/7 activity. The data on each point is a result of three independent experiments. ($p < 0.005$).

WEHI-3B to chemotherapeutic agents *in vivo* was studied.

Firstly, the effect of the diacylated lipopeptide Pam2CSK4 on the rate of tumor progression was assessed. Forty 18–20 g animals (female BALB/C mice) participated in the experiment. The animals were divided into four groups, 10 mice per group. The control group (the first group) consisted of intact mice. The second group included mice that received three doses of Pam2CSK4 intramuscularly. The third group was comprised of the mice transplanted with WEHI-3B cells (2×10^6 cells per mouse). The mice from the fourth group were intraperitoneally transplanted with WEHI-3B cells of identical dose. Each mouse from this group received 5 μ g of Pam2CSK4 on days 1, 3, and 5 following tumor transplantation. The mice were euthanized with diethyl ether in order to assess the tumor progression after 20 days; the liver and spleen were removed from the mice and were subsequently used for macroscopic and histological studies. The average weight of the spleen was determined in each experi-

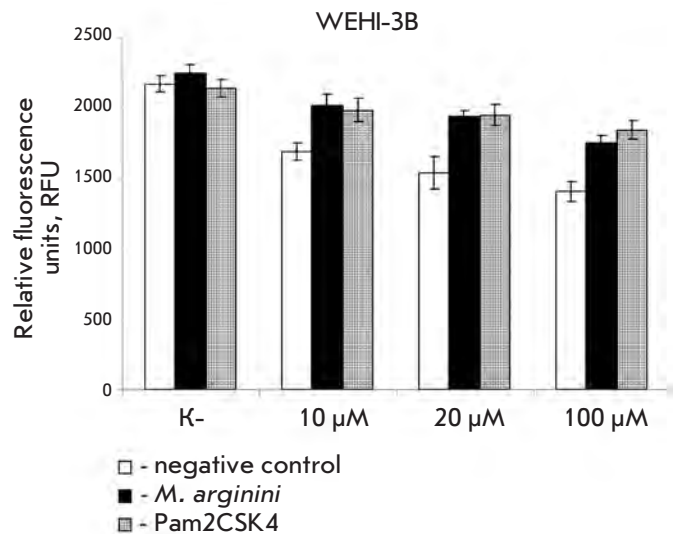


Fig. 4. Membrane mitochondrial potential level ($\Delta\psi_m$) in WEHI-3B cells after exposure to different concentrations of cisplatin. The data on each point is a result of three independent experiments. ($p < 0.005$).

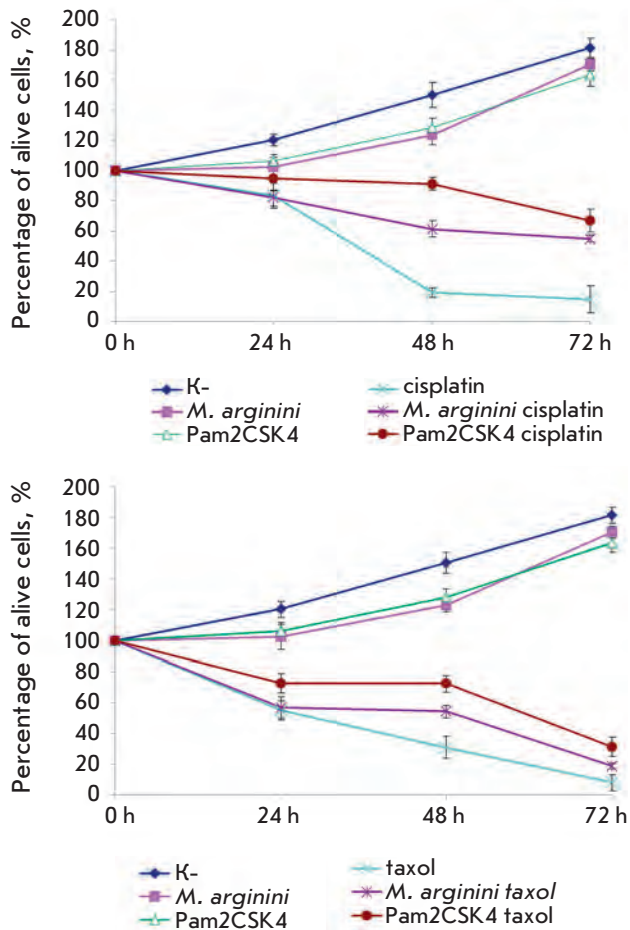


Fig. 5. Proliferation rate of WEHI-3 cells. K – control cells; *M. arginini* – cells infected with *M. arginini*; Pam2CSK4 – cells treated with diacylated lipopeptide; cisplatin – control cells treated with cisplatin; *M. arginini* cisplatin – cells infected with *M. arginini* and treated with cisplatin; Pam2CSK4 cisplatin – cells treated with diacylated lipopeptide and cisplatin; taxol – control cells treated with taxol; *M. arginini* taxol – cells infected with *M. arginini* and treated with taxol; Pam2CSK4 taxol – cells treated with diacylated lipopeptide and taxol. ($p < 0.005$).

mental group (Fig. 6A–B). According to the data obtained in the macroscopic study, no visible pathological changes were observed in mice from groups 1 and 2 (Fig. 6A). However, a negligible increase in the average weight of the spleen was observed in mice from group 2 (Fig. 6B). The changes typical of leukaemia (increase of spleen size and slightly swollen liver) were detected in the liver and spleen of the mice with transplanted myelomonocytic mouse leukaemia cells (group 3) by macroscopic studies. Sparse tumors were detected on the liver and spleen surface. When performing the mac-

roscopic study of the liver and spleen obtained from mice transplanted with leukaemia cells and that had received Pam2CSK4 (group 4), the changes typical of leukaemia were also observed. The spleen was considerably swollen. Loose neo-formations (which turned out to be myelomonocytic leukaemia cells) were found on the spleen and liver surface.

The measurements of the average weight of the spleen demonstrated a significant increase in the weight of this organ in mice with leukaemia (groups 3 and 4) as compared to the mice from the control groups 1 and 2. The introduction of Pam2CSK4 to mice from group 4 resulted in an even greater increase in the average weight of the spleen ($p < 0.05$) in comparison with the animals from group 3 (Fig. 6B).

No pathological changes were revealed in a histological study of the spleen and liver of the mice from groups 1 and 2. An identical pattern was observed in the spleen of the mice from groups 3 and 4. Diffuse dense infiltration of pulp with myelomonocytic leukaemia elements was observed; lymphatic follicles were atrophied. The greatest differences were observed between the liver samples of the mice from groups 3 and 4. Numerous small myelomonocytic leukaemia infiltrates were present in the livers of the mice from group 3, whereas the mice livers from group 4 were considerably larger (Fig. 6C). Infiltrates mostly localized along sinusoids. Leukaemia cell aggregation was also detected in individual blood vessels. A clearly defined surface infiltration of a liver with leukaemia cells was observed in mice from group 4, in contrast to those from group 3.

The macro- and microscopic studies of spleen and liver samples obtained from mice which were intraperitoneally transplanted with WEHI-3B cells allowed us to arrive at the conclusion that micoplasma diacylated lipopeptide promotes tumor progression.

The effect of the diacylated lipopeptide Pam2CSK4 on the rate of tumor progression was assessed at the next stage. The nature of the effect of Pam2CSK4 on the resistance of the transplanted cells to chemotherapeutic agents was simultaneously determined. This experiment was performed according to the scheme described in the Experimental section. Figure 6D shows the diagram of the survival rate of the experimental mice.

It was shown via an analysis of the Kaplan–Meier survival curves that the mice receiving the synthetic diacylated lipopeptide demonstrated a less favorable response to 5-fluorouracil in comparison with those that did not receive Pam2CSK4. The last mouse from the group receiving chemotherapy died on day 33, whereas the mice that received Pam2CSK4 simultaneously with chemotherapy died as early as on day 26.

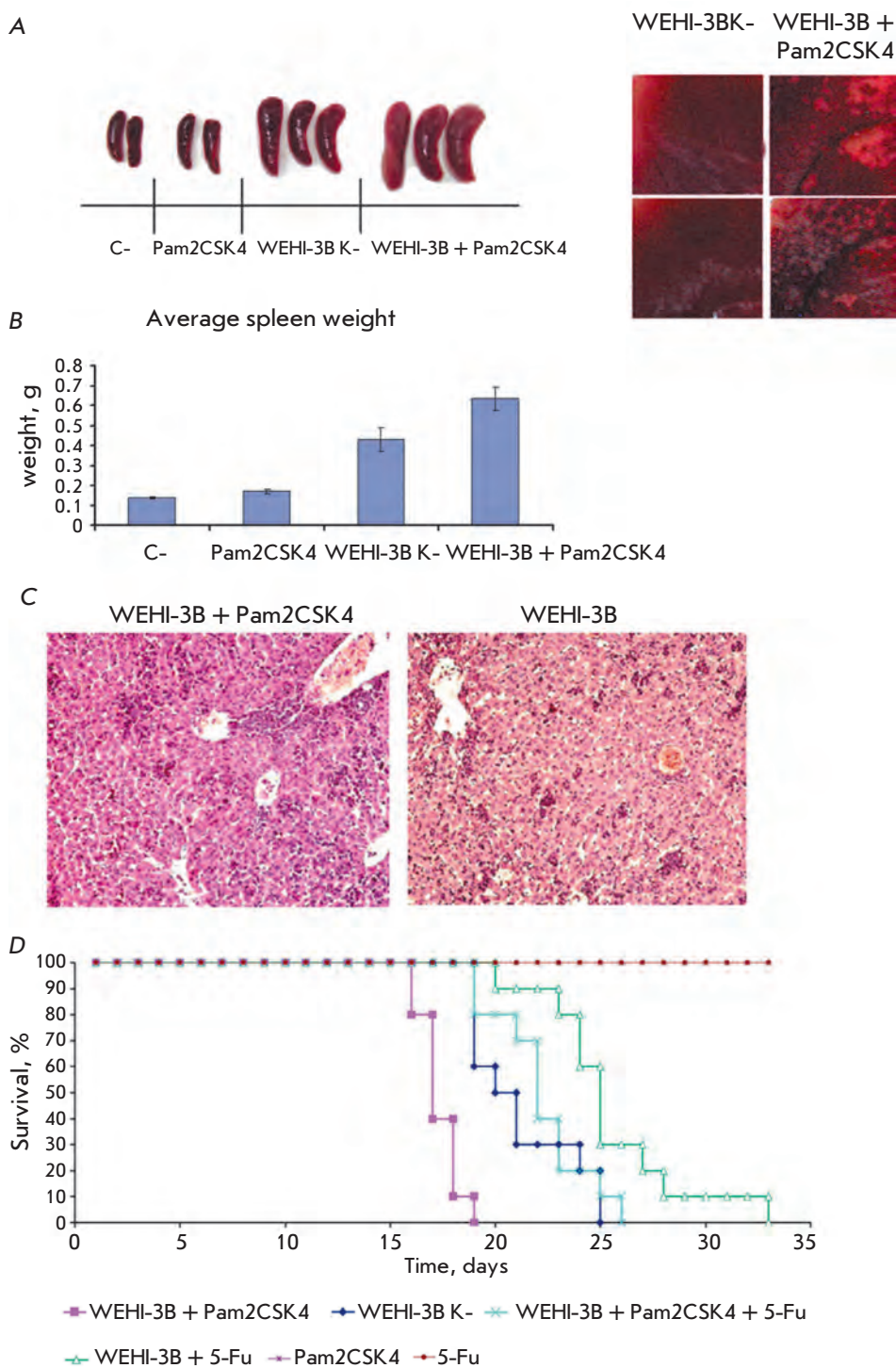


Fig. 6. Influence of diacylated lipopeptide Pam2CSK4 on the proliferation rate and chemotherapy resistance of WEHI-3B tumor cells *in vivo*. (A) – macrophotographs of mouse organs. The macrophotograph of the spleen is presented on the left-hand side; the macrophotograph of liver sections with infiltrations is presented on the right-hand side. C – group of intact mice injected with PBS; Pam2CSK4 – group of mice injected with diacylated lipopeptide Pam2CSK4; WEHI-3B – group of mice injected with WEHI-3B tumor cells; WEHI-3B + Pam2CSK4 – group of mice injected with WEHI-3B tumor cells and treated with Pam2CSK4. (B) – the average weight of spleens. Five organs from different groups of mice were used to determine the average weight. (C) – macrophotographs of a liver slice. Liver samples were placed into 10% formalin for fixation. The samples were then embedded into paraffin blocks according to the standard protocol; slides were stained with hematoxylin and eosin. (D) – survival curves of Balb/C mice. WEHI-3B K – group of mice with i.p. injected WEHI-3B cells; WEHI-3B + Pam2CSK4 – group of mice with i.p. injected WEHI-3B cells and i.m. injected Pam2CSK4; WEHI-3B + 5-Fu – group of mice with i.p. injected WEHI-3B and treated with 5-fluorouracil; WEHI-3B + Pam2CSK4 + 5-Fu – group of mice with i.p. injected WEHI-3B cells and i.m. injected Pam2CSK4 and treated with 5-fluorouracil ($p < 0.001$).

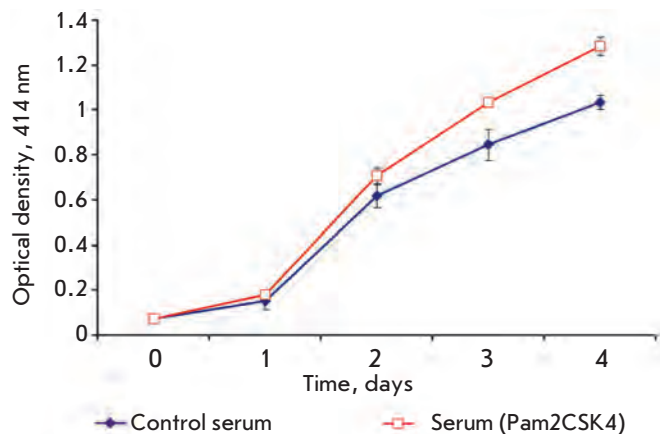


Fig. 7. Proliferation rate of myelomonocytic leukaemia cells WEHI-3B after exposure to serum of mice injected with Pam2CSK4 ($p < 0.005$).

The *in vivo* survival rate of mice was in complete correlation with the results previously obtained on culture cells. Moreover, as follows from the diagram, all mice into which WEHI-3B and Pam2CSK4 cells were simultaneously introduced died as early as on day 19, whereas the lifetime of those mice that did not receive Pam2CSK4 was equal to 25 days. These data attest to the fact that the intramuscular administration of Pam2CSK4 results in accentuated tumor progression and a decrease in the lifetime of mice. It is noteworthy that these experimental results showed no agreement with the data obtained for a cell culture, where the addition of Pam2CSK4 into the culture media did not result in an increase in the proliferation rate of WEHI-3B cells.

The effect of diacylated lipopeptide Pam2CSK4 on production of the factors stimulating the *in vivo* proliferation of myelomonocytic mouse leukaemia cells WEHI-3B

Taking into account the major difference between the *in vitro* and *in vivo* growth of WEHI-3B cells in the presence of Pam2CSK4, it was assumed that the factors that are essential for the proliferation of WEHI-3B cells can occur in the organism of the experimental animals after diacylated lipopeptide is introduced, thus determining the kinetics of the *in vivo* growth of these cells.

To corroborate this hypothesis, we studied the effect of serum obtained from the mice that had received Pam2CSK4 on the proliferation rate of WEHI-3B cells. BALB/c mice received intramuscular injections of 5 μ g of diacylated lipopeptide Pam2CSK4. Twenty-four hours after the injection, blood samples were

taken to obtain serum. Serum from mice that received a phosphate saline buffer was used as a control. The sera were used to prepare 5% of the medium for culturing WEHI-3B (RPMI) cells. The media were added to WEHI-3B cells, which were then seeded into a 96-well plate at a concentration of 10^3 cells per well. The kinetics of cell growth was determined based on the accumulation of cell biomass in the reaction with the MTT substrate during 72 h (Fig. 7).

As follows from Fig. 7, the addition of blood serum obtained from the mice that intramuscularly received Pam2CSK4 to WEHI-3B cells resulted in an increase in their proliferation rate. The results of this experiment corroborated the assumption earlier made about the possible production of the factor inducing the growth of the myelomonocytic mouse leukaemia cells WEHI-3B in response to the introduction of Pam2CSK4.

An attempt to identify the factors promoting the accentuated growth of WEHI-3B cells was undertaken at the next stage.

For this purpose, the synthesis of chemokines and cytokines in the organism in response to the introduction of diacylated lipopeptide was analyzed (Fig. 8). The cytokine expression was determined according to the procedure described in the Experimental section. Figure 8 shows the data for cytokines whose expression level changed in response to the introduction of Pam2CSK4. It is clear that the introduction of Pam2CSK4 resulted in a change in the expression of eight of the 14 cytokines. An analysis of the published data demonstrated that five of these cytokines (IL-6, MCP-1, MCP-3, RANTES, and TNF α) are capable of direct or indirect promotion of tumor growth [21].

Hence, it was shown that the activation of the TLR2-dependent signalling pathway in WEHI-3B cells after the introduction of diacylated lipopeptide Pam2CSK4 or *M. arginini* cells leads to the constitutive activation of the transcription factor NF- κ B in WEHI-3B cells. In turn, the activation of NF- κ B results in increased resistance of these cells to various assaults induced by chemotherapeutic agents (cispatin, taxol, and fluorouracil).

It was demonstrated via *in vitro* experiments that apoptosis suppression in the cells infected with *M. arginini*, which was caused by the activation of the transcription factor NF- κ B, had no effect on the rate of cell proliferation. However, the data obtained *in vivo* differs: the intramuscular introduction of Pam2CSK4 promoted the growth of myelomonocytic mouse leukaemia cells WEHI-3B in the organism of experimental animals. This fact is mostly accounted for by the ability of Pam2CSK4 to stimulate the expression of the factors (IL-6, MCP-1, MCP-3, RANTES, and TNF α) boosting the growth of tumor cells.

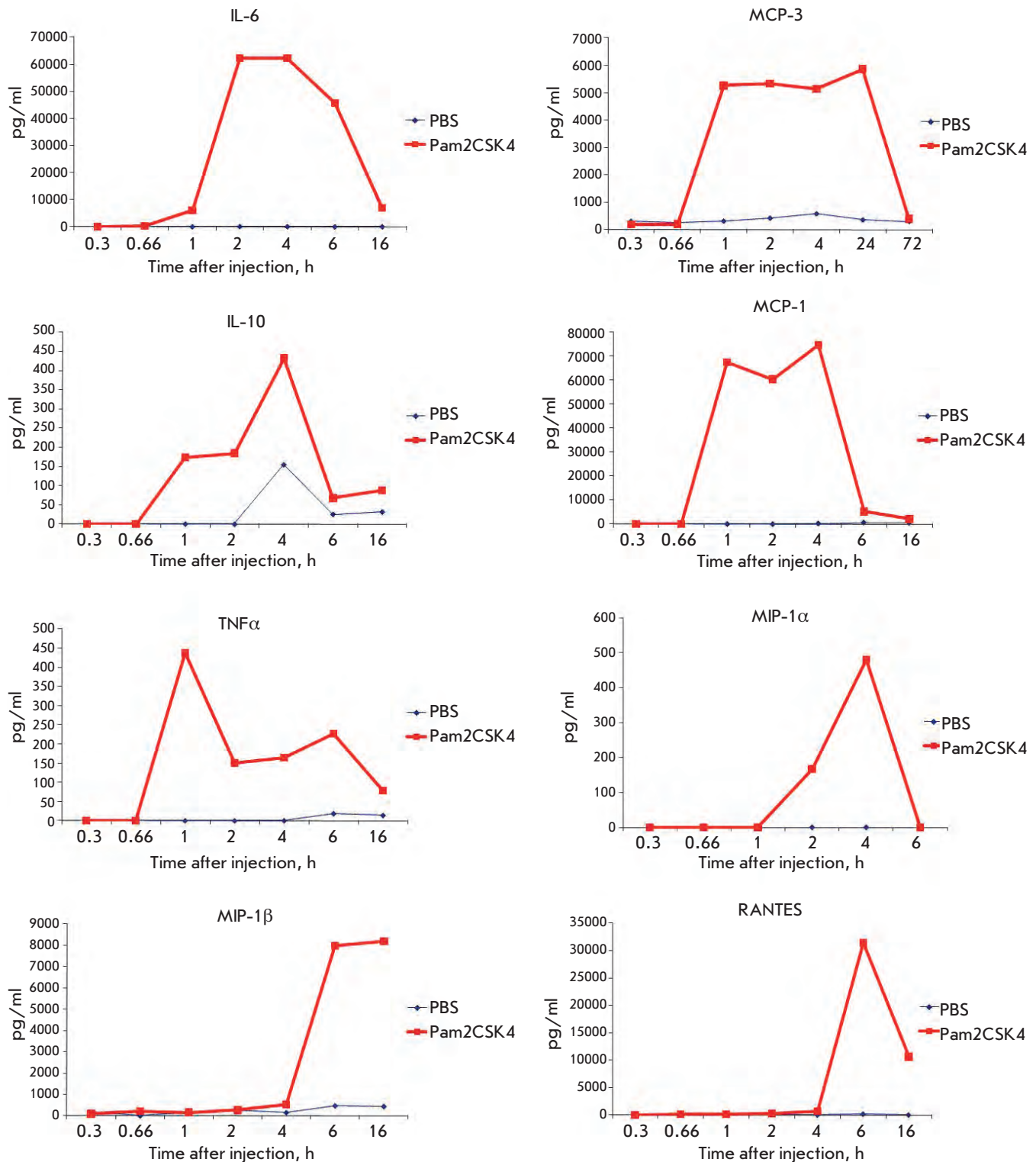


Fig. 8. Determination of serum cytokine concentrations in mice injected with Pam2CSK4. BALB/C mice were injected with diacylated lipopeptide Pam2CSK4 or PBS. Blood samples were collected for serum preparation after the indicated time intervals. Cytokine concentrations were determined in serum samples. Each point is the average value of three independent experiments.

The results obtained for the model WEHI-3B cells show that the activation of the Toll-like receptor 2 in tumor cells of myelomonocytic origin caused by mycoplasmal infection or the direct action of the TLR2 agonist (diacylated lipopeptide) promotes the growth of these cells. Meanwhile, studying the effect of mycoplasma and its structural component diacylated lipopeptide Pam2CSK4 on the development of the tumor allows one to arrive at the conclusion that the mycoplasmal in-

fection may impact not only the rate of disease progression, but also the effectiveness of anti-tumor therapy. This observation is valid not only for mycoplasmas, but also for the other pathogens causing various infections in patients with malignancies. The potential exists to conduct efficient therapy in the case of myelomonocytic leukaemias, provided that the disease is not stimulated by the factors of pathogenic microorganisms, or their antigens, circulating in the body. ●

REFERENCES

1. Medzhitov R. // *Nat. Rev. Immunol.* 2001. V. 1. P. 135–145.
2. Pasare C., Medzhitov R. // *Nature.* 2005. V. 438. № 7066. P. 364–368.
3. Uematsu S., Akira S. // *Handb. Exp. Pharmacol.* 2008. V. 183. P. 1–20.
4. Bianchi M.E. // *J. Leukoc. Biol.* 2007. V. 81. P. 1–5.
5. Diebold S.S. // *Handb. Exp. Pharmacol.* 2009. V. 188. P. 3–30.
6. West A.P., Koblansky A.A., Ghosh S. // *Annu. Rev. Cell. Dev. Biol.* 2006. V. 22. P. 409–437.
7. Tukhvatulin A.I., Logunov D.Y., Shcherbinin D.N., Shmarov M.M., Naroditsky B.S., Gudkov A.V., Gintsburg A.L. // *Biochemistry.* 2010. V. 75 (9). P. 1224 – 1243
8. Aravind L., Dixit V.M., Koonin E.V. // *Science.* 2001. V. 291. P. 1279–1284.
9. Kawai T., Akira S. // *Semin. Immunol.* 2007. V. 19. P. 24–32.
10. Iwasaki A., Medzhitov R. // *Nat. Immunol.* 2004. V. 5. № 10. P. 987–995.
11. Pasare C., Medzhitov R. // *Adv. Exp. Med. Biol.* 2005. V. 560. P. 11–18.
12. Palm N.W., Medzhitov R. // *Immunol. Rev.* 2009. V. 227. № 1. P. 221–233.
13. Shcheblyakov D.V., Logunov D.Y., Tukhvatulin A.I., Shmarov M.M., Naroditsky B.S., Gintsburg A.L. // *Acta Naturae.* V. 2. № 3 (6). 2010. P. 21–29.
14. Krieg A.M. // *J. Clin. Invest.* 2007. V. 117. P. 1184–1194.
15. Chicoine M.R., Zahner M., Won E.K. // *Neurosurgery.* 2007. V. 60. P. 372–381.
16. Stockfleth E., Trefzer U., Garcia-Bartels C. // *Br. J. Dermatol.* 2003. V. 149 (Suppl. 66). P. 53–56.
17. Logunov D., Scheblyakov D., Zubkova O., Shmarov M., Rakovskaya I., Gurova K., Tararova N., Burdelya L., Naroditsky B., Ginzburg A., Gudkov A. // *Oncogene.* 2008. V. 27. № 33. P. 4521–4531.
18. Harmey J.H., Bucana C.D., Lu W. // *Int. J. Cancer.* 2002. V. 101. P. 415–422.
19. Hayden M.S., Ghosh S. // *Genes Dev.* 2004. V. 18. P. 2195–2224.
20. Huang B., Zhao J., Shen S. // *Cancer. Res.* 2007. V. 67. P. 4346–4352.
21. Karin M., Yamamoto Y., Wang Q.M. // *Nat. Rev. Drug.* 2004. V. 3. P. 17–26.

Inhibition of DNA Gyrase by Levofloxacin and Related Fluorine-Containing Heterocyclic Compounds

V.L. Tunitskaya^{1*}, A.R. Khomutov¹, S.N. Kochetkov¹, S.K. Kotovskaya^{2,3}, V.N. Charushin^{2,3}

¹Engelhardt Institute of Molecular Biology, Russian Academy of Sciences

²Postovsky Institute of Organic Synthesis, Ural Branch, Russian Academy of Sciences

³Urals Federal University, Yekaterinburg, Russia

*E-mail: ve_tun@mail.ru

Received 28.09.2011

Copyright © 2011 Park-media, Ltd. This is an open access article distributed under the Creative Commons Attribution License, which permits unrestricted use, distribution, and reproduction in any medium, provided the original work is properly cited.

ABSTRACT Fluoroquinolones are an important class of modern and efficient antibacterial drugs with a broad spectrum of activity. Levofloxacin (the optically active form of ofloxacin) is one of the most promising fluoroquinolone drugs, and its antibacterial activity is substantially higher than the activity of other drugs of the fluoroquinolone family. Earlier, in the Postovsky Institute of Organic Synthesis, UB RAS, an original method of levofloxacin synthesis was developed, and now the pilot batch of the drug is being prepared. Bacterial DNA gyrase is a specific target of fluoroquinolones; hence, the study of the enzyme-drug interaction is of theoretical and practical importance. Moreover, the parameters of DNA gyrase inhibition may serve as a criterion for drug quality. Here, we present the results of studying the interaction of DNA gyrase with a number of fluoroquinolones and their analogs: intermediates and semi-products of the levofloxacin synthesis, and also samples from the pilot batches of this drug. The importance of two structural elements of the levofloxacin molecule for the efficiency of the inhibition is revealed. The data obtained may be useful for the design of new drugs derived from levofloxacin.

KEYWORDS fluoroquinolones; levofloxacin; derivatives; bacterial DNA gyrase; enzymatic activity; inhibition.

INTRODUCTION

Fluoroquinolones are among the most important classes of effective antibacterial drugs with a broad spectrum of activity. They effectively compete with and can partly substitute cephalosporins and other antibiotics, which are widely used in clinical practice to cure infectious diseases [1–11]. The first fluoroquinolones (pefloxacin, ciprofloxacin, norfloxacin, and ofloxacin) appeared in the global pharmaceutical market in the early 1990s [1–6]. Now, sales of ciprofloxacin amount to about 10 billion US dollars, and novel promising drugs of this family, such as levofloxacin [12] (one of the enantiomers of ofloxacin) and moxifloxacin, have been developed. Therefore, fluoroquinolones occupy an important place among the arsenal of antibiotics currently in use.

Fluoroquinolones are effective against a large number of diseases: severe suppurative-septic infections, including those of the respiratory tract, urinary tract, skin and soft tissues; bones and joints; liver and biliary; gastrointestinal tract, eyes and the central nervous system; and sexually transmitted infections [1–4]. The high efficiency of fluoroquinolones and wide spectrum

of antibacterial activity is due to their ability to affect the reproduction of bacteria inhibiting bacterial topoisomerase II (DNA gyrase), an enzyme responsible for the breaking and restoration of the DNA double helix. It is of importance that the mechanism of fluoroquinolone action differs from that of the other groups of antibiotics (e.g., penicillin antibiotics, cephalosporins, and aminoglycosides), which enables the effective use of fluoroquinolones for the treatment of infectious diseases caused by antibiotic-resistant strains [1–4].



One of the most effective drugs from the group of tricyclic fluoroquinolones is levofloxacin, which is an

optically active from (*S*-isomer) of ofloxacin. The antibacterial activity of levofloxacin is twice higher than the activity of racemic ofloxacin and 128 times higher than the activity of its *R*-antipode [13]. Levofloxacin is rightly referred to as a drug of the 21st century. This drug, at low doses, affects clinically important gram-positive and atypical microorganisms. Besides, it exhibits high activity towards many gram-negative bacteria [12]. Original methods for the preparation of a family of fluoroquinolones and the corresponding synthetic precursors, including enantiomerically pure semi-products of levofloxacin synthesis, based on kinetic separation of optical antipodes using chiral reagents were recently developed at the Postovsky Institute of Organic Synthesis, UB RAS, and the Urals Federal University [5, 7, 11]. The impact of these studies, mainly the synthesis of optically active levofloxacin and its analogs, has been confirmed by a series of publications [14–20], including an original and effective method for the production of (*S*)-7,8-difluoro-2,3-dihydro-3-methyl-4H-[1,4]-benzoxazine, which is a key semi-product of levofloxacin synthesis [14, 15].

Currently, in the Postovsky Institute of Organic Synthesis, UB RAS, the design and synthesis of new fluoroquinolone derivatives and their analogs with antibacterial activity are in progress. An important constituent of these studies is the investigation of the interaction of new compounds with DNA gyrase, which may be considered among the criterion for the purity of levofloxacin. In this paper, we present results of the investigation of the interaction of DNA gyrase with new fluoroquinolone derivatives, as well as with levofloxacin samples from the pilot batch.

EXPERIMENTAL

Materials

GyrA-pET19 and GyrB-pET19m plasmids containing genes encoding the A and B subunits of DNA gyrase were kindly provided by K.V. Severinov and I.S. Shkundina (Institute of Molecular Genetics, RAS) and were used as producers of DNA gyrase. The substrates for the gyrase reaction (i. e., a relaxed plasmid pBR322 or pHOT) were purchased from Topogen (USA).

Isolation and Purification of DNA Gyrase

Escherichia coli Rosetta (DE3) {*F- ompT hsdSB (rbmB)- gal dcm lacY1 (DE3) pRARE6 (CmR)*} (“Novagen”, USA) was used as the expression strain. The DNA gyrase subunits encoded by the plasmids contained six histidine residues at the *N*-terminus; the latter facilitated their isolation with affinity chromatography using Ni-NTA-agarose.

The cells transformed with plasmids were grown overnight in 5 ml of the LB medium containing 150 mg/l ampicillin (A150) and 15 mg/l chloramphenicol (C15) at 37°C. The cell pellet was obtained by centrifugation and finally re-suspended in 250 ml of the fresh medium containing A150 and C15 and grown up to an optical density (OD_{550}) of 0.5 at 37°C. Then, isopropylthio- β -*D*-galactoside (IPTG) was added (final concentration 1 mM), and cultivation was continued for an additional 18 h at 17°C. Cells were collected by centrifugation at 4000 rpm for 20 min, washed with a GTE buffer (25 mM Tris-HCl, pH 7.6, 50 mM glucose, and 10 mM EDTA), and kept frozen at –85°C. Furthermore, the cells were suspended in 15 ml of buffer A (20 mM Tris-HCl, pH 8.0, 500 mM NaCl, 10% (v/v) glycerol, 1% (v/v) Triton X-100, and 1 mM 2-mercaptoethanol), and protease inhibitors (1 mM phenylmethylsulfonyl fluoride (PMSF) and 10 μ g/ml aprotinin) were added. The suspension of cells was sonicated on ice and centrifuged for 15 min at 10000 g. The supernatant was applied on the column with Ni-NTA-agarose (2 ml) equilibrated with buffer A. The column was subsequently washed with buffer A containing 10, 30, and 50 mM of imidazole (5 ml each), and the target proteins were eluted with the same buffer containing 200 mM of imidazole. The fractions containing gyrase A and gyrase B were dialyzed against buffer A without Triton X-100 and then against the same buffer containing 50% of glycerol. The yield and the purity of the enzymes were analyzed by 12% polyacrylamide gel electrophoresis in accordance with the procedure described by Laemmli. The yield of gyrase A was 40 mg/l of the cell culture; gyrase B, around 60 mg/l. Equivalent amounts of the thus-obtained DNA gyrase subunits A and B were mixed, and the aliquots at a volume of 30–50 μ l could be stored at –80°C for several weeks without a significant loss of activity, while these enzyme samples remained active for only 2–3 days at –18°C.

Determination of the Activity of DNA Gyrase

The reaction mixture (30 μ l) contained 35 mM Tris-HCl (pH 7.5), 24 mM KCl, 4 mM $MgCl_2$, 1.4 mM ATP, 5 mM DTT, 1.8 mM spermidine, and 0.1 mg/ml of a bovine serum albumin. A mixture of DNA gyrase A and B subunits (0.4 μ g) and 0.25–0.5 μ g of the substrate (relaxed plasmid pBR322) were added to the reaction probe. The reaction was performed for 60 min at 25°C (for multiple samples, 96-well plates were used). After the reaction was completed, the samples were extracted with an equal volume of chloroform (30 μ l). Then, 7 μ l of the mixture containing 50% of sodium dodecyl sulfate, 25% of glycerol, and 0.25% of bromphenol blue were added to the aqueous phase. The mixture was applied on a 1.2% agarose gel in TAE buffer (40 mM Tris-acetate,

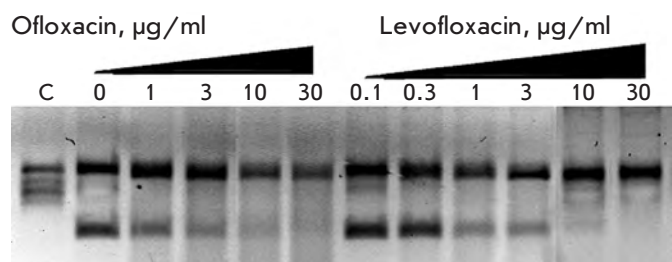


Fig. 1. Inhibition of DNA gyrase by levofloxacin and ofloxacin. Figures specify the concentrations of inhibitors in the reaction mixtures. C – control (plasmid without the enzyme).

pH 8.0, 2 mM EDTA) and analyzed with electrophoresis (50 V, 2 h). The products were visualized under UV-light after staining with ethidium bromide. The activity of the enzyme (%) was determined from the intensity of the band corresponding to the super-coiled form of plasmid pBR322 and estimated using the Total Lab v2.01 software.

Inhibition of DNA Gyrase by Fluoroquinolones and Related Fluorine-Containing Heterocycles

The reaction mixture in a volume of 30 µl contained 35 mM Tris-HCl (pH 7.5), 24 mM KCl, 4 mM MgCl₂, 1.4 mM ATP, 5 mM DTT, 1.8 mM spermidine, 0.1 mg/ml bovine serum albumin, and a solution of levofloxacin or fluorine-containing heterocyclic derivatives (see below) in DMSO (1–3 µl). An equal volume of DMSO was added to the control. The reaction was started upon addition of DNA gyrase (0.4 µg) and relaxed plasmid pBR322 (0.25–0.5 µg), which was used as a substrate, and performed as described above. Calculations were made using the Total Lab v2.01 program.

RESULTS AND DISCUSSION

The cellular target of fluoroquinolones is bacterial DNA gyrase, which consists of two subunits with M_r of 105 and 95 kDa and encoded by the *gyrA* and *gyrB* genes, respectively. DNA gyrase has an A₂B₂-type tetrameric structure [1–5]. Although this enzyme does not only break but also ligate the breaks in the DNA chains, normally, only one reaction is used to determine the enzyme activity *in vitro*; namely, the ability of the enzyme to produce a negative super coil form of the plasmid from the relaxed circular DNA. Respectively, the substrate and the product can be separated and determined quantitatively using agarose gel electrophoresis.

The DNA gyrase from *E. coli*, which was used in this work, had high specific activity that enabled us to use these enzyme samples for testing the inhibitory activity of fluoroquinolones. First, levofloxacin (a left-rotating

isomer of ofloxacin) with *ee* of about 99% was studied using ofloxacin (racemic form) as a control. Ofloxacin is well-known to clinicians as a fluoroquinolone of the first generation that has been in use in practical therapy for more than 15 years [1–4].

Inhibition of DNA gyrase by the above fluoroquinolones are presented in Fig. 1. The IC₅₀ values calculated from the results of three independent experiments were 2.50 ± 0.14 µg/ml and 6.20 ± 0.17 µg/ml for levofloxacin and ofloxacin, respectively, and they are in general agreement with the published data [7–10]. Moreover, the IC₅₀ ratios for these substances indicate the stereospecificity of DNA gyrase. The IC₅₀ value for the racemate (ofloxacin) is approximately twice higher than that for the individual stereoisomer (levofloxacin), which is roughly equal to its content in the racemic mixture.

Since the IC₅₀ value is widely used to describe the efficiency of the inhibition, it can be used to control the quality of levofloxacin. Taking into account that only one isomer of ofloxacin efficiently inhibited the enzyme, one can also consider the IC₅₀ value as a criterion of drug purity. Hence, biological activity, as well as chemical purity and the *ee* value, is considered to be an important characteristic of the quality of levofloxacin.

The structural formulas of levofloxacin, the key intermediates and semi-products of its pilot-scale synthesis performed in the Postovsky Institute of Organic Synthesis, UB RAS, are presented in Table 1.

All 19 samples of the levofloxacin taken from the pilot batch had close IC₅₀ values (2.4–2.8 µg/ml); i.e., they are in close correlation, since the error of the methods used is about 20%, and they are in agreement with the data published for the sample of levofloxacin of 99%

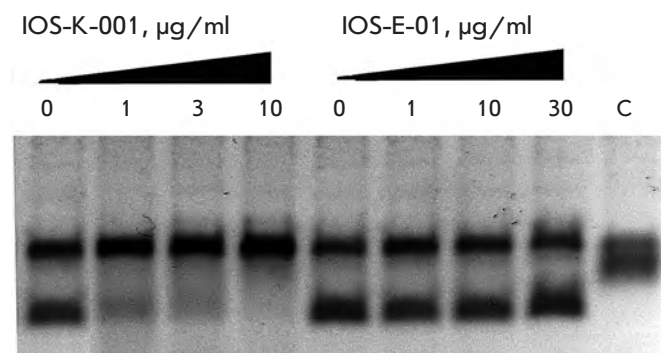
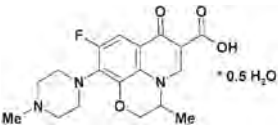
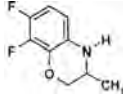
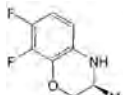
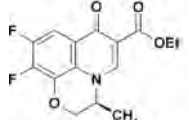
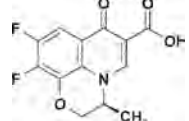


Fig. 2. Inhibition of DNA gyrase by IOS-K-001 and IOS-E-01. Figures specify the concentrations of inhibitors in the reaction mixtures. C – control (plasmid without the enzyme). Reaction conditions are described under “Experimental.”

Table 1. Structural formulas of levofloxacin, intermediates, and semi-products of its synthesis

Structural formula	Substance	Type of the substance	Code
	Levofloxacin (3 <i>S</i>)-9-Fluoro-3-methyl-10-(4-methyl piperazine-1-yl)-7-oxo-2,3-dihydro-7H-pyrido[1,2,3- <i>d,e</i>]-benzoxazine-6-carboxylic acid hemihydrate	Substance	IOS-001 – IOS-019
	(<i>R,S</i>)-7,8-Difluoro-3-methyl-2,3-dihydro-4H-benzo[<i>b</i>][1,4]-oxazine	Intermediate	IOS-RS-01, IOS-RS-02
	(3 <i>S</i>)-2,3-Dihydro-3-methyl-7,8-difluoro-1,4-benzoxazine	Intermediate	IOS-S-01, IOS-S-02
	Ethyl ester of (3 <i>S</i>)-(-)-9,10-difluoro-3-methyl-7-oxo-2,3-dihydro-7H-pyrido[1,2,3- <i>d,e</i>][1,4]-benzoxazine-6-carboxylic acid	Semi-product	IOS-E-01, IOS-E-02
	(3 <i>S</i>)-(-)-Difluoro-3-methyl-7-oxo-2,3-dihydro-7H-pyrido[1,2,3- <i>d,e</i>][1,4]-benzoxazine-6-carboxylic acid	Semi-product	IOS-K-001, IOS-K-002

purity. Among the key intermediates and semi-products of levofloxacin synthesis, racemic benzoxazine (**IOS-RS**), enantiomerically pure benzoxazine (**IOS-S**), and the ester (**IOS-E**) exhibited no significant activity. The activity of the semi-product **IOS-K** was found to be lower by an order of magnitude as compared with that of levofloxacin (*Fig. 2*).

The comparison of the structural formulas for the semi-products **IOS-E** and **IOS-K** reveals that these samples differ only by the ethoxycarbonyl group in **IOS-E**, instead of the free carboxyl group in **IOS-K**. It is important to note that this difference is crucial for the activity; i. e., the substance possessing the carboxyl group shows significant inhibitory activity, while the ethoxycarbonyl derivative is practically inactive. This observation indicates the significant impact of the charged carboxyl group in the inhibition. These data are in accordance with the known mechanism of the interaction of fluoroquinolones with DNA gyrase and should be taken into account when designing novel and more effective inhibitors of the enzyme.

In this paper, the ability of several new fluoroquinolone derivatives and fluorine-containing heterocycles to inhibit DNA gyrase was also investigated. These substances were synthesized in the Postovsky Institute of Organic Synthesis, UB RAS. The results of the experiments demonstrated that the majority of the studied compounds are inactive as depicted in *Table 2*. The

only exceptions is fluoroquinolone **EV-465**, the activity of which is lower than the activity of levofloxacin by approximately for two orders of magnitude and the known compounds from the fluoroquinolone group, i.e. **IOS-NORFL_01** (norfloxacin) and **IOS-PEFL_02** (pefloxacin) (*Figs. 3, 4*).

The compound **IOS-NORFL_01** turned out to be a poor inhibitor, while substance **IOS-PEFL_02** showed moderate activity, which was significantly lower than the activity of levofloxacin. It is important to note that these compounds differ only by the presence of an ad-

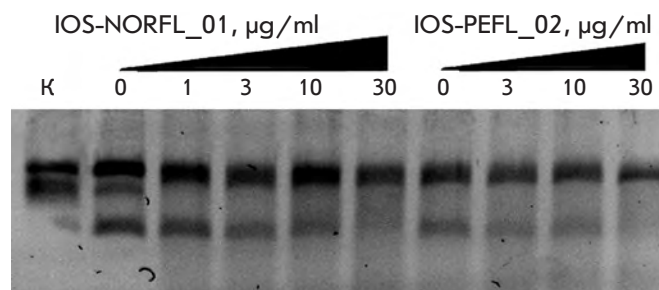


Fig. 3. Inhibition of DNA-gyrase by norfloxacin **IOS-NORFL_01** and pefloxacin **IOS-PEFL_02**. Figures specify the concentrations of inhibitors in the reaction mixtures. C – control (plasmid without the enzyme). Reaction conditions are described under “Experimental.”

Table 2. Inhibition activity of a series of fluoroquinolones and fluorine-containing heterocycles towards DNA gyrase

CODE/ I_{50} $\mu\text{g/ml}$	Structural formula	CODE/ I_{50} $\mu\text{g/ml}$	Structural formula
EV-465 >30		EV-X149 Inactive	
EV-591 Inactive		EV-T150-C Inactive	
EV-452-D Inactive		EV-T156 Inactive	
EV-313-D Inactive		EV-T143-B Inactive	
EV-572 Inactive		EV-N51-B Inactive	
EV-X58-A Inactive		EV-N119-2 Inactive	
IOS-NORFL_01 >11		IOS-PEFL_02 2.8	

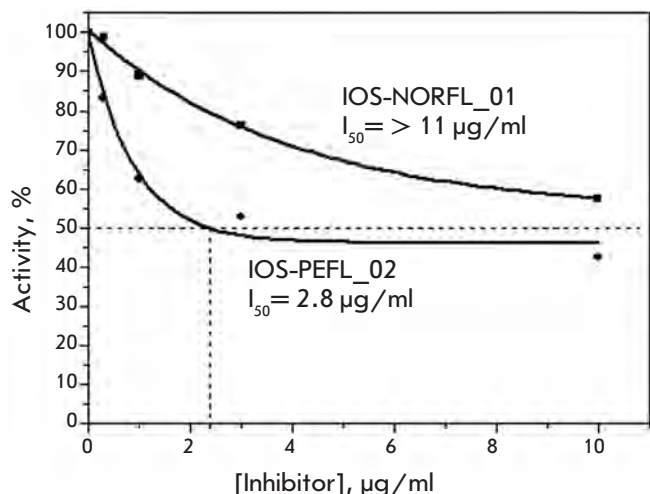


Fig. 4. Determination of the I_{50} value for the compounds **IOS-NORFL_01** and **IOS-PEFL_02** (from the data shown in Fig. 3). The I_{50} value corresponds to the point at which dash lines intersect the X-axis.

ditional methyl group in the piperazine ring of **IOS-PEFL_02**. The introduction of the methyl group results in an increase in the efficiency of the inhibition by approximately an order of magnitude, and this observation is of importance for the future design of novel biologically active fluoroquinolones.

The data obtained confirm that the degree of inhibition of bacterial DNA gyrase by levofloxacin and other fluoroquinolones is an important addition to physico-chemical methods, when the quality of the synthesized drugs is controlled. Using this method, the quality of 19 samples from the pilot batch of levofloxacin was assessed, along with eight intermediates and semi-products, as well as 14 new fluoroquinolone derivatives and their analogs.

Structure-activity relationship data outlined the importance of the carboxyl group in the **IOS-K** structure, the etherification of which leads to the loss of the inhibitory activity, and the N-methyl group in compound **IOS-PEFL**, which is also essential for the activity. The data obtained should be considered during the design of novel drugs based on fluorine-containing heterocycles. ●

The authors would like to thank K.V. Severinov and I.S. Shkundina (Institute of Molecular Genetics, Russian Academy of Sciences) for providing plasmids GyrA-pET19 and GyrB-pET19m.

This work was supported by the Federal Target Scientific and Technical Program "Research and Development in Priority Areas of Science and Technology for 2007–2013" (Government Contract № 02.522.12.2011).

REFERENCES

- The New Generation of Quinolones. / Eds Siporin C., Heifetz C.L., Domagala J.M. 1990. 422 p.
- Shen L.L. Quinolone Antibacterial Agents. Washington: American Soc. Microbiol., 1993. 344 p.
- Quinolone Antimicrobial Agents. / Eds Hooper D.S., Wolfson J.S. 1993.
- Padeyskaya E.N., Yakovlev V.P. // Fluoroquinolones Moscow: Bioinform, 1995. 208 p.
- Mokrushina G.A., Charushin V.N., Chupakhin O.N. // Pharmaceutical Chemistry Journal, 1995. № 1. P. 5–19.
- Ball P. The Quinolones. / Ed. Andriole T.V. San Francisco: Acad. Press, 1998. P. 1–28.
- Mokrushina G.A., Nosova E.N., Lipunova G.N., Charushin V.N. // Russian Journal of Organic Chemistry 1999. V. 35. № 10. P. 1447–1462.
- Granik V.G. // Basic Medicinal Chemistry Moscow: Vuzovskaya Kniga, 2001.
- Furin G.G. // Fluorine-containing Heterocyclic compounds: Synthesis and Applications Novosibirsk: Nauka, 2001.
- Mokrushin V.P., Vavilov G.A. // Principles of the Chemistry and Technology of bioorganic and synthetic medical preparations. Ekaterinburg: UGTU–UPI, 2004.
- Nosova E.V., Mochulskaya N.N., Kotovskaya S.K., Lipunova G.N., Charushin V.N. // Heteroatom. Chemistry. 2006. V. 17. № 6. P. 579–586
- Yakovlev V.P. Yakovlev S.V. // Infections and Antimicrobial Therapy 2004. V. 6. № 4. (http://old.consilium-medicum.com/media/infektion/04_04/108.shtml)
- Hayakawa I, Atarashi S, Yokohama S, Imamura M, Sakano K, Furukawa M. // Antimicrob. Agents Chemother. 1986. V. 29. №1. P. 163–164.
- Krasnov V.P., Levit G.L., Korolyova M.A., Kodess M.I., Chupakhin O.N., Kim M.H., Lee H.S., Park Y.J., Kim K.-C. // Tetrahedron: Asymmetry, 1999. V. 10. P. 2691–2702.
- Japanese Patent JP 2000178265. Production of (S)-benzoxazine derivative and racemization of (R)-benzoxazine derivative. / Chupakhin O.N., Krasnov V.P., Levit G.L., Charushin V.N., Korolyova M.A., Tzoi E.V., Lee H.S., Park Y.J., Kim M.H., Kim K.Ch.; publication date 27.06.2000 (Chem. Abstr., 2000. V. 133. P. 43530).
- Krasnov V.P., Levit G.L., Bukrina I.M., Andreeva I.N., Sadretdinova L.Sh., Korolyova M.A., Kodess M.I., Charushin V.N., Chupakhin O.N. // Tetrahedron: Asymmetry, 2003. V. 14. P. 1985–1988.
- Potemkin V.A., Krasnov V.P., Levit G.L., Bartashevich E.V., Andreeva I.N., Kuzminsky M.B., Anikin N.A., Charushin V.N., Chupakhin O.N. // Mendeleev Comm. 2004. P. 69–71.
- Krasnov V.P., Levit G.L., Kodess M.I., Charushin V.N., Chupakhin O.N. // Tetrahedron: Asymmetry. 2004. V. 15. № 5. P. 859–862.
- Gruzdev D.A., Levit G.L., Krasnov V.P., Chulakov E.N., Sadretdinova L.Sh., Grishakov A.N., Ezhikova M.A., Kodess M.I., Charushin V.N. // Tetrahedron: Asymmetry. 2010. V. 21. P. 936–942.
- Levit G.L., Gruzdev D.A., Krasnov V.P., Chulakov E.N., Sadretdinova L.Sh., Ezhikova M.A., Kodess M.I., Charushin V.N. // Tetrahedron: Asymmetry. 2011. V. 22. P. 185–189.

The Fate of the Nucleolus during Mitosis: Comparative Analysis of Localization of Some Forms of Pre-rRNA by Fluorescent *in Situ* Hybridization in NIH/3T3 Mouse Fibroblasts

K.V. Shishova, O.O. Zharskaya, O.V. Zatssepina

Shemyakin and Ovchinnikov Institute of Bioorganic Chemistry, Russian Academy of Sciences

*E-mail: kseniya.shishova@inbox.ru

Received 10.06.2011

Copyright © 2011 Park-media, Ltd. This is an open access article distributed under the Creative Commons Attribution License, which permits unrestricted use, distribution, and reproduction in any medium, provided the original work is properly cited.

ABSTRACT Nucleolus is the major structural domain of the cell nucleus, which in addition to proteins contains ribosomal RNA (rRNA) at different stages of maturation (or pre-rRNA). In mammals, the onset of mitosis is accompanied by the inhibition of rRNA synthesis, nucleolus disassembly, and the migration of pre-rRNA to the cytoplasm. However, the precise role of cytoplasmic pre-rRNA in mitosis remains unclear, and no comparative analysis of its different forms at consequent mitotic stages has thus far been performed. The focus of this research was the study of the localization of pre-rRNA in mitotic NIH/3T3 mouse fibroblasts by fluorescent *in situ* hybridization (FISH) with probes to several regions of mouse primary 47S pre-rRNA transcripts and by confocal laser microscopy. The results reveal that all types of pre-rRNA appear in the cytoplasm at the beginning of mitosis, following the breakdown of the nucleolus and nuclear envelope. However, not all pre-rRNA are transported by chromosomes from maternal cells into daughter cells. At the end of mitosis, all types of pre-rRNA and 28S rRNA can be visualized in nucleolus-derived foci (NDF), structures containing many proteins of mature nucleoli the appearance of which indicates the commencement of nucleologenesis. However, early NDF are enriched in less processed pre-rRNA, whereas late NDF contain predominantly 28S rRNA. Altogether, the results of this study strengthen the hypotheses that postulate that different forms of pre-rRNA may play various roles in mitosis, and that NDF can be involved in the maturation of pre-rRNA, remaining preserved in the cytoplasm of dividing cells.

KEYWORDS nucleolus; mitosis; nucleolus-derived foci (NDF); NIH/3T3 mouse fibroblasts; fluorescence *in situ* hybridization (FISH).

ABBREVIATIONS rRNA – ribosomal RNA; 47S pre-rRNA – 47S precursor of rRNA; NDF – nucleolus-derived foci; PNB – prenucleolar bodies; 5'ETS, 3'ETS – 5'- and 3'-external transcribed spacers; ITS1, ITS2 – internal transcribed spacer 1 and 2; bp – base pairs; snoRNA – small nucleolar RNA; DAPI – 4',6-diamidino-2-phenylindole; FISH – fluorescent *in situ* hybridization.

INTRODUCTION

Nucleolus is the major structural domain of the cell nucleus, whereby the transcription of ribosomal genes (rDNA), the processing (maturation) of primary transcripts (pre-rRNA), and the assembly of the ribosomal particles occur [1, 2]. In mammalian cells, three types of cytoplasmic rRNA (18S, 5.8S, and 28S) are synthesized in nucleoli in the form of the common precursor 46S pre-rRNA. Maturation of 47S pre-rRNA into rRNA is a complex multistage process which includes the excision of several spacer fragments transcribed within 47S pre-rRNA (5'-external transcribed spacer (5'ETS), as

well as the first (ITS1) and the second (ITS2) internal transcribed spacers) in addition to the chemical modifications of 18S, 5.8S, and 28S rRNAs (*Fig. 1*). It is known that the maturation time of 18S rRNA and 28S rRNA is 20 and 40 min, respectively. Consequently, in addition to primary rRNA transcripts, partially processed pre-rRNA of varying size are also found in the fraction of isolated nucleoli [3]. In mice, a 650 bp fragment located at the 5'-terminus of ETS is the shortest lived one, its half-life being less than 2 min [4]. According to the existing notion, the excision of internal spacer in mammals begins following completion of the synthesis and

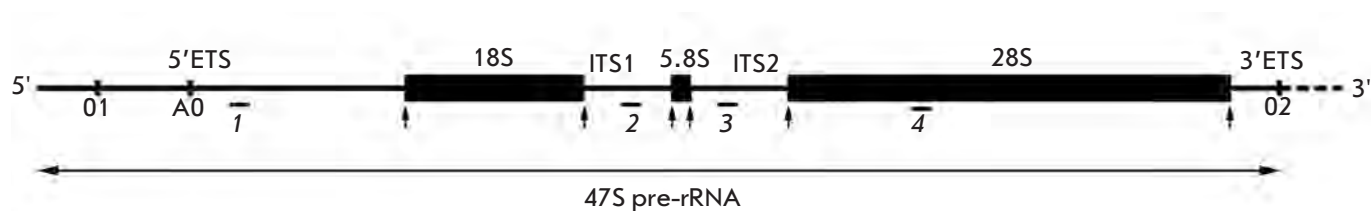


Fig. 1. Structure of primary mouse transcript (47S pre-rRNA) and location of probes for *in situ* hybridization. 5'ETS – 5'-external transcribed spacer; ITS1 – internal transcribed spacer 1; ITS2 – internal transcribed spacer 2; 3'-ETS – 3'-external transcribed spacer. 18S, 5.8S, 28S – coding regions of pre-rRNA. The sequence location of probes for *in situ* hybridization is shown below the 47S pre-rRNA diagram: for 5'ETS +2251/+2280 (probe 1); for ITS1 +6391/+6420 (probe 2); for ITS2 – +7471/7500 (probe 3), for 28S rRNA – +9571/9600 (probe 4). 01, 02, A0 – endonucleolytic cleavage sites in pre-rRNA.

detachment of the primary pre-rRNA transcript from the matrix rRNA. The half-life of the internal spacers in mammals is at least 30 min [3–5].

It is well known that mitosis in higher eukaryotes is accompanied by the termination of pre-rRNA synthesis, the disassembly of the nucleolus, and the migration of the major nucleolar components, proteins and rRNA, into the cytoplasm [6–10].

The methods of biochemical [11, 12] and cytological analysis [13] were used to demonstrate that pre-rRNA synthesized before mitosis remains preserved in the cellular cytoplasm up to its completion. However, the role of this stable pre-rRNA in mitosis has yet to be elucidated. The features of localization of different pre-rRNA forms in mitosis have not been sufficiently studied, although research in this area will shed light on their role in the recovery of nucleoli during the latter stages of mitosis.

The recovery of nucleoli during mitotic cell division begins immediately after the chromosomes separate and move to the mitotic spindle poles and numerous discrete bodies (of 0.2–2.0 μm diameter), and the so-called nucleolus-derived foci (NDF) emerge in the cytoplasm. Currently, NDF are reported to include numerous proteins of mature nucleoli participating in pre-rRNA processing (B23/nucleophosmin, C23/nucleolin, fibrillarin, etc.), U3 and U14 small nucleolar RNA (snoRNA), as well as mature 18S and 28S rRNA). The methods of immunocytochemistry [13, 14] and the expression of protein markers of NDF fused with fluorescent proteins were used in order to demonstrate the gradual decrease in the amount of NDF-containing proteins of early pre-rRNA processing (e.g., fibrillarin) following the completion of mitosis. On the contrary, the proteins participating in the late stages of pre-rRNA processing (e.g., B23/nucleophosmin) are retained among NDF up to the G1 phase of the subsequent cell cycle [15]. The presence of the proteins and snoRNAs,

which are required for pre-rRNA processing in interphase nucleoli, among NDF allows one to reasonably assume that at least some of the stages of maturation of pre-rRNA (which remains preserved in cells during mitosis) can take place in NDF. However, at the time of writing no experiments have been performed to verify this assumption. The presence of different forms of pre-rRNA in early and late NDF has been insufficiently studied.

The major aim of this study was to perform a comparative analysis of the localization of different forms (intermediates) of partially processed pre-rRNA and 28S rRNA at sequential phases of mitosis in NIH/3T3 mouse fibroblasts via fluorescent *in situ* hybridization and confocal laser microscopy.

EXPERIMENTAL

Cell culture

NIH/3T3 mouse fibroblasts were obtained from the Russian Cell Culture Collection of the Institute of Cytology of the Russian Academy of Sciences; the cells were free of micoplasma. The cells were cultured in a DMEM medium (PanEco, Russia) containing 10% fetal bovine serum (HyClone, USA), 2 mM *L*-glutamine, penicillin and streptomycin (250 U of each antibiotic) at 37°C and 5% CO₂, with re-culturing twice a week.

Fluorescent *in situ* hybridization

In this study, we used oligonucleotide probes labelled by biotin at the 5'-terminus, which were capable of specific detection of the following fragments of mouse 47S pre-rRNA: the core fragment of the 5'-external transcribed spacer (5'ETS, probe 1) – 5'aga gag aga ccg atg ccg aca cac cga tgc (+2251/+2280); the first internal transcribed spacer (ITS1, probe 2) – 5'aaa cct ccg cgc cgg aac gcg aca gct agg (+6391/+6420); the second internal transcribed spacer (ITS2, probe 3) – 5'cag

aca acc gca ggc gac cga ccg gcc (+7471/+7500); and a 28S rRNA fragment (probe 4) 5'gag gga acc agc tac tag atg gtt cga tta (+9571/+9600). The probes were synthesized by Sintol (Russia); the probe concentration in stock solutions was approximately equal to 2 µg/µl. The localization of probes with respect to the mouse 47S pre-rRNA is shown in *Fig. 1*. As can be seen in *Fig. 1*, probe 1 detected the less processed pre-rRNA form; probes 2 and 3 could hybridize both with longer or shorter (i.e., processed to a larger extent) forms of pre-rRNA; probe 4 mainly detected the mature 28S rRNA, but it could also hybridize with the immature pre-rRNA as well.

The cells grown on coverslips were washed with a phosphate saline buffer (PSB, 140 mM NaCl, 2.7 mM KCl, 1.5 mM KH₂PO₄, and 8.1 mM Na₂HPO₄, pH 7.2–7.4), followed by subsequent fixation with a 4% formalin solution (MP Biomedicals, Inc., France) in PBS for 30 min at room temperature. The cells were then washed with PBS (3 × 5 min), treated with 0.5% Triton X-100 (10 min at 4°C), washed with PBS, followed by a two-fold washing with a standard saline buffer (2×SSC, 0.3 M NaCl, 0.03 M Na₃C₆H₅O₇, pH 7.0) for 5 min.

The hybridization mixture was composed of 50% of deionized formamide (Sigma, USA), 10% of dextran sulphate (Loba Chemie, Fischamend, Austria), 5% of 20×SSC (3 M NaCl, 0.3 M Na₃C₆H₅O₇, pH 7.0), and 8 ng/µl oligo samples. Hybridization was performed in a wet chamber for 16 h at 42°C. The cells were then sequentially washed with 50% formamide (Panreac, Spain) in 2×SSC (3 × 10 min) at 42°C, 2×SSC at 42°C (10 min), and 2×SSC (1 min) at room temperature. The hybridization sites were detected using rhodamine-conjugated avidin (Roche, Switzerland) after 1 : 200 dilution in the buffer containing 4×SSC (0.06 M NaCl, 0.06 M Na₃C₆H₅O₇, pH 7.0) for 1 h at room temperature. The cells were then washed with 4×SSC (10 min) and PBS (3 × 10 min). Chromatin and chromosomes were stained with a DAPI dye (1 µg/ml, 4'-6-diamidino-2'-phenylindole, Sigma) for 10 min. The cells were embedded in Mowiol (Calbiochem, USA) and examined on an LSM510 DuoScanMETA confocal laser scanning microscope (Carl Zeiss, Germany) equipped with argon (Ar) and helium-neon (He-Ne) lasers, using a Plan-Apochromat 63×/1.40 numerical aperture immersion lens. In order to obtain the control sample, the fixed cells were treated with RNase A (200 µg/ml) in PBS for 30 min at 37°C according to the previously described procedure [16]. The treatment with RNase A resulted in the complete blockage of the emergence of fluorescent signals in nucleoli during interphase and of the mitotic signals after FISH was performed (not shown). A minimum of 20 cells for the control and experimental samples were analyzed for each stage.

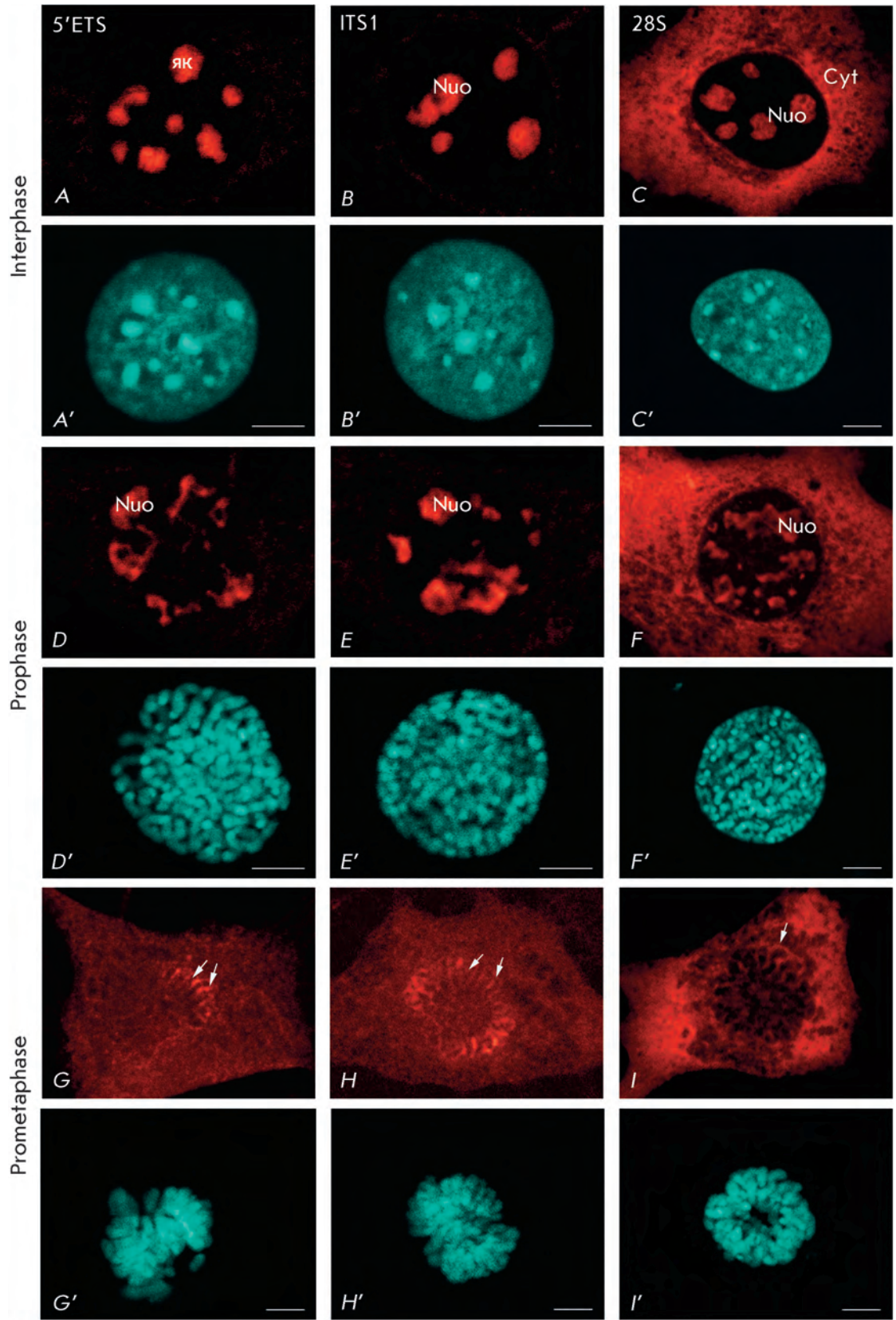
RESULTS AND DISCUSSION

The localization of pre-rRNA and 28S rRNA in interphase cells NIH/3T3 is shown in *Fig. 3*. It is clear that all pre-rRNA forms were detected in nucleoli only (*Fig. 2A,B*), whereas 28S rRNA was detected both in the nucleolus and the cytoplasm of mature ribosomes (*Fig. 2C*). These observations are in close agreement with data published by other authors [5, 7, 14]; however, the hybridization signals in this case were brighter and more distinct. We believe that this can be accounted for both by the efficiency of the labelling of oligonucleotide probes and by the conditions of the FISH experiment, including the parameters of the washing in the buffer, which enabled the removal of the unbound probes, thereby reducing the background (nonspecific) fluorescence.

At the initial mitotic stage (during prophase), the cells were identified based on the presence of long condensed chromosomes, which were distinctly detected by the DAPI dye in nuclei (*Fig. 2G'–E'*). It was known that all the proteins participating in pre-rRNA processing migrate from the nucleoli into the nucleus during prophase, and that they are diffusely arranged between chromosomes [9, 16–18]. Among these proteins are the following: fibrillarin (the early pre-rRNA processing factor) [19], B23/nucleophosmin (the ribosome assembly factor) [20], and SURF-6 (the late pre-rRNA processing factor) [16, 17]. The results obtained in this study show that the immature rRNAs detected by probes to 5'ETS (*Fig. 2D*), ITS1 (*Fig. 2E*), ITS2 (not shown), and 28S rRNA (*Fig. 2F*) were mostly located in the nucleolar area and were quasi absent in the nucleus during prophase, as opposed to proteins. No differences were detected in the localization of the pre-rRNAs revealed by probes to ITS1 and ITS2. The differences in the behavior of the pre-rRNAs and proteins participating in its maturation during nucleolar disassembly have yet to be described. It is reasonable to assume that these differences indicate the partial disassembly of pre-rRNA–protein complexes, which accompanies the termination of the processing of the pre-rRNA that was synthesized prior to mitosis, or in the very beginning of this process.

Nuclear envelope disassembly relates to the progression of cells from prophase into metaphase. It is marked by additional condensation of chromosomes and the alteration of the contour of the area occupied by them. It is known that nucleolar disassembly is terminated and most nucleolar proteins migrate to the cytoplasm during prometaphase [15]. According to the results obtained in this study, all pre-rRNA forms can be distinctly detected in the cytoplasm and on the chromosome surface during prometaphase (*Fig. 2G,H*). However, the fluorescent signals detected by a probe

Fig. 2. Pre-rRNA location in NIH/3T3 cells detected by fluorescent *in situ* hybridization with probes to 5'ETS (probe 1) (A, D, G), ITS1 (probe 2) (B, E, H), and 28S rRNA (probe 4) (C, F, I) in interphase (A–C), prophase (D–F) and prometaphase (G–I). (A–I) – pre-rRNA and 28S location; (A'–I') – chromatin staining with DAPI in interphase and chromosomes in mitosis. nuo – nucleoli; cyt – cytoplasm; arrows – perichromosomal material. Bars, 5 μ m.



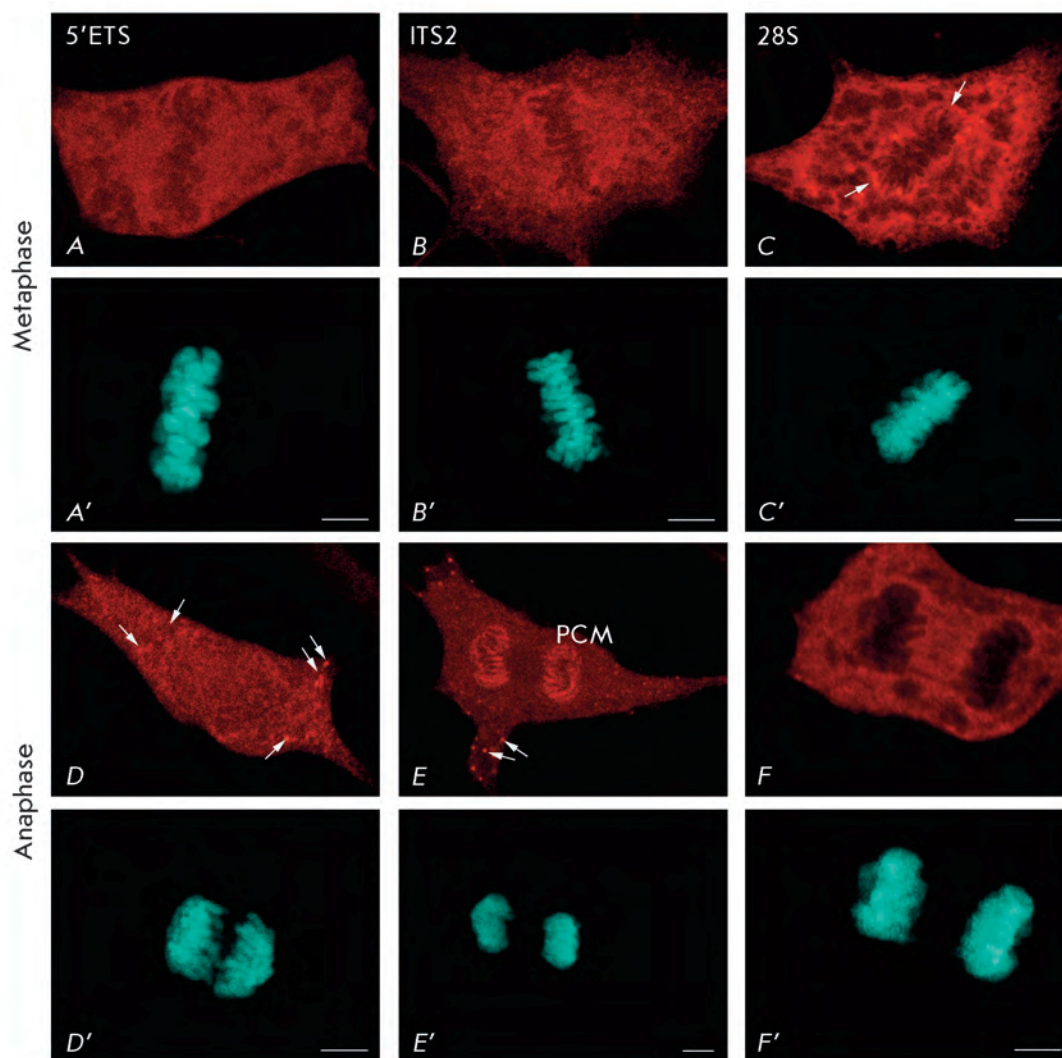


Fig. 3. Pre-rRNA location in NIH/3T3 cells detected by FISH with probes to 5'ETS (probe 1) (A, D, G), ITS2 (probe 3) (B, E, H), and 28S rRNA (probe 4) (C, F, I) in metaphase (A–C) and anaphase (D–F). (A–F) – pre-rRNA and 28S location; (A'–F') – chromatin and chromosome staining with DAPI. PCM – peripheral chromosomal material; arrows (D, E) – nucleoli-derived foci (NDF); arrows (C) – PCM. Bars, 5 μ m.

to 5'ETS were present on the surface of only a number of chromosomes (Fig. 2G), whereas the signals detected by the probes to ITS1 (Fig. 2H) and ITS2 (not shown) could be seen on the surface of all chromosomes. An identical pattern was also observed during the subsequent stage of mitosis (metaphase), when the chromosomes formed a characteristic plate at the center of the cell (Fig. 3A–B'). However, the best defined distinctions in the localization of different pre-rRNA forms can be observed during anaphase, when chromosomes separate and move to the spindle poles (Fig. 3D–F'). It is clear from the comparison of Figs. 3D and 3E that the probe to ITS2 brightly stains the chromosome surface, whereas almost no hybridization occurs between the probe to 5'-ETS and the chromosome surface. These observations enable one to conclude that the less mature pre-rRNA detected by the probe to 5'-ETS was not transported by chromosomes from maternal cells

into daughter cells, as opposed to the more mature (short) pre-rRNA forms that were detected by the probes to ITS1 and ITS2.

Nucleolar disassembly during prophase causes the migration of 28S rRNA, along with the processed pre-rRNA forms, into the cytoplasm (Fig. 2F). Therefore, starting with the early prometaphase, the FISH method does not allow one to distinguish between 28S rRNA of nucleolar and cytoplasmic origin. During the late prometaphase (Fig. 2I), metaphase (Fig. 3C), and anaphase (Fig. 3F), the FISH signals detected by the probe to 28S rRNA were visualized in the cytoplasm. Moreover, more intense signals in many cells could be seen on the chromosome surface in the form of perichromosomal material (Fig. 3C, F). The presence of perichromosomal material detected by the probe to 28S rRNA can be accounted for by the presence of either mature pre-rRNA or immature 28S rRNA. This assumption agrees

with the data of an *in situ* analysis of mitotic chromosomes using electron microscopy. According to these data, RNP particles of a size corresponding to that of ribosomes are located on the chromosome surface. These particles are one of the major structural components of the so-called perichromosomal material (or perichromosomal layer) [21]. It has been known that the nucleolar proteins that constitute the perichromosomal material are used to promote the formation of the nucleoli of daughter cells. On the contrary, protein material, not being a component of the perichromosomal layer, is an unlikely participant in this process [22–24]. One can assume that a similar pattern exists for different forms of pre-rRNA; i.e., less processed pre-rRNA forms (such as those detected by the probe to 5'-ETS) do not participate in nucleogenesis.

According to current theories, one of the earliest stages in nucleolar recovery during mitosis in mammals corresponds to the formation of NDF, cytoplasmic bodies, with the proteins participating in rRNA processing as its major component [18]. However, several rRNA forms, including those of mature rRNA and pre-rRNA, have been reportedly detected within NDF, both in animal and plant cells [7, 13, 15]. The results obtained in this study unequivocally attest to the fact that mouse NDF also contain pre-rRNAs, although the labelling of NDF with the probes to various pre-rRNA forms differs for the various stages of mitosis. Early NDF (i.e., NDF during anaphase (Fig. 3D'–F') and at the beginning of telophase (Fig. 4A')) are mostly labelled by the probe to 5'-ETS (Figs. 3D,E; 4A), although they can hardly be labelled by the probe to 28S rRNA (Figs. 3E; 4B). On the contrary, during the late telophase and G1 period (Fig. 4C', D'), NDF are detected by the probe to 28S rRNA (Fig. 4G) but cannot be labelled by the probes to 5'-ETS (Fig. 4C), ITS1, and ITS2 (not shown). It is noteworthy that the late NDF detected by the probe to 28S rRNA (Fig. 4D) are larger than those that can be detected at the same stage of mitosis by the probe to 5'-ETS (Fig. 4C).

Based on these observations, a conclusion can be made that the composition of NDF is gradually altered during the latter stages of mitosis: the less processed pre-rRNAs disappear, while the more mature rRNAs remain preserved or are even accumulated during these stages. These observations imply the participation of NDF in the processing of pre-rRNA, which remains preserved during mitosis. It should be noted that NDF contain no rDNA; they are therefore incapable of synthesizing 47S pre-rRNA [15]. NDF are structures with a shorter lifespan in comparison with nucleoli. Therefore, if pre-rRNA processing indeed occurs within them, it occurs during a limited time period, coinciding with the termination of mitosis. The biological meaning of this phenomenon may be associated with the rational use of

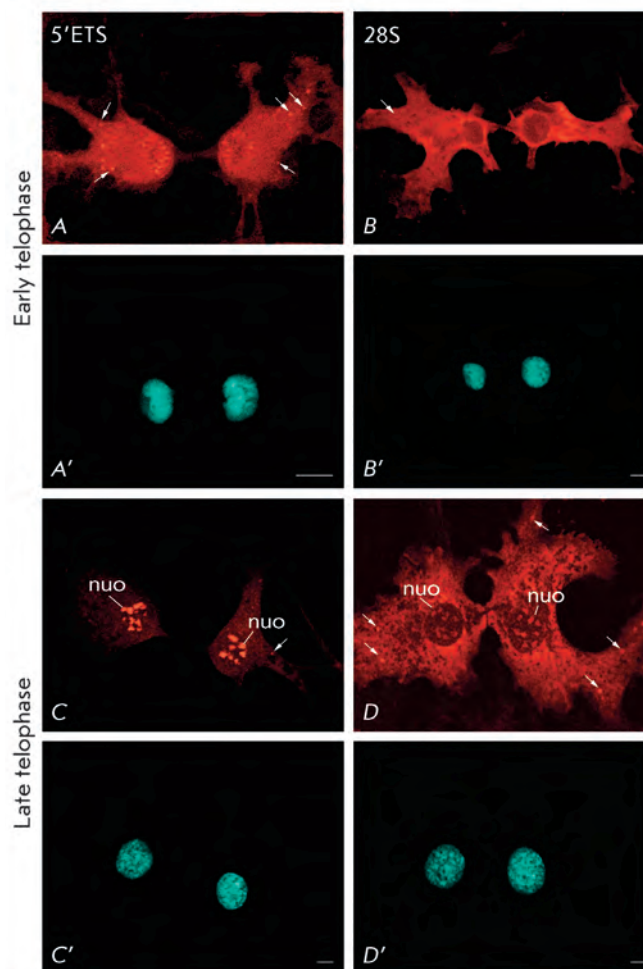


Fig. 4. Pre-rRNA location in NIH/3T3 cells detected by FISH with probes to 5'-ETS (probe 1) (A, C) and 28S rRNA (probe 4) (B, D) in early telophase (A, B) and late telophase (C, D). (A–D) – pre-rRNA and 28S location; (A'–D') – chromatin and chromosome staining with DAPI. nuo – nucleoli; arrows – nucleoli-derived foci (NDF). Bars, 10 μ m.

pre-rRNA synthesized prior to mitosis and in providing the cell with additional ribosomes at the active growth phase after mitosis.

Pre-nucleolar bodies (PNB) also participate in nucleogenesis at the latter stages of mitosis [15]. Similar to NDF, pre-nucleolar bodies are discrete formations up to 1 μ m in size, which contain nucleolar rRNA processing factors. Unlike NDF, these bodies are generated not in the cytoplasm but in the daughter cell nuclei [25, 26]. Proteins are the major markers of these bodies, and the question of the presence of different pre-rRNA forms and mature rRNA in pre-nucleolar bodies remains poorly studied. Nevertheless, it has been shown that pre-

nucleolar bodies in HeLa and CMT3 (green monkey) cells, as well as those in plant cells (*Pisum sativum* and *Allium cepa*), may contain 32S pre-rRNA and mature 28S rRNA, although the presence of 18S rRNA in pre-nucleolar bodies is not obvious (Table and References in [15]). Our observations is evidence that in NIH/3T3 cells pre-nucleolar bodies are hybridized with the same probes that hybridize with NDF, although the early PNB are hard to detect with the probe to 28S rRNA (Fig. 4B, B'). In other words, they are devoid of this form of rRNA. However, the rRNA compositions in PNBs at different stages of their existence require a special investigation. This issue could only be resolved at the cytological level, when approaches that enable one to combine high-sensitivity *in situ* hybridization with the probes to various pre-rRNA sequences, and the detection of the marker proteins of pre-nucleolar bodies, have been developed.

CONCLUSIONS

A procedure for high-sensitivity detection of different forms of pre-rRNA and mature 28S rRNA in mitotic

NIH/3T3 mouse fibroblasts using biotin-labelled oligonucleotide probes was proposed. It was shown that pre-rRNA is preserved in disassembling nucleoli for a longer period of time than the proteins participating in pre-rRNA processing and that it does not disintegrate during mitosis. Only a portion of the forms of pre-rRNA were transported by chromosomes from maternal cells into daughter cells. Pre-rRNA and 28S rRNA were detected within nucleolar cytoplasmic derivatives (NDF) immediately after their formation during anaphase or early telophase. However, the disappearance of immature pre-rRNA from the NDF fabric occurred at an earlier stage than that of 28S rRNA. This observation argues for the fact that NDF participates in the processing of pre-rRNA, which is preserved in the cell cytoplasm during mitosis. ●

This study was supported by the Ministry of Education and Science of the Russian Federation (Government Contracts № 14.740.11.0121 and 14.740.11.0925).

REFERENCES

1. Sirri V., Urcuqui-Inchima S., Roussel P., Hernandez-Verdun D. // *Histochem. Cell. Biol.* 2008. V. 129. P. 13–31.
2. Henras A.K., Soudet J., G erus M., Lebaron S., Caizergues-Ferrer M., Mougin A., Henry Y. // *Cell. Mol. Life Sci.* 2008. V. 65. P. 2334–2359.
3. Wang M., Pestov D.G. // *Nucl. Acids Res.* 2011. V. 39. P. 1811–1822.
4. Kent T., Lapik Y.R., Pestov D.G. // *RNA.* 2009. V. 15. P. 14–20.
5. Lazdins I.B., Delannoy M., Sollner-Webb B. // *Chromosoma.* 1997. V. 105. P. 481–495.
6. Gautier T., Dauphin-Villemant C., Andr e C., Masson C., Arnoult J., Hernandez-Verdun D. // *Exp. Cell Res.* 1992. V. 200. P. 5–15.
7. Dundr M., Misteli T., Olson M.O. // *J. Cell. Biol.* 2000. V. 150. P. 433–446.
8. Hernandez-Verdun D. // *The nucleolus.* N.Y.: Kluwer Acad./Plenum Publ., 2004. P. 41–57.
9. Leung A.K.L., Lamond A.I. // *Crit. Rev. Eukaryot. Gene Expr.* 2004. V. 13. P. 39–54.
10. DiMario P.J. // *Int Rev. Cytol.* 2004. V. 239. P. 99–178.
11. Pi nol-Roma S. // *Mol. Biol. Cell.* 1999. V. 10. P. 77–90.
12. Okuwaki M. // *J. Biochem.* 2008. V. 143. P. 441–448.
13. Dundr M., Olson M.O. // *Mol. Biol. Cell.* 1998. V. 9. P. 2407–2422.
14. Beven A.F., Lee R., Razaz M., Leader D.J., Brown J.W., Shaw P.J. // *J. Cell. Sci.* 1996. V. 109. P. 1241–1251.
15. Zharskaya O.O., Zatssepina O.V. // *Tsitologia.* 2007. V. 49 (5). P. 355–369.
16. Gurchenkov V.V., Polzikov M.A., Magoulas C., Romanova L.G., Zatssepina O.V. // *Bioorg. Khim.* 2006. V. 31. P. 1–8.
17. Magoulas C., Zatssepina O.V., Jordan P.W., Jordan E.G., Fried M. // *Eur. J. Cell. Biol.* 1998. V. 75. P. 174–183.
18. Angelier N., Tramier M., Louvet E. // *Mol. Biol. Cell.* 2005. V. 16. P. 2862–2871.
19. Turner A.J., Knox A.A., Prieto J. // *Mol. Cell. Biol.* 2009. V. 29. P. 3007–3017.
20. Huang N., Negi S., Szebeni A., Olson M.O.J. // *J. Biol. Chem.* 2005. V. 280. P. 5496–5502.
21. Chentsov Yu.S. // *Russ. J. Dev. Biol.* 2000. V. 31. P. 388–399.
22. Hernandez-Verdun D. // *Histochem. Cell. Biol.* 2006. V. 125. P. 127–137.
23. Hernandez-Verdun D. // *Histochem. Cell. Biol.* 2006a. V. 126. P. 135–148.
24. Olson M.O., Dundr M. // *Histochem. Cell. Biol.* 2005. V. 123. P. 203–216.
25. Raska I., Shaw P.J., Cmarko D. // *Int. Rev. Cytology.* 2006. V. 255. P. 177–235.
26. Hernandez-Verdun D. // *Nucleus.* 2011. V. 2. P. 189–194.

Effect of Sodium Chloride on Aggregation of Merocyanine 540 and Photosensitized Inactivation of *Staphylococcus aureus* and *Pseudomonas aeruginosa*

T.A. Shmigol¹, V.A. Bekhalo^{2*}, E.V. Sysolyatina², E.V. Nagurskaya², S.A. Ermolaeva², A.Ya. Potapenko¹

¹Pirogov Russian National Research Medical University

²Gamaleya Research Institute of Epidemiology and Microbiology, Ministry of Health and Social Development of the Russian Federation

*E-mail: bekhalo@gamaleya.org

Received 07.07.2011

Copyright © 2011 Park-media, Ltd. This is an open access article distributed under the Creative Commons Attribution License, which permits unrestricted use, distribution, and reproduction in any medium, provided the original work is properly cited.

ABSTRACT Merocyanine 540 (MC540) is used as a photosensitizer for the inactivation of microorganisms. The following is already known about MC540: firstly, MC540 exists in distilled water in both monomeric and dimeric forms, and the addition of salts into a MC540 solution leads to the formation of large aggregates that can be detected by the resonance light scattering technique. Secondly, singlet oxygen can only be photogenerated by MC540 monomers. In the present work, we studied the effect of MC540 in the aggregated state on the rate of photosensitized inactivation of *Staphylococcus aureus* and *Pseudomonas aeruginosa*. To this end, bacteria either in MC540-containing distilled water or in a 0.25 M sodium chloride aqueous solution also containing MC540 are irradiated (546 nm). The results show that, in the presence of salt, the aggregation of MC540 greatly increases the efficiency of the MC540-photosensitized inactivation of *P. aeruginosa* and *S. aureus*. In the presence of salt, the rates of *P. aeruginosa* and *S. aureus* inactivation increase by factors of 10 and 30, respectively, in comparison with the rate of inactivation observed in the case of distilled water. Our results suggest that a salt-induced photosensitization mechanism can switch from the singlet oxygen to the free-radical pathway.

KEYWORDS antimicrobial photodynamic therapy; merocyanine 540; *Staphylococcus aureus*; *Pseudomonas aeruginosa*.

ABBREVIATIONS CAC – critical aggregation concentration; MC540 – merocyanine 540; RLS – resonance light scattering; PS – photosensitizer; CFU – colony-forming unit.

INTRODUCTION

The search for effective methods of antibacterial protection has led to the development of antimicrobial photodynamic therapy. The photodynamic effect was first described by Raab in 1900, and the term “photodynamic reaction” was first introduced by Tappeiner in 1904 [1]. The photodynamic inactivation of bacteria occurs under the action of light in the presence of photosensitizers (FSs) and molecular oxygen. Through exposure to light, photosensitizers are activated, thereby producing free radicals or singlet oxygen, which are fatal to infectious agents.

MC540 is known to be capable of inactivating infectious agents [2–5]. This happens as a result of the occurrence of two types of photodynamic reactions: types I

and II. In type I reactions, a photosensitizer in the triplet-excited state reacts directly with a substrate, but it does not react with molecular oxygen. During reactions of this type, the electron (or hydrogen) is transferred from a photosensitizer molecule found in the triplet-excited state to a substrate found in the ground state. Depending on the reacting pair, both transfer from a substrate to a photosensitizer and *vice versa* are possible. Free radicals are produced as a result of such reactions; oxygen enters into the reaction at later stages, thereby leading to the photooxidation of the substrate [6].

In type II reactions, the primary reaction occurs between a photosensitizer in the triplet-excited state and molecular oxygen. This type of reaction causes the occurrence of an excited singlet oxygen or superoxide

radical anion. The main role in subsequent reactions is played by the singlet oxygen, which oxidizes a substrate. The detachment of an electron from the excited photosensitizer, accompanied by the formation of a superoxide anion, may also occur. In the subsequent reactions of substrate oxidation, only the superoxide anion and other active forms of oxygen participate [6].

In preliminary studies performed *in vitro*, MC540 aggregates were shown to photobleach faster than monomers and dimers [7, 8]. Resonance light scattering (RLS) is the most sensitive and selective method for studying aggregation processes in dyes. The principle of RLS lies in the drastic increase in Rayleigh light scattering in the region of the absorption band of aggregated dye molecules. The above-mentioned phenomenon is typical of strongly absorbing chromophores that form large aggregates in which exciton interaction between the π -electron systems of dye molecules occurs [9].

Herein, we describe the effect of sodium chloride on the aggregation of MC540, on the rate of its photobleaching, and on the photosensitized inactivation of *Staphylococcus aureus* and *Pseudomonas aeruginosa* bacteria.

EXPERIMENTAL

Reagents

Merocyanine 540 (Sigma, USA) and chemically pure NaCl (REAKHIM, Russia) were used. A stock solution of MC540 (10^{-3} M) in distilled water was prepared in the day of the experiment. Working solutions (25 μ M) were obtained by diluting the stock solution with water or with a 0.25 M NaCl solution.

Merocyanine 540 solutions and suspensions of microorganisms were irradiated with light generated by a DRSh-250 mercury quartz lamp (Zelenograd, Russia). Monochromatic light was obtained via a 546-nm glass filter (Russia).

The intensity of light was measured using an IM-1-2 photodiode (Russia) calibrated for 546 nm. The irradiation of MC540 solutions was performed in cells with a thickness of 1 cm under side lighting and continuous stirring with a magnetic stirrer at a temperature of 23°C.

The absorption spectra were measured using a Shimadzu UV-1601 PC spectrophotometer (Japan).

The resonance light scattering spectra were measured using a Shimadzu RF-1501 Spectrofluorimeter (Japan). The spectral measurements were performed using quartz cells with a thickness of 1 cm. The measured RLS spectra were corrected taking into account the effects of the inner optical filtering effect and the sensitivity of the instrument, in accordance with the procedure described in [10] by Tikhomirov *et al.*

Cell Cultures

In this work, we used *S. aureus* and *P. aeruginosa* clinical isolates of strains 78 (*Sa78*) and 104 (*Pa104*), respectively. The microorganisms were taken from the collection of the Gamaleya Research Institute of Epidemiology and Microbiology of the Ministry of Health and Social Development of the Russian Federation.

Preparation of Cell Suspension

S. aureus and *P. aeruginosa* were incubated in a brain heart infusion broth (Difco, USA) for 12 h at 37°C and then diluted in a phosphate-buffered saline solution to an optical density value (D_{600}) of 1, which corresponds to a concentration of 10^9 CFU/ml. The bacterial suspension (1 ml) was washed twice by centrifugation in sterile distilled water (7000 rot/min, 3 min) and then resuspended in 10 ml of sterile distilled water.

In order to obtain samples for irradiation, a 50 μ M solution of MC540 in distilled water was mixed with the bacterial suspension, which was prepared according to the aforementioned process, at a ratio of 1:1. The 25 μ M MC540 sample in a salt solution was prepared by mixing 100 μ M MC540, 1 M NaCl, and the bacterial suspension at a ratio of 1:1:2, respectively. Prior to irradiation, a MC540 solution with a final concentration of 25 μ M was incubated with cells for 10 min in the dark at room temperature. Following irradiation, the sample underwent a series of 10-fold dilutions in a GRM-1 agar medium (Obolensk, Russia) and was poured into Petri dishes. Both the treated and control samples were incubated in a thermostat at 37°C. The amount of grown colonies was calculated after 24 h. The bactericidal effect was determined as a ratio of the survived bacteria in the experimental to the control groups, respectively.

Kinetics of Photobleaching of MC540 and Photoinactivation of Bacteria

A kinetic analysis of the photobleaching of 25 μ M MC540 in the distilled water solution and the sodium chloride (0.25 M) solution was carried out for the initial range of the dose-dependence curve (at which decay of the photosensitizer has a mono exponential behavior) plotted in semilogarithmic coordinates. The photobleaching constant (m^2/kJ) was ascertained according to the following: $k = \ln(D/D_0)$, where D_0 and D are the optical densities at a wavelength of 518 nm in the initial moment of time and under irradiation at a dose of F (kJ/m^2), respectively.

A kinetic analysis of the photoinactivation of *P. aeruginosa* and *S. aureus* bacteria in a the 25 μ M MC540 distilled water and sodium chloride (0.25 M) solutions was performed for the initial segment of the dose-dependence curve constructed in semi-logarithmic co-

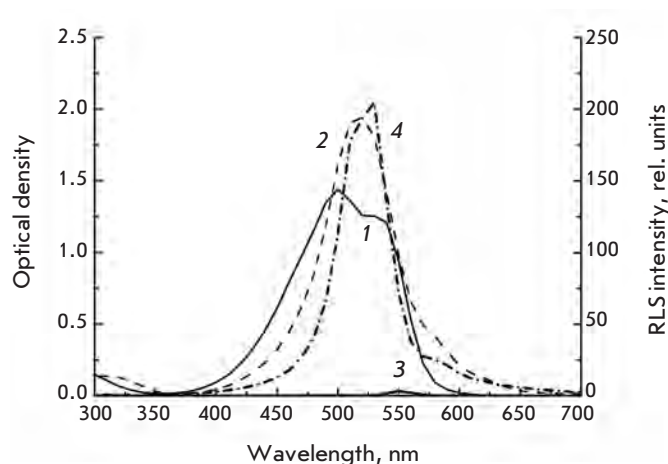


Fig. 1. Absorption (1, 2) and resonance light scattering (3, 4) spectra of a 25 μM MC540 in distilled water (1, 3) solution and in 0.25 M NaCl solution (2, 4).

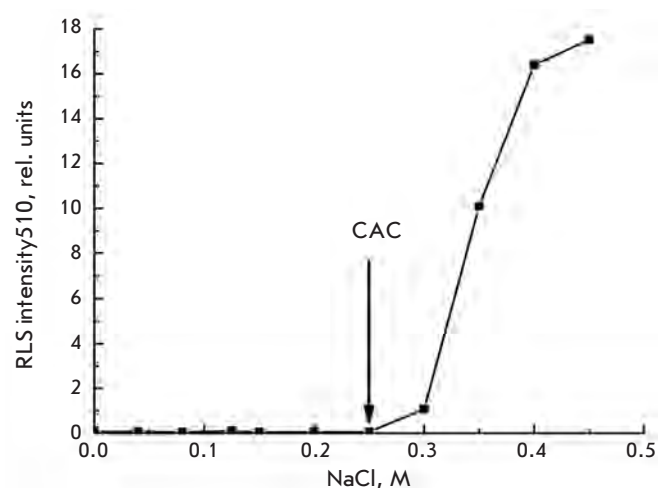


Fig. 2. Dependence of the RLS intensity at 510 nm in a 7.6 μM MC540 solution on the NaCl concentration. An arrow indicates the critical aggregation concentration (CAC) of NaCl above which formation of MC540 aggregates occurs; the latter are detected by the RLS technique.

ordinates. The photoinactivation constant was determined in accordance with the following formula:

$$\beta = \ln(CFU_0/CFU)/F,$$

where CFU_0 and CFU are the parameters that characterize the ability to form colonies at the initial time and under irradiation at a dose of F (kJ/m^2), respectively.

Statistical Analysis

The mean values for the magnitudes studied were determined, and their standard errors of mean were estimated as follows: $SEM = \pm s/\sqrt{n}$, where s is the sample standard deviation.

RESULTS

Absorption Spectra of MC540

The absorption spectra of the MC540 water and water-salt solutions differ in both amplitude and shape.

In the absorption spectra of a MC540 aqueous solution, there are two peaks (Fig. 1, curve 1): at around 500 and 533 nm. These peaks are associated with dimers and monomers, respectively; they are referred to as “water peaks” [11]. When 0.25 M of sodium chloride is added to an aqueous solution of MC540, the water peaks disappear and a new band with a maximum at approximately 518 nm and two weak shoulders at around 570 and 620 nm occurs (Fig. 1, curve 2). This new band appears as a result of the formation of aggregates [12], which is confirmed by the appearance of a band in the RLS spectrum [10] (Fig. 1, curve 4).

The RLS spectra measured under the same conditions as the absorption spectra are shown in Fig. 1 (Fig. 1, curves 3 and 4). In the absence of salt, a low-intensity band at around 550 nm is observed in the RLS spectrum (Fig. 1, curve 3); the appearance of this band is a result of the fluorescence of MC540 in the anti-Stokes region (0^2-0 -transition). In the absorption region of both the MC540 monomers and dimers, no resonance light scattering is observed. Resonance light scattering is observed for a 0.25 M NaCl solution of MC540, which confirms the formation of MC540 aggregates. The shape of the RLS spectrum resembles the shape of the measured absorption spectrum of a salt solution of MC540. The measured absorption spectrum of a water-salt solution of MC540 has an intense, symmetric and unstructured band with a maximum at around 518 nm and two less intense shoulders at 580 and 620 nm. The RLS spectrum is similar to the absorption spectrum. The most intense light scattering band overlaps with the most intense absorption band; however, the former band is slightly shifted towards the long-wavelength region and is found to have a fine structure with maximums at about 506 and 528 nm. On the long-wavelength side from the main RLS band, there is a tail observed in the absorption spectrum, as well (Fig. 1, curve 4).

The dependence of the RLS intensity on the concentration of NaCl added into a 7.6 μM solution of MC540 is shown in Fig. 2. It is clear that, at a salt concentration of less than 0.25 M, no RLS signal is observed. Upon further increase in the salt concentration, an abrupt growth in the intensity of light scattering occurs; this is indicative of the formation of dye aggregates. The

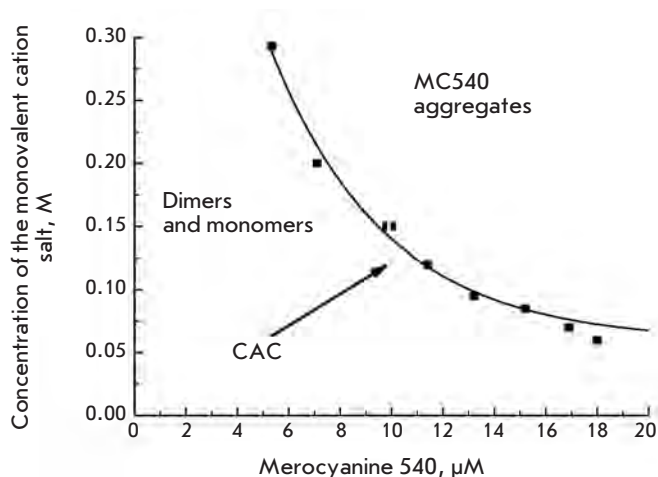


Fig. 3. Dependence of the critical aggregation concentration (CAC) for monovalent cation salts on the MC540 concentration.

concentration of the salt above which the formation of aggregates occurs was called the “critical aggregation concentration” (CAC). It should be noted that the CAC value does not change if we substitute NaCl for KCl; in other words, the critical aggregation concentration depends only on the valence of salt cations. The CAC values were determined for MC540 concentrations ranging from 5 to 25 μM . The dependence of the CAC value on the concentration of MC540 is presented in Fig. 3. According to these data, the CAC *vs.* MC540 concentration curve can be described as hyperbole and the $[\text{CAC}] \times [\text{MC540}]$ product remains constant within the entire concentration range studied; its value is $(1.4 \pm 0.05) \times 10^{-6} \text{ M}^{-2}$. This product is the solubility

product of MC540 (like the solubility product of water). The data presented in Fig. 3 allows us to calculate the fraction of the nonionized molecules of MC540, which form the extended aggregates. In 25 μM solutions of MC540 containing NaCl (0.25 M), this value exceeds 3/4 of the total amount of MC540 molecules.

Photobleaching of MC540

The process of photobleaching proceeds differently in an aqueous MC540 solution from the way it proceeds in a solution containing NaCl (0.25 M).

In the absorption spectra of an aqueous MC540 solution, it is obvious that an increase in the dose of irradiation leads to a comparable drop in the optical density (Fig. 4A) of both “water peaks” corresponding to MC540 monomers and dimers, respectively; the shape of the spectrum in this case does not change within the studied range of doses.

In the presence of NaCl, the rate at which MC540 photobleaches is significantly higher than in an aqueous solution (Fig. 4B). In addition, the shape of the absorption spectra changes during irradiation. After approximately 10 min of irradiation, disappearance of the peak at 518 nm becomes noticeable and the intensity of “water peaks” grows (the insertion in Fig. 4B).

From Fig. 5 it follows that the beginning segment of the bleaching *vs.* dose curves constructed for water and water–salt (NaCl, 0.25 M) solutions of MC540 has the shape of a straight line in semilogarithmic coordinates and can consequently be described by a mono-exponential function.

The photobleaching constants (k) were calculated for 25 μM MC540 solutions from the slope of the corresponding lines (see “Experimental”), and their values were as follows: $(70 \pm 3) \times 10^{-6} \text{ m}^2/\text{kJ}$ for the distilled

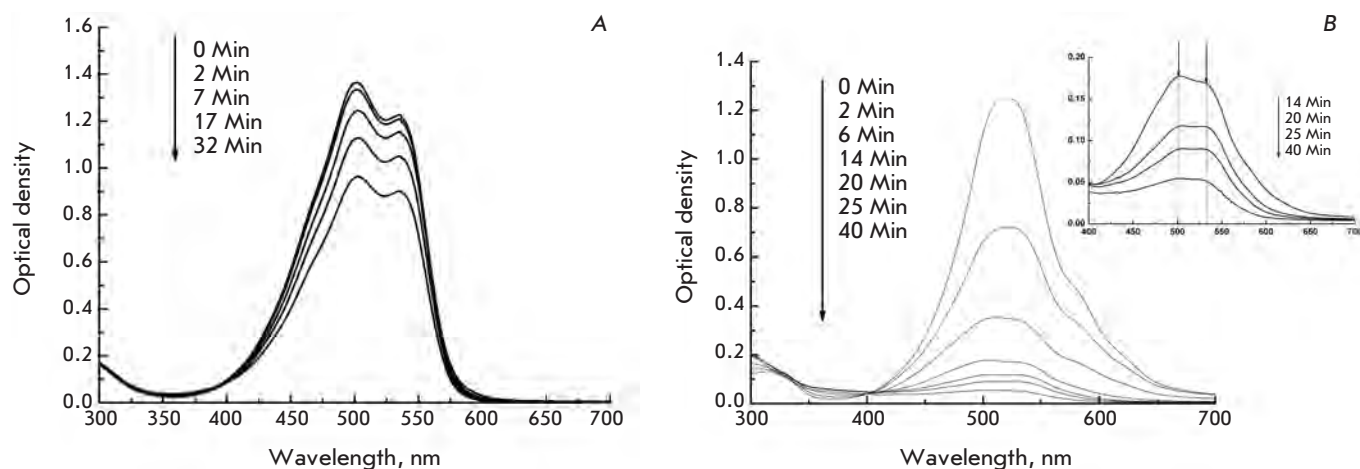


Fig. 4. Photobleaching of MC540 (25 μM) in distilled water (A) and in NaCl containing (0.25 M) solutions (B).

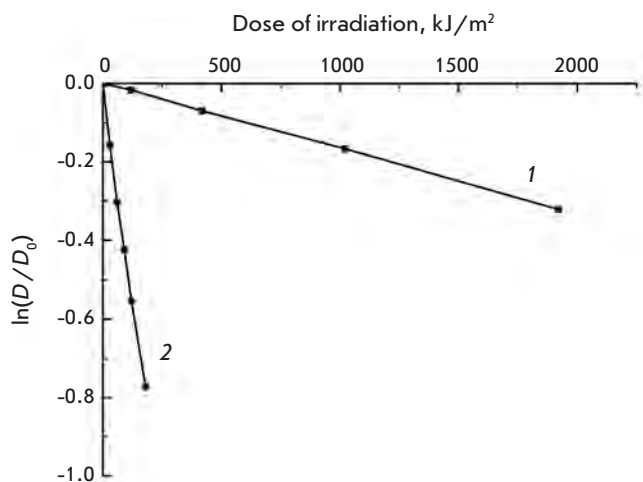


Fig. 5. Dose-response curves of photobleaching of a 25 μM MC540 in distilled water (1) and in NaCl-containing (0.25 M) solutions (2). D and D_0 are the optical densities at 518 nm measured in irradiated and nonirradiated solutions, respectively.

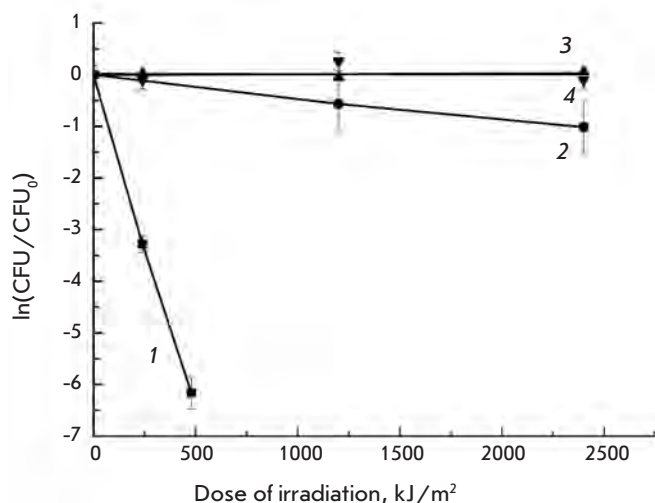


Fig. 6. Dose-response curves of *S. aureus* inactivation photosensitized by 25 μM MC540 in distilled water (2) and in NaCl containing (0.25 M) solutions (1). Curves 3 and 4 correspond to the photoinactivation of *S. aureus* in distilled water and 0.25 M NaCl solutions without MC540, respectively.

water solution and $(2080 \pm 80) \times 10^{-6} \text{ m}^2/\text{kJ}$ for the water solution containing sodium chloride (0.25 M). It is obvious that the rate of MC540 photobleaching is 30 times higher in the presence of NaCl in a water solution compared to a solution containing only distilled water. In a salt solution, MC540 is encountered mainly in its aggregated state, which in turn defines the optical density of the solutions. Accordingly, the reason for the

higher rate of MC540 photobleaching observed in a salt solution in comparison with a distilled water solution could be the higher photolability of MC540 aggregates, rather than the dimers and monomers.

The curves, in semilogarithmic coordinates, which characterize how the dose affects MC540 photosensitized inactivation of *S. aureus* in distilled water and NaCl containing (0.25 M) water solutions, are shown in Fig. 6 (Fig. 6, curve 1).

Irradiating cells in the absence of the photosensitizer caused inactivation neither in the distilled water solution (Fig. 6, curve 3) nor in the 0.25-M NaCl solution (Fig. 6, curve 4). In the preliminary experiments, it was established that the incubation of *P. aeruginosa* and *S. aureus* cells in a 25 μM MC540 solution without irradiation had no effect on their survival (data not presented).

The rate constants for MC540 photosensitized inactivation of bacteria are listed in Table; the values were calculated as described in "Experimental." According to these data, MC540 photosensitized inactivation of *S. aureus* proceeds faster in the presence of salt as compared to a distilled water solution.

The dose dependences of MC540 photosensitized inactivation of *P. aeruginosa* in distilled water and in a 0.25 M NaCl solution are shown in Fig. 7 (curves 1 and 2, respectively). Irradiation in the absence of MC540 caused inactivation neither in distilled water (curve 3) nor in a 0.25 M NaCl solution (curve 4).

Under irradiation in the presence of MC540, in the initial segments of the doseresponse curves, a shoulder was observed when no inactivation of *P. aeruginosa* had occurred (Fig. 7, curves 1 and 2). The initial nonlinear segments of curves 1 and 2 (Fig. 7) are most likely related to the repair of photodamage; the processes compensate for the damage caused by antimicrobial photodynamic therapy at the early stages of photoinactivation. At high doses of irradiation, the inactivation curves displayed exponential behavior and assumed the shape of a straight line in semilogarithmic coordinates. The extrapolation of the linear segments before their intersection with the horizontal line corresponding to $\ln(\text{CFU}/\text{CFU}_0) = 0$ enabled us to determine the doses for which linear regions occur. These doses were called thresholds (F_{th}). For water suspensions, $F_{\text{th,water}} = 140 \text{ kJ}/\text{m}^2$, and for cell suspensions in a salt solution, $F_{\text{th,salt}} = 81 \text{ kJ}/\text{m}^2$. Thus, we introduced this variation, which takes into account the dose threshold value, into the equation for calculating the photoinactivation constant:

$$\beta = \ln(\text{CFU}/\text{CFU}_0)/(F - F_{\text{th}}),$$

where CFU_0 and CFU are the parameters that characterize the ability to form colonies at the initial time and

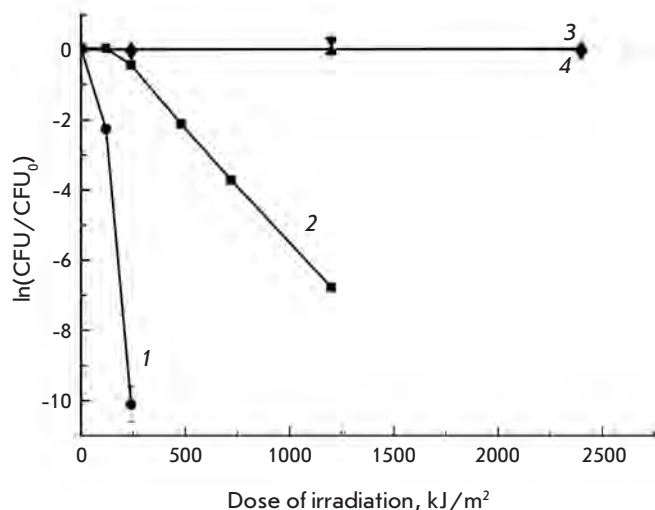


Fig. 7. Dose-response curves of *P. aeruginosa* inactivation photosensitized by 25 μM MC540 in distilled water (2) and in NaCl containing (0.25 M) solutions (1). Curves 3 and 4 correspond to the photoinactivation of *P. aeruginosa* in distilled water and in 0.25 M NaCl solutions without MC540, respectively.

under irradiation at a dose (kJ/m^2) of $(F - F_{\text{th}})$, respectively.

The values of the photoinactivation constants are listed in Table.

It can be observed that the photosensitized inactivation of *P. aeruginosa* proceeds 10 times more effectively in the presence of salt than it does in just distilled water.

DISCUSSION

It is known that the aggregation state of MC540 defines the type of photodynamic reactions that occur and affects the formation of active products, which can inflict damage on biological molecules [13] and can also influence the rate of MC540 photobleaching [7, 8]. The production of singlet oxygen ($^1\text{O}_2$) was believed to play the main role in the bactericidal activity of photosensitizers [5, 14]. At the same time, it was shown that singlet oxygen can generate only monomeric forms of MC540 [15].

In this work, we studied how the aggregation state of MC540 affects its rate of photobleaching in the presence of 0.25 M NaCl and the rate of MC540 photosensitized inactivation of bacteria. The calculations that we performed relying on the data from Figs. 2 and 3 reveal that, at the given concentration of sodium chloride and MC540, 3/4 of the dye molecules are found in the aggregated state. In previously published works devoted to the study of the MC540 photosensitized inactivation of bacteria, no attempts were made to influence the aggregation state of this dye and by this the efficiency of inactivation [2, 3].

MC540 is an anionic photosensitizer. In distilled water, this compound exists in the form of dimers and monomers, which have absorption peaks at 533 and 500 nm, respectively [11]. Since the cell wall of bacteria is negatively charged [16–19], just as MC540 dimers and monomers, the penetration of the photosensitizer through the bacterial cell wall is hindered by electrostatic repulsion; in this case, the efficiency of MC540 photosensitized inactivation of bacteria decreases. However, when salt is added to the solution, its cations shield the anionic group of MC540; the latter leads to a reduction in the electrostatic repulsion between the molecules of MC540 and, thereby, to the formation of extended MC540 aggregates, which are detected by the RLS method. In addition, salt cations shield negative charges on the bacterial cell wall; this may facilitate the interaction of the photosensitizer with bacteria.

In our work, we demonstrated by means of the RLS method that when salt is added to an aqueous solution of MC540, there is a critical aggregation concentration (CAC) of salt above which aggregation of MC540 occurs; the CAC value depends on the concentration of MC540 (Fig. 2). The product of the CAC and the MC540 concentration in solutions of monovalent cations remains constant, and its value is $[\text{CAC}] \times [\text{MC540}] = (1.4 \pm 0.05) \times 10^{-6} \text{ M}^2$.

The results obtained in this work show that the rate of photobleaching of a 25 μM MC540 in a NaCl containing solution is 30 times higher than that in a distilled water solution; the rate constants of photobleaching are $(2080 \pm 80) \times 10^{-6}$ and $(70 \pm 3) \times 10^{-6} \text{ m}^2/\text{kJ}$, re-

Photoinactivation constants (β , m^2/kJ) for *P. aeruginosa* and *S. aureus* for 25 μM MC540 in distilled water and in NaCl-containing (0.25 M) solutions

<i>P. aeruginosa</i> 104		<i>S. aureus</i> 78	
in water	in 0.25 M NaCl	in water	in 0.25 M NaCl
$(6700 \pm 600) \times 10^{-6}$	$(66900 \pm 2500) \times 10^{-6}$	$(500 \pm 60) \times 10^{-6}$	$(13800 \pm 600) \times 10^{-6}$

spectively. In the case of MC540 photosensitized inactivation of *P. aeruginosa*, the photoinactivation constant increases by a factor of ten in the presence of sodium chloride (0.25 M), in comparison with its value in distilled water; the values of the photoinactivation constants are $(66900 \pm 2500) \times 10^{-6}$ and $(6700 \pm 600) \times 10^{-6} \text{ m}^2/\text{kJ}$, respectively. In the case of *S. aureus*, the photoinactivation constant in the presence of 0.25 M NaCl is approximately 28 times higher $[(13800 \pm 600) \times 10^{-6} \text{ m}^2/\text{kJ}]$ than the inactivation constant in distilled water $[(500 \pm 60) \times 10^{-6} \text{ m}^2/\text{kJ}]$. We suggest that such a difference in the rate constants of photobleaching (k) and photoinactivation (β) can be accounted for by the influence of salt cations on both the photosensitizer and the bacterial cell wall.

Only monomers of MC540 possess the ability to generate $^1\text{O}_2$ [14]. During aggregation, the concentration of monomers drastically decreases; consequently, the increase in the bactericidal activity occurring in the presence of sodium chloride cannot be associated with the

prevailing effect of $^1\text{O}_2$ on bacteria. It may be suggested that the transfer of an electron between the excited and unexcited molecules of the dye is facilitated in the aggregates of MC540. In all likelihood, the presence of the salt causes the activation of photodynamic reactions in the aggregates of MC540, which results in the generation of free radicals [13], the latter having the ability to attack bacteria and, subsequently, to kill them.

CONCLUSIONS

The data obtained in this work indicating an increase in the bactericidal effects of a photosensitizer in the presence of salts can be used in the development of promising new antibacterial treatments especially in light of the current problems connected with multiple antibiotic resistance. ●

This work was supported by the Federal Agency on Science and Innovations (Government Contract № 02.740.11.0310).

REFERENCES

- Geinitz A.V., Sorokaty A.E., Yagudajev D.M., Trukhmanov R.S. // *Laser medicine*. 2007. V.11. P. 42–46
- O'Brien J.M., Gaffney D.K., Wang T.P., Sieber F. // *Blood*. 1992. V. 80. P. 277–285.
- Lin H.Y., Chen C.T., Huang C.T. // *Appl. Environ. Microbiol.* 2004. V. 70. P. 6453–6458.
- Sbarra M.S., Di Poto A., Arciola C.R., Saino E., Sharma M., Bragheri F., Cristiani I., Speziale P., Visai L. // *Int. J. Artif. Organs*. 2008. V. 31. P. 848–857.
- Pervaiz S. // *FASEB J*. 2001. V. 15. P. 612–617.
- Foote C.S. // *Photochem. Photobiol.* 1991. V. 54. P. 659.
- Kozhinova E.A., Kozyr L.A., Tikhomirov A.M., Kyagova A.A., Potapenko A.Y. // *Bulletin of RSMU* 2005. V.7. P. 47–52
- Kozhinova E.A., Tikhomirov A.M., Kozyr L.A., Kyagova A.A., Potapenko A.Y. // *Russian Journal of Physical Chemistry A*. 2007. V.81. P. 1335–1340
- Pasternack R.F., Collings P.J. // *Science*. 1995. V. 269. P. 935–939.
- Tikhomirov A.M., Shmigol T.A., Kozhinova E.A., Kyagova A.A., Potapenko A.Y., Bezdetnaya L.N. // *Biophysics*. 2009. V.54. P. 584–589
- Cunderlíková B., Sikurová L., Moan J. // *Bioelectrochemistry*. 2003. V. 59. P. 1–10.
- Adenier A., Aaron J. // *Spectrochim. Acta. A. Mol. Biomol. Spectrosc.* 2002. V. 58. P. 543–551.
- Davila J., Harriman A., Gulliya K.S. // *Photochem. Photobiol.* 1991. V. 53. P. 1–11.
- Kalyanaraman B., Feix J.B., Sieber F., Thomas J.P., Girotti A.W. // *Proc. Natl. Acad. Sci. USA*. 1987. V. 84. P. 2999–3003.
- Feix J.B., Kalyanaraman B. // *Arch. Biochem. Biophys.* 1991. V. 291. P. 43–51.
- Grimmecke H.D., Knirel Y.A., Kiesel B., Voges M., Rietschel E.T. // *Carbohydrate Res.* 1994. V. 259. P. 45–58.
- Zähringer U., Lindner B., Rietschel E.T. // *Adv. Carbohydrate Chem. Biochem.* 1994. V. 50. P. 211–276.
- Raetz C.R., Ulevitch R.J., Wright S.D., Sibley C.H., Ding A., Nathan C.F. // *FASEB J*. 1991. V. 5. P. 2652–2660.
- Navarre W.W., Schneewind O. // *Microbiol. Mol. Biol. Rev.* 1999. V. 63. P. 174–229.

Deficient Response to Experimentally Induced Alkalosis in Mice with the Inactivated *insrr* Gene

I.E. Deyev¹, D.I. Rzhovsky², A.A. Berchatova¹, O.V. Serova¹, N.V. Popova¹, A.N. Murashev², A.G. Petrenko^{1*}

¹Shemyakin and Ovchinnikov Institute of Bioorganic Chemistry, Russian Academy of Sciences

²Branch of Shemyakin and Ovchinnikov Institute of Bioorganic Chemistry, Pushchino, Russian Academy of Sciences

*E-mail: petrenkoag@gmail.com

Received 12.05.2011

Copyright © 2011 Park-media, Ltd. This is an open access article distributed under the Creative Commons Attribution License, which permits unrestricted use, distribution, and reproduction in any medium, provided the original work is properly cited.

ABSTRACT Currently, the molecular mechanisms of the acid-base equilibrium maintenance in the body remain poorly understood. The development of alkalosis under various pathological conditions poses an immediate threat to human life. Understanding the physiological mechanisms of alkalosis compensation may stimulate the development of new therapeutic approaches and new drugs for treatment. It was previously shown that the orphan insulin receptor-related receptor (IRR) is activated by mildly alkaline media. In this study, we analyzed mutant mice with targeted inactivation of the *insrr* gene encoding IRR, and revealed their phenotype related to disorders of the acid-base equilibrium. Higher concentrations of bicarbonate and CO₂ were found in the blood of *insrr* knockout mice in response to metabolic alkalosis.

KEYWORDS alkalosis; IRR.

INTRODUCTION

The insulin receptor-related receptor (IRR) is a receptor tyrosine kinase that belongs to the minifamily of the insulin receptor, which also includes the insulin receptor and insulin-like growth factor receptor [1]. The cDNA sequence of IRR was cloned in 1989 [2]; however, as of now no natural agonists for IRR possessing a peptide or protein character have been found [3].

Contrary to its close homologs, which are present in a large number of tissues and cells, IRR is produced only in some tissues and specific cell populations. The largest concentration of IRR is found in the kidneys, where this receptor is present only in β -intercalated cells (a subpopulation of epithelial cells lining the distal ducts) [4]. These cells are in contact with the renal filtrate, the pH of which, in contrast to blood, may vary to become alkaline. IRR is also expressed in gastric enterochromaffin-like cells [5] secreting histamine, which, in turn, stimulates the secretion of acid, accompanied by an outflow of alkali from the stomach wall to the blood stream. A significant amount of IRR was detected in β - and α -cells of the islets of Langerhans, which may be in contact with the alkaline pancreatic juice [6]. It was found that IRR, in contrast to its homologs, can be activated at pH > 8.0 [7, 8] and presumably is a cellular sensor of mildly alkaline media. The postulated func-

tion of IRR correlates well with its known tissue and cell distribution.

In order to reveal the functional properties of IRR, we performed a phenotypic analysis of the mice with the genetically ablated *insrr* gene that encodes IRR. It was found that the *insrr* knockout mice had a defect in the compensatory response to experimentally induced alkalosis.

EXPERIMENTAL

Antibodies and Western-Blot Analysis

We used the rabbit antibody against the 539–686 mouse IRR fragment fused with glutathione S-transferase (GST) [8]. Monospecific antibodies were purified on a matrix with the 539–686 mouse IRR fragment and a 6-His tag coupled with BrCN-Sepharose. The proteins were separated by electrophoresis on a 10% polyacrylamide gel (PAAG) in the presence of sodium dodecyl sulfate (SDS) and were subsequently transferred to a nitrocellulose membrane. In order to reduce nonspecific sorption, the membrane was incubated in a milk/TBS-T buffer (5% non-fat milk, 20 mM Tris-HCl, pH 7.6, 140 mM NaCl, and 0.1% Tween-20) overnight at a temperature of 4°C. In order to detect the proteins, the membrane was incubated with the primary anti-

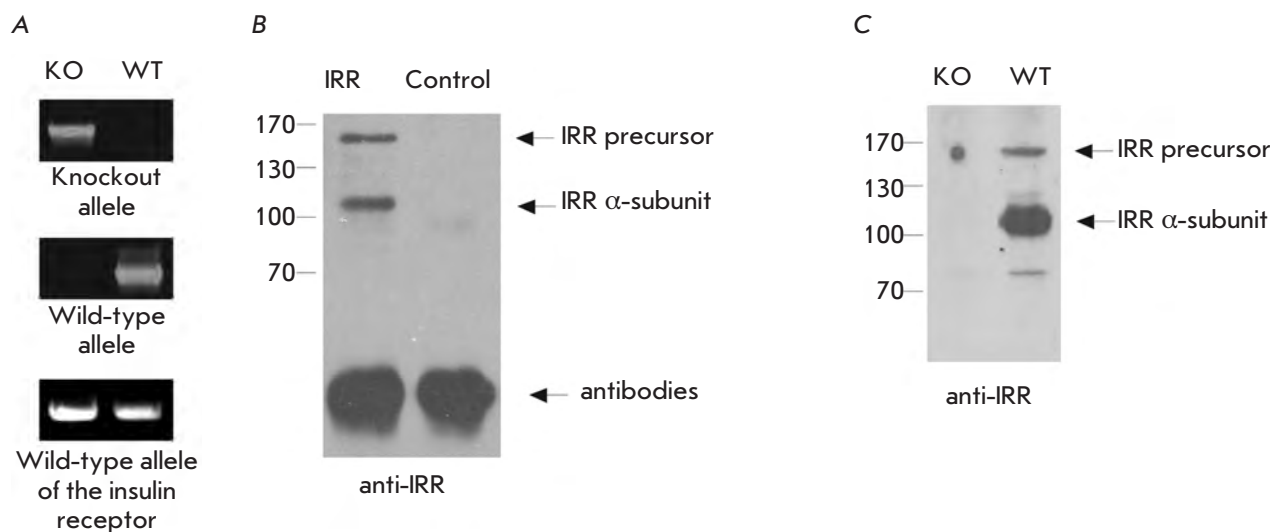


Fig. 1. Analysis of the inactivation of the *insrr* gene in mice. (A) – PCR on the genomic DNA of the wild-type and *insrr* knockout mice with the use of the primers to the wild-type allele of IRR, IR and the *insrr* knockout allele. (B) – Western blotting with the use of antibodies against the IRR ectodomain. Lysates from transfected HEK293 cells with IRR-HA expressing plasmid and non-transfected cells (as the negative control) were blotted with the anti-ectodomain IRR antibodies. (C) – Equal amounts of WGA-eluates (about 10 μ g) from the kidney membrane fraction of wild-type and *insrr* knockout mice were blotted with anti-ectodomain antibodies.

bodies (1 : 5000 by volume) for 60 min at room temperature, washed with TBS-T, and then incubated with the secondary anti-rabbit antibodies conjugated with horseradish peroxidase (1 : 10000 by volume) for 1 h. The bound antibodies were detected by SuperSignal West Pico chemiluminescent substrate [9].

Animal Experiments

The *insrr* knockout mice were obtained by *in vitro* fertilization with frozen sperm of the insulin receptor family triple knockout mice [10]. The wakeful, sexually mature male mice with targeted inactivation of only the *insrr* gene were examined. Genotyping was performed in accordance with [10]. The C57BL6 mice were taken as a control group. The animals were kept in the Laboratory Animal Breeding Facility (Branch of the Institute of Bioorganic Chemistry, Pushchino) under ambient conditions (temperature of $21 \pm 2^\circ\text{C}$, humidity of 30–70%, and a lighting cycle of 12/12 h), mice were given *ad libitum* access to food and water.

The experiments were performed upon wakeful animals. A 1.3% solution of NaHCO_3 (200 $\mu\text{l}/10$ g of body weight) was injected into the tail vein of mice within 5 s. The blood samples were taken 30 min prior to the injection of NaHCO_3 (point 0), as well as 5 and 15 min after the injection. Blood was collected from the retro-orbital sinus into plastic capillaries (Lithin-Heparin, 50 unit/ml) and analyzed with the help of a Rapid-

point 405 blood gas analyzer (Siemens). All manipulations were performed in accordance with the protocol certified by the Institute Committee on the Control of the Housing and Use of Laboratory Animals.

RESULTS

In order to obtain a homozygous line of the *insrr* knockout mice, animals with the *insrr* gene, as well as those with the insulin receptor and insulin-like growth factor receptor genes knocked out (triple heterozygous knockout [10]), were crossed with the C57BL6 mice of the wild type. The presence of alleles with the *insrr* gene knocked out and the absence of alleles with the insulin receptor and insulin-like growth factor receptor genes knocked out were verified by PCR on the genomic DNA of mice (Fig. 1A).

The synthesis of IRR protein in mice with the *insrr* gene knocked out was analyzed using the antibody that specifically recognizes the ectodomain of IRR (Fig. 1B). The Western blots of partially purified renal membrane extracts of the normal mice and the *insrr* knockout mice were stained with these antibodies. This analysis confirmed that no IRR protein was present in the obtained mice (Fig. 1C).

The primary analysis performed under normal conditions did not reveal any significant differences between the normal mice and the mice with the *insrr* gene knockout [11]; hence, we performed two series

Blood parameters in wild-type (WT) and *insrr* knockout mice (KO)

Electrolytes in blood	WT mice		KO mice	
	Mean value	Error	Mean value	Error
pH	7.21	0.03	7.29	0.02
PCO ₂ , mm Hg	50	1.5	49	1.5
PO ₂ , mm Hg	41	0.8	42	0.8
BE, mmol/l	-8.4	1.8	-4.2	1.2
TCO ₂ , mmol/l	21.4	1.6	24.4	1.0
HCO ₃ ⁻ , mmol/l	19.9	1.6	22.9	1.0
Na, mmol/l	148	0.9	148	0.8
K, mmol/l	6.2	0.1	6.3	0.2
Ca, mmol/l	1.25	0.0	1.24	0.0
tHb, g/l	16.8	0.3	18.0	0.4
Hct, %	50	1.0	54	1.1

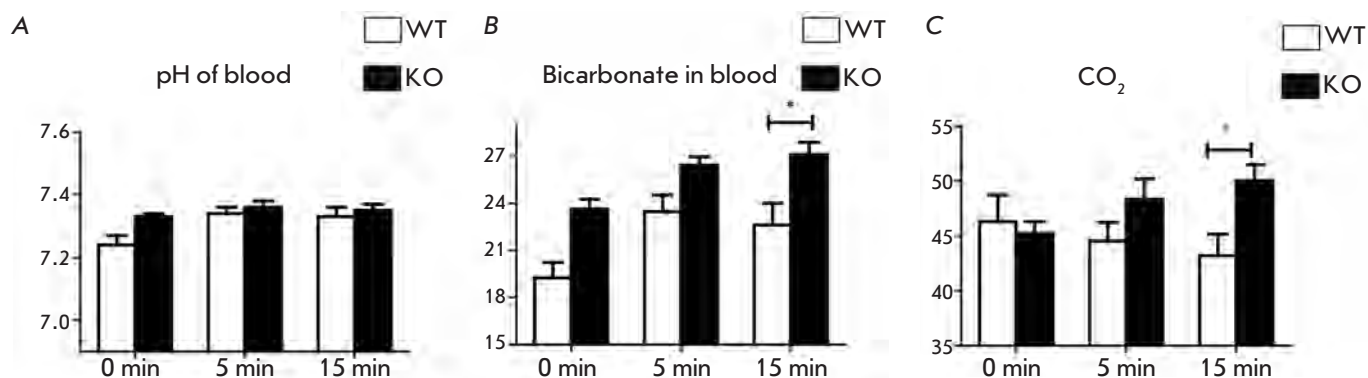


Fig. 2. Blood gas analysis of blood from wild-type (WT) and *insrr* knockout (KO) mice before and after injection of a bicarbonate solution. (A) – pH of blood; (B) – concentration of bicarbonate in blood (mmol/l); (C) – concentration of CO₂ in blood (mm Hg). * $p < 0.05$ by the Student's test.

of experiments with the wild-type and knockout mice both under normal conditions, as well as under induced alkalosis.

In the first series of experiments, we determined 11 blood parameters in mice from both groups (eight animals per group) under normal conditions. It was found that in mice with the inactivated *insrr* gene, the concentration of bicarbonate in blood (22.9 ± 1.0 against 19.9 ± 1.6 , $p < 0.05$), as well as pH (7.29 ± 0.02 against 7.21 ± 0.03 , $p < 0.05$), and the hematocrit (54 ± 1.1 against 50 ± 1.0 , $p < 0.05$) was higher than that in the wild-type animals. All other determined blood parameters did not differ significantly (Table).

For the second series of experiments, two groups of animals were selected: 10 wild-type mice and 12 knockout mice. Metabolic alkalosis was induced by an intravenous injection of a 1.3% NaHCO₃ solution

(200 μ l/10 g of body weight). The blood parameters were determined at intervals of 5 and 15 min following the alkaline injection. Five minutes after the injection of the alkaline solution, the dynamics of the variation in the concentration of bicarbonate and blood pH in mice with IRR knocked out was the same as that in the wild-type mice; i.e., pH increased (from 7.24 ± 0.03 to 7.34 ± 0.02 , $p < 0.05$ in wild-type mice and from 7.33 ± 0.01 to 7.36 ± 0.02 , $p < 0.2$ in knockout mice) and so did the concentration of bicarbonate (from 19.25 ± 0.98 to 23.47 ± 1.06 , $p < 0.05$ in wild-type mice and from 23.64 ± 0.63 to 26.43 ± 0.53 , $p < 0.05$) (Figs. 2A, B). Fifteen minutes after the induction of alkalosis, the blood pH value in mice from both groups became somewhat lower than that recorded after 5 min (7.33 ± 0.03 in wild-type mice and 7.35 ± 0.02 in knockout mice). However, after 5 min, a significant increase

was observed both in the concentrations of bicarbonate and CO₂ in the blood of the mice with IRR knocked out in comparison with these values in the wild-type mice (Figs. 2B, C); thus, the wild-type animals and the animals with the *insrr* gene knockout displayed different responses to acute alkalosis, which was experimentally induced via the injection of bicarbonate into the blood.

CONCLUSIONS

It was demonstrated in our previous studies that IRR is a sensor of extracellular alkaline media. The absence of this gene in the body leads to a disturbance in the compensation of metabolic alkalosis, induced by feeding animals with alkaline food for several days. This effect resulted from a defect in bicarbonate secretion by the kidneys of the *insrr* knockout mice [8]. The results obtained in studying the compensation of induced alkalosis under acute conditions (5–15 min) confirm our hypothesis on the compensatory role of IRR in the secretion of bicarbonate. It can be concluded that IRR-dependent compensation of alkalosis proceeds rather fast.

It is important to note that, in mice with IRR knocked out, compensation of alkalosis is also observed (since the blood pH value decreases). However, this occurs not due to the secretion of excess amounts of bicarbonate, but as a result of the increase in the concentration of CO₂ in the blood; the latter most likely results from the decelerated breathing or accelerated metabolism. Thus, it can be concluded that IRR plays a significant role in the physiological mechanisms of regulation of the acid-base equilibrium and that mice with IRR knocked out can be used as animal models to study pathological development of metabolic alkalosis. ●

This work was supported by the Russian Foundation for Basic Research (Grants № 06-04-49706a, 09-04-01644-a, 10-04-01794-a, and 09-04-12201-ofi_m), by the Fundamental Research Programs of the Presidium of the Russian Academy of Sciences “Fundamental Sciences to Medicine” and “Molecular and Cell Biology.”

REFERENCES

1. Marino-Buslje C., Martin-Martinez M., Mizuguchi K., Siddle K., Blundell T.L. // *Biochem. Soc. Trans.* 1999. V. 27. P. 715–726.
2. Shier P., Watt V.M. // *J. Biol. Chem.* 1989. V. 264. P. 14605–14608.
3. Dissen G.A., Garcia-Rudaz C., Tapia V., Parada L.F., Hsu S.Y., Ojeda S.R. // *Endocrinology*. 2005. V. 147. № 1. P. 155–165.
4. Bates C.M., Merenmies J.M., Kelly-Spratt K.S., Parada L.F. // *Kidney Int.* 1997. V. 52. P. 674–681.
5. Tsujimoto K., Tsuji N., Ozaki K., Ohta M., Itoh N. // *Endocrinology*. 1995. V. 136. P. 558–561.
6. Hirayama I., Tamemoto H., Yokota H., Kubo S.K., Wang J., Kuwano H., Nagamachi Y., Takeuchi T., Izumi T. // *Diabetes*. 1999. V. 48. P. 1237–1244.
7. Deev I.E., Vasilenko K.P., Kurmangaliev E., Serova O.V., Popova N.V., Galagan Y.S., Burova E.B., Zozulya S.A., Nikol'skii N.N., Petrenko A.G. // *Dokl. Biochem. Biophys.* 2006. V. 408. P. 184–187.
8. Deyev I.E., Sohet F., Vassilenko K.P., Serova O.V., Popova N.V., Zozulya S.A., Burova E.B., Houillier P., Rzhnevsky D.I., Berchatova A.A., et al. // *Cell Metab.* 2011. V. 13. P. 679–689.
9. Deyev I.E., Petrenko A.G. // *Biochimie*. 2010. V. 92. P. 418–422.
10. Nef S., Verma-Kurvari S., Merenmies J., Vassalli J.D., Efstratiadis A., Accili D., Parada L.F. // *Nature*. 2003. V. 426. P. 291–295.
11. Kitamura T., Kido Y., Nef S., Merenmies J., Parada L.F., Accili D. // *Mol. Cell Biol.* 2001. V. 21. P. 5624–5630.

GENERAL RULES

Actae Naturae publishes experimental articles and reviews, as well as articles on topical issues, short reviews, and reports on the subjects of basic and applied life sciences and biotechnology.

The journal is published by the Park Media publishing house in both Russian and English.

The journal *Acta Naturae* is on the list of the leading periodicals of the Higher Attestation Commission of the Russian Ministry of Education and Science

The editors of *Actae Naturae* ask of the authors that they follow certain guidelines listed below. Articles which fail to conform to these guidelines will be rejected without review. The editors will not consider articles whose results have already been published or are being considered by other publications.

The maximum length of a review, together with tables and references, cannot exceed 60,000 symbols (approximately 40 pages, A4 format, 1.5 spacing, Times New Roman font, size 12) and cannot contain more than 16 figures.

Experimental articles should not exceed 30,000 symbols (20 pages in A4 format, including tables and references). They should contain no more than ten figures. Lengthier articles can only be accepted with the preliminary consent of the editors.

A short report must include the study's rationale, experimental material, and conclusions. A short report should not exceed 12,000 symbols (8 pages in A4 format including no more than 12 references). It should contain no more than four figures.

The manuscript should be sent to the editors in electronic form: the text should be in Windows Microsoft Word 2003 format, and the figures should be in TIFF format with each image in a separate file. In a separate file there should be a translation in English of: the article's title, the names and initials of the authors, the full name of the scientific organization and its departmental affiliation, the abstract, the references, and figure captions.

MANUSCRIPT FORMATTING

The manuscript should be formatted in the following manner:

- Article title. Bold font. The title should not be too long or too short and must be informative. The title should not exceed 100 characters. It should reflect the major result, the essence, and uniqueness of the work, names and initials of the authors.
- The corresponding author, who will also be working with the proofs, should be marked with a footnote *.
- Full name of the scientific organization and its departmental affiliation. If there are two or more scientific organizations involved, they should be linked by digital superscripts with the authors' names. Abstract. The structure of the abstract should be very clear and must reflect the following: it should introduce the reader to the main issue and describe the experimental approach, the possibility of practical use, and the possibility of further research in the field. The average length of an abstract is 20 lines

(1,500 characters).

- Keywords (3 – 6). These should include the field of research, methods, experimental subject, and the specifics of the work. List of abbreviations.

- INTRODUCTION
- EXPERIMENTAL PROCEDURES
- RESULTS AND DISCUSSION
- CONCLUSION

The organizations that funded the work should be listed at the end of this section with grant numbers in parenthesis.

- REFERENCES

The in-text references should be in brackets, such as [1].

RECOMMENDATIONS ON THE TYPING AND FORMATTING OF THE TEXT

- We recommend the use of Microsoft Word 2003 for Windows text editing software.
- The Times New Roman font should be used. Standard font size is 12.
- The space between the lines is 1.5.
- Using more than one whole space between words is not recommended.
- We do not accept articles with automatic referencing; automatic word hyphenation; or automatic prohibition of hyphenation, listing, automatic indentation, etc.
- We recommend that tables be created using Word software options (Table → Insert Table) or MS Excel. Tables that were created manually (using lots of spaces without boxes) cannot be accepted.
- Initials and last names should always be separated by a whole space; for example, A. A. Ivanov.
- Throughout the text, all dates should appear in the “day.month.year” format, for example 02.05.1991, 26.12.1874, etc.
- There should be no periods after the title of the article, the authors' names, headings and subheadings, figure captions, units (s – second, g – gram, min – minute, h – hour, d – day, deg – degree).
- Periods should be used after footnotes (including those in tables), table comments, abstracts, and abbreviations (mon. – months, y. – years, m. temp. – melting temperature); however, they should not be used in subscripted indexes (T_m – melting temperature; T_{pt} – temperature of phase transition). One exception is mln – million, which should be used without a period.
- Decimal numbers should always contain a period and not a comma (0.25 and not 0,25).
- The hyphen (“-”) is surrounded by two whole spaces, while the “minus,” “interval,” or “chemical bond” symbols do not require a space.
- The only symbol used for multiplication is “×”; the “×” symbol can only be used if it has a number to its right. The “.” symbol is used for denoting complex compounds in chemical formulas and also noncovalent complexes (such as DNA·RNA, etc.).
- Formulas must use the letter of the Latin and Greek alphabets.

GUIDELINES FOR AUTHORS

- Latin genera and species' names should be in italics, while the taxa of higher orders should be in regular font.
- Gene names (except for yeast genes) should be italicized, while names of proteins should be in regular font.
- Names of nucleotides (A, T, G, C, U), amino acids (Arg, Ile, Val, etc.), and phosphonucleotides (ATP, AMP, etc.) should be written with Latin letters in regular font.
- Numeration of bases in nucleic acids and amino acid residues should not be hyphenated (T34, Ala89).
- When choosing units of measurement, SI units are to be used.
- Molecular mass should be in Daltons (Da, KDa, MDa).
- The number of nucleotide pairs should be abbreviated (bp, kbp).
- The number of amino acids should be abbreviated to aa.
- Biochemical terms, such as the names of enzymes, should conform to IUPAC standards.
- The number of term and name abbreviations in the text should be kept to a minimum.
- Repeating the same data in the text, tables, and graphs is not allowed.

GUIDENESS FOR ILLUSTRATIONS

- Figures should be supplied in separate files. Only TIFF is accepted.
- Figures should have a resolution of no less than 300 dpi for color and half-tone images and no less than 500 dpi.
- Files should not have any additional layers.

REVIEW AND PREPARATION OF THE MANUSCRIPT FOR PRINT AND PUBLICATION

Articles are published on a first-come, first-served basis. The publication order is established by the date of acceptance of the article. The members of the editorial board have the right to recommend the expedited publishing of articles which are deemed to be a priority and have received good reviews.

Articles which have been received by the editorial board are assessed by the board members and then sent for external review, if needed. The choice of reviewers is up to the editorial board. The manuscript is sent on to reviewers who are experts in this field of research, and the editorial board makes its decisions based on the reviews of these experts. The article may be accepted as is, sent back for improvements, or rejected.

The editorial board can decide to reject an article if it does not conform to the guidelines set above.

A manuscript which has been sent back to the authors for improvements requested by the editors and/or reviewers is reviewed again, after which the editorial board makes another decision on whether the article can be accepted for publication. The published article has the submission and publication acceptance dates set at the beginning.

The return of an article to the authors for improvement does not mean that the article has been accepted for publication. After the revised text has been received, a decision is made by the editorial board. The author must return the improved text, together with the original text and responses to all comments. The date of acceptance is the day on which the final version of the article was received by the publisher.

A revised manuscript must be sent back to the publisher a week after the authors have received the comments; if not, the article is considered a resubmission.

E-mail is used at all the stages of communication between the author, editors, publishers, and reviewers, so it is of vital importance that the authors monitor the address that they list in the article and inform the publisher of any changes in due time.

After the layout for the relevant issue of the journal is ready, the publisher sends out PDF files to the authors for a final review.

Changes other than simple corrections in the text, figures, or tables are not allowed at the final review stage. If this is necessary, the issue is resolved by the editorial board.

FORMAT OF REFERENCES

The journal uses a numeric reference system, which means that references are denoted as numbers in the text (in brackets) which refer to the number in the reference list.

For books: the last name and initials of the author, full title of the book, location of publisher, publisher, year in which the work was published, and the volume or issue and the number of pages in the book.

For periodicals: the last name and initials of the author, title of the journal, year in which the work was published, volume, issue, first and last page of the article. Must specify the name of the first 10 authors. Ross M.T., Grafham D.V., Coffey A.J., Scherer S., McLay K., Muzny D., Platzer M., Howell G.R., Burrows C., Bird C.P., et al. // Nature. 2005. V. 434. № 7031. P. 325–337.

References to books which have Russian translations should be accompanied with references to the original material listing the required data.

References to doctoral thesis abstracts must include the last name and initials of the author, the title of the thesis, the location in which the work was performed, and the year of completion.

References to patents must include the last names and initials of the authors, the type of the patent document (the author's rights or patent), the patent number, the name of the country that issued the document, the international invention classification index, and the year of patent issue.

The list of references should be on a separate page. The tables should be on a separate page, and figure captions should also be on a separate page.

The following e-mail addresses can be used to contact the editorial staff: vera.knorre@gmail.com, actanaturae@gmail.com, tel.: (495) 727-38-60, (495) 930-80-05

NANOTECHNOLOGIES

in Russia

Peer-review scientific journal

Nanotechnologies in Russia
(*Rossiiskie Nanotekhnologii*)

focuses on self-organizing structures and nanoassemblages, nanostructures including nanotubes, functional nanomaterials, structural nanomaterials, devices and facilities on the basis of nanomaterials and nanotechnologies, metrology, standardization, and testing in nanotechnologies, nanophotonics, nanobiology.

—> **Russian edition:** <http://nanoru.ru>

—> **English edition:** <http://www.springer.com/materials/nanotechnology/journal/12201>

Issued with support from:



The Ministry of Education and Science of the Russian Federation